



**An investigation of the mechanisms of cellular
transformation by hERG potassium channels**

Thesis submitted for the Degree of
Doctor of Philosophy
at the University of Leicester

by

George S. G. Shehatou

Department of Cell Physiology and Pharmacology

University of Leicester

Leicester, UK

April 2011

**An investigation of the mechanisms of cellular transformation
by hERG potassium channels**

Human ether-à-go-related gene 1 (hERG1) potassium channels are expressed in a variety of tumour cells and expression of hERG1 K⁺ channels in normal cells can induce a transformed phenotype.

The transformative potential of hERG1 appears to be extracellular matrix-dependent. hERG1-expressing NIH-3T3 cells maintained a normal cell morphology when plated on collagen-1 and cell migration speeds were not different to those measured for empty vector-transfected NIH-3T3 cells (NIH-VC). However, hERG1-expressing NIH-3T3 cells displayed a transformed morphology and enhanced cell migration speeds when plated on laminin-1 or fibronectin, and this was associated with a reduction in vinculin protein cell content and cytoskeletal rearrangements.

I have provided evidence to indicate that the ion flux through the hERG1 pore and its cell-surface localization is important for its oncogenic potential. Unlike for wild-type hERG1, stable expression of a non-conducting G628S hERG1, or a trafficking-deficient A561V hERG1 mutant did not induce a transformed phenotype in NIH-3T3 cells. Pentamidine, a compound which inhibits hERG1 trafficking to the cell-surface, inhibited fibronectin-dependent migration of wild-type hERG1-expressing cells. Although dofetilide, which blocks the ion conductance of hERG1, did not alter the transformative effect of wild-type hERG1 expression in cell grown on fibronectin, chronic application of this hERG1 inhibitor at a therapeutically-relevant concentration (100 nM) did cause a near-complete reversion of hERG1-expressing cells to a normal cell phenotype within 14 days.

NIH-3T3 cells transiently transfected with a plasmid encoding both hERG1 and hERG1b exhibited increases in cell proliferation relative to cells expressing either isoform alone, suggesting a potential role for the hERG1b isoform in regulating hERG1 pro-oncogenic effects.

In summary, the transforming potential of hERG1 expression appears to be dependent on hERG1 trafficking to the cell-surface and its ion channel functionality. Chronic administration of hERG1-blockers may be able to impair oncogenic progression in hERG1-expressing tumours.

Acknowledgements

First of all, I would like to express my deepest gratitude to my supervisors Dr. John Mitcheson and Professor John Challiss who have provided me with invaluable guidance and continuous support throughout this research project. Their expertise, patience and advice have enriched my experience and endowed me with the tools to pursue a scientific career.

I gratefully acknowledge the staff in the Department of Pharmacology and Toxicology, Mansoura University, Egypt for awarding me the scholarship, which gave me the opportunity to pursue my research at the University of Leicester.

I would like to thank everyone in the Department of Cell Physiology and Pharmacology at the University of Leicester, who supported me with a friendly chat, helpful advice and useful guidance. I would like to thank in particular: Raj. Mistry for his support with ligand binding assays, Steve Thomson for his help in cell patching, Dr. Sarah Nelson for her help in cell culture, Dr. Carl Nelson for his help in confocal imaging and Dr. Christine Pullar for her support and valuable advice regarding single cell migration experiments.

I must also acknowledge Dr. Dave Lodwick (Cardiovascular sciences, University of Leicester) for his guidance and support in molecular biology, Dr Salvador Macip (Department of Biochemistry, University of Leicester) and Roger Snowden (MRC Toxicology Unit, University of Leicester) for their help in flow cytometry and cell sorting and Dr. Lev Solyakov (MRC Toxicology Unit, University of Leicester) for his advice regarding Western blotting.

I would also like to thank members of my family: my father, my mother, Janet and Bassem. They have always supported me and loved me. Thanks for believing in me and for being always there for me. I am also indebted to my wife, Nariman, who encouraged me throughout the last four years. You chose to live in a foreign country that you hardly knew her language and sacrificed the company of family and friends to support me in every way you could. Thanks for giving birth to our kids, Mariam, Youssif and the forthcoming baby. They are the light and joy of my life. To them I dedicate this thesis.

List of abbreviations

4-AP	4-aminopyridine
AP	Action potential
ATCC	American type culture collection
ATP	Adenosine 5'-triphosphate
AVD	Apoptotic volume decrease
BK _{Ca}	Large conductance Ca ²⁺ -activated K ⁺ channels
CaM	Calmodulin
CaMKII	Calcium calmodulin kinase II
CAMs	Cell-cell adhesions molecules
CDK	Cyclin-dependent kinase
CHO	Chinese hamster ovary
CMV	Cytomegalovirus
cNBD	Cyclic nucleotide-binding domain
CO	Collagen
cRNA	Complementary RNA
C _T	Cycle threshold
DEPC	Diethylpyrocarbonate
DMEM	Dulbecco's modified Eagle's medium
DMSO	Dimethylsulphoxide
EAG	Ether-à-go-go gene
ECG	Electrocardiogram
ECM	Extracellular matrix
ELK	Ether-à-go-go like gene
ER	Endoplasmic reticulum
ERG	Ether-à-go-go related gene
ERK	Extracellular signal-regulated protein kinase

FA I-V	Fully-activated current-voltage
FAK	Focal adhesion kinase
FBS	Fetal bovine serum
FN	Fibronectin
GAPDH	Glyceraldehyde 3-phosphate dehydrogenase
GIRK	G protein-coupled inwardly-rectifying K ⁺ channels
HEK293	Human embryonic kidney 293
hERG	Human ether-à-go-go related gene
HIF-1	Hypoxia inducible factor-1
HRP	Horseradish peroxidase
IK _{Ca}	Intermediate conductance Ca ²⁺ -activated K ⁺ channels
I _{Kr}	Rapid component of cardiac delayed-rectifier potassium current
I-V	Current-voltage
K _{2P}	Two-pore domain K ⁺ channels
K _{ATP}	ATP-sensitive inwardly-rectifying K ⁺ channels
K _{Ca}	Ca ²⁺ -activated K ⁺ channels
K _D	Dissociation constant
K _{ir}	Inwardly-rectifying K ⁺ channels
K _v	Voltage-gated K ⁺ channels
LA	Laminin
LB	Luria-Bertani
LQTS	Long QT syndrome
MAPK	Mitogen-activated protein kinase
MinK	Minimum conductance potassium channel
MiRP1	MinK-related protein 1
MMP	Matrix metalloproteinase
MTT	Methylthiazolyldiphenyl-tetrazolium

NF- κ B	Nuclear factor- κ B
NTC	No template control
PAS	Per-arnt-sim
PCR	Polymerase chain reaction
ROS	Reactive oxygen species
RT	Reverse transcriptase
RVD	Regulatory volume decrease
SA	Surface area
SDF-1	Stromal cell-derived factor-1
SDS	Sodium dodecylsulfate
shRNA	Short hairpin RNA
siRNA	Small interfering RNA
SK _{Ca}	Small conductance Ca ²⁺ -activated K ⁺ channels
SQTS	Short QT syndrome
TASK	TWIK-related acid-sensitive K ⁺ channels
TdP	Torsades de points
TGF β	Transforming growth factor β
TM	Transmembrane
TNF α	Tumour necrosis factor α
TRH	Thyrotropin-releasing hormone
VC	Vector control
VEGF	Vascular endothelial growth factor
V _m	Membrane voltage
V _{REST}	Resting membrane potential
WT	Wild-type

Table of Contents

Title page.....	I
Abstract.....	II
Acknowledgements.....	III
List of abbreviations	IV
Contents.....	VII
Introduction	1
1.1 Ion channels.....	1
1.2 Potassium channels.....	2
1.2.1 Basic structure of K ⁺ channels	2
1.2.2 Classification of K ⁺ channels: structural and functional diversity	5
1.2.2.1 Inwardly rectifying K ⁺ (K _{ir}) channels	7
1.2.2.2 Ca ²⁺ -activated K ⁺ (K _{Ca}) channels	7
1.2.2.3 Two-pore domain K ⁺ (K _{2P}) channels	8
1.2.2.4 Voltage-gated K ⁺ (K _v) channels.....	8
1.3 hERG1 channels	9
1.3.1 Structure and gating kinetics of hERG1	9
1.3.2 Biophysical properties of hERG1 currents	13
1.3.3 Physiological roles of hERG1.....	15
1.3.4 hERG heterogeneity: hERG genes and isoforms.....	17
1.3.5 Auxiliary β -subunits associated with hERG1	21
1.3.6 Pharmacological modulators of hERG1 channel activity.....	21
1.3.6.1 hERG1 blockers	21
1.3.6.2 hERG1 activators	24
1.3.6.3 hERG1 trafficking modulators.....	24
1.4 Potassium channels and cancer.....	25
1.4.1 Self-sufficiency in growth signals	27
1.4.1.1 Regulation of membrane potential.....	29
1.4.1.2 Regulation of cell volume.....	30

1.4.1.3	Involvement in signalling pathways leading to proliferation	31
1.4.1.4	Limitations	32
1.4.2	Insensitivity to anti-growth signals	33
1.4.3	Evasion of apoptosis	34
1.4.4	Unlimited proliferation	36
1.4.5	Sustained angiogenesis	37
1.4.6	Tissue invasion and metastasis	38
1.4.6.1	Cell migration	38
1.4.6.2	Integrins	39
1.4.6.3	Integrins and cancer	41
1.4.6.4	K ⁺ channels and tumour cell migration	42
1.5	Limitation of studies on the contribution of K⁺ channels to tumorigenesis	46
1.6	Oncogenic potential of specific types of K⁺ channels	46
1.6.1	TWIK-related acid-sensitive K ⁺ channels (TASK-3, K _{2p} 9.1 or KCNK9).....	46
1.6.2	EAG	48
1.6.3	hERG1	51
1.6.3.1	Evidence for implication of hERG1 in cancer.....	51
1.6.3.2	hERG1 and tumour proliferation	55
1.6.3.3	The role of hERG1 in tumour cell migration and invasiveness.....	61
1.6.3.4	hERG1 and tumour angiogenesis	62
1.6.3.5	Interaction of hERG1 channels with integrins.....	63
1.6.3.6	Are hERG1 channels involved in tumour adaptation to hypoxia?	67
1.6.3.7	hERG1: a regulator of tumour apoptosis?	69
1.6.3.8	hERG1 expression in tumours as a prognostic indicator.....	70
1.6.3.9	Role of hERG1 isoforms in cancer	71
1.7	Thesis aims	73

Methods	74
2.1 Cell culture	74
2.1.1 Cell-lines and their maintenance.....	74
Wild-type (WT) and stably-transfected NIH-3T3 cell-lines.....	74
WT HEK-293 (WT-HEK) and HEK-hERG cells.....	75
2.1.2 Cell-freezing (cryopreservation).....	77
2.1.3 Recovery of frozen cells	77
2.2 Molecular biology	78
2.2.1 Preparation of DNA stocks	78
2.2.1.1 Bacterial transformation	78
2.2.1.2 Preparation of glycerol stocks of DNA.....	79
2.2.1.3 Recovery and purification of DNA.....	79
2.2.2 Site-specific DNA digestion	80
2.2.3 DNA extraction from agarose gels	81
2.2.4 Ligation of DNA fragments.....	81
2.2.5 DNA sequencing.....	82
2.3 Characterization of hERG1 channel properties by expression in	
<i>Xenopus</i> oocytes	82
2.3.1 Preparation of cRNA by <i>in vitro</i> transcription.....	83
2.3.2 Preparation of template DNA	83
2.3.3 cRNA synthesis.....	84
2.3.4 Recording of hERG1 currents expressed in <i>Xenopus</i> oocytes.....	84
2.4 Generation of stable cell-lines.....	86
2.4.1 DNA constructs.....	86
2.4.2 Transfection	86
2.4.3 Generation of a kill curve	87
2.4.4 Clonal selection.....	87
2.5 Screening of clones for hERG1 expression	88

2.5.1	Real-time reverse transcription (RT RT) PCR	88
2.5.1.1	RNA extraction	88
2.5.1.2	cDNA synthesis (reverse transcription)	89
2.5.1.3	Checking the efficiency of cDNA synthesis by polymerase chain reaction (PCR)	90
2.5.1.4	Quantification of relative hERG1 expression by real-time RT PCR.....	92
2.5.2	[³ H]dofetilide binding assay	95
2.5.2.1	Membrane preparation	96
2.5.2.2	[³ H]dofetilide saturation binding	97
2.5.2.3	[³ H]dofetilide displacement assay	98
2.5.2.4	Screening of transfected NIH-3T3 clones	99
2.5.3	Western blotting to analyze hERG1 protein expression.....	99
2.5.3.1	Preparation of total cell extracts	99
2.5.3.2	Lowry protein assay	100
2.5.3.3	hERG1 antibodies	100
2.5.3.4	Blotting	101
2.6	Migration assays	102
2.6.1	Scratch-wound assay.....	102
2.6.2	Analysis of migration of single-cells using time-lapse microscopy	104
2.6.2.1	Analysis of cell morphology and migration parameters.....	105
2.7	Analysis of β1-integrin, β-actin and vinculin expression levels on culture plasticware and fibronectin by Western blotting.....	107
2.8	Immunocytochemistry	108
2.8.1	Vinculin and actin double-staining	108
2.9	Proliferation assays	109
2.9.1	Saturation-density assay	109
2.9.2	MTT proliferation assay	109
2.10	Statistical analysis of data.....	111

Chapter 3.....	112
Investigating the effects of extracellular matrix on the transforming properties of NIH-3T3 cells stably expressing hERG1.....	112
3.1 Introduction	112
3.2 Results.....	114
3.2.1 hERG1 expression in NIH-3T3 cells allow over-growth and increased post-confluent cell density	114
3.2.2 hERG1 expression in NIH-3T3 cells enhances cell migration.....	116
3.2.3 Does ECM-mediated signalling influence the over-growth capacity of hERG1-expressing cells?	118
3.2.4 Effect of ECM adhesion on morphology and migration properties of NIH-3T3 cells expressing hERG1	122
3.2.4.1 Tissue culture plasticware.....	123
3.2.4.2 Migration of hERG1-expressing cells on collagen-1.....	125
3.2.4.3 Migration of hERG1-expressing cells on laminin-1	129
3.2.4.4 Migration of hERG1-expressing cells on fibronectin.....	132
3.2.5 Do hERG1-expressing cells exhibit altered levels of β 1-integrin, vinculin or actin proteins on adhesion to fibronectin?.....	135
3.2.6 Does adhesion to fibronectin induce cytoskeletal modulation in hERG1-expressing cells?	140
3.2.7 Does modulation of hERG1 function and/or cell-surface expression influence the migration of hERG1-expressing cells on fibronectin?	141
3.2.7.1 Effect of high $[K^+]_o$ and the hERG1 channel activator ICA-105574 on fibronectin-dependent cell migration in hERG1-expressing cells.....	144
3.2.7.2 Effect of hERG1 trafficking inhibitors on fibronectin-dependent migration of hERG1-expressing cells.....	150
3.2.7.3 Effect of acute and chronic hERG1 current inhibition on fibronectin-dependent migration of hERG1-expressing cells.....	151

3.3 Discussion	155
3.3.1 hERG1-expressing cells exhibit changes in shape, spreading and migratory phenotype on adhesion to fibronectin and laminin-1.....	155
3.3.2 hERG1-expressing cells exhibit decreased vinculin expression on adhesion to fibronectin.....	157
3.3.3 hERG1-expressing cells exhibit alterations in cytoskeletal organization and focal adhesion formation following adhesion to fibronectin.....	158
3.3.4 hERG1-expressing cells display an integrin-dependent transformed phenotype	159
3.3.5 Is hERG1 current required for integrin-mediated changes in the transforming behaviour of hERG1-expressing cells?.....	161
 Chapter 4.....	 164
K⁺ channel function is required for the transforming potential of hERG1	164
4.1 Introduction	164
4.2 Results.....	167
4.2.1 Is the biological activity of hERG1 channel blockers lost under cell culture conditions?	167
4.2.2 Do G628S hERG1 and A561V hERG1 exhibit a dominant-negative suppression of hERG1 current?	172
4.2.3 Generation of stable, WT and mutant hERG1 transfectants.....	176
4.2.3.1 Optimizing real-time reverse transcription PCR conditions for screening of NIH-3T3 clones	176
4.2.3.2 [³ H]dofetilide binding assay	183
4.2.3.3 Quantification of hERG1 expression in transfected clones	185
4.2.3.4 Detection of hERG1 expression in mutant hERG1 transfectants using Western blotting	186

4.2.4	Do G628S hERG1 and A561V hERG1 transfectants exhibit a transformed phenotype?	190
4.3	Discussion	199
4.3.1	Biological activity of hERG1 channel blockers is not lost under culture conditions.....	199
4.3.2	G628S hERG1 and A561V hERG1 exhibit dominant-negative suppression on the WT hERG1 current.....	200
4.3.3	Differences between hERG1 mRNA and protein levels in screened clones ..	203
4.3.4	The link between hERG1 channel conduction and transformation	203
4.3.5	Why are high concentrations of hERG1 inhibitors required to block cell transformation?	208
Chapter 5		210
Does transient transfection of hERG1 and the splice-variant hERG1b induce cellular transformation?		210
5.1	Introduction	210
5.2	Methods	213
5.2.1	Generation of bicistronic cDNA constructs encoding hERG1 and hERG1b ..	213
5.2.2	Characterization of hERG currents expressed by C1 and C2 constructs by voltage clamp recording	220
5.2.3	Transient transfection	220
5.2.4	Flow cytometry analysis and fluorescence-activated cell sorting (FACS)	221
5.2.5	Detection of hERG1 expression by measurement of membrane potential changes	222
5.2.6	Cell culture-based assays.....	223
5.3	Results.....	224
5.3.1	Functional expression of hERG1 and hERG1b in <i>Xenopus</i> oocytes	224

5.3.2	Functional expression of hERG1, hERG1-pIRES-hERG1b (C1) and hERG1-pCMV-hERG1b (C2) in mammalian cells	229
5.3.3	Detection of hERG1 and hERG1b expression levels in NIH-3T3 cells by Western blotting	231
5.3.4	Optimization of transient transfection conditions	235
5.3.5	Membrane potential changes in a sorted cell population transiently transfected with hERG1	237
5.3.6	Effect of transient expression of hERG1b, hERG1 or hERG1/1b on cell migration, proliferation and overgrowth.....	240
5.4	Discussion	244
5.4.1	Characterization of hERG1-pIRES-hERG1b (C1) and hERG1-pCMV-hERG1b (C2)	244
5.4.2	Transient expression of hERG1 does not affect NIH-3T3 cell migration or growth properties	246
5.4.3	Transient expression of hERG1 and hERG1b enhances NIH-3T3 cell proliferation	247
Chapter 6	249
	hERG1 expression does not affect survival of Chinese hamster ovary cells at low oxygen tension	249
6.1	Introduction	249
6.2	Methods	252
6.2.1	CHO-VC and CHO-hERG cells	252
6.2.2	Exposure of CHO cells to low oxygen tension.....	252
6.2.3	MTT viability assay	253
6.2.4	Analysis of apoptosis and cell cycle distribution by flow cytometry	253
6.2.5	Flow cytometry acquisition parameters and data analysis.....	254

6.3 Results and Discussion	256
6.3.1 hERG1 expression in CHO-hERG cells	256
6.3.2 Response of CHO-VC and CHO-hERG cells to 5% oxygen levels	256
6.3.3 Response of CHO-VC and CHO-hERG cells to severe hypoxia (<1% O ₂) ..	258
Chapter 7.....	264
Concluding Discussion	264
7.1 Technical considerations.....	265
7.2 Extracellular matrix-dependent signalling is important for hERG1-mediated oncogenic effects	267
7.3 hERG1 channel conductance and cell-surface localization are necessary for hERG1-induced cell transformation.....	270
7.4 Co-expression of hERG1 and hERG1b enhances cell proliferation	274
7.5 What is the potential contribution of hERG1 to tumour progression?	275
Bibliography.....	281

Introduction

1.1 Ion channels

Ion channels are transmembrane proteins, embedded in the phospholipid bilayer of the plasma membrane (or organellar membranes) of cells, which passively allow the flow of ions in and out of the cell down their electrochemical gradient. Ion channels regulate ion flux in response to specific signalling stimuli that trigger the channels to switch between an “open” (in presence of the gating stimulus) and “closed” (in absence of the gating stimulus) conformational states. Some ion channel types may also transit into an additional non-conducting “inactivated or desensitized” state on sustained activation. Most ion channels are highly selective as they allow the conduction of certain ion species and exclude others and therefore, they can be classified, according to the species of ion(s) that selectively pass through them, into potassium, sodium, calcium, proton, chloride and non-selective cation channels.

In addition to their physiological roles in maintaining normal cellular ion homeostasis and controlling the bioelectrical properties of the cell membrane, it has been shown that dysregulation of ion channel function is important in many pathological diseases (channelopathies) (Kass, 2005, Sanguinetti, 2010) and in cancer (Kunzelmann, 2005, Schonherr, 2005, Felipe *et al.*, 2006, Prevarskaya *et al.*, 2010), establishing them as potential diagnostic markers, as well as therapeutic targets. Interestingly, some studies have reported that some ion channel actions can occur independently of ion conduction and may be mediated via a catalytic activity of specific ion channel domains, which directly activate effector enzymes, or through conformational coupling with other transmembrane proteins to modulate intracellular signal transduction pathways (Kaczmarek, 2006).

1.2 Potassium channels

The potassium channel gene family is the largest and the most diverse of the ion channel families creating a “superfamily” of ion channels. These channels are highly selective for K^+ over other cations. The normal physiological K^+ ion concentration in blood is around 4.5 mM relative to ~ 140 mM inside the cell. Upon activation, these channels open to allow the movement of K^+ ions down their electrochemical gradient to exit the cells, which gives rise to a hyperpolarizing current. Conversely, inhibition of K^+ channel function tends to result in membrane depolarization.

K^+ channels fulfil many functions in both excitable and non-excitable cells. In excitable cells, they help set the resting membrane potential, repolarize the plasma membrane after action potential firing, and thus regulate the frequency and duration of action potentials. Moreover, K^+ channels may serve other important physiological roles in both excitable and non-excitable cells, such as the regulation of osmolarity and electrolyte balance, cell size, Ca^{2+} signalling, secretion, lymphocyte activation, migration, differentiation, proliferation and apoptosis (O'Grady *et al.*, 2005).

1.2.1 Basic structure of K^+ channels

Much of our understanding of K^+ channel structure comes from the crystallographic studies of bacterial and mammalian K^+ channels and structure-function studies on Shaker K^+ channels. Moreover, computational, mutational and electrophysiological studies have also added to our understanding of the mechanisms of ion permeation.

All K^+ channels from prokaryotic and eukaryotic origins have a similar pore structure, as evidenced by a highly conserved amino acid “signature” sequence that lines the selectivity filter

of their pores and similar pharmacological properties (Schrempf *et al.*, 1995, MacKinnon *et al.*, 1998). The first crystal structure of a bacterial K⁺ channel, KcsA from *Streptomyces lividans*, was solved in 1998 (Doyle *et al.*, 1998). Despite its simple topology, the KcsA channel closely resembles eukaryotic K⁺ channels in terms of ion permeation, selectivity to K⁺ ions and block by scorpion toxins (MacKinnon *et al.*, 1998, LeMasurier *et al.*, 2001), which established it as a useful structural model to study ion permeation in eukaryotic K⁺ channels.

The crystal structure of the KcsA channel revealed that this K⁺ channel consists of four identical subunits that form an inverted tepee structure surrounding a central ion conduction pathway, which extends across (spans) the cell membrane. Each subunit contains two transmembrane helices (denoted M1 and M2). The inner helices (M2) from each subunit cross over close to one another at the cytoplasmic side of the membrane to form an intracellular activation gate. This crossing of inner helices prevents ion conduction, which suggested that the KcsA channel had been crystallized in its closed state (Fig. 1.1). On the extracellular side, the M1 and M2 helices of each subunit are separated by a linker region, the re-entrant P- loop, which forms a narrow selectivity filter lined by a specific signature sequence of amino acids (Gly-Tyr-Gly). The carbonyl oxygen atoms of this peptide coordinate K⁺ ions and help them to shed their hydration shell. A water-filled cavity, the inner vestibule, exists between the selectivity filter and the activation gate. This cavity is lined by hydrophobic amino acids, which prevent the contact of K⁺ ions with the pore allowing a fast ion conduction rate (Doyle *et al.*, 1998, Choe, 2002).

The mechanism of K⁺ channel pore opening was elucidated when the prokaryotic calcium-activated MthK (Jiang *et al.*, 2002a), bacterial voltage-gated K_vAP (Jiang *et al.*, 2003a) and mammalian voltage-gated Kv1.2 (Long *et al.*, 2005) K⁺ channels were crystallized in the open

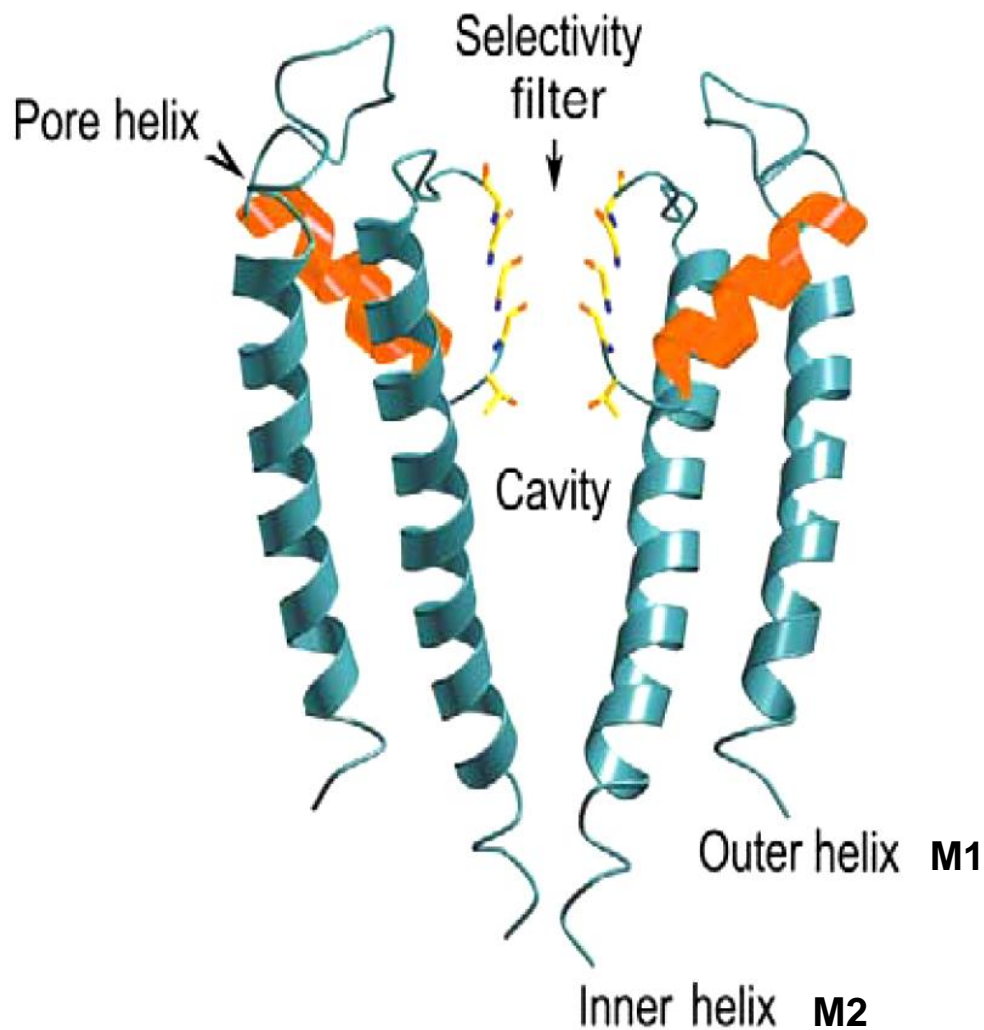


Figure 1.1 A cartoon of the crystal structure of KcsA K⁺ channel in its closed conformation as viewed from the side. Only two subunits are shown for clarity. The inner helices of the four subunits forming the channel cross over on the cytoplasmic side of the cell membrane closing an intracellular gate to prevent ion conduction. The positions of the selectivity filter, central cavity and pore helix are marked (adapted from Gulbis *et al.*, 2004).

state. In this conformation, the cytoplasmic ends of inner helices splay wide and bend, thereby opening the activation gate to the cytoplasm to allow the passage of K^+ ions through the pore.

1.2.2 Classification of K^+ channels: structural and functional diversity

There are a large number of K^+ channel types, which help support their varied and numerous physiological functions. Structurally, K^+ channels vary in the number of transmembrane domains per subunit. This allows their division into three main groups that contain two (2TM), four (4TM) or six (6TM) transmembrane helices in each monomer subunit. However, some K^+ channels do not conform to this classification and may have 7 or 8 TM domains (Fig. 1.2).

Another popular means of classification is based on how K^+ channels respond to intracellular signals. K^+ channels open (activate) in response to a wide variety of stimuli, such as changes in membrane potential or a change in the concentration of intracellular modulating molecules (e.g. intracellular Ca^{2+} [Ca^{2+}_i], adenosine 5'-triphosphate (ATP), G proteins, polyamines, pH). The K^+ channel superfamily can be broadly classified into four main types according to their mode of activation: inwardly-rectifying K^+ channels (K_{ir}), two-pore domain K^+ channels (K_{2P} , also known as leak K^+ channels), Ca^{2+} -activated K^+ channels (K_{Ca}) and voltage-gated K^+ channels (K_v) (Korn *et al.*, 2005).

There are many aspects of K^+ channel diversity. First, within each category, these channels also vary in their gating kinetics, activating stimulus threshold and single-channel conductances. Moreover, it has been shown that, under physiological conditions, the pore-forming α -subunits of one channel can form functional heterotetrameric complexes with different α -subunits from the same or a related family producing channels with different biophysical properties.

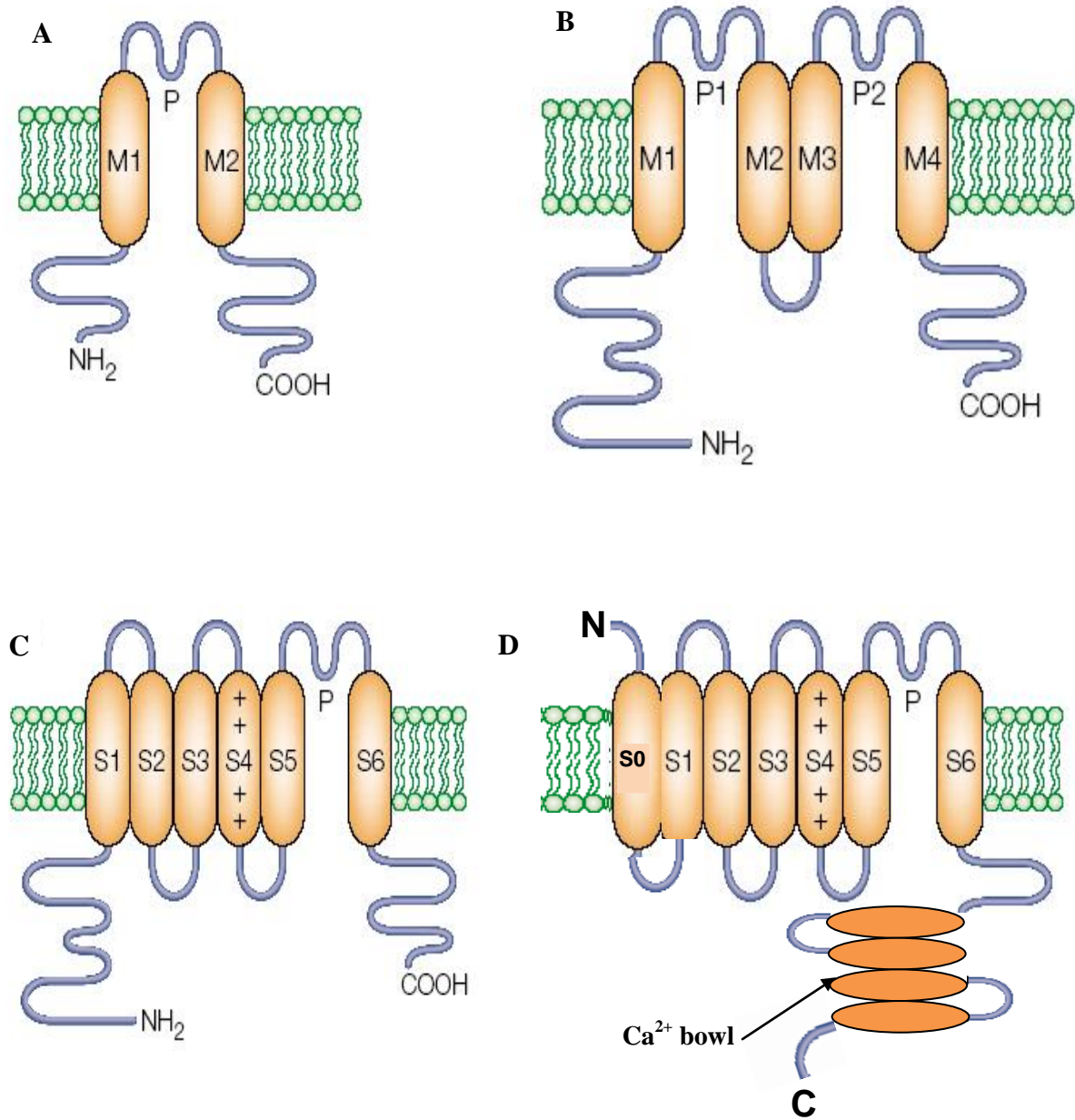


Figure 1.2 Schematic illustration of K⁺ channels topology. K⁺ channels can be classified according to the number of transmembrane (TM) segments per subunit into 2-TM (A, e.g. K_{ir} channels), 4-TM (B, e.g. K_{2P} channels) and 6-TM (C, e.g. K_v channels). In each case, the amino (N-) and carboxy (C-) termini are located intracellularly. BK_{Ca} channels (D) contain 7-TM per subunit. Its N-terminus is located extracellularly and its C-terminus contains a binding site for Ca²⁺ (Ca²⁺ bowl). P denotes the pore region and positive charges indicate the voltage sensor (modified from Choe, 2002).

Finally, K^+ channel diversity is further increased through the regulation of the pore-forming α subunits by various auxiliary β -subunits (Li *et al.*, 2006; O'Grady *et al.*, 2005).

1.2.2.1 Inwardly rectifying K^+ (K_{ir}) channels

K_{ir} channels have two transmembrane spanning segments per α -subunit. They activate in response to membrane hyperpolarization and moderately elevated external K^+ levels. They are so-called as they exhibit an inward rectification property, which means K^+ ions are conducted more efficiently in the inward direction. Although they lack a voltage sensor, this inward rectification is voltage-dependent. That is, they pass a large inward current upon hyperpolarization and a small current at more depolarized potentials, which is caused by voltage-dependent block of outward currents by endogenous Mg^{2+} ions and polyamines. K_{ir} channels comprise 7 subfamilies ($K_{ir1.x}$ - $K_{ir7.x}$), which include the G protein-regulated $K_{ir3.x}$ (GIRK) and the ATP-sensitive $K_{ir6.x}$ (K_{ATP}) sub-families (Nichols *et al.*, 1997).

1.2.2.2 Ca^{2+} -activated K^+ (K_{Ca}) channels

K_{Ca} channels are activated by increases in $[Ca^{2+}]_i$. They are sub-categorized into three groups according to their single channel conductance namely: small (SK), intermediate (IK) and large (BK) -conductance Ca^{2+} -activated K^+ channels. Activation of IK_{Ca} and SK_{Ca} channels is weakly voltage-dependent. On the other hand, BK_{Ca} channels are regulated by changes in membrane voltage. Structurally, all K_{Ca} channels contain 6 transmembrane (6TM) helices per subunit (S1-S6), except the BK_{Ca} channels that possess an additional transmembrane domain (S0) at their *N*-terminus. The Ca^{2+} sensitivity of these channels is conferred by the presence of a Ca^{2+} 'bowl' in the *C*-terminal of BK_{Ca} , and a calmodulin (CaM) binding site in the *C*-terminal of IK_{Ca} and SK_{Ca} channels (Berkefeld *et al.*, 2010).

1.2.2.3 Two-pore domain K⁺ (K_{2P}) channels

K_{2P} channels have a unique structure where each α -subunit possesses two pore-forming domains and four transmembrane helices and only two subunits are required to form a functional channel. K_{2P} channels are regarded as leak or background K⁺ channels, as they are voltage-independent and are open at resting membrane potentials. However, their activity can be modulated by other factors, such as polyunsaturated fatty acids, pH and oxygen tension (Enyedi *et al.*, 2010).

1.2.2.4 Voltage-gated K⁺ (K_v) channels

K_v channels are normally closed at resting membrane potential and open in response to membrane depolarization to potentials more positive than the resting membrane potential (V_{REST}). The functional channel is a tetramer, with each subunit possessing 6 transmembrane domains (denoted S1-S6) and large N- and C-termini within the cytoplasm. The S5/S6 helices and P-loop form the pore domain and the selectivity filter of the channel (analogous to M1 and M2 domains described in KcsA channels). The S4 domain contains positively charged residues and the whole S1-S4 domain act as a voltage-sensor for the channel coupling changes in the transmembrane electric field to the channel pore.

There are 12 K_v subfamilies denoted K_v1.x- K_v12.x. These comprise K_v1.x-4.x (mammalian homologues of *Shaker*, *Shab*, *Shaw* and *Shal* channels respectively, originally identified in *Drosophila*) and K_v7.x (also known as KCNQ) channels. K_v5, 6, 8, and 9 are silent channels that do not conduct a functional current. However, they can assemble with other K_v subunits to form conductive channels with altered current properties. K_v10.x (ether-à-go-go (EAG)), K_v11.x (EAG-related gene (ERG)) and K_v12.x (EAG-like gene (ELK)) are three closely related K_v sub-families and together they comprise the EAG family of K_v channels. A defining feature

of members of this family is the presence of an 135 amino acid EAG domain at the *N*-terminus that folds to form a Per-Arnt-Sim (PAS) domain (Morais Cabral *et al.*, 1998, Vilorio *et al.*, 2000). Human ether-à-go-go-related gene 1 (hERG1) K⁺ channels are the focus of this Thesis.

1.3 hERG1 channels

1.3.1 Structure and gating kinetics of hERG1

The identification and cloning of the *hERG1* gene was first reported by Warmke *et al.* (1994), who used a mouse homologue of *Drosophila* EAG channels to screen a human hippocampal cDNA library. The authors also showed that hERG1 proteins have the typical architecture of K_v channels (described above), comprising 6 transmembrane-spanning helices per subunit and a positively charged S4 domain (Fig. 1.3A) (Warmke *et al.*, 1994). Expression of hERG1 channels (also known as hERG1a and K_v11.1) in a *Xenopus* oocyte expression system elicited a current with biophysical properties similar to the cardiac delayed-rectifier potassium current I_{Kr} and hERG1 was identified as the pore-forming α -subunit that conducts I_{Kr} (Sanguinetti *et al.*, 1995, Trudeau *et al.*, 1995).

Each hERG1 subunit has a large intracellular *N*-terminus that contains a PAS domain and a large *C*-terminus with a cyclic nucleotide-binding domain (cNBD) (Morais Cabral *et al.*, 1998). Both the *N*- and *C*-termini are located intracellularly and may be targets of regulatory pathways. The *N*-terminal domain has been shown to be important for hERG1 deactivation (see below), whereas the cNBD domain appears to have a minor effect on hERG1 gating (Cui *et al.*, 2000). The physiological role of cNBD in hERG1 is still elusive. Cyclic AMP has been shown to bind with low affinity to isolated cNBD of hERG1 channels (Brelidze *et al.*, 2009).

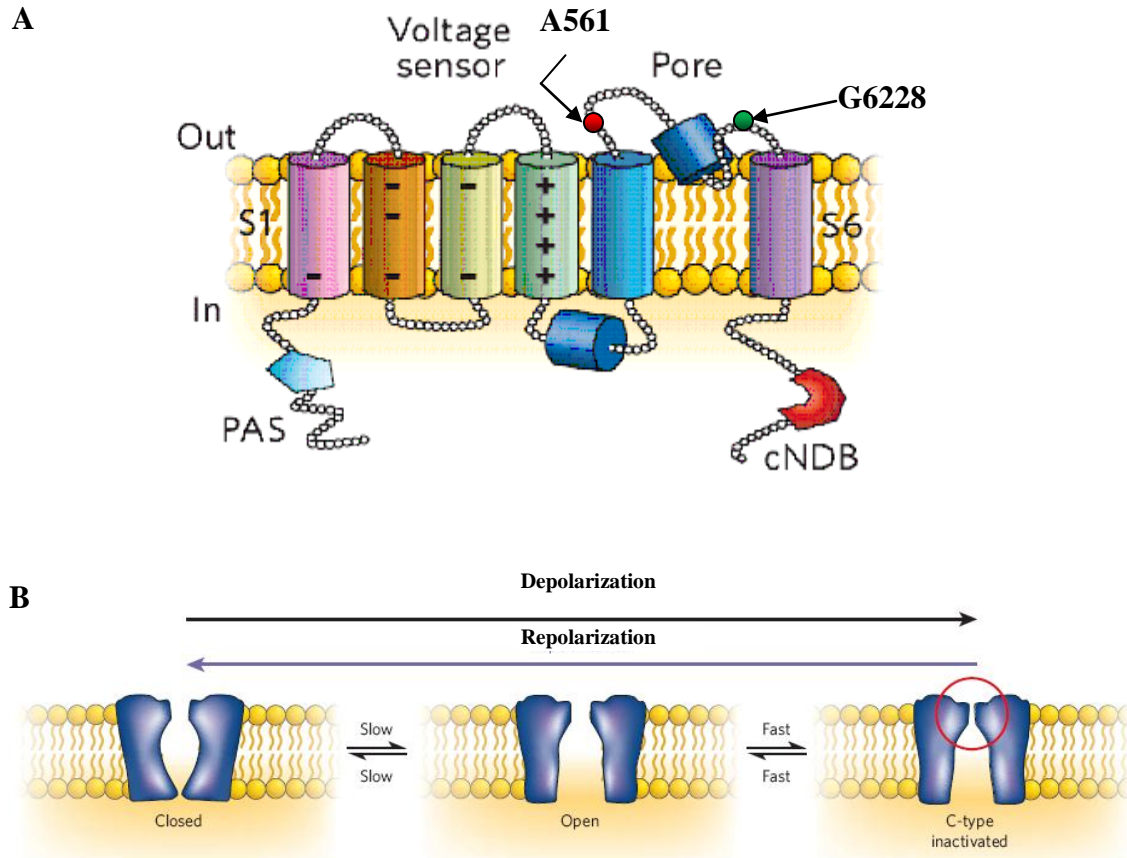


Figure 1.3 Structure and gating of hERG1. **A.** A diagrammatic representation of a single hERG1 protein α - subunit containing six helical transmembrane domains, S1–S6. The voltage sensor, S4, contains multiple positive charges. The locations of the N-terminal Per-Arnt-Sim (PAS) domain and the C-terminal cyclic-nucleotide-binding domain (cNBD) are marked. Also, the relative positions of A561 and G628 residues are shown. **B.** A simplified diagram showing gating of hERG1. hERG1 may exist in one of 3 conformations: closed, open or inactive. Activation occurs via an opening of an intracellular cytoplasmic gate while inactivation is mediated via closure of an extracellular inactivation gate (circled in red) (taken from Sanguinetti *et al.*, 2006).

However, high concentrations of cyclic AMP failed to modulate hERG1 current when applied to inside-out patches (Brelidze *et al.*, 2009). On the other hand, the cNBD domain may be important for post-translational processing and proper hERG1 channel trafficking (Akhavan *et al.*, 2005).

The hERG1 channel has unusual gating kinetics, which include slow activation and deactivation, but rapid voltage-dependent inactivation and recovery from inactivation (Fig.1.3B, Wang *et al.*, 1997b). hERG1 channels may exist in one of 3 main conformational states: closed, open and inactive (Trudeau *et al.*, 1995). In the closed conformation, the four inner S6 domains lining the channel pore are tilted and bundle together near the cytoplasmic interface forming a narrow aperture: an intracellular cytoplasmic gate, which prevents passage of K⁺ ions. Interactions between specific residues in the S4-S5 linker and C-terminal end of S6 stabilize the channel in its closed state (Tristani-Firouzi *et al.*, 2002, Ferrer *et al.*, 2006). Activation involves an outward movement of the voltage-sensor caused by changes in the transmembrane electrical field, which in turn causes the opening of the activation gate by outward splaying and kinking of the S6 domains at a gating hinge (Jiang *et al.*, 2002b, Yifrach *et al.*, 2002, Jiang *et al.*, 2003b). The voltage-sensor is coupled to the activation gate through the S4-S5 linker, which acts as a mechanical lever to transduce voltage-sensor movement to the activation gate. Upon membrane repolarization, the S4 helix moves inward, which forces the S4-S5 linker against the C-terminal end of S6, closing the activation gate (Ferrer *et al.*, 2006). The slow activation of the hERG1 channels may be due to the slow movement of the S4 domains on depolarization (Smith *et al.*, 2002b, Piper *et al.*, 2003), which may be attributed to electrostatic interactions between negatively-charged residues in the S1, S2 and S3 domains and positively-charged residues in S4 (Zhang *et al.*, 2005).

The *N*-terminus (residues 1-390) of hERG1 plays an important role in the deactivation process. Deletion of the whole *N*-terminus (Schonherr *et al.*, 1996, Spector *et al.*, 1996), EAG domain (Morais Cabral *et al.*, 1998), or just the first 16 residues of the *N*-terminus (Wang *et al.*, 1998) resulted in channels having much faster deactivation kinetics. Moreover, the normal slow deactivation gating of hERG1 channels was recovered by adding a soluble peptide that corresponds to residues 1-16 of the *N*-terminus-truncated channel (Wang *et al.*, 2000). Recently, NMR spectroscopic analysis of residues 1-26 (NT1-26) of hERG1 showed that this structural domain has a positively-charged surface. Neutralization of basic residues on this face resulted in an acceleration of deactivation mimicking the effect of *N*-terminus deletion. Moreover, charge reversal mutations of acidic residues on cNBD can also accelerate channel closure (Muskett *et al.*, 2010). Based on these findings, the authors have suggested that the slow deactivation of hERG1 is due to binding of NT1-26 to the cNBD, thereby stabilizing the open state (Muskett *et al.*, 2010).

Inactivation is a non-conducting state that channels can transition to on sustained membrane depolarization. It involves the closure of an extracellular inactivation gate, elicited by subtle conformational changes of the selectivity filter that lead to constriction of the conduction pathway and inhibition of ion permeation, and is similar to C-type ‘collapse of the pore’ inactivation of Shaker K⁺ channels (Schonherr *et al.*, 1996, Smith *et al.*, 1996). Recovery from inactivation refers to the opening of the inactivation gate. It has been suggested that the S4 domain may also act as a voltage-sensor for inactivation gating (Smith *et al.*, 2002b). These authors showed that voltage-dependent changes in fluorescence, seen as a result of movement of fluorescent probes attached to residues in the S4 domain, consisted of a slow and a rapid component whose kinetics corresponded to activation and inactivation gating, respectively (Smith *et al.*, 2002b). In another study, alanine-scanning mutagenesis approach was used to

identify residues in the S4 domain that are important for activation and inactivation gating (Piper *et al.*, 2005). While mutations that affect activation are spread throughout S4, mutations that affect inactivation are localized to a distinct face of S4, suggesting that S4 contributes to both processes albeit via different regions (Piper *et al.*, 2005). On the other hand, other studies suggest that the voltage-sensor for hERG1 inactivation may be different from that for activation and a role for the pore and S5-P domains in voltage-sensitivity of inactivation has been postulated. In agreement with this, S620T hERG1 is a pore mutant that does not inactivate, but can readily activate (Ficker *et al.*, 1998). Moreover, manipulation of charges on the S5-P domain alters the voltage-dependence of hERG1 inactivation while having minimal effect on activation (Clarke *et al.*, 2006).

1.3.2 Biophysical properties of hERG1 currents

The unique gating kinetics displayed by hERG1 channels gives rise to currents with distinctive biophysical properties. At negative membrane potentials (below -50 mV), hERG1 channels are closed and deactivated. At weakly depolarized membrane potential (below 0 mV), the channels activate very slowly reaching steady-state after a few seconds (Wang *et al.*, 1997b). Stronger depolarizations produce only a small outward current as the channels rapidly inactivate reducing overall channel conductance at positive potentials. This results in a bell-shaped current (I) – voltage (V) relationship (Fig. 1.4B) for hERG1 currents measured at the end of the depolarizing pulse (Fig. 1.4A). On repolarization, the channels pass a large tail current, despite the decrease in the electrochemical driving force for the outward flux of K^+ , which is caused by a rapid recovery from inactivation and slower deactivation rates. Collectively, the rapid voltage-dependent inactivation of hERG1 channels leads to strong inward rectification behaviour, that is, when fully activated, they pass little current in the outward direction, but

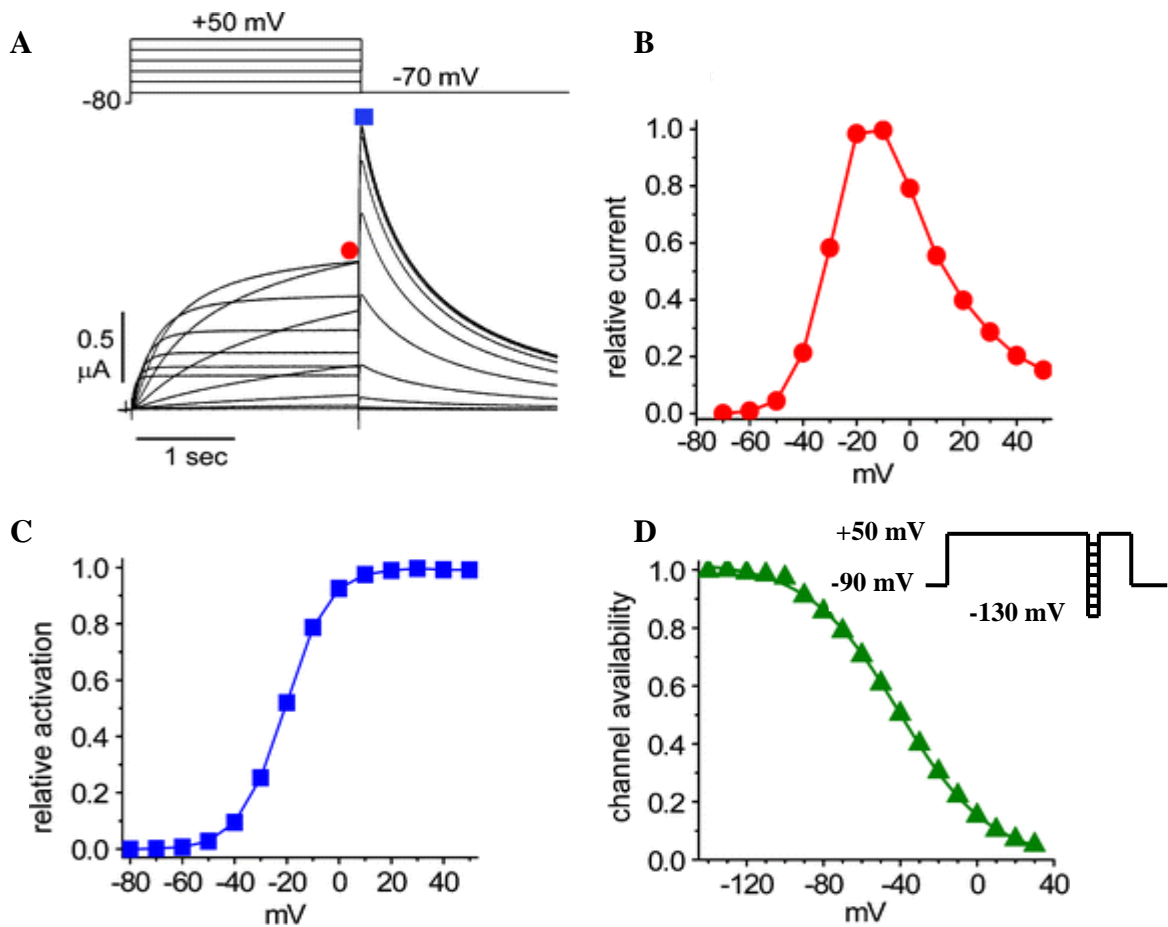


Figure 1.4 Biophysical properties of hERG1 channel currents. **A, top.** Voltage clamp I-V protocol. From a holding potential of -80 mV, a family of test potentials ranging from -70 to +50 mV are applied and tail currents elicited by stepping to -70 mV after each test potential. **A, bottom.** hERG1 currents obtained using the I-V protocol. **B.** Current–voltage (I–V) relationship for hERG1 currents measured at the end of depolarizing pulses (indicated by red circle in **A**). The decrease in current amplitude observed at potentials > 0 mV is due to fast inactivation of hERG channels. **C.** Voltage dependence of hERG1 current activation. The peak of tail currents measured at -70 mV (indicated by blue square in **A**) are normalized to the largest peak tail current amplitude and plotted against the preceding test potential. **D.** Voltage dependence of hERG1 current inactivation. Expressed hERG1 channels are allowed to fully activate by a strong depolarizing pulse then tail currents are measured following brief pulses to a range of test potentials (current traces are not shown). At positive potentials, hERG1 channels inactivate and thereby the channel availability is decreased (taken from Sanguinetti, 2010).

significant current in the inward direction (Smith *et al.*, 1996). The inward rectification is due to voltage-dependent inactivation and is distinct from that of K_{ir} channels (Sanguinetti *et al.*, 1995, Schonherr *et al.*, 1996, Smith *et al.*, 1996, Spector *et al.*, 1996).

The amplitude of peak tail current measured at a certain membrane potential reflects the number of hERG1 channels activated by the preceding depolarizing pulse, and the direction of tail current is determined by the electrochemical driving-force. Based on this, peak tail current (I)-voltage (V) curves can be used to determine the voltage-dependence of activation (Fig. 1.4A, C). To study the voltage-dependence of hERG1 inactivation, hERG1 channels are fully activated by a strong depolarizing pulse (e.g. to +40-50 mV) and then the membrane potential is stepped briefly to a range of test voltages. The peak instantaneous tail current with a third pulse at + 40 mV is measured and the I-V curve plotted. In this case, the tail current amplitude at any potential represents the number of channels that are still active (“available”) and have not undergone inactivation: this is also sometimes referred to as the current-availability relationship (Fig. 1.4D). The voltages required for half-activation and half-inactivation are around -20 and -85 mV, respectively (Schonherr *et al.*, 1996, Smith *et al.*, 1996, Spector *et al.*, 1996).

1.3.3 Physiological roles of hERG1

hERG1 channels are expressed in the heart, where their roles are well established. hERG1 channels are the pore-forming channel subunits of the rapid component of the cardiac delayed-rectifier potassium current I_{Kr} , responsible for termination of the plateau phase of the action potential (AP) (Sanguinetti *et al.*, 1995, Trudeau *et al.*, 1995). The unique kinetics displayed by I_{Kr} current (see above) account for its importance in cardiac AP repolarization. During the plateau phase of AP (phase II), I_{Kr} slowly activates, but rapidly inactivates producing only a small outward current which prevents repolarization of AP occurring at too faster rate.

However, at the end of phase II, values of ventricular membrane potential are appropriate for recovery from inactivation and I_{Kr} increases. Since hERG1 channels deactivate very slowly, I_{Kr} exerts a strong repolarizing influence that brings potentials into range of I_{K1} (inwardly-rectifying K^+ current), which is responsible for final rapid phase of repolarization (Hancox *et al.*, 1998).

Loss of function mutations in hERG1 (Curran *et al.*, 1995), or blockade of hERG1 activity by a variety of drugs (Lagrutta *et al.*, 2008) can induce long QT syndrome (LQTS), which is associated with an increased risk of a cardiac arrhythmia known as Torsades de points (TdP). ECG traces of patients with LQTS show a characteristic prolonged QT interval, which is the time between the initial depolarization and final repolarization phases of the ventricular AP. Mechanisms that mediate the genetic loss of hERG1 channel function include (i) disruption of protein folding or assembly (defective synthesis), (ii) defective protein trafficking, (iii) the generation of non-functional channels and (iv) changes of channel gating (that decrease channel open probability (P_o)) (Zhou *et al.*, 1998a, Anderson *et al.*, 2006, Perrin *et al.*, 2008). Conversely, gain-of-function mutations of hERG1 can lead to short QT syndrome (SQTS), a cardiac condition associated with atrial and ventricular arrhythmias (Brugada *et al.*, 2004). An example is the N588K hERG1 mutation located in the S5-P linker region, which disrupts hERG1 channel inactivation, leading to an enhancement of I_{Kr} current and an early repolarization of the ventricular AP (McPate *et al.*, 2005).

Cardiac hERG1 currents have also been shown to play a crucial anti-arrhythmic role by suppressing the propagation of premature beats, as they pass a large transient outward current that opposes depolarization elicited by premature stimuli (Lu *et al.*, 2001).

ERG1 channels in many different species are also expressed in several non-cardiac tissues, such as neuronal tissues (Guasti *et al.*, 2005), smooth muscle (Akbarali *et al.*, 1999), pancreatic β -cells (Rosati *et al.*, 2000), lactotrophs (Bauer *et al.*, 2003), chromaffin cells (Gullo *et al.*, 2003) and carotid body (Overholt *et al.*, 2000). In these tissues, ERG1 channels contribute to maintenance of resting membrane potential and regulation of membrane excitability.

ERG1 is abundantly expressed in the CNS in the olfactory bulb, cerebral cortex, hypothalamus, hippocampus, basal ganglia, cerebellum and peripheral sympathetic ganglia (Shi *et al.*, 1997, Papa *et al.*, 2003). ERG1 channels have been shown to be important for spike frequency adaptation (Chiesa *et al.*, 1997, Sacco *et al.*, 2003, Pessia *et al.*, 2008), suggesting a critical role for ERG in regulation of neuronal excitability. Indeed, it has been suggested that ERG1 channels may be implicated in the aetiology of schizophrenia (Huffaker *et al.*, 2009) and epilepsy (Johnson *et al.*, 2009, Omichi *et al.*, 2009). Furthermore, ERG1 channels are involved in regulating smooth muscle contractile responses (Akbarali *et al.*, 1999, Ohya *et al.*, 2002, Farrelly *et al.*, 2003, Mewe *et al.*, 2008), oxygen-sensing (Overholt *et al.*, 2000) and neurotransmitter and hormone secretion (Chiesa *et al.*, 1997, Bauer, 1998, Akbarali *et al.*, 1999, Overholt *et al.*, 2000, Rosati *et al.*, 2000, Bauer *et al.*, 2003, Farrelly *et al.*, 2003, Gullo *et al.*, 2003, Guasti *et al.*, 2005).

1.3.4 hERG heterogeneity: hERG genes and isoforms

Three different *hERG* genes have been identified: *hERG1* (encoding K_v11.1), *hERG2* (encoding K_v11.2) and *hERG3* (encoding K_v11.3). The expression of *ERG2* and *ERG3* gene products has been shown to be restricted to the nervous system (Shi *et al.*, 1997). Amino acid sequence alignment of the three proteins reveals three highly conserved domains: the *N*-terminus sequence, the hydrophobic core (S1-S6 domains), and the cNBD, which share ~60% sequence

identity. ERG2 channels have similar kinetic properties to ERG1, although its activation curve is shifted to more positive potentials. On the other hand, ERG3 channels exhibit faster activation and deactivation kinetics and slower inactivation rates than ERG1, resulting in a left-shift in its activation curve (Shi *et al.*, 1997). When co-expressed in Chinese hamster ovary (CHO) cells, proteins encoded by different *ERG* genes co-assemble to form functional heteromultimeric ERG channels with distinct biophysical properties (Wimmers *et al.*, 2001, Wimmers *et al.*, 2002).

Alternative splicing of hERG1 mRNA can produce variant proteins that possess distinct properties (Fig. 1.5, Larsen, 2010). A C-terminal spliced variant, hERG1_{USO}, has been identified in the heart. This isoform lacks nearly all of the C-terminal domain, including all of the cNBD, encoded by exons 9 to 15 in hERG1, which is substituted by an 88 amino acid domain encoded by the small USO exon (Kupersmidt *et al.*, 1998). In heterologous systems, expression of hERG1_{USO} alone did not elicit any functional current. When hERG1_{USO} was expressed with hERG1 in a 1:1 ratio, it had no effect on hERG1-generated currents. However, when co-expressed with hERG1 in a 10:1 ratio, it reduced hERG1 current amplitude by ~2-3 fold and accelerated activation kinetics of the resulting current by ~3-5 fold, suggesting that hERG1_{USO} can coassemble with hERG1 to modify its gating (Kupersmidt *et al.*, 1998). This isoform is abundantly expressed in the heart and its physiological role (s) is presently not very clear (Kupersmidt *et al.*, 1998, Guasti *et al.*, 2008).

hERG1b is another isoform that lacks most of the hERG1 N-terminus, including the PAS domain. The first 36 residues in hERG1b are unique to this isoform and are encoded by a specific exon not present in the hERG1 transcript, suggesting that hERG1b is an alternative transcript, rather than a splice variant. Indeed, a separate promoter region for hERG1b has been

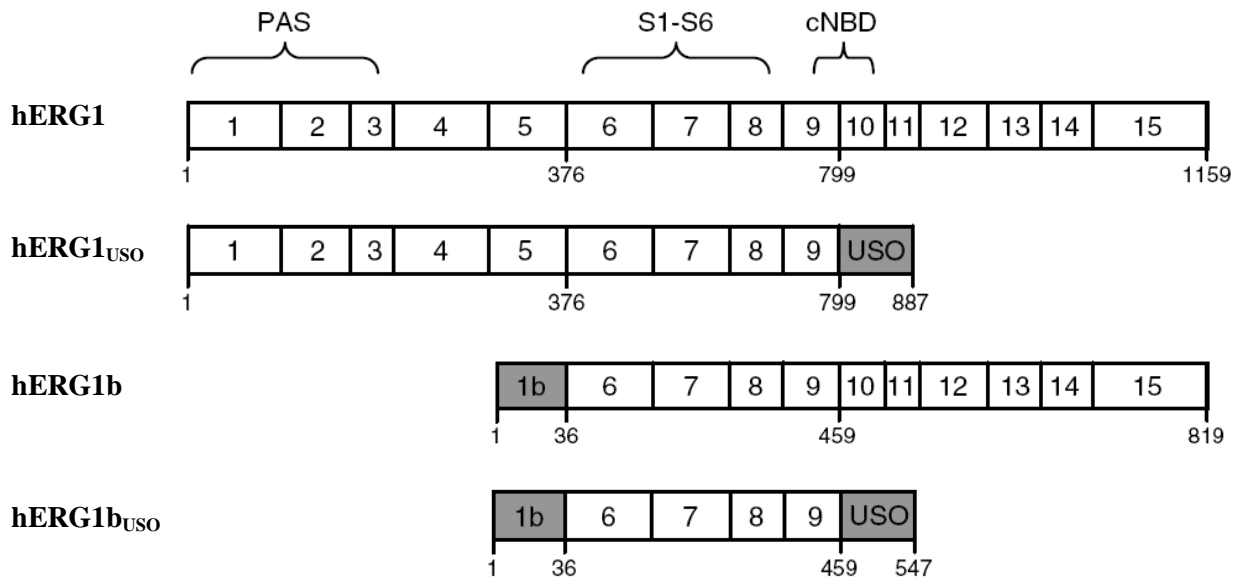


Figure 1.5 Diagrammatic comparison of hERG1 isoforms. The full-length hERG1 protein is encoded by the KCNH2 gene comprising 15 coding exons, indicated by numbers in boxes. The relative positions of the PAS domain, S1–S6 helices and the cNBD are labelled. Numbers below the boxes refer to residue numbers. Grey boxes mark sequences unique to shorter hERG1 isoforms (taken from Larsen, 2010).

identified (Luo *et al.*, 2008). hERG1b can produce a functional current on its own, which exhibits ~5 fold faster deactivation kinetics than the hERG1-generated current (Lees-Miller *et al.*, 1997, London *et al.*, 1997, Crociani *et al.*, 2003, Larsen *et al.*, 2008). Both the full length hERG1 and its shorter isoform, hERG1b co-assemble in the heart (Jones *et al.*, 2004), brain (Guasti *et al.*, 2005) and tumour cells (Crociani *et al.*, 2003). In heterologous systems, hERG1/hERG1b heteromeric currents have altered biophysical properties that are intermediate to the homomeric forms and closely mimick I_{Kr} kinetic properties, indicating a potentially overlooked physiological role of this isoform in the heart (Kirchberger *et al.*, 2006, Larsen *et al.*, 2008, Sale *et al.*, 2008).

Another isoform, hERG1b_{USO}, which has *N*- and *C*-termini identical to hERG1b and hERG1_{USO} respectively, has been described in tumour cells (Guasti *et al.*, 2008), and a brain-specific isoform, ERG1c has also been identified (Huffaker *et al.*, 2009).

Co-expression of different hERG1 isoforms has been reported in several tissue types. The functional importance of this overlapping expression is still elusive. However, it has been speculated that the relative expression of the shorter hERG1 isoforms may modulate the physiological functions of the full-length hERG1 transcript through modulating its cell-surface expression, trafficking, electrophysiological properties and/or post-translational processing (Guasti *et al.*, 2008, Larsen *et al.*, 2010). According to this proposal, it seems likely that modulating the relative abundance of hERG1 isoforms may be a physiologically relevant regulatory mechanism to modify hERG1 cellular function.

1.3.5 Auxiliary β -subunits associated with hERG1

The pore-forming α -subunit of hERG1 channels can associate with other auxiliary β -subunits that can modulate channel function. Co-expression of minK (KCNE1) with hERG1 increases hERG1 current amplitude, shifts activation to more negative potentials and increases steady-state inactivation (McDonald *et al.*, 1997). In addition, it has been claimed that hERG1 channels alone cannot recapitulate the biophysical characteristics of a native cardiac I_{Kr} current and require co-assembly with another β -subunit, minK-related protein 1 (MiRP1; KCNE2) (Abbott *et al.*, 1999). However, the potential physiological role of MiRP1 has been questioned in another study based on a comparison with native I_{Kr} currents of hERG1 currents expressed with and without MiRP1 coexpression in CHO cells (Weerapura *et al.*, 2002). Moreover, expression of MiRP1 in heart is mostly restricted to the cardiac conduction system (Yu *et al.*, 2001a), which suggests perhaps a specialized physiological role.

1.3.6 Pharmacological modulators of hERG1 channel activity

1.3.6.1 hERG1 blockers

hERG1 channels can be selectively blocked by an enormous number of compounds having diverse structures and various therapeutic indications. The sensitivity of hERG1 channels to blockade may be explained by the presence of a large pore cavity, which enables them to accommodate various drugs (Mitcheson *et al.*, 2000a). In addition, the presence of multiple aromatic residues, especially Tyr 652 and Phe 656, in the S6 domain region lining the cavity may facilitate high-affinity binding of drugs containing aromatic residues (Fig. 1.6A, Mitcheson *et al.*, 2000c). Moreover, the rapid inactivation of the hERG1 channels is suggested

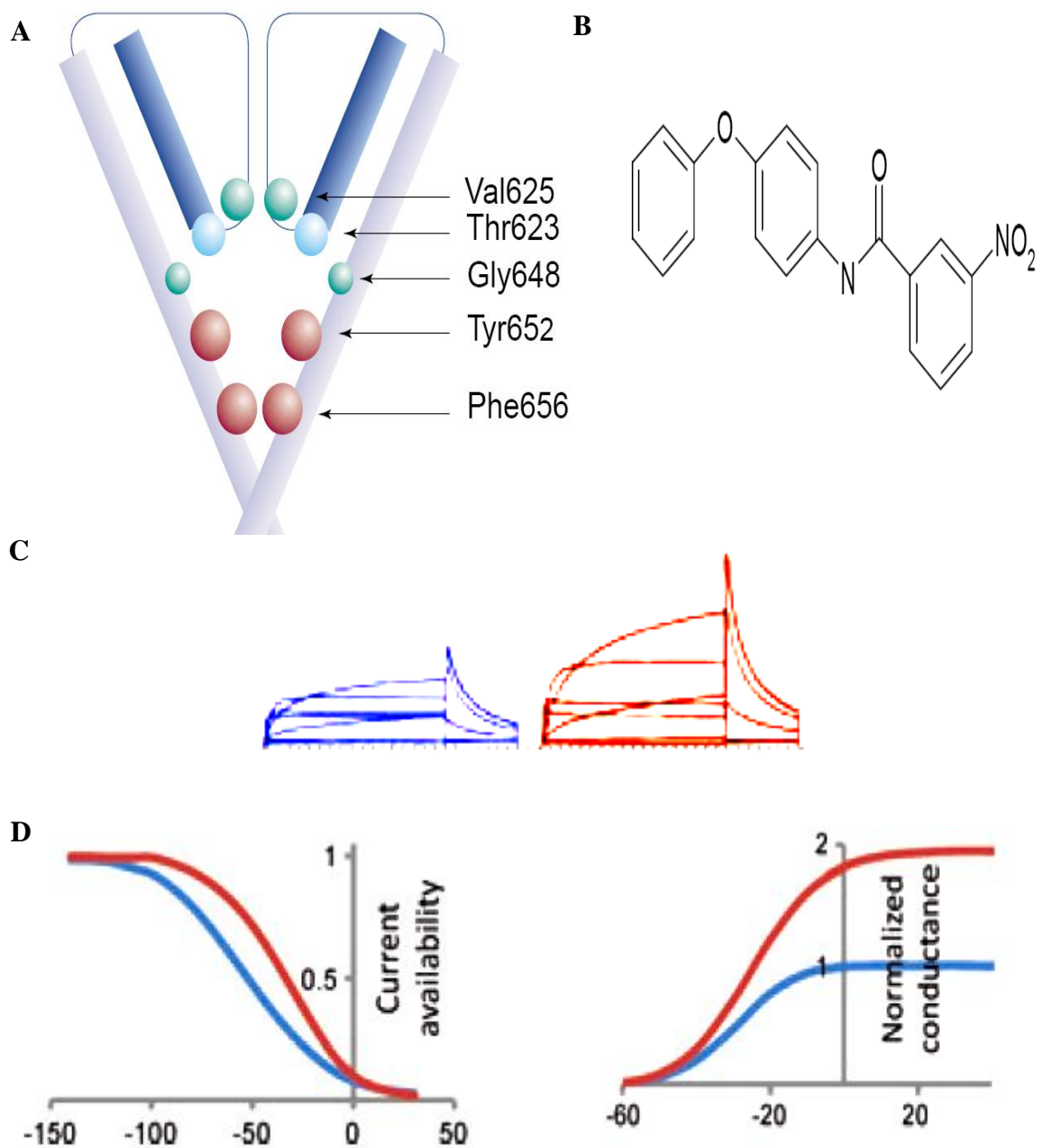


Figure 1.6 hERG1 block and activation. **A.** A cartoon of hERG1 channel cavity. The residues involved in high affinity drug block are highlighted. **B.** Structure of the hERG1 activator ICA-105574. **C.** hERG1 currents obtained using a standard IV protocol (Fig. 1.4A) under control (blue) and ICA-105574-modulated (red) conditions. **D.** Comparison of voltage-dependence of inactivation (left) and activation (right) curves of hERG1 currents in the absence (blue) and presence (red) of ICA-105574 (adapted from Mitcheson *et al.*, 2000bb, Gerlach *et al.*, 2010, Perry *et al.*, 2010).

to stabilize drug interaction with hERG1 channels, an effect that may be mediated via allosteric changes in the drug binding site (Chen *et al.*, 2002).

hERG1 blockers can have different sites of action on hERG1 channel structure. Although most hERG1 blockers do not affect hERG1-gating properties, they can specifically affect different gating states of the channels and thereby produce a voltage-dependent blockade. Most blocking drugs approach the channel from the intracellular side to act on binding sites inside the pore cavity. High-affinity blockers (e.g. dofetilide) block the channel in its open/inactivated state by binding to S6 aromatic residues lining the pore cavity. Other mechanisms of hERG1 blockade include closed-state- and mixed-state-dependent blockade. Conversely, the scorpion toxin BeK-m1 blocks hERG1 channels by acting extracellularly on the S5-pore linker of the channel in its closed state (Witchel, 2007).

The promiscuity of hERG1 channel block and the associated risk of cardiac arrhythmias represent a considerable problem for new drug development. A number of non-cardiac drugs, such as the anti-histamines terfenadine and astemizole, the prokinetic agent cisapride and the antipsychotic sertindole have been withdrawn from the market, or their use has to be carefully monitored, due to their unwanted cardiac side-effects caused by hERG1 blockade. Currently, drug regulatory authorities require that every new drug must be tested for its liability to cause LQTS. It has now become common practice in pharmaceutical companies to screen all new drugs for hERG1 channel blockade at an very early stage of the drug development process. It has been estimated that 40-70% of compounds are discarded during this initial screening. Moreover, some therapeutically valuable compounds might be discarded despite having minimal (or at least manageable) cardiac side-effects (Witchel, 2007). Advances in understanding of hERG1 channel structure and drug binding

sites may help in design of new drugs that lack hERG1-blocking activity (Sanguinetti *et al.*, 2005)

1.3.6.2 hERG1 activators

A new class of hERG1 modulator has been described; the hERG1 activators. These small molecule activators seem to act via a common mechanism by attenuating hERG1 inactivation and shifting its voltage-dependence to more depolarized potentials. They may be further divided into two sub-groups, depending on whether or not they affect channel deactivation. Type I activators (e.g. RPR260243) strongly slow hERG1 deactivation, whereas type 2 activators (e.g. PD118057 and ICA-105574; Fig. 1.6B) minimally affect hERG1 deactivation properties, but may enhance single channel open probability (Fig. 1.6C; Perry *et al.*, 2010). ICA-105574 (Gerlach *et al.*, 2010) has been shown to cause a 2-fold decrease in channel deactivation and a minor hyperpolarizing shift in the I-V activation curve when used at higher concentrations ($\geq 3 \mu\text{M}$; Fig. 1.6D). An exception to the common mechanism of action of other hERG1 activators is mallotoxin, which does not affect hERG1 inactivation and primarily acts by increasing the rate of hERG1 activation (Zeng *et al.*, 2006).

1.3.6.3 hERG1 trafficking modulators

hERG1 proteins are synthesized, in the endoplasmic reticulum (ER), as core glycosylated monomers, which are then assembled into tetramers to be transported to the Golgi apparatus. The presence of ER quality control mechanisms ensures that any misfolded or misassembled proteins are retained in the ER, so that only properly folded tetrameric hERG1 proteins exit the ER. In the Golgi, hERG1 proteins undergo maturation via complex glycosylation. Finally, the mature channels are transported to the cell-surface (Zhou *et al.*,

1998a, Perrin *et al.*, 2008). A number of compounds (e.g. pentamidine, arsenic trioxide, fluoxetine) impair correct trafficking of hERG1 channels, which results in their failure to reach the plasma membrane (Raschi *et al.*, 2008). On the other hand, other compounds have the ability to correct such abnormal trafficking and rescue the surface expression of trafficking-deficient hERG1 mutants; effects that may be dependent (Ficker *et al.*, 2002) or independent (Rajamani *et al.*, 2002) of hERG1 channel blockade. These compounds act as pharmacological chaperones to stabilize hERG1 proteins in a conformation that can bypass ER quality control mechanisms and exit the ER. The ability of the high-affinity hERG1 blockers astemizole, cisapiride and E-4031 to rescue the trafficking-deficient G601S hERG1 mutant varied with their hERG1 blockade potency and the concentrations required to rescue the mutant were ~ 100 fold higher than those needed to block the channel (Ficker *et al.*, 2002). On the other hand, the weak hERG1 blocker fexofenadine was able to rescue the trafficking-deficient N470D hERG1 and G601S hERG1 mutants at concentrations that do not block hERG1 channels (Rajamani *et al.*, 2002).

1.4 Potassium channels and cancer

Cancer is a disease caused by the occurrence of dynamic genomic changes at multiple sites. These changes may range from subtle point mutations to major chromosome arrangements. Examples of such genetic alterations include mutations that lead to the dominant gain-of-function of oncogenes and recessive loss-of-function of tumour suppressor genes. Importantly, tumorigenesis is a multistep process, as these genetic changes occur sequentially and successively, conferring growth advantages and acquired capabilities to normal cells, which collectively drive their progressive transformation into malignant cancer cells (Farber, 1984, Hanahan *et al.*, 2000, Duesberg *et al.*, 2003, Weinberg, 2008).

Chapter 1

In a landmark review, Hanahan and Weinberg (2000) suggested that all cancer cell-types acquire six functional capabilities during cancer development. These “hallmarks of cancers” are self-sufficiency in growth signals, insensitivity to inhibitory growth signals, resistance to apoptosis, unlimited replication, sustained angiogenesis, and tissue invasion and metastasis (Hanahan *et al.*, 2000). Recently, the same authors have proposed two additional capabilities to be important for the development of cancer that should be added to the originally outlined list of hallmarks of cancer (Hanahan *et al.*, 2011). These are the ability of tumour cells to evade immune destruction and the capability to modify cellular metabolism to support cancer cell proliferation (Hanahan *et al.*, 2011).

The hallmarks of cancers are traits that are acquired in tumours via a variety of different mechanisms. Moreover, the pathways that normal cells adopt on their way to malignancy are highly variable. The acquisition of these novel capabilities by cancer cells can appear at different times of multi-step tumour progression (Hanahan *et al.*, 2000). Although formation of secondary metastases has been thought to be the last step in primary tumour progression, which is likely the case in most tumour types, recent evidence has indicated that cells can disseminate early from pre-malignant lesions (Coghlin *et al.*, 2010). This may suggest that the mechanisms underlying metastatic dissemination to distant tissues and subsequent colonization in these new microenvironments are independent of or different from those mediating primary tumour progression (Hanahan *et al.*, 2011).

Many K⁺ channels are up-regulated in cancerous cell-lines and primary tumours when compared to the corresponding healthy cells from which they originate (O'Grady *et al.*, 2005, Schonherr, 2005). Several reports have also shown that specific K⁺ channel subtypes, including TASK-3 (Mu *et al.*, 2003), EAG (Pardo *et al.*, 1999) and hERG1 channels (Pier,

2007) may possess oncogenic potential. I will first provide a general overview of possible contributions of K^+ channels to each feature of the neoplastic phenotype before discussing the current knowledge on involvement of specific K^+ channels, with a specific focus on hERG1 channels, in cancer.

1.4.1 Self-sufficiency in growth signals

In order to proliferate, normal cells require to receive mitogenic growth signals from their microenvironment. Signalling molecules, including soluble growth factors and components of the extracellular matrix (ECM), bind to and activate transmembrane receptors (growth factor receptors and integrins, respectively), which transduce signals that activate intracellular signalling pathways responsible for proliferation. In contrast, tumour cells can proliferate independently of exogenous growth stimulation. This growth signal autonomy in cancer cells can be evoked via a number of mechanisms. Many cancer cells can produce growth factors that stimulate their own proliferation through an autocrine stimulation mechanism. Moreover, several types of cancers over-express growth factor receptors, an effect that can increase their response to low levels of growth factors, or alternatively, elicit their constitutive (ligand-independent) activation. In addition, tumour cells can change their pattern of integrin expression, favouring those that transduce pro-proliferative signals. Tumour cells may also show genetic alterations in the components of intracellular transduction pathways (e.g. SOS-Ras-Raf-MAPK), which promote mitogen-independent proliferation. Finally, tumour cells may induce other cells present in the tumour microenvironment (stromal cells), such as tumour-associated fibroblasts, endothelial and inflammatory cells, to release growth signals. In this way, tumours can be regarded as

complex tissues, rather than the former view of tumours as unicellular masses (Hanahan *et al.*, 2000).

A large number of reports indicate that K^+ channels are essential for neoplastic cell proliferation. These studies also generally report that tumour cells over-express functional K^+ channels belonging to diverse K^+ channel families (Wang, 2004, Haren *et al.*, 2010). Moreover, inhibition of K^+ channel conduction through different types of K^+ channels often impairs proliferation in a variety of tumour cell-types, including breast carcinoma, melanoma, neuroblastoma, leukaemia, prostate, colon cancer cells as well as others (Wonderlin *et al.*, 1996, Pardo, 2004, Wang, 2004). Mitogen-treated tumour cells often show increased K^+ channel activity and/or expression (Wang *et al.*, 1997a, Gamper *et al.*, 2002, Borowiec *et al.*, 2007). In addition, oncogene- and oncovirus-mediated cell transformation has been associated with an increase in K^+ channel activity (Teulon *et al.*, 1992, Repp *et al.*, 1993, Huang *et al.*, 1994, Draheim *et al.*, 1995). Some K^+ channel agonists increased DNA synthesis and proliferation in some cell-types (Harmon *et al.*, 1993, Malhi *et al.*, 2000, Abdul *et al.*, 2002, Parihar *et al.*, 2003, Spitzner *et al.*, 2007). Moreover, the activities or expression of some K^+ channels are cell cycle-regulated (Pardo *et al.*, 1998, Kunzelmann, 2005). In general, it is well established that increased K^+ channel expression/activity correlates well with an enhancement of cancer cell proliferation. The mechanisms accounting for the contribution of K^+ channels to tumour cell proliferation are not well understood. Nevertheless, several hypotheses have been proposed that might explain the importance of K^+ channels in tumour cell proliferation. These mechanisms are discussed below.

1.4.1.1 Regulation of membrane potential

The ability of K^+ channels to regulate membrane potential is thought to be essential for passage through cell cycle checkpoints. An increase in K^+ current flow at G1 has been reported which leads to a relatively hyperpolarized membrane potential that may be necessary for progression through the G1-S phase checkpoint (Wonderlin *et al.*, 1996). Supporting a role of membrane potential modulation in proliferation, treatment of human carcinoma cells with epidermal growth factor (EGF) (Pandiella *et al.*, 1989) and Ras-transformed NIH-3T3 cells with bradykinin caused an initial membrane hyperpolarization followed by fluctuations in membrane potential with alternating depolarization and hyperpolarization (Pandiella *et al.*, 1989, Lang *et al.*, 1991, Lang *et al.*, 1992). The K_v channel blocker 4-aminopyridine (4-AP, 0.5-2 mM) has been shown to reduce insulin-induced proliferation in human myeloblastic leukaemic ML-1 cells, leading to arrest in the G1 phase of the cell cycle (Guo *et al.*, 2005). The anti-proliferative effect of K^+ channel blockers may be due to their interference with the transient hyperpolarization required for progression from the G1 phase of the cell cycle (Wonderlin *et al.*, 1996). In agreement with this, membrane depolarization through increasing external K^+ concentration (to 30-120 mM), or by using the depolarizing drug ouabain (200 μ M) impaired proliferation of mitogen-treated Schwann cells (Wilson *et al.*, 1993). Since tumour cells have relatively depolarized membrane potentials (Redmann *et al.*, 1972, Smith *et al.*, 1975, Binggeli *et al.*, 1980), it is plausible that such cells need to up-regulate expression of certain types of K^+ channel to produce the transient hyperpolarization necessary to pass the G1 checkpoint (Prevarskaya *et al.*, 2010).

However, some reports have indicated that a depolarization, rather than a hyperpolarization, is required at the G1 checkpoint. This is based on reports that the resting potential of terminally differentiated cells in G0 is markedly hyperpolarized, while quiescent cells are moderately hyperpolarized, and cycling cells (e.g. tumour cells) that do not enter G0 are relatively depolarized (Redmann *et al.*, 1972, Smith *et al.*, 1975, Arcangeli *et al.*, 1995, Wonderlin *et al.*, 1996). It has also been shown that hyperpolarizing membrane potentials inhibit DNA synthesis (Arcangeli *et al.*, 1995). The sometimes contradictory results on the required changes in membrane polarity for cell cycle progression may be due to differences between the types of cell studied to date.

A hyperpolarized membrane potential may maintain the driving force for Na⁺-dependent nutrient transport (Pardo, 2004) and pH regulation (Spitzner *et al.*, 2007), which are important for cell cycle progression. More importantly, modulation of the cell membrane potential under the control of K⁺ channels is usually associated with an increased [Ca²⁺]_i (Nilius *et al.*, 1993, Lepple-Wienhues *et al.*, 1996, Yao *et al.*, 1999, Spitzner *et al.*, 2007) (Pandiella *et al.*, 1989, Lang *et al.*, 1991, Lang *et al.*, 1992), which is crucial for signal transduction processes during cell proliferation (Nilius *et al.*, 1993, Means, 1994). In contrast, the anti-proliferative effects of the K_{ATP} channel inhibitor glibenclamide on mitogen-treated rat hepatocytes was not associated with any changes in [Ca²⁺]_i (Malhi *et al.*, 2000), suggesting that some K⁺ channels may affect cell proliferation independently of Ca²⁺ influx and that other mechanisms may mediate their contribution to cell proliferation.

1.4.1.2 Regulation of cell volume

An additional mechanism linking K⁺ channel conductance to cell proliferation is the ability of these channels to regulate cell volume. Proliferation is associated with an increase in cell

volume during G1 phase, but excessive cell-swelling can inhibit proliferation (Lang *et al.*, 2000). A plot of proliferation rate versus cell volume gives a bell-shaped curve indicating that there is an optimal cell volume for growth (Dubois *et al.*, 2004). Mitogens induce cell-swelling, which is associated with an increase in Ca^{2+} entry (Shen *et al.*, 2002). K^+ channel blockers can produce an increase in cell volume and a decrease in cell proliferation (Rouzair-Dubois *et al.*, 1998). A higher expression of K^+ channels in tumour cells may allow a tight regulation of cell volume, allowing maintenance of the optimal concentration of cell cycle effectors (Rouzair-Dubois *et al.*, 2004). On the other hand, excessive cell volume increases can also be damaging to the cell, while significant cell shrinking can induce apoptosis (Maeno *et al.*, 2006). Therefore, K^+ channels may have dual roles in proliferation and apoptosis, but a much larger K^+ flux is required to induce apoptosis relative to the ionic K^+ currents necessary for cell cycle progression (Kunzelmann, 2005).

1.4.1.3 Involvement in signalling pathways leading to proliferation

K^+ channel activity may also be contributory to growth factor-mediated signalling. Suppression of K^+ channel activity using either 4-AP (2 mM) or extracellular K^+ (60 mM) inhibited EGF- induced activation of extracellular signal-regulated protein kinase 2 (ERK2). Elimination of extracellular Ca^{2+} did not affect the influence of K^+ channel blockade on ERK2 activation. These data appear to show that K^+ channels are required for initiation of mitogen-activated protein kinase (MAPK) pathways in response to growth factors (Xu *et al.*, 1999).

Moreover, certain types of K^+ channel may enhance cell cycle progression through formation of supramolecular complexes with other proteins involved in proliferation. This has been shown for a $\text{K}_v1.3$ interaction with $\beta 1$ -integrin (Levite *et al.*, 2000) and p56^{lck}

(Szabo *et al.*, 1996, Hanada *et al.*, 1997). Also, hERG1 channels can physically associate with Src (Cayabyab *et al.*, 2002), TNF α receptors (Wang *et al.*, 2002a), 14-3-3 proteins (Kagan *et al.*, 2002), VEGF receptor1 (VEGFR1) and β 1-integrin (Pillozzi *et al.*, 2007). The significance for these hERG1-protein complexes will be discussed later in a different context.

1.4.1.4 Limitations

The evidence for an important role of K⁺ channels in tumour cell proliferation is presently far from conclusive. The anti-proliferative effect of K⁺ channel inhibitors is usually observed at high doses, at which they may have undefined effects on other cellular proteins (Wonderlin *et al.*, 1996). Moreover, only a few specific types of K⁺ channel were able to induce malignant transformation when expressed in heterologous systems (Pardo *et al.*, 1999, Mu *et al.*, 2003, Pier, 2007). Furthermore, in most of the studies that highlight the pro-proliferative effects of K⁺ channels in tumours, the authors usually identify a particular type of K⁺ channel in a cancer cell-line and then try to correlate the gene and functional expression of the identified channel(s) to proliferation. However, tumour cells invariably express multiple types of K⁺ channel at their cell membrane, which may indicate that a co-ordination of their functions may be required to facilitate cancer cell proliferation. Interestingly, it has been suggested that hEAG and IK_{Ca} channels co-operate to regulate cell cycle progression in MCF-7 breast cancer cells (Ouadid-Ahidouch *et al.*, 2004). In these cells, activation of hEAG channels produced a transient hyperpolarization at early G1 phase (Ouadid-Ahidouch *et al.*, 2001). Moreover, IK_{Ca} channel expression and activity were greatly enhanced at the end of G1 and in early S phase, which was associated with membrane hyperpolarization and an increase of [Ca²⁺]_i (Ouadid-Ahidouch *et al.*, 2004).

Astemizole (a non selective hEAG channel blocker, 5 μ M) and clotrimazole (a selective IK_{Ca} channel blocker, 5 μ M) inhibited proliferation of MCF-7 cells by 60% and 20% respectively, whereas their combined used produced an at least additive inhibitory effect with $\geq 80\%$ inhibition of proliferation and 99% G1 arrest. Based on these results, the authors proposed a model in which hEAG and IK_{Ca} channels co-operate to maintain a hyperpolarized membrane potential during G1 phase, facilitating G1/S cell cycle transition (Oquadid-Ahidouch *et al.*, 2004).

1.4.2 Insensitivity to anti-growth signals

As described above, growth signals are essential for the life of normal cells. However, normal cells also require anti-proliferative signals to maintain normal tissue homeostasis. These inhibitory signals can limit cell proliferation by either temporarily forcing cells out of the active cell cycle into a quiescent (G0) state, or irreversibly causing cells to lose their proliferative potential and specify (differentiate). Anti-growth signals (e.g. transforming growth factor β (TGF β)) act on cognate surface receptors. Binding of TGF β to its receptor induces phosphorylation of Smad4 protein, which then translocates to the nucleus to stimulate synthesis of cyclin-dependent kinase (CDK) inhibitors p21 and p27, which in turn block association of cyclins and CDKs, leading to cell cycle block at G1 (Peng *et al.*, 2002).

Obviously, cancer cells need to ignore these inhibitory messages in order to proliferate. In agreement with this, some cancer cell types down-regulate their TGF β receptors and others express mutant non-responsive TGF β receptors. Moreover, this inhibitory factor-mediated signalling may be disrupted in cancer cells in such a way that they support proliferation rather than blocking it (Hanahan *et al.*, 2000).

K^+ channels may help tumour cells overcome TGF β -mediated cell cycle block. Inhibition of K_v channel activity in small cell lung cancer (SCLC) NCI-H209 and NCI-H146 and leukaemic Jurkat tumour cell-lines using 4-AP produced an increase in CDK inhibitor p27 and a decrease in cyclin A expression, leading to G1 arrest (Renaudo *et al.*, 2004). Similarly, the anti-proliferative effect of K^+ channel blockers on oligodendrocyte progenitor cells has been attributed to accumulations of the CDK inhibitors p27 and p21 (Ghiani *et al.*, 1999).

1.4.3 Evasion of apoptosis

Apoptosis (programmed cell death) is an essential process for maintaining normal tissue homeostasis. Cells can start the apoptotic program after sensing extracellular death signals (induced by abnormal conditions, e.g. exposure to carcinogens) via death receptors located at the plasma membrane (e.g. FAS receptor responding to FAS-ligand and TNF-R1 receptors responding to TNF α). Alternatively, cells can sense unfavourable intracellular signals (e.g. DNA damage induced by cancer) through the tumour suppressor p53, which triggers mitochondria to initiate apoptosis. Both intrinsic (mitochondria-mediated) and extrinsic (death receptor-mediated) mechanisms of apoptosis converge to stimulate caspases, intracellular proteases that perform a series of sequential steps, including degrading cell organelles and DNA, that eventually cause cell death. Apoptosis is considered to be a major barrier to cancer and tumour cells have to avoid apoptosis. Many types of cancer display mutated dysfunctional death receptors. Alternatively, the components of the apoptotic signalling circuitry in cancer cells may be genetically inactivated (Hanahan *et al.*, 2000).

K^+ channels play a major role in the regulation of apoptosis. The higher activity of K^+ channels and the associated loss of intracellular K^+ ions due to K^+ efflux can lead to apoptosis. This might be due to induction of an apoptotic volume decrease (AVD) in the early phase of apoptosis and loss of the inhibitory effect of K^+ ions on executioner caspases and DNA-degrading endonucleases (Yu *et al.*, 2001b, Wang, 2004). According to this hypothesis, it would seem a logical corollary that tumour cells need to down-regulate K^+ channel expression/activity in order to evade apoptosis. Supporting this notion, the expression of the redox-sensitive $K_v1.5$ channel is down-regulated in various human cancers and its blockade was shown to increase the resistance of SGC790 gastric cancer cells to apoptosis induced by chemotherapeutic agents (Bonnet *et al.*, 2007, Han *et al.*, 2007b). Moreover, increased survival of glioma cells correlated well with decreased activity of TASK3 channels induced by higher extracellular K^+ , whereas the TASK3 channel-opener isoflurane reduced glioma cell survival by ~ 30% (Meuth *et al.*, 2008). In contrast, heterologous expression of TASK3 in mouse fibroblast (C8) cells enhanced their resistance to TNF α -induced apoptosis (Pei *et al.*, 2003).

On the other hand, K^+ channels expressed in tumour cells may also contribute to evasion of apoptosis via signalling mechanisms. 4-aminopyridine (4AP) caused an apoptotic effect in the U87 astrocytoma cell-line at a 4AP concentration (4mM) that caused approx. 50% inhibition of the K^+ current in these cells. Moreover, 4 mM 4AP failed to induce apoptosis in another astrocytoma cell-line A172 that expresses a mutant p53 protein, suggesting that K^+ channels have an inhibitory effect on wild-type (WT) p53-mediated apoptosis in malignant astrocytoma cells (Chin *et al.*, 1997). In agreement with this, blockade of BK $_{Ca}$

in human HeLa cervical and A2780 ovarian cancer cell-lines caused apoptosis and G1 arrest, associated with an increase in p53 expression (Han *et al.*, 2007a).

Apoptosis is a Ca^{2+} -dependent process (Orrenius *et al.*, 2003). K^+ channels may modulate tumour response to apoptosis through regulation of $[\text{Ca}^{2+}]_i$ via altering membrane potential. In agreement with this, the apoptotic effect of 4AP in HepG2 human hepatoblastoma cells has been attributed to a sustained Ca^{2+} influx, which was inhibited by the non-selective cation channel blocker flufenamic acid. These data suggest that 4AP-induced apoptosis may be due to activation of voltage-dependent Ca^{2+} permeable non-selective cation channels caused by 4AP-mediated membrane depolarization (Kim *et al.*, 2000).

1.4.4 Unlimited proliferation

Normal cells have a finite replicative potential as they stop growing after a certain number of divisions (senescence). The terminal parts of the chromosome, called telomeres, determine the number of cell divisions. Telomeres contain thousands of non-coding six base pair short sequence repeats, which protect the ends of the chromosome. Each replication cycle causes 50-100 base pairs of telomeric DNA to be lost. This progressive shortening eventually causes loss of the protective ends of the chromosome, leading to chromosome fusion and eventually cell death. Cancer cells replicate indefinitely and become immortalized as they usually up-regulate telomerase enzyme, which catalyzes the synthesis and extension of telomeric DNA (Hanahan *et al.*, 2000, Artandi *et al.*, 2010).

So far, it has not been reported whether K^+ channels can affect telomerase activity. However, since telomerase activity is regulated by Ca^{2+} homeostasis (Alfonso-De Matte *et al.*, 2002), which in turn can be modulated by K^+ channels activity, it is possible that such a link between K^+ channels and telomerase exists.

1.4.5 Sustained angiogenesis

Oxygen and nutrients provided by the vasculature are essential for normal cell function and survival. This necessitates that all living cells are located no more than 100 μm from the nearest capillary blood vessel. Based on this, for a neoplastic mass to develop in size, tumour cells must acquire angiogenic capability, that is, to synthesize new blood vessels from the endothelium of existing vasculature. A tumour “angiogenic switch” is attained via an interference with the normal balance between pro-angiogenic and anti-angiogenic factors. Many tumours over-express pro-angiogenic factors, such as vascular endothelial growth factor (VEGF), whereas others down-regulate the angiogenic inhibitor thrombospondin-1 (Hanahan *et al.*, 2000, Folkman, 2002).

Several reports have suggested that K_{Ca} channels are involved in tumour angiogenesis. Higher expression of K_{Ca} channels has been detected in metastatic brain tumour tissue and tumour capillary endothelium as compared to normal brain tissue (Hu *et al.*, 2007). Likewise, in patients with colonic adenocarcinoma, the number of endothelial cells expressing K_{Ca} channels per mesenteric artery was 2.5 times higher than corresponding levels in non-cancer patients. This resulted in a 2.7-fold potentiation of bradykinin-induced endothelial hyperpolarization compared with control. Endothelial hyperpolarization can increase the electrochemical driving force for Ca^{2+} influx and thus facilitate Ca^{2+} entry, which is an essential requirement for synthesis of vasodilating factors and gene expression (Kohler *et al.*, 2000). Moreover, the increased proliferation of human vascular endothelial cells mediated by basic fibroblast growth factor (bFGF) or vascular endothelial growth factor-A (VEGF-A) has been shown to be accompanied by an increase of BK_{Ca} activity (Wiecha *et al.*, 1998, Faehling *et al.*, 2001). The angiogenic effect of bFGF was inhibited

by 50% when endothelial cells were exposed to the BK_{Ca} inhibitor, iberiotoxin (100 nM)(Wiecha *et al.*, 1998).

Alternatively, both EAG1 (Downie *et al.*, 2008) and hERG1 (Masi *et al.*, 2005, Pillozzi *et al.*, 2007) channels have been shown to contribute to production and secretion of VEGF by tumour cells (covered in more detail later).

1.4.6 Tissue invasion and metastasis

Upon progressive development of tumours, nutrients and space within the tumour become limiting. This triggers individual cancer cells to break away from the primary tumour mass, invade nearby capillaries and travel to distant sites where they form new colonies (metastases). Metastasis is considered to be a major cause of death of cancer patients.

Acquisition of metastatic and invasive phenotype requires that tumour cells acquire three novel traits. First, tumour cells have to decrease their adhesive contacts with the tumour microenvironment by altering the expression of proteins involved in cell-cell adhesion (cadherins and cell-cell adhesion molecules (CAMs)) and cell-extracellular matrix (ECM) interaction (integrins). Secondly, cancer cells tend to secrete extracellular proteases (e.g. matrix metalloproteinases (MMP)), which enable them to degrade surrounding matrices and tissue structure. Finally, tumour cells acquire enhanced migratory properties (Hanahan *et al.*, 2000, Wang *et al.*, 2005).

1.4.6.1 Cell migration

When cells migrate, they tend to polarize, that is, the front part of the cell extends protrusions that may be sheet-like lamellipodia or thin filopodia. These protrusions are induced by polymerization of actin monomers at the leading edge toward the direction of

movement. The cell body forms the rear of the cell. In this way, migration can be described as a cyclic process of three co-ordinated basic steps that take place repeatedly: (i) extension of lamellipodia or filopodia at the leading edge of migrating cells in the direction of movement, (ii) formation of adhesion sites with the substratum via transmembrane receptors linked to the actin cytoskeleton and (iii) contraction of the cell body leading to release of contacts at the rear of the cell and allowing rear retraction (Wang, 1985, Mogilner *et al.*, 2003, Ridley *et al.*, 2003). Integrins are one of the most important components of the migration machinery of normal and metastatic tumour cells.

1.4.6.2 Integrins

Integrins are cell-surface adhesion receptors that physically mediate cell adhesion to the ECM and direct cell-cell adhesion. Moreover, they can also transduce messages from the extracellular environment into the cytoplasm that help cells regulate their shape, as well as many physiological processes, such as proliferation, survival, spreading, migration, cytoskeletal arrangement and gene transcription. Integrins are glycoprotein heterodimers formed of two non-covalently-linked α and β subunits. So far, 18 α and 8 β subunits have been identified in mammals, which pair to produce 24 different integrins with distinct affinities for ECM proteins (e.g. fibronectin, collagen, laminin, fibrinogen). Each integrin subunit possesses a large extracellular domain, a single transmembrane helix and a short cytoplasmic tail. An exception is the $\beta 4$ subunit that has a large (1000 amino acid) cytoplasmic domain. The extracellular domains recognize specific amino acid sequences, which accounts for their high-specificity/high affinity binding to substrates. Their cytoplasmic domains interact with actin-associated proteins, thus facilitating linkage of the ECM to the cytoskeleton (Shattil *et al.*, 2010).

It is well established that integrins mediate bidirectional signalling through the plasma membrane (Schoenwaelder *et al.*, 1999, Coppelino *et al.*, 2000). That is, they can transmit messages both out of the cell, “inside-out”, and into the cell, “outside-in”. Inside-out signalling (integrin activation) refers to the ability of intracellular signalling molecules to modulate the binding affinity of integrins. Under normal conditions the extracellular binding site of integrins is partially blocked, which diminishes its affinity for the substrate (low-affinity state). Interaction of integrin cytoplasmic domains with cytoplasmic and cytoskeletal proteins lead to conformational changes to the integrin extracellular domains, which then bind with greater affinity to the ECM (high-affinity state).

Integrin outside-in signalling is induced via their ligation to ECM proteins. Unbound integrins are usually diffusely located at the cell membrane. Engagement of the extracellular sites of integrins localizes them at fixed points at the cell membrane, which allow them to cluster, in the plane of the membrane, with other integrins nearby. Integrin clustering is thought to cause conformational changes that are transduced to the cytoplasmic domains, which can then in turn recruit various signalling molecules, cytoskeletal and scaffolding proteins, to be arranged in macromolecular complexes called focal adhesions or focal complexes. These structures comprise integrins, non-receptor tyrosine kinases (such as focal adhesion kinases (FAK) and Src-family kinases (SFKs)) and cytoskeletal proteins, including talin, paxillin, vinculin, α -actinin, and other proteins connected to the actin cytoskeleton (Schoenwaelder *et al.*, 1999, Coppelino *et al.*, 2000, Brakebusch *et al.*, 2003, Shattil *et al.*, 2010).

Moreover, it has been shown that integrins can also associate with other cell-surface proteins, such as growth factor receptors (Bill *et al.*, 2004, Walker *et al.*, 2005, Pillozzi *et*

et al., 2007), chemokine receptors and ion channels (Arcangeli *et al.*, 2006). Based on these findings, it has been suggested that these associations localize these membrane proteins at the cell membrane, allowing a reciprocal regulatory relationship between associated proteins and forming extensive signalling platforms that modulate intracellular signalling.

1.4.6.3 Integrins and cancer

Acquisition of a transformed phenotype is usually associated with alterations in integrin expression patterns. Among the numerous integrins reported to be up-regulated in cancerous cells are $\alpha 6\beta 4$, $\alpha_v\beta 3$, $\alpha 5\beta 1$ and $\alpha_v\beta 6$ (Mizejewski, 1999, Desgrosellier *et al.*, 2010). Indeed, in some tumour cell-types the expression of specific integrins correlates with increased tumour progression, poor prognosis and reduced patient survival. Conversely, the expression levels of some integrins, such as $\alpha 2\beta 1$, are down-regulated in tumour cells. Moreover, re-expression of $\alpha 2\beta 1$ in breast cancer cells reversed some aspects of the neoplastic phenotype, which may suggest that this particular integrin may function as a tumour suppressor (Zutter *et al.*, 1995). Integrin localization can also be modulated on neoplastic transformation. In general, integrins become more diffuse in cancer cells (Mizejewski, 1999), whereas some integrins, such as the $\alpha 6\beta 4$, become localized to the leading edge of migrating cancer cells (Hood *et al.*, 2002).

Integrin signalling can affect diverse functions of tumour cells, such as migration, proliferation, invasion and survival. Integrins may contribute to the migratory and invasive phenotype of tumour cells via regulation of the activity of FAK and matrix-degrading proteases, respectively (Felding-Habermann, 2003) However, integrins do not have oncogenic activity as they lack the ability to transform cells. Instead, it has been suggested that integrin-mediated effects on cancer cells may require their co-operation with growth

factor receptors, cytokine receptors or oncogenes to enhance tumorigenesis (Guo *et al.*, 2006, Pylayeva *et al.*, 2009). In fact, it has been shown that ErbB2 growth factor receptor can up-regulate the transcription of $\alpha 5\beta 1$ integrin improving survival of tumour cells (Spangenberg *et al.*, 2006) and that $\alpha 6\beta 4$ can regulate ErbB2 expression leading to Ras activation (Yoon *et al.*, 2006). These findings confirm mutual regulatory mechanisms between integrins and growth factor receptors in tumour cells.

The aberrant expression and/or localization of integrins in tumour cells, their contribution to tumour progression and their involvement in signalling complexes with oncogenes/growth factors has attracted attention to their possible therapeutic use as targets of anticancer agents. Anti-integrin $\beta 1$ antibodies have been shown to reduce the growth of human breast tumour cells both *in vitro* and *in vivo* (Park *et al.*, 2006). The integrin antagonist cilengitide (inhibiting $\alpha_v\beta 3$ and $\alpha_v\beta 5$) is currently being assessed in phase III clinical trials in glioblastoma patients (Desgrosellier *et al.*, 2010).

1.4.6.4 K^+ channels and tumour cell migration

Several reports have indicated a correlation between the expression of some K^+ channels in tumours and their metastatic abilities (Stringer *et al.*, 2001, Lastraioli *et al.*, 2004, Haren *et al.*, 2010). The possible roles of K^+ channels in enhancing migration and invasion of tumour cells are considered below.

Several studies have demonstrated a functional role of different types of K^+ channels in the migration of healthy and tumour cells, especially members of K_{Ca} (Schwab *et al.*, 1994, Schwab *et al.*, 1999a, Schneider *et al.*, 2000, Potier *et al.*, 2006, Schwab *et al.*, 2006, Weaver *et al.*, 2006, Kessler *et al.*, 2008, Sciaccaluga *et al.*, 2010) and K_v families (Levite *et al.*, 2000, Artym *et al.*, 2002, Rao *et al.*, 2002, Nutile-McMenemy *et al.*, 2007, Pier, 2007,

Pillozzi *et al.*, 2007). Inhibition of K^+ channel activity in migrating cells can modulate their migration speed. Fibroblast growth factor-2 (FGF-2) mediated migration of transformed renal epithelial (MDCK-F) cells is dependent on both ERK1/2 and IK_{Ca} channel activation (Kessler *et al.*, 2008). Similarly, glioblastoma cell migration induced by the chemokine CXCL12 is completely abolished when the activity of the IK_{Ca} channel is inhibited (Sciaccaluga *et al.*, 2010). Moreover, heterologous expression of some K^+ channels in mammalian systems increased rates of migration (Schwab *et al.*, 2006, Pier, 2007) and increased expression of some K^+ channels subtypes in tumour cells correlated with an enhanced migratory phenotype (Potier *et al.*, 2006, Chantome *et al.*, 2009).

K^+ channels might modulate cell migration via different mechanisms. One possible mechanism relates to their ability to regulate membrane potential, an effect that controls the electrical driving force for ion fluxes across the membrane. In agreement with this hypothesis, increasing extracellular K^+ concentration, which depolarizes the membrane, inhibited migration of transformed epithelial cells (Schwab *et al.*, 1994). Likewise, knockdown of SK_{Ca} channel in melanoma cells led to plasma membrane depolarization and decreased cell motility (Chantome *et al.*, 2009). Membrane potential regulates intracellular Ca^{2+} levels, which are critical for cell migration. An increase of $[Ca^{2+}]_i$ can lead to actin depolymerization and a low level of Ca^{2+} favours polymerization. Therefore, cells maintain an intracellular gradient of Ca^{2+} with lower concentrations at the leading edge, which provides optimum conditions for actin polymerization (Brundage *et al.*, 1991, Schwab *et al.*, 1997). Moreover, Ca^{2+} is important for the release of cell-matrix contacts at the rear end (Franco *et al.*, 2005) and transient increases in Ca^{2+} levels occur just before rear retraction (Doyle *et al.*, 2004). Over-expression of SK_{Ca} in melanoma MDA-MB-435 cells has been

suggested to control migration by regulating membrane potential and $[Ca^{2+}]_i$ (Potier *et al.*, 2006). In addition, it has been suggested that the role of $K_v1.1$ and $K_v1.5$ in wound healing is mediated via their effect on $[Ca^{2+}]_i$. K_v channels hyperpolarize the cell membrane potential, increasing the driving force for Ca^{2+} influx and increased $[Ca^{2+}]_i$ (Rao *et al.*, 2002). Supporting this notion, transformed MDCK-F cells transfected with $K_v1.4$ channels exhibited clustering of these channels at the leading edge of the lamellipodia, which could account for localized membrane potential changes needed to modulate $[Ca^{2+}]_i$ level and migration-related cytoskeletal mechanisms (Reinhardt *et al.*, 1998). Moreover, the fluxes of Na^+ and Cl^- ions are also controlled by membrane potential. These ions have also been reported to have a role in cell migration (Fraser *et al.*, 2003, Fraser *et al.*, 2004, Fraser *et al.*, 2005, Fulgenzi *et al.*, 2006).

Another mechanism that can explain the involvement of K^+ channels in cell migration is their influence on cell volume regulation. Phases of cell migration may involve localized transient changes of cell volume, where protrusion of the leading edge is accompanied by an increase in cell volume, whereas rear retraction is associated with cell shrinkage (Rotsch *et al.*, 2001). In addition, maintaining the proper cell volume is essential for the normal functioning of actin cytoskeleton (Pedersen *et al.*, 2001). Supporting this concept, the role of IK_{Ca} channels in cell migration might be mediated via cell volume regulation. These channels are distributed all over the cell membrane with higher channel densities at the front edge (Schwab *et al.*, 2006). However, they are more active at the rear of the cell, probably due to the $[Ca^{2+}]_i$ gradient across the cell. Opening of these channels leads to K^+ efflux, which may cause a localized cell shrinkage necessary for retraction of the trailing edge (Schwab *et al.*, 1999b, Schneider *et al.*, 2000). Based on these findings, it has been

suggested that IK_{Ca} channels are part of the cell migration machinery (Schwab *et al.*, 2006). Moreover, the ability of BK_{Ca} and Cl^- channels to regulate dynamic changes of cell shape and cell volume may be essential for glioma cell invasion through the narrow extracellular spaces in the brain (McFerrin *et al.*, 2006).

Many K^+ channels are highly expressed at the leading edge of migrating cells (Reinhardt *et al.*, 1998, Kindzelskii *et al.*, 2005, deHart *et al.*, 2008). It has been suggested that K^+ channels may act as sensors of the external electrical field and thereby effect directional migration of the cell in response to an external electric field (galvanotaxis) (Kindzelskii *et al.*, 2004, Kindzelskii *et al.*, 2005), a phenomenon suggested to take place in epithelial wound healing (McCaig *et al.*, 2005) and tumour cell invasion (Mycielska *et al.*, 2004).

Finally, it has been shown that some K^+ channels may physically associate with important protein components of the migratory machinery, such as integrins (Levite *et al.*, 2000, Artym *et al.*, 2002, Cherubini *et al.*, 2005) and FAK (Rezzonico *et al.*, 2003). Kir4.2 was shown to co-localize with $\alpha 9$ -integrins in focal adhesions at the leading edge of migrating fibroblasts and inhibition of these channels impaired integrin-dependent cell migration (deHart *et al.*, 2008). Interestingly, it has been shown that there is a reciprocal relationship between K^+ channels and the coupled migration-related proteins, since modulating the activity of one protein affects the activation state of the other. An important example is $K_v1.3$, which physically interacts with $\beta 1$ -integrin in lymphocytes (Levite *et al.*, 2000) and melanoma cells (Artym *et al.*, 2002). Such association can be initiated by cell adhesion and prevented by K^+ channel blockers. Moreover, $\beta 1$ -integrin activation stimulates $K_v1.3$ channels, whereas opening of $K_v1.3$ channels can lead to $\beta 1$ -integrin activation. This mutual relationship might be mediated via conformational coupling between the proteins.

hERG1 has also been reported to interact with components of focal adhesion complexes in tumour cells. I will discuss these studies later.

1.5 Limitation of studies on the contribution of K⁺ channels to tumorigenesis

Most of the above-mentioned studies that highlight the importance of K⁺ channels in tumorigenesis were performed in model cell-lines, which may have altered properties through maintenance in cell culture. Studies performed on primary tumours cells are essential to establish the functional contributions of K⁺ channels in cancer. Moreover, electrophysiological analysis of functional ion channels in tumours may require accurate simulation of the media conditions used for isolated cells to those found in the tumour microenvironment, since conditions such as hypoxia, presence/absence of growth factors and ionic composition can modulate channel expression and activity. Finally, it is not clear whether the altered expression of K⁺ channels in cancer cells has a role in initiation of tumorigenesis, or K⁺ channels are just some of an array of genes dysregulated in cancer cells. An alternative approach to investigate the role of certain K⁺ channels in tumour initiation is to test their abilities to transform epithelial cells upon transient or stable transfection. So far, only TASK-3 (Mu *et al.*, 2003), EAG (Pardo *et al.*, 1999) and hERG1 (Pier, 2007) channels have been reported to have oncogenic effects.

1.6 Oncogenic potential of specific types of K⁺ channels

1.6.1 TWIK-related acid-sensitive K⁺ channels (TASK-3, K_{2P}9.1 or KCNK9)

TASK-3 is a member of K_{2P} channels. These channels have been found to be over-expressed, mainly through genomic amplification, in several tumours including breast, lung,

prostate and colorectal cancers (Mu *et al.*, 2003, Kim *et al.*, 2004). It has been suggested that enhanced expression of these channels provides specific advantages to tumour cells, such as potentiation of proliferation and resistance to hypoxia and serum-deprivation. Over-expression of TASK-3 in partially transformed mouse embryonic fibroblast (C8) cells increased their survival rates in low serum and hypoxic conditions, promoted resistance to TNF α -induced apoptosis and induced tumour formation when injected in athymic mice (Mu *et al.*, 2003, Pei *et al.*, 2003). It has been proposed that the oncogenic effects of TASK-3 channels might be mediated through their oxygen-sensing capabilities, since TASK-3 has been identified as the O₂-sensitive K⁺ channel in the small cell lung carcinoma H146 cells (Hartness *et al.*, 2001). These effects are unlikely to be due to TASK-3 conductance, since hypoxia inhibits TASK-3 channel activity (Patel *et al.*, 2004).

In contrast, the oncogenic potential of these channels has been demonstrated to be dependent on ion conduction (Pei *et al.*, 2003). In this study, immunodeficient mice injected with C8 cells expressing WT TASK-3 channels developed larger tumours than those injected with a dominant-negative non-functional mutant (G95E TASK-3). This mutation lies within the selectivity filter and completely abolished K⁺ channel activity when expressed in *Xenopus* oocytes. Moreover, transfection of a lung cancer cell-line that highly expresses TASK-3 with G95E TASK-3 reduced its proliferation rate (Pei *et al.*, 2003). Taken together, these results strongly indicate a role of TASK-3 channel activity in tumour progression

On the other hand, TASK-3 channels have also been reported to play a role in neuronal apoptosis (Lauritzen *et al.*, 2003). This paradox might be explained if these channels play a pro-apoptotic or oncogenic roles dependent on cellular context (Patel *et al.*, 2004). In

addition, the magnitude of TASK-3 currents may be a critical factor for induction of either apoptosis or cell proliferation, since apoptosis require a large loss of cytosolic K^+ ions, an effect that leads to caspase activation and cell-shrinkage (Kunzelmann, 2005). In agreement with this, the magnitude of TASK-3 currents in proliferating cancer cells (Pei *et al.*, 2003) are much smaller than that in neurons (Lauritzen *et al.*, 2003).

1.6.2 EAG

EAG expression is widespread during development, but disappears from most tissues after differentiation and becomes localized to brain and placenta. However, EAG is found to be up-regulated in many cancer cell-lines, including HeLa, MCF-7 (breast cancer) and SH-SY5Y (retinoblastoma) cells (Pardo *et al.*, 1999), as well as in many primary cancer tumours, such as cervix carcinomas (Farias *et al.*, 2004), neuroblastomas (Meyer *et al.*, 1998), gliomas (Patt *et al.*, 2004) and melanomas (Meyer *et al.*, 1999). Moreover, using immunohistochemistry and real-time reverse transcription PCR techniques, two studies have confirmed the aberrant expression of EAG channels in more than 75% of tumour cells obtained from diverse origins (Hemmerlein *et al.*, 2006, Mello de Queiroz *et al.*, 2006). A functional EAG current has been demonstrated in various tumour cells indicating the proper cell-surface expression of these channels in tumours (Meyer *et al.*, 1998, Meyer *et al.*, 1999.). The limited expression of EAG channels in normal tissue outside the CNS has prompted investigators to suggest the use of these channels as tumour markers, as well as potential therapeutic targets (Pardo *et al.*, 2008).

It has been shown that the biophysical properties EAG currents can be modulated during the cell cycle (Bruggemann *et al.*, 1997). In this study, EAG currents expressed in *Xenopus* oocytes were reduced on stimulation of mitosis, an effect attributed to an increased

sensitivity to blockade by $[\text{Na}^+]_i$, since CHO cells stably transfected with EAG channels exhibited a greater block by $[\text{Na}^+]_i$ when synchronized into M phase (Pardo *et al.*, 1998). The strongest evidence for the oncogenic potential of EAG channels has been provided by Pardo *et al.* (1999). In this study, it was shown that expression of EAG, but not $\text{K}_v1.4$, in CHO cells could produce a transformed phenotype characterized by an increase in cell proliferation, loss of contact inhibition, substratum-independence of growth and *in vivo* tumour formation following injection of EAG-expressing CHO cells into immunodeficient (SCID) mice. In addition, the down-regulation of EAG expression in cancer cell-lines, using siRNAs or monoclonal antibodies, reduced cell proliferation (Pardo *et al.*, 1999, Mello de Queiroz *et al.*, 2006, Weber *et al.*, 2006, Gomez-Varela *et al.*, 2007). EAG expression may confer a selective growth advantage to tumours, since EAG-positive tumours showed an increased vascularization compared to EAG-negative tumours (Downie *et al.*, 2008). Moreover, EAG-expressing HEK cells showed higher HIF-1 α activity under mild hypoxic conditions and higher VEGF secretion than mock-transfected cells (Downie *et al.*, 2008).

The oncogenic potential of EAG is considered to be mediated through ion flux, since non-specific EAG blockers could be shown to decrease proliferation in breast cancer and melanoma cells (Gavrilova-Ruch *et al.*, 2002). Moreover, a monoclonal antibody that effectively blocks EAG channels, by targeting a sequence close to the channel pore region, was able to reduce colony formation for several EAG-expressing tumour cell-lines. Another antibody that did not affect the ion flow through EAG channels had no effect on colony formation. In addition, *in vivo* administration of the blocking antibody reduced tumour growth in two different models (Gomez-Varela *et al.*, 2007). Interestingly, another

paper has provided evidence that EAG-mediated effects may be independent of a functional current (Hegle *et al.*, 2006). In this study, expression of a non-conducting F465A EAG mutant (point mutation in the selectivity filter of the channel pore) in NIH-3T3 cells was shown to increase proliferation when compared to vector-transfected cells, to a similar extent to WT EAG channels, suggesting that EAG-mediated effects on cell proliferation can occur independently of EAG ion conduction. Moreover, mutations that increased the proportion of channels in the open state did not increase cell proliferation, which suggests that EAG-induced proliferation requires the channels to be in a closed conformation. The authors also showed that p38 MAPK inhibitors could block the proliferative effects of EAG expression. Based on these findings, these authors hypothesized that EAG may be acting as a 'hub' for the assembly of a signalling scaffold with conformational change exposing regions within the channel protein that interact with downstream signalling molecules (Hegle *et al.*, 2006). It has also been shown that NIH-3T3 cells and CHO cells stably expressing a non-conducting EAG pore mutant (G440S EAG) are able to induce tumour formation when injected into SCID mice. However, tumours were significantly lower in mass than those produced by cells expressing WT EAG channels, indicating that tumour progression may be only partly independent of ion permeation. However, in the same study, oral administration of the non-selective EAG blocker astemizole reduced the size of tumours induced by implantation of WT EAG-expressing CHO cells into SCID mice (Downie *et al.*, 2008). The authors explained this paradox by suggesting a conformational state-mediated oncogenic effect of EAG channels. Astemizole is open-channel blocker, which locks the channel in this conformation, whereas pore mutant channels are still able to undergo normal gating transitions (Downie *et al.*, 2008). Supporting this notion, EAG protein domains may have signalling roles. The PAS domain located at its *N*-terminus is

reported to regulate protein kinase activity and gene transcription (Gilles-Gonzalez *et al.*, 2004). Moreover, the EAG cytoplasmic domain can bind and constitutively activate Ca^{2+} /calmodulin-dependent protein kinase II (CaMKII) in *Drosophila*. The C terminal of the EAG channel has a CaMKII-binding motif, which shows homology to the auto-inhibitory domain of this kinase. Therefore, binding of CaMKII to EAG can block interaction of the auto-inhibitory domain to the catalytic site, rendering the kinase Ca^{2+} -independent (Griffith, 2004, Sun *et al.*, 2004).

1.6.3 hERG1

1.6.3.1 Evidence for implication of hERG1 in cancer

Changes in the gene expression and function of hERG1 channels during development may have provided the first clue of a potential role for these channels in cell proliferation and consequently, when dysregulated, tumorigenesis. hERG1 channels are widely expressed in embryonic tissues, but this expression is lost during differentiation. Thus, hERG1 expression is limited to excitable tissues, such as neuronal tissues, smooth muscle and the heart in adults. Interestingly several studies have shown that adult tissues may up-regulate hERG1 expression on neoplastic transformation. An important study that investigated the developmental changes of cardiac K^+ currents in mouse hearts has shown that I_{Kr} , the physiological ERG1 current in the heart, is the predominant repolarizing current in fetal mouse heart and disappears in adult mouse myocardium (Wang *et al.*, 1996a, Wang *et al.*, 1996b). These authors have shown, using electrophysiological methods, that I_{Kr} was the only K^+ current in fetal ventricular myocytes. In addition, dofetilide, a selective hERG1 blocker, was able to prolong the cardiac action potential duration in fetal ventricle by 137% while failing to affect action potential duration in adult myocardium. Moreover, using

radioligand binding techniques, [^3H]-dofetilide bound specifically and with affinity in preparations of fetal, but not adult, mouse ventricle. Intriguingly, it has also been shown that adult cardiac cells that undergo de-differentiation, or carcinogenesis, re-express the I_{hERG1} current (Bhattacharyya *et al.*, 1997, Yang *et al.*, 1997, Claycomb *et al.*, 1998, Kabir *et al.*, 2000). Similarly, quail neural crest-derived neurons and muscle cells only transiently express hERG1 currents at very early stages of their development. At later stages, hERG1 currents disappeared from mature neurons, which showed morphological and biochemical markers of differentiation, and are primarily replaced by inward rectifier-like K^+ currents (Arcangeli *et al.*, 1997, Crociani *et al.*, 2000). Moreover, various neuroblastomas, which arise from malignant transformation of neural crest cells, highly express a cell cycle-regulated hERG1 current (Arcangeli *et al.*, 1995, Faravelli *et al.*, 1996).

This unusual pattern of hERG1 expression has suggested a role of these channels in proliferation and implied that re-expression of hERG1 channels in adult tissues may induce unlimited proliferation and neoplastic transformation. It has been suggested that during development, hERG1 channel expression allows the cells to divide and, as cells differentiate, hERG1 channel expression is replaced by that of other inward rectifier-like K^+ channels, which are able to hyperpolarize fully the membrane potential, and inhibit proliferation (Arcangeli *et al.*, 1997, Crociani *et al.*, 2000). During transformation and de-differentiation, the highly proliferating cancer cell phenotype correlates with re-expression of hERG1 channels (Bianchi *et al.*, 1998). In agreement with this assumption, normal human myotube cells display a K^+ current that is similar to a classical inward rectifier-like K^+ channel (Cs^+ -sensitive, E4031-insensitive). However, these currents were not detected in neoplastic TE671 rhabdomyosarcoma cells, which showed a current with characteristics

similar to hERG1 (Bianchi *et al.*, 1998). Moreover, induction of differentiation in neuroblastoma cells, via long-term treatment with retinoic acid, triggers the expression of an inward rectifier-like K⁺ current (Arcangeli *et al.*, 1998), without loss of hERG1 expression (Arcangeli *et al.*, 1999).

The ectopic expression of the full-length hERG1 protein and its splice variants in neoplastic cells has provided additional evidence for their role in oncogenesis. It has been shown that many transformed cell-lines (including SH-SY5Y, rhabdomyosarcoma TE671, mammary adenocarcinoma SK-BR3, hematopoietic K562, monoblastic leukaemia FLG29, breast cancer MCF-7, melanoma MDA-MB-435S, colon cancer H630 and HCT116, and gastric cancer SGC7901, AGS, MGC803 and MKN45 cells) express hERG1 (Bianchi *et al.*, 1998, Smith *et al.*, 2002a, Lastraioli *et al.*, 2004, Chen *et al.*, 2005b, Shao *et al.*, 2005, Li *et al.*, 2008, Roy *et al.*, 2008, Afrasiabi *et al.*, 2010). hERG1 channels have also been found to be expressed in many primary tumours, such as human endometrial cancer (Cherubini *et al.*, 2000), chronic lymphocytic leukaemia (Smith *et al.*, 2002a), myeloid leukaemia (Pillozzi *et al.*, 2002), colorectal carcinomas (Lastraioli *et al.*, 2004, Dolderer *et al.*, 2009), gastric cancer (Shao *et al.*, 2005, Shao *et al.*, 2008, Ding *et al.*, 2009), esophageal carcinoma (Ding *et al.*, 2008), low grade gliomas (Patt *et al.*, 2004) and high grade astrocytic gliomas (glioblastoma multiforme (GBM)) (Masi *et al.*, 2005). hERG1 mRNA was also detected in leukaemic stems cells, but not normal hematopoietic stem cells (Li *et al.*, 2008). Moreover, hERG2 is expressed in a human retinoblastoma cell-line and the neural tissue-specific hERG3 gene is surprisingly expressed in SK-Br3 mammary adenocarcinoma cells (Crociani *et al.*, 2003). Both hERG2 and hERG3 genes have also been detected in several squamous and endometrial uterine cancer cell-lines (Suzuki *et al.*, 2004). In contrast,

hERG1 expression has never been reported in the corresponding non-cancerous tissues from which these tumours originate. It has also been suggested that hERG1 might be used as a tumour marker of colorectal carcinomas. hERG1 mRNA expression (assayed by RT-PCR) and hERG1 protein (assayed by immunohistochemistry (IHC)) was detected in all primary carcinomas tested (23 samples), whereas all non-carcinoma negative-control samples (43 samples) did not show hERG1 expression, except for one sample from a patient who developed tumour recurrence and large adenomas. These results indicate that hERG1 expression can occur at very early stages in tumour development and can be a marker of a pre-cancerous phenotype (Dolderer *et al.*, 2009).

The transcriptional mechanisms underlying hERG1 up-regulation during tumorigenesis have been revealed (Lin *et al.*, 2007). In this study, it was shown that the promoter region of the hERG1 gene contains binding sites for several oncoproteins (e.g. Sp1 and NF- κ B) and tumour suppressors (e.g. NKx3.1), which regulate hERG1 transcription in tumour cells. Inhibiting the activity of the oncoproteins Sp1 or NF- κ B, using inhibitors, siRNAs, or by mutational disruption of their binding sites in hERG1 promoter, decreased hERG1 promoter activity (assayed by measuring promoter-derived luciferase expression) and endogenous hERG1 transcription (determined by realtime-PCR) in the SK-Br3 tumour cell-line. Conversely, impairing NKx3.1 activity increased hERG1 transcription (Lin *et al.*, 2007).

It has also been demonstrated that leukemic (e.g. acute myeloid leukaemia (AML)) (Bianchi *et al.*, 1998, Pillozzi *et al.*, 2002, Pillozzi *et al.*, 2007) and neuroblastoma (Crociani *et al.*, 2003) tumour cells also co-express the N-truncated hERG1b form alongside full-length hERG1 protein. When hERG1b is expressed at the plasma membrane

it can form heterotetramers with hERG1. In fact, hERG1b is the predominantly expressed isoform in leukemic FLG-29 cells resulting in hERG1 currents with faster deactivation rates and a right-shifted I-V curve (Bianchi *et al.*, 1998). The expression of both isoforms in human neuroblastoma SH-SY5Y cells is cell cycle-dependent, where hERG1 is up-regulated during G1 phase and hERG1b is up-regulated during S phase (Crociani *et al.*, 2003). Another variant, hERG1b_{USO}, which lacks both the PAS and cNBD domains, has been cloned from neuroblastoma and leukaemia cells (Guasti *et al.*, 2008). The USO-hERG1 isoforms (hERG1_{USO} and hERG1b_{USO}) are highly expressed, both at the mRNA and protein level, in various tumour cell-lines and primary tumours despite being minimally expressed in healthy human tissues (Guasti *et al.*, 2008).

1.6.3.2 hERG1 and tumour proliferation

hERG1 channels have been implicated in different aspects of cancer progression. Several reports suggest a role for hERG1 in cancer cell proliferation. hERG1 mRNA expression was easily detected in peripheral blood mononuclear cells enriched in CD34⁺ (PBCD34⁺; taken as representative of hemopoietic progenitors) only when these cells were stimulated to enter S phase of the mitotic cycle by *in vitro* treatment with cytokines or growth factors for 12 h (Pillozzi *et al.*, 2002). The specific hERG1 inhibitors E4031 and WAY123398 reduced proliferation of leukemic K562, CEM, U937 and FLG29.1 cell-lines that express hERG1. However, the same inhibitors failed to affect proliferation in leukaemic HL60 cells that lack hERG1 expression (Pillozzi *et al.*, 2002, Smith *et al.*, 2002a). Similarly, E4031 and WAY123398 impaired the proliferation of hERG1-expressing SH-SY5Y cells, but did not affect that of neuroblastoma LAN1 clone AE12 cells, which do not express hERG1 (Crociani *et al.*, 2003). Another selective hERG1 inhibitor, cisapride produced

concentration-dependent inhibitory effects on gastric cancer SGC7901, AGS, MGC803 and MKN45 cell proliferation (Shao *et al.*, 2005). Moreover, WAY123398 also showed a strong inhibition of colony formation from primary AML-blasts when seeded in semi-solid medium (Pillozzi *et al.*, 2002). Furthermore, erythromycin (which blocks hERG1) reduced the proliferation of the highly hERG1-expressing human colon adenocarcinoma cell-line-HT-29 and displayed synergistic effects with the anti-cancer agents, vincristine and paclitaxel (Chen *et al.*, 2005b). It has also been suggested that hERG1 over-expression in tumour cells mediates the growth-promoting effects induced by activation of oncoproteins Sp1 and NF- κ B and inactivation of the tumour suppressor NKx 3.1 (Lin *et al.*, 2007). In this study, inhibition of hERG1 activity by dofetilide, E4031 or cisapiride slowed the proliferation of hERG1-expressing SK-Br3 and SH-SY5Y tumour cells, but failed to affect proliferation of A549 tumour cells that do not express hERG1. Moreover, transiently expressing hERG1, but not K_v4.3, in A549 tumour cells increased their proliferation rate, an effect that was reversed by dofetilide treatment. Furthermore, knocking-down Sp1 and NF- κ B expression using specific siRNAs decreased, while knocking-down NKx 3.1 increased, proliferation of several tumour cell-lines and these effect was partly abolished by pre-treating cells with dofetilide, indicating that hERG1 can mediate the growth signals elicited by oncoprotein activation, or the silencing of a tumour suppressor (Lin *et al.*, 2007). In a recent study, E4031 or cisapiride was able to attenuate the proliferation of melanoma MDA-MB-435S cell-line that expresses hERG1 mRNA and protein (Afrasiabi *et al.*, 2010). However, the results obtained using hERG1 inhibitors should be interpreted cautiously and I will discuss this aspect of previous studies further later.

Interestingly, although stable hERG1 expression in NIH-3T3 did not affect proliferation rate, it increased the ability of cells to grow over each other in confluent cultures, possibly due to loss of contact inhibition, resulting in a substantial increase in post-confluency cell density (Pier, 2007). Silencing hERG1 and hERG1b gene expression using short-hairpin RNA (shRNA) interference in SH-SY5Y neuroblastoma cells resulted in a decrease in cell proliferation (Zhao *et al.*, 2008). These authors also investigated the effect of hERG1 inhibition on tumour growth *in vivo* using a mouse model of human neuroblastoma xenograft. Intra-tumour injection with a shRNA-expressing plasmid that targets hERG1/hERG1b substantially reduced the size of tumours during a 14 day follow-up period (Zhao *et al.*, 2008).

The suggested anti-proliferative effect mediated by hERG1 inhibition has been argued to be due to a retardation of cell cycle progression (Pillozzi *et al.*, 2002, Shao *et al.*, 2005, Li *et al.*, 2007a, Shao *et al.*, 2008, Zhao *et al.*, 2008) and/or induction of apoptosis (Shao *et al.*, 2005, Shao *et al.*, 2008). Cell cycle analysis of leukemic FLG29.1, gastric cancer and neuroblastoma SH-SY5Y cells after hERG1 channel inhibition revealed an increase in the number of cells in G1 phase (Pillozzi *et al.*, 2002, Shao *et al.*, 2005, Zhao *et al.*, 2008), whereas blocking hERG1 channels in hERG1-expressing uterine cancer cells arrested the cells in G2/M phase (Suzuki *et al.*, 2004). It has also been shown that hERG1 channels may be important for cell volume regulation, an essential process for cell cycle progression, of the hERG1-expressing breast cancer MCF-7 cells, since E4031 inhibited their ability to undergo a regulatory volume decrease (RVD) after initial cell swelling when placed into a hypo-osmotic environment (Roy *et al.*, 2008). More recently, Afrasiabi *et al.* (2010) attributed the anti-proliferative effect of the hERG1 inhibitor E4031 on the hERG1-

expressing melanoma MDA-MB-435S cell-line to a decrease in phosphorylation of mitogen-activated protein kinase (MAPK) and a decrease in expression of *c-fos*, a transcription factor downstream of MAPK signalling known to be important for cell proliferation (Afrasiabi *et al.*, 2010).

The mechanisms underlying hERG1 channel involvement in tumour cell proliferation are being actively debated. On the one hand, it has been postulated that hERG1 can affect tumour cell proliferation via regulation of membrane potential. Typical hERG1 currents were identified in neuroblastoma, as well as non-neuronal, transformed cell-lines, and were suggested to be a key determinant of resting membrane potential. In contrast, normal parental cells from the relevant cell-lineages did not express hERG1 currents and only expressed inward rectifier-like K^+ currents. The substitution of native inward rectifier-like K^+ currents in normal tissues by hERG1 current after neoplastic transformation may contribute to the depolarized membrane potential of transformed cells, which is thought to be a prerequisite for unlimited cell proliferation. This hypothesis is consistent with the biophysical properties of hERG1 currents. First, the crossover between steady-state activation and inactivation curves of hERG1 produces a significant current at a V_m around -40 mV, a value close to resting membrane potential of tumours cells. Second, hERG1 currents have a limited hyperpolarizing effect (when compared to inward rectifier-like K^+ currents), since hERG1 channels are deactivated at membrane potentials negative to -50 mV. In agreement with this, the resting potential (V_{REST}) values of several tumour cell-lines that express I_{hERG1} have been found to be more depolarized than those of the corresponding (non-hERG1-expressing) normal tissues, from which they originate (Arcangeli *et al.*, 1995, Bianchi *et al.*, 1998). hERG1 channel activity can be enhanced by the tumour

microenvironment. Tumour cells exhibit a high extracellular K^+ ($[K^+]_o$) and lower oxygen (PO_2) tension. These conditions can contribute to a higher hERG1 channel activity as increased $[K^+]_o$ increases open probability of the channels and chronic exposure to hypoxia may also modulate hERG1 current (Fontana *et al.*, 2001). Moreover, the voltage-dependence of activation and inactivation of hERG1 currents varies throughout the cell cycle (Arcangeli *et al.*, 1995, Meyer *et al.*, 1998). Synchronizing neuroblastoma cells into S phase was associated with a positive shift of the $V_{0.5}$ of hERG1 current inactivation that correlated with a depolarization of resting membrane potential. This may suggest that hERG1 channels are regulated to affect the resting potential at critical points of the cell cycle, which may be important for cell cycle progression. The up-regulation of hERG1b during S1 phase of the cell cycle may also contribute to the relative depolarization of the membrane (Crociani *et al.*, 2003), which may be essential for DNA synthesis as cells in the active proliferative and DNA-synthetic phase have relatively depolarized V_{REST} (Binggeli *et al.*, 1986, Crociani *et al.*, 2003). The importance of hERG1 channel activity in cell cycle progression in tumour cells is further supported by reports that demonstrate that hERG1 current inhibition by pharmacological inhibitors or siRNAs in leukaemic FLG 29.1, gastric colon cancer and neuroblastoma SH-SY5Y cells inhibited proliferation and colony formation and led to a partial block of cells in G1 (Pillozzi *et al.*, 2002, Shao *et al.*, 2005, Li *et al.*, 2008, Shao *et al.*, 2008, Zhao *et al.*, 2008).

In contrast, some studies do not support a role for the hERG1 current in cancer progression. Although specific blockers of hERG1 channels were able to reduce proliferation (Pillozzi *et al.*, 2002, Smith *et al.*, 2002a, Shao *et al.*, 2005, Li *et al.*, 2008), these blockers were often used at very high concentrations which might have induced additional hERG1-independent

non-specific effects. WAY123398 (at 1 μM) is able to inhibit completely hERG1 current in leukaemic FLG 29.1 cells, however a 40-fold higher concentration of this compound was needed to reduce cell proliferation (Pillozzi *et al.*, 2002). Although the half-maximal inhibitory concentration (IC_{50}) of E4031 for hERG1 current in leukaemic K562 cells was found to be ~ 5 nM (Cavarra *et al.*, 2007) and 1 μM E4031 completely abolished hERG1 currents in K562, CEM and U937 cells, this concentration of inhibitor only reduced the proliferation in these cells by 14-17% (Smith *et al.*, 2002a, Li *et al.*, 2008). Moreover, the proliferation of NIH-3T3 cells stably-expressing hERG1 was not affected by the hERG1 inhibitor terfenadine (10 μM) (Pier, 2007). Similarly, E4031 (3 μM) and ERGtoxin (300 nM) failed to affect cell proliferation in hERG1-expressing breast cancer MCF-7 cells (Roy *et al.*, 2008). Moreover, the hERG1 activator PD118057 (10 μM) failed to affect the proliferation of the hERG1-expressing melanoma MDA-MB-435S cell-line (Afrasiabi *et al.*, 2010).

In another study by Wang *et al.* (2002), hERG1 expression in three tumour cell-lines (SH-SY5Y, SK-BR-3, HL-1) was found to enhance proliferation induced by low $\text{TNF}\alpha$ concentrations. However, the increase in proliferation was unaffected by hERG1 channel blockade by dofetilide (1 μM). A similar enhancing effect of $\text{TNF}\alpha$ -induced cell proliferation was seen in HEK293 cells expressing S633A hERG1, a non-conducting dominant-negative mutant form of hERG1 that is trafficked to the membrane. These authors suggested that hERG1 channels may help recruit the TNF receptor-1 (TNFR1) to the cell-surface, since hERG1 could be co-immunoprecipitated with TNFR1. Moreover, hERG1 channel expression correlated with an increased translocation and activation of NF-

κ B (Wang *et al.*, 2002a), which is a downstream target of the TNFR1 and its activation may have an oncogenic effect (Richmond, 2002).

If hERG1-mediated effects were merely due to K^+ ion flux and the resulting effects on membrane potential, it would be expected that increased expression of any K^+ channels could possess oncogenic potential. However, only stable expression of EAG in CHO cells (Pardo *et al.*, 1999), TASK-3 in mouse embryonic (C8) fibroblasts, or hERG1 in NIH-3T3 cells (Pier, 2007) produced a transformed phenotype.

1.6.3.3 The role of hERG1 in tumour cell migration and invasiveness

hERG1 channels have also been implicated in the control of cell migration and tumour invasion. The first evidence for this was provided by Lastraioli *et al.* (2004), who studied the effects of hERG1 channel activity on the migration of colon cancer cells through synthetic matrix-coated filters inserted into Boyden chambers. Colon cancer cell-lines expressing high levels of hERG1 exhibited increased cell migration relative to cells expressing lower levels of hERG1. Moreover, the migration of these cells was reduced in the presence WAY123398 (albeit at a high (40 μ M) concentration). The same authors showed that the migration of HEK293 cells stably transfected with hERG1 cDNA were about 2-fold higher compared to cells transfected with empty vector (Lastraioli *et al.*, 2004). It has also been suggested that hERG1 currents mediate stromal cell-derived factor-1 (SDF-1) -induced migration of leukemic cell-lines, leukaemic stem cells and primary acute leukaemic cells (Li *et al.*, 2009). In this study, E4031 (1 μ M) decreased the number of leukemic cells migrating towards a SDF-1-containing compartment. Moreover, SDF-1 has been shown to enhance hERG1 currents expressed in oocytes and HEK-hERG cells (Li *et al.*, 2009). More recently, treatment of melanoma MDA-MB-435D cells that express

hERG1 mRNA and protein with E4031 (10 μ M) or siRNAs against hERG1 decreased the number of cells migrating through a collagen matrix. In the same study, addition of the hERG1 activator PD118057 (10 μ M) produced a 3-fold increase in the number of migrated cells compared to vehicle-treated cells (Afrasiabi *et al.*, 2010).

hERG1 channels have also been shown to mediate VEGF-dependent migration of AML cells (Pillozzi *et al.*, 2007). In this study, treatment of AML with a specific FLT-1 ligand (VEGF₁₆₅) alone, or in combination with a β 1-integrin-activating antibody (TS2/16) increased the level of tyrosine phosphorylation of FLT-1 and increased phosphorylation of Akt (a downstream signalling molecule of FLT-1 activation). These treatments also enhanced cell migration through fibronectin-coated porous membranes. The VEGF₁₆₅ \pm TS2/16-mediated effects on AML cells were abolished by pre-treatment with hERG1 inhibitors WAY123398 or E4031. Moreover, immunodeficient mice injected with primary hERG1-positive AML-blasts displayed higher blood, hepatic and splenic invasion and increased angiogenesis than those injected with hERG1-negative AML-blasts (Pillozzi *et al.*, 2007). Taken together, these data suggest that hERG1 channel activity can switch on FLT-1 signalling leading to an increase in cell motility and trans-endothelial migration (Pillozzi *et al.*, 2007). In addition, stable expression of hERG1 in NIH-3T3 cells produced an increased rate of cell migration into an artificial wound made in a confluent cell monolayer, when compared to mock-transfected cells (Pier, 2007).

1.6.3.4 hERG1 and tumour angiogenesis

hERG1 channel activity may contribute to malignancy through increasing vascular endothelial growth factor (VEGF) secretion, which can stimulate neo-angiogenesis typical of high-grade gliomas and metastatic leukaemias (Pillozzi *et al.*, 2002, Masi *et al.*, 2005,

Pillozzi *et al.*, 2007). Inhibition of hERG1 current in U138, a glioma cell-line that expresses hERG1, by WAY123398 or E4031 produces concentration-dependent reductions in both VEGF mRNA expression and secretion (Masi *et al.*, 2005).

1.6.3.5 Interaction of hERG1 channels with integrins

There is growing evidence suggesting that ion channels may be able to modulate intracellular signal transduction pathways independently of ion conduction or changes in membrane potential (Kaczmarek, 2006). Integrins interact with some ion channels, including hERG1, and via this association, can affect cellular functions. Integrins may transduce extracellular signals that affect ion fluxes. On the other hand, ion channel signalling/activity may modulate integrin expression and activation and influence adhesion to the extracellular matrix (ECM). Modulation of adhesion to ECM could contribute to the previously mentioned oncogenic role of hERG1 in improving cell motility and enhancing invasion and neo-angiogenesis of tumour cells. These integrin-ion channel interactions may require the formation of supramolecular complexes at the plasma membrane of tumour cells that can recruit other transmembrane proteins (e.g. growth factor and chemokine receptors), scaffolding proteins, cytoskeletal proteins and cytoplasmic signalling proteins. These multiprotein complexes localize integrins and ion channels at the plasma membrane where they can act as signalling platforms affecting many aspects of tumour progression.

hERG1 current density (current amplitude normalized to capacitance, a measure of membrane surface area) was increased when hERG1-expressing cells adhered to ECM: examples include the binding of mouse neuroblastoma cells to fibronectin (Arcangeli *et al.*, 1993), human neuroblastomas to soluble or bound laminin (Arcangeli *et al.*, 1996, Cherubini *et al.*, 2005), FLG29.1 leukemic cells to fibronectin and/or vitronectin (Hofmann

et al., 2001), and HEK cells stably expressing hERG1 to fibronectin (Cherubini *et al.*, 2005). No increase in hERG1 current density was observed when these cells adhered to albumin-coated surfaces. Moreover, hERG1 currents were enhanced without any increase in hERG1 mRNA levels or hERG1 surface protein expression. Furthermore, this effect was mimicked by treating ECM-bound or suspended tumour cells with antibodies that activate β 1-integrins. Overall, these findings indicate that β 1-integrin activation *per se*, not necessarily being induced via ligation to ECM proteins, causes hERG1 channel activation. It has been suggested that signalling proteins downstream of integrin activation can modulate hERG1 channel activity (Cayabyab *et al.*, 2002, Miranda *et al.*, 2005). Indeed, the β 1-integrin-dependent activation of hERG1 may be mediated by pertussis toxin-sensitive G_i proteins, since pre-incubating FLG29.1 cells with pertussis toxin for 12 h inhibited hERG1 current activation observed on binding to fibronectin, or exposure to activating β 1-antibodies (Arcangeli *et al.*, 1993, Hofmann *et al.*, 2001). hERG1 channels can also affect integrin expression and/or activation (Arcangeli *et al.*, 1993, Hofmann *et al.*, 2001, Cherubini *et al.*, 2005). hERG1 activation induced by binding of leukemic FLG29.1 cells to fibronectin via β 1-integrins has been shown to be necessary for up-regulation of another integrin, the vitronectin receptor $\alpha_v\beta_3$ (Hofmann *et al.*, 2001). Moreover, hERG1 channels are important for activation of focal adhesion kinase (FAK) and the small GTPase, Rac1 (Cherubini *et al.*, 2005) and both of these effectors can modulate integrin activity as well as integrin-regulated downstream signalling. In this context, hERG1 channels function can be viewed as becoming bidirectional (Arcangeli *et al.*, 2006).

This reciprocal relationship between β 1-integrin subunits and hERG1 channels has been shown to occur through a physical association based on co-immunoprecipitation

experiments performed on AML, neuroblastoma and HEK293 cells expressing recombinant hERG1 (Cherubini *et al.*, 2002, Cherubini *et al.*, 2005, Pillozzi *et al.*, 2007). These associations may be mediated via the N-terminal of hERG1 as β 1-integrins were only able to form a complex with the full length hERG1, not hERG1b (Cherubini *et al.*, 2005). These β 1-integrin-hERG1 complexes are also suggested to localize in caveolae/lipid rafts, as both proteins co-immunoprecipitated with caveolin-1. Surprisingly, the immature form of hERG1 also associates with β 1-integrins (Cherubini *et al.*, 2005). Since most hERG1 immature forms are retained in the endoplasmic reticulum, such association may occur early before full protein maturation and translocation to the plasma membrane.

There is also an evidence for a physical association between ERG and Src tyrosine kinases in rat microglia MLS-9 cells. Src and ERG proteins co-immunoprecipitate, and ERG has sequences that resemble SH2 and SH3 binding motifs used by Src proteins (Cayabyab *et al.*, 2002). Tyrosine phosphorylation of hERG1 by Src increases ERG current and produces a slowed deactivation and a left-shift in the voltage-dependence of activation (Cayabyab *et al.*, 2002). An association between hERG1 channels and 14-3-3 proteins has also been reported (Kagan *et al.*, 2002).

The functional importance of hERG1- β 1-integrin complexes with other proteins in tumour cells could be many-fold. hERG1-mediated Rac1 activation may be essential for an increased motility and invasive phenotype of hERG1-expressing tumour cells. hERG1 is suggested to recruit and activate FAK, which is known to be involved in transformation, and many cancers exhibit increased FAK activation (Weiner *et al.*, 1993, Agochiya *et al.*, 1999, Xu *et al.*, 2000). The assembly of a hERG1- β 1-integrin-FLT-1 complex in AML cells has been proposed to be important for activation of FLT-1 and its downstream

signalling pathways, which play a role in VEGF secretion, proliferation and migration of AML cells leading to an enhanced ability to invade the peripheral circulation and extra-medullary sites in immunodeficient mice (Pillozzi *et al.*, 2007). A hERG1- β 1-integrin-CXCR4 complex in childhood Acute B Lymphoblastic Leukaemia (B-ALL) may contribute to its drug resistance, since hERG1 channel blockade increases the chemosensitivity of these cells to corticosteroids (Pillozzi *et al.*, 2010).

Reports about interactions of hERG1 with cell surface receptors and signalling proteins in tumour cells may suggest that the oncogenic role of hERG1 may occur independently of ion flux. hERG1 might affect signalling by partner proteins via conformational coupling rather than channel-mediated ion fluxes and/or changes in membrane potential. However, many reports indicate, through use of specific hERG1 inhibitors, that hERG1 channel activity is important for the signalling activity of the entire complex. An alternative explanation is that the role of hERG1 in these complexes may still be dependent on membrane potential changes if the channel modulatory domains are conformationally restricted to certain gating state(s) of the channel; in other words, hERG1 effects on associated partner proteins may be mediated via a voltage-dependent conformational state. Whether or not these states are associated with ion flux needs to be elucidated, particularly if hERG1 is to be as a target for treating cancer given the known cardiac side effects of hERG1 inhibitors.

Finally, the above-mentioned interactions are presently based solely on co-immunoprecipitation experiments and therefore should be interpreted cautiously and confirmed using alternate experimental approaches.

1.6.3.6 Are hERG1 channels involved in tumour adaptation to hypoxia?

Cancer cells develop in a hypoxic microenvironment. Tumour hypoxia is caused by uncontrolled cell proliferation and a lack of blood supply due to angiogenesis not keeping up with the metabolic demand of the growing mass. Overcoming hypoxia is a critical stage in cancer development (Vaupel *et al.*, 1989).

hERG1 channels may be involved in oxygen-sensing. ERG1 currents have been detected in the glomus cells of the rabbit carotid body, where they may contribute to maintenance of resting membrane potential. Blocking ERG currents with dofetilide depolarized resting membrane potential, increased $[Ca^{2+}]_i$ and increased impulse frequency recorded from carotid sinus nerve innervating the carotid body, mimicking the effect of hypoxia on the carotid sinus nerve (Overholt *et al.*, 2000). However, this does not mean that hERG1 channels are acting as chemoreceptors in these cells. Moreover, direct evidence of oxygen tension acutely altering hERG1 channel function has not been reported.

Hypoxia can modulate hERG1 currents by modulating the redox state of the cells or the levels of reactive oxygen species (ROS). ROS, generated by prolonged hypoxia, have been shown to decrease hERG1 current in HEK-hERG cells by inhibiting hERG1 maturation and trafficking (Nanduri *et al.*, 2009). The ROS-mediated inhibition of hERG1 currents can lead to membrane depolarization and thereby increase sensory activity. Conversely, enhancement of ROS production, induced by the perfusion with iron/ascorbic acid, have been reported to acutely increase hERG1 outward currents expressed in *Xenopus* oocytes (Taglialatela *et al.*, 1997). Moreover, it has been shown that hERG1 currents in SH-SY5Y cells are modulated by longer-term exposure to hypoxia, which produces a slowing in deactivation kinetics and a negative shift in the voltage-dependence of activation (Fontana

et al., 2001). This modulation results in an increase in hERG1 current at the range of membrane potentials typical for V_{REST} of tumour cells and therefore may help to counteract hypoxia-mediated membrane depolarization (Fontana *et al.*, 2001). Hypoxia can produce a depolarization of V_{REST} due to an increase of extracellular K^+ (Hansen, 1985). However, sustained ischemia during tumour progression can eventually lead to ATP deficits and failure of the Na^+/K^+ ATPase, resulting in an increase of $[\text{Na}^+]_i$ and enhanced membrane depolarization (Calabresi *et al.*, 1995). Such effects may be counterbalanced by an increase of hyperpolarizing hERG1 currents in hypoxic tumour cells (Fontana *et al.*, 2001).

The presence of a PAS domain in hERG1 channels is another reason for them being candidates for oxygen-sensing. The PAS domain belongs to a family of sensor domains used in signal transduction. These domains are reported to play roles in detection and adaptation to environmental changes (Gu *et al.*, 2000). Although PAS domains in different proteins share little sequence homology, they have conserved regions of flexibility. This may indicate that PAS domains signal in a similar manner regardless of the ligand bound (Vreede *et al.*, 2003) and the PAS domain has been shown to give oxygen-sensing capability to other unrelated proteins (Kurokawa *et al.*, 2004). A protein with a PAS domain can transduce a signal by binding to another PAS-containing protein and changing its conformation. PAS domains bind heme and confer sensitivity to signalling molecules such as nitric oxide, carbon monoxide, as well as O_2 (Gilles-Gonzalez *et al.*, 2004). Whether this occurs in hERG1 is unknown, although it may be supported by the findings of a recent study by Kolbe *et al.* (2010) who showed that hERG1b (which lacks a PAS domain) or a hERG1 mutant with a small deletion (Δ 2-15) within the PAS domain exhibited lower sensitivity to inhibition by ROS than hERG1. Using mutagenesis, these authors also

showed that Cys-723 within the hERG1-linker region is essential for hERG1 functional modification by ROS (Kolbe *et al.*, 2010), highlighting an alternative (PAS-independent) mechanism for hERG1 regulation by hypoxia.

Crociani *et al.* (2003) have suggested that the ability of some tumour cells to modulate relative expression of hERG1 and hERG1b (which lacks a PAS domain) could play a role in their adaptation to hypoxia (Crociani *et al.*, 2003). According to this hypothesis, tumour cells reduce their hERG1b/hERG1 expression ratio during hypoxia, which induces a hyperpolarization of V_{REST} . When normoxic conditions are restored, the hERG1b/hERG1 ratio can be up-regulated to facilitate membrane depolarization and sustain cell growth (Crociani *et al.*, 2003). However, this model is speculative and requires convincing experimental support.

1.6.3.7 hERG1: a regulator of tumour apoptosis?

It has been shown that hERG1 conductance facilitates apoptosis induced by high concentrations of TNF α (1-10 ng mL⁻¹), or H₂O₂ (400 μ M) in hERG1-expressing tumour cell-lines and HEK-hERG cells, as compared to tumour (and HEK) cell-lines that do not express hERG1 (Wang *et al.*, 2002a, Han *et al.*, 2004). The enhancement of apoptosis observed in hERG1-expressing cells can be blocked by treating cells with dofetilide or E4031. Moreover, H₂O₂ exposure increased hERG1 current and produced a leftward-shift in the voltage-dependency of hERG1 activation. Interestingly, on H₂O₂ exposure, HEK-hERG displayed higher levels of caspase activity, phospho-p38 and -JNK1 compared to HEK cells (Han *et al.*, 2004), indicating that these signalling pathways may be involved in hERG1-facilitated apoptosis. In sharp contrast, it has also been shown that inhibition of

hERG1 by the anti-hypertensive agent doxazosin promotes apoptosis in HEK-hERG cells via an uncharacterized mechanism (Thomas *et al.*, 2008).

1.6.3.8 hERG1 expression in tumours as a prognostic indicator

The expression of hERG1 in a variety of different cancers raised the question of whether there is a link between expression level and prognostic outcome, and whether hERG1 could be used as a biomarker. The level of expression of the hERG1 protein correlates well with metastatically-aggressive tumours. Lastraioli *et al.* (2004) performed an immunohistochemical analysis of hERG1 protein expression in normal and neoplastic colorectal tissues. Expression of hERG1 protein was not detected in normal human colonic mucosa and adenomas. However, 75% of non-metastatic primary colorectal cancers displayed hERG1 protein expression while metastatic colonic adenocarcinoma tissues studied were 100% positive for hERG1 protein expression and showed widespread homogenous staining for the hERG1 protein (Lastraioli *et al.*, 2004). In another study by Masi *et al.* (2005), high-grade primary astrocytic gliomas displayed higher expression of hERG1 mRNA and I_{hERG1} current compared to low-grade gliomas. hERG1 protein was also detected by IHC in the cytoplasm of high-grade gliomas (Masi *et al.*, 2005). hERG1 expression in leukaemia patients also correlated with a higher probability of relapse and shorter survival times (Pillozzi *et al.*, 2007). Likewise, in patients with gastric cancer or esophageal carcinoma, hERG1 protein expression is linked to shorter survival times compared to patients negative for hERG1 expression (Ding *et al.*, 2008, Ding *et al.*, 2009). Moreover, tumour cell-lines that highly express hERG1 showed high resistance to the chemotherapeutic agent doxorubicin compared to those with lower hERG1 expression. Erythromycin, which can block hERG1 channels, synergistically enhanced the

chemosensitivity of doxorubicin (Chen *et al.*, 2005a). Collectively, these data appear to suggest that hERG1 expression level in tumours may be an indicator of poor prognostic outcome.

1.6.3.9 Role of hERG1 isoforms in cancer

The aberrant expression of different hERG1 isoforms alongside the full-length hERG1 protein in tumours has complicated our understanding of their contribution to oncogenic transformation. It has been shown that USO isoforms, abundantly expressed in many tumours, regulate the cell surface expression of hERG1 channels and I_{hERG} current density in heterologous systems and tumour cells. These isoforms are retained intracellularly in the endoplasmic reticulum and are not trafficked to the cell surface. Moreover, they can form heteromultimeric complexes with full-length hERG1. The resultant complexes fail to translocate to the cell surface and undergo ubiquitin-dependent degradation leading to a decrease in cellular hERG1 current. Such a regulatory mechanism may be important to maintain a finite number of functional hERG1 channels in the tumour cell membrane that clamp the membrane voltage at values appropriate for cell proliferation and avoidance of apoptosis and differentiation. In agreement with this hypothesis, knocking down USO isoforms in tumour cell-lines using siRNAs results in an increase in hERG1 current, an effect that is associated with neurite outgrowth in neuroblastomas and apoptosis in leukaemia cells (Guasti *et al.*, 2008). Moreover, differentiation of NG108-15 neuroblastoma x glioma cells is associated with a 2-fold increase of hERG1-like current compared to undifferentiated and proliferating cells (Pancrazio *et al.*, 1999).

Immunoprecipitation experiments confirm that both hERG1 and hERG1b proteins are expressed at the plasma membrane and can form heterotetramers in SH-SY5Y, FLG 29.1

and K562 cells (Crociani *et al.*, 2003, Cavarra *et al.*, 2007). This is consistent with patch-clamp studies in K562 cells (Cavarra *et al.*, 2007). Native hERG1 currents in K562 cells had a $V_{0.5}$ for activation similar to that of the heterotetrameric I_{Kr} current of ventricular myocytes measured under the same conditions. Furthermore, hERG1b deactivation is faster than hERG1 and the deactivation time constant for the K562 cell hERG1 current was slower than that of homotetrameric hERG1b channels, but much faster than that of WT hERG1 homotetramers (Cavarra *et al.*, 2007). Nevertheless, the role of hERG1b in tumorigenesis remains elusive.

1.7 Thesis aims

The aims of the present study were as follows:

1. To investigate the role of ECM-integrin-mediated signalling on the “transformed” behaviour exhibited by hERG1 expressing NIH-3T3 cells.
2. To elucidate the role of hERG1 channel conduction and surface expression in hERG1-induced cellular transformation. Non-functional hERG1 mutants were stably transfected into NIH-3T3 cells, expression confirmed by a variety of screening methods and migratory and proliferative behaviours compared to cells expressing WT hERG1 channels.
3. To explore the contribution of the hERG1b isoform to cellular transformation. The effect of transient transfection of NIH-3T3 cells with WT hERG1, hERG1b and a plasmid that allows co-expression of both isoforms has been studied.
4. To investigate the effect of hERG1 expression on cell survival under hypoxic conditions. CHO cells stably expressing hERG1 channels (CHO-hERG) were maintained at low oxygen tension for different lengths of time and cell-viability and hypoxia-induced cell death compared to mock-transfected (CHO-VC) cells.

Methods

2.1 Cell culture

2.1.1 Cell-lines and their maintenance

A number of different mammalian cell-lines were used in this project:

Wild-type (WT) and stably-transfected NIH-3T3 cell-lines

WT NIH-3T3 cells (purchased from American Type Culture Collection (ATCC), USA) were used in this work for transient and stable transfection with hERG1 channel constructs. NIH-16 and NIH-50 are stably transfected clones expressing WT hERG1 in pcDNA3 vector. Previous work from my lab had shown that these cells express a ‘transformed’ phenotype compared to NIH-3T3 cells transfected with the vector control plasmid alone (NIH-VC).

NIH -C3, -C10, -C12 and -C36 are NIH-3T3 clones stably expressing the non-functional hERG1 mutants G628S hERG1 (NIH-C3 and NIH-C36) and A561V hERG1 (NIH-C10 and NIH-C12). They were generated by stable transfection and subsequent clonal selection as described in Section 2.4. NIH-Ras cells stably express V12-Ras, a constitutively-active mutant of Ras, a small GTPase and a well-characterized oncogene. These cells were a kind gift from Dr. Julian Downward (formerly at the MRC Cancer Research Institute, London, UK) and were used as positive control for a transformed phenotype during this project.

WT NIH-3T3 and NIH-Ras cell-lines were maintained in high glucose (4.5 mg mL⁻¹) Dulbecco’s modified Eagle’s medium (DMEM), with 10% v/v fetal bovine serum (FBS), 50 U mL⁻¹ penicillin and 50 µg mL⁻¹ streptomycin. 500 µg mL⁻¹ geneticin (G418) was

added to the culture medium for maintaining clones stably expressing WT hERG1 (NIH-16 and NIH-50), hERG1 mutants (NIH- C3, - C10, - C12 and - C36) or pcDNA3 alone (NIH-VC). Cells were maintained at 37°C in the atmosphere of 5% CO₂ : humidified air. To lift the cells from culture flasks, the culture medium was aspirated and the cell monolayer was washed twice with divalent cation-free Dulbecco's phosphate-buffered saline (D-PBS). 30 µL of trypsin/EDTA per cm² of flask surface area was added to dissociate cells. When cells started to round and detach from the surface, they were diluted in fresh medium and split at a ratio of 1:10. This was repeated every 3 days, or when cells reached ~70% confluency. When cells reached passage 30, they were discarded and new cells were grown.

WT HEK-293 (WT-HEK) and HEK-hERG cells

WT human embryonic kidney-293 (HEK-293) cells were maintained in DMEM supplemented with 10% v/v FBS, 50 U mL⁻¹ penicillin and 50 µg mL⁻¹ streptomycin. For HEK-293 cells stably expressing WT hERG1 (HEK-hERG cells), 400 µg mL⁻¹ G418 was added to the culture medium. Cells were cultured at 37°C in 5% CO₂ : humidified air. Cells were grown in 25 cm² flasks and split at a ratio of 1:4 every 3-4 days. HEK-hERG cells were a kind gift from Prof. Craig January (University of Wisconsin, USA). HEK-hERG cells express high levels of hERG1 and were used as a positive control for hERG1 protein expression in this study.

A brief description of all cell-lines used in the present study is shown in table 1.

Table 1 Stable cell lines used in the present study.

Cells	Description	Use	Source
NIH-VC	NIH-3T3 cells stably transfected with an empty vector	As a negative control for hERG1 expression	The present study and Pier, (2007)
NIH-16 and NIH-50	NIH-3T3 cells stably expressing WT hERG1	Investigation of ECM signalling in hERG1 expressing cells	(Pier, 2007)
NIH -C3 and NIH-C36	NIH-3T3 cells stably expressing G628S hERG1, a non conducting hERG1 mutant	Investigation of the role of hERG1 channel conduction and surface localization in hERG1-induced transformation	The present study
NIH -C10 and NIH-C12	NIH-3T3 cells stably expressing A561V hERG1, a trafficking-defective hERG1 mutant		
NIH-Ras	NIH-3T3 cells stably expressing V12-Ras, a constitutively active mutant of H-Ras	As a positive control for a transformed phenotype	Dr. Julian Downward (Rodriguez-Viciano <i>et al.</i> , 1997)
HEK-hERG	HEK cells stably expressing WT hERG1	As a positive control for hERG1 expression in molecular biology and biochemical techniques.	Prof. Craig January (University of Wisconsin, USA).
CHO-VC	CHO cells stably transfected with an empty vector	As a negative control for hERG1 expression	(Pier, 2007)
CHO-hERG	CHO cells stably expressing WT hERG1	Investigation of the survival capacity of hERG1-expressing cells under hypoxic conditions	(Pier, 2007)

2.1.2 Cell-freezing (cryopreservation)

Exponentially growing cells (cells in logarithmic phase of growth) can be stored frozen for long periods of time using a cryoprotective agent such as dimethylsulphoxide (DMSO). Culture medium was aspirated from T-25 cm² flasks containing sub-confluent cells (~ 70% confluent) and the cell monolayer was washed with D-PBS to remove FBS. 1 mL of pre-warmed trypsin/EDTA was added to cover the cells. Trypsin/EDTA was then aspirated and flasks were incubated at 37°C until all cells were rounded. Cells were then resuspended in 1 mL of freezing medium (10% v/v DMSO (Sigma) / 90% v/v FBS (Gibco)) and transferred to sterile cryogenic vials which were labelled, wrapped in paper tissue and frozen at -80°C for 24 h. Cryogenic vials were then unwrapped and stored at -80°C or in liquid nitrogen for long-term storage.

2.1.3 Recovery of frozen cells

Frozen vials were rapidly thawed in a waterbath at 37°C and cells were added slowly to 10 mL of pre-warmed culture medium in a T-25 cm² flask and incubated at 37°C for 24 h. After the cells had attached, the medium was exchanged for fresh medium to remove floating, dead cells and DMSO, which may be damaging to cells on prolonged exposure. When cells reached 70% confluency, they were split as described earlier.

2.2 Molecular biology

Several molecular biology techniques were used throughout this study to prepare hERG1 channel constructs for expression in *Xenopus* oocytes or mammalian cell-lines. A brief description of each protocol is provided in the following sections. Specific strategies for making constructs for dual expression of hERG1 and hERG1b are given in Chapter 5.

2.2.1 Preparation of DNA stocks

2.2.1.1 Bacterial transformation

Transformation is a process of introducing exogenous plasmid DNA into competent bacteria, which is then copied and amplified as the bacteria divide to enable large amounts of DNA to be purified. Bacteria are made competent through a chemical treatment process, which enhances their ability to take-up exogenous DNA. Plasmid DNA is added to the cells and they are heat-shocked to take up the DNA. The plasmids contain an antibiotic-resistance gene, which allows selection of bacteria that have taken up the DNA by growing them in an antibiotic-containing medium. The protocol in brief is: DH5 α -competent *E. coli* (Invitrogen, UK) were slowly thawed on ice. DNA of interest (2-5 μ L) was then added and the mixture was incubated on ice for 30 min. The cells were heat-shocked (by placing the tube in a water bath at 42°C for 45 s then returning to ice for 2 min). Pre-warmed salt-optimized and carbon (SOC) medium (Invitrogen) was added and cells were incubated at 37°C in a shaking (230 r.p.m.) incubator for 1 h to provide time for expression of antibiotic resistance. Cells were plated onto Luria-Bertani (LB) agar plates containing 100 μ g mL⁻¹ ampicillin and incubated at 37°C overnight. A known quantity of control plasmid DNA (puc 19) was used as a positive control (to test for efficiency of transfection) and 5 μ L H₂O

as a negative control (to test for non-specific DNA contamination of reagents). Single colonies were picked and grown up in LB broth with $100 \mu\text{g mL}^{-1}$ ampicillin. This culture was used to make a glycerol stock, or to extract plasmid DNA.

2.2.1.2 Preparation of glycerol stocks of DNA

A glycerol stock of bacteria that have been transformed with DNA can be used for long-term storage. 0.5 mL of a bacterial culture (grown from a single colony of bacteria) was mixed with 0.5 mL sterile 65% v/v glycerol solution in a cryovial tube, which was briefly vortex-mixed and stored at -80°C . When plasmid DNA was required, the glycerol stock was placed on dry-ice and a wooden stick was used to pick a portion and streak an ampicillin-agar plate, which was incubated at 37°C overnight. The following day, a single colony was picked and grown in an appropriate volume of ampicillin-containing LB broth prior to DNA extraction.

2.2.1.3 Recovery and purification of DNA

DH5 α -competent *E. coli* transformed with plasmid DNA were grown overnight in LB broth with $100 \mu\text{g mL}^{-1}$ ampicillin in a shaking incubator (250 r.p.m.) at 37°C . DNA was then recovered by alkaline lysis and column purification using commercial Qiagen plasmid purification kits (Qiagen, CA, USA). Briefly, bacterial cultures were pelleted by centrifugation and lysed using a strong alkaline lysis buffer. The cell lysate was neutralized and treated with a high-salt solution to precipitate genomic DNA and large protein complexes, while the smaller plasmid DNA remained in solution. The precipitate was then removed by centrifugation and the clear supernatant was added to a silica-based anion exchange resin, which binds plasmid DNA in a pH-dependent manner. RNA, proteins, and

low molecular weight impurities were removed by a medium-salt wash. Finally, plasmid DNA was eluted from the column in a high-salt buffer, concentrated and desalted by isopropanol precipitation. DNA yield was quantified by running against a quantitative DNA ladder (Hyperladder 1, Bioline, London, UK) on a 1% w/v agarose gel. The gel contained $0.5 \mu\text{g mL}^{-1}$ ethidium bromide, which intercalates with DNA and allows visualization under UV light. Alternatively, DNA was quantified by spectrophotometry at 260 nm, where an absorbance value of 1 corresponds to $50 \mu\text{g mL}^{-1}$ DNA. DNA was stored at -20°C or -80°C until required.

2.2.2 Site-specific DNA digestion

Restriction endonucleases are enzymes that recognize specific nucleotide sequences and cut DNA producing either overhanging (sticky), or blunt ended fragments. They are frequently used for cutting DNA fragments from one source and inserting into a plasmid (subcloning) and to check the correct size of inserted fragments, or PCR products. Briefly, DNA was incubated with the selected restriction endonuclease in the correct buffer provided by the manufacturer with the enzyme (New England Biolabs, UK). In cases where two restriction enzymes were used, a buffer that provides optimal reaction conditions for both was used. A double digest for some enzyme combinations was not possible and therefore a sequential digestion was necessary. The incubation temperature and the length of incubation was dependent on the type of enzyme and amount of DNA. One unit of the enzyme digests $1 \mu\text{g}$ DNA in 1 h. The amount of glycerol present was always $\leq 5\%$ to avoid non-specific digestion ('star' activity). For cloning purposes, restriction enzymes that produce sticky ends were used to generate complementary fragments that could be specifically ligated. To

check for complete digestion, the digestion products were separated by gel electrophoresis on a 1% w/v agarose gel. The size and number of fragments were compared to those predicted by DNA and protein sequence analysis software (Vector NTI, Invitrogen, UK).

2.2.3 DNA extraction from agarose gels

DNA fragments can be extracted from agarose gels following their separation by electrophoresis. This was performed using a QIAquick gel extraction kit (Qiagen, USA). Briefly, DNA bands (from an ethidium bromide-stained gel) were visualized under UV and the band of interest was carefully excised using a sharp, clean razor blade. The gel slice was weighed, placed in a dissolving buffer at 3:1 ratio (buffer volume to gel weight) and heated at 50°C for 10 min. An equal volume of isopropanol was added to fragments of sizes <500 bp or >4 Kb to improve the DNA yield. The solution was then added to an anion-exchange column, which was centrifuged (13,500 xg, 1 min) to allow DNA binding. The column was then washed and the DNA was eluted with 30 µL of an elution buffer containing 10 mM Tris/HCl (pH 8.5) by centrifugation (13,500 xg, 1 min).

2.2.4 Ligation of DNA fragments

Vector and insert DNA fragments were prepared by cutting with appropriate restriction enzymes that each cut at a single site and produce fragments with single-stranded complementary overhanging (sticky) ends. The purified vector and insert were mixed to give a molecular ratio of 3 molecules of insert DNA to each molecule of vector DNA. 1 µL T4 ligase enzyme (New England Biolabs, UK) and 1 x T4 buffer were added. Control samples having no T4 ligase (to check for presence of uncut vector DNA), no vector DNA (to check for self-ligation of the DNA insert) and no insert (to check for self-ligation of the

vector DNA) were prepared in parallel. The ligation mixtures were incubated at room temperature for 1 h and 5 μ L of each solution transformed into DH5 α -competent bacteria. A successful ligation was predicted on the basis that the test sample produced colonies on ampicillin-agar plates, due to the presence of an ampicillin-resistance gene marker on the ligated circular DNA, while the three control samples produced no colonies. Single colonies were then picked and grown in LB broth cultures to allow DNA amplification and were subsequently purified as previously described. The size of the inserted fragment was checked by digestion with restriction enzymes flanking the ligation site. If the size was correct, a sample was sent for sequencing.

2.2.5 DNA sequencing

DNA sequencing was performed to check DNA constructs following ligation, or site-directed mutagenesis. DNA samples were sent to an in-house facility - PNACL (Protein and Nucleic Acid Chemistry Laboratory, University of Leicester) that uses an automated DNA sequencer (ABI PRISM Model 377). Primers used for sequencing were chosen to be about 100 bp upstream (5') of target sequence. Sequencing files were analyzed using Vector NTI software (Invitrogen, UK).

2.3 Characterization of hERG1 channel properties by expression in *Xenopus* oocytes

Oocytes from *Xenopus laevis* frogs are a valuable expression system for studying ion channel function. They efficiently translate exogenous complementary RNA (cRNA) and traffic channel proteins to the plasma membrane. Levels of expression can be titrated with

the amount of cRNA injected and robust currents can be recorded using relatively simple apparatus.

2.3.1 Preparation of cRNA by *in vitro* transcription

cRNA is a complementary RNA strand of DNA that is derived by *in vitro* DNA transcription using RNA polymerase. This is more efficient with linearization of circular DNA plasmid to create template DNA, which should contain the promoter site to which the RNA polymerase can bind and initiate cRNA synthesis.

2.3.2 Preparation of template DNA

A restriction enzyme was chosen to cut plasmid DNA at a single specific site downstream of the 3' end to enhance the efficiency of RNA synthesis. *EcoRI* restriction enzymes (New England Biolabs, UK) were used to linearize the pcDNA 3.0 plasmid. 10 μg of plasmid DNA was incubated with the restriction enzyme under appropriate conditions to ensure linearization, which was confirmed by running a sample of the restriction digest on 1% w/v agarose gel against uncut DNA. The DNA template was then incubated with proteinase K (100 $\mu\text{g mL}^{-1}$) and 0.5% w/v SDS at 50°C for 30 min to denature contaminating RNAses. Finally, the linearized DNA was purified using Qiaquick gel extraction kit (Qiagen, USA) as described previously. Template DNA was then quantified and diluted in diethylpyrocarbonate (DEPC)-treated water to a final concentration of 0.2 $\mu\text{g mL}^{-1}$ and stored at -80°C until required.

2.3.3 cRNA synthesis

In vitro transcription was performed using mMessage mMachine kit (Ambion, USA). During this process, care was taken to avoid contamination by RNAses through using autoclaved glassware and sterile filter-pipette tips. Briefly, a solution containing 1 μL nuclease-free water, 10 μL NTP/CAP mix, 2 μL 10x reaction buffer, 2 μL RNA polymerase enzyme and 1 μg of template DNA was incubated at 37°C for 2 h. This yields approx. 20 μg of RNA, which was treated with DNAase1 (Amibion, USA) for 15 min at 37°C to digest remaining template DNA. RNA was quantified by running on a 1% w/v agarose denaturing formaldehyde gel against an RNA standard. This gel contained 5% v/v formaldehyde and 10x MOPS EDTA/sodium acetate (MESA) buffer made up of 2 M MOPS, 50 mM sodium acetate and 10 mM EDTA at pH 7.0. RNA was diluted to a final concentration of 0.5 $\mu\text{g } \mu\text{L}^{-1}$, aliquoted into 3.1 μL samples and stored at -80°C until required.

2.3.4 Recording of hERG1 currents expressed in *Xenopus* oocytes

cRNAs (5-15 ng) encoding WT, G628S, and A561V hERG1 were injected into oocytes isolated from *Xenopus laevis*. Oocytes were maintained at 16-18°C in modified Barth's solution containing 88 mM NaCl, 1 mM KCl, 0.41 mM CaCl₂, 0.33 mM Ca(NO₃)₂, 1 mM MgSO₄, 2.4 mM NaHCO₃, 10 mM HEPES, pH 7.4, 1 mM sodium pyruvate and 50 $\mu\text{g } \mu\text{L}^{-1}$ gentamycin. 2-7 days later, currents were recorded at room temperature by two-electrode voltage clamp using a Gene Clamp 500B amplifier (Molecular Devices, USA). Microelectrodes were filled with 3 M KCl and had a resistance of 1-2 M Ω . Voltage protocols were generated by a computer running pCLAMP software (Axons Instruments,

Molecular Devices, USA), which was also used to save data for off-line analysis. An analogue to digital converter (Digidata 1320A, Molecular Devices) interfaced with the voltage clamp amplifier. Current signals are filtered at 1 KHz and sampled at 2-5 KHz.

WT and mutant hERG currents were measured in normal 5 mM K⁺ extracellular recording solution containing (in mM): 93 NaMES, 5 KMES, 2 Ca (MES)₂, 1 MgCl₂ and 5 HEPES or a high (20 mM) K⁺ solution containing (in mM): 78 NaMES, 20 KMES, 2 Ca (MES)₂, 1MgCl₂ and 5 HEPES. Extracellular recording solutions were prepared and pH was adjusted to 7.6 with NaOH. Currents were elicited with current-voltage relationship (I-V) protocols or a fully-activated current-voltage (FA I-V) protocol. In the I-V protocol, a family of 5 s test pulses were applied to potentials between -70 and +50 mV from a holding potential of -90 mV followed by a 400 ms step to a potential of -70 mV or -120 mV to record tail currents. The magnitude of peak tail current amplitude was normalized to the maximum and plotted as a function of test potential and the results fitted with a Boltzmann function to determine parameters for the voltage-dependence of activation. With the FA I-V protocol, a 1 s test pulse to +40 mV from a holding potential of -90 mV was applied, then membrane potential stepped for 5 s to a range potentials between -150 to +30 mV in 10 mV increments The decay phase of the tail current was fit with the double-exponential function (insert) to determine the time constants for deactivation. Resting membrane potentials were also recorded in current clamp mode (set up mode) on the voltage clamp amplifier.

2.4 Generation of stable cell-lines

2.4.1 DNA constructs

The DNA cloning vector pcDNA3 was selected for generation of stable cell-lines in this study. This expression vector contains a multi-cloning region which has many restriction sites and therefore is suitable for inserting a target gene. A cytomegalovirus (CMV) promoter drives the expression of the inserted gene. pcDNA3 also contains an ampicillin resistance gene, which allows the use of ampicillin for selection of bacteria that have been transformed with the vector to be used for DNA amplification. Another promoter, SV40 drives the expression of a neomycin-resistance gene. This confers mammalian cells, which have incorporated the plasmid DNA in their genome after stable transfection, with resistance to the selection compound G418. WT hERG1 cDNA was subcloned between Hind III and EcoRI restriction sites. hERG1 channels mutants A561V (a trafficking-deficient mutant) and G628S (a non-conducting mutant) were made by site-directed mutagenesis. The DNA constructs were checked by restriction enzyme digestion and sequencing.

2.4.2 Transfection

Lipofection is a lipid-based transfection technology used to introduce DNA into cells using cationic lipid reagents. The transfection reagent is allowed to complex with DNA molecules through ionic interaction. These complexes fuse with the cell membrane and introduce DNA into the cell. NIH-3T3 cells were transfected with either empty vector, WT, A561V or G628S hERG1-pcDNA3. NIH-3T3 cells were cultured to ~70% confluency in a 6-well plate. The culture medium was changed prior to transfection. 7.5 μ L of the

transfection agent, Lipofectamine (Invitrogen, UK) was added to 95 μL of serum-free medium and incubated at room temperature for 5 min. Plasmid DNA (3 μg) was then added to the solution and allowed to complex with Lipofectamine for 20 min at room temperature. The DNA-Lipofectamine complex was then added to the cells. The plate was rocked several times to ensure uniform distribution of complexes over the cells and incubated at 37°C for 5 h. After this time the Lipofectamine-containing medium was replaced by fresh culture medium.

2.4.3 Generation of a kill curve

pcDNA3 plasmid expresses G418 resistance that can be used as a selection marker to grow cells that have taken-up the plasmid and so may also express WT hERG1/hERG1 mutants. The concentration of G418 used should be sufficient to kill untransfected cells, but not too high to be toxic. To determine the optimum concentration of G418, untransfected NIH-3T3 cells were cultured in medium containing 0, 250, 500, 750, or 1000 $\mu\text{g mL}^{-1}$. Cells were observed over 3 weeks. G418 at a concentration of 500 $\mu\text{g mL}^{-1}$ caused death of only ~70% of cells after 10 days. A concentration of 750 $\mu\text{g mL}^{-1}$ was found to kill 100% of cells in 10 days and was the concentration used for selection.

2.4.4 Clonal selection

Stable cell-lines will only constitutively express the protein of interest if the transfected DNA is incorporated into an active region of chromosomal DNA. This is a rare event and therefore careful selection of clones that express the target protein is essential. Clones are grown from single cells with the expectation that there will be more uniform level of hERG1 protein across the cell population. 48 h after transfection cells were ~80-90%

confluent and were passaged at a 1:6 dilution into fresh culture medium containing $750 \mu\text{g mL}^{-1}$ G418 (selection medium). This was repeated when the cells again reached $\sim 70\%$ confluency. Only cells that had taken up the hERG1/hERG1 mutant cDNA were able to survive in the selection G418-supplemented medium. Culture medium was exchanged every 2-3 days to remove dead cells. As stated earlier, clones were produced from single cells within the population to ensure that all cells of the clone express the DNA of interest at the same level. To do that, 2 weeks after selection, cells from a single well were trypsinized, counted and diluted to 10 cells mL^{-1} in selection medium. One hundred μL of this cell dilution was then plated in each well of a 96-well plate. Wells that contained single cells were identified and allowed to grow into colonies of a harvestable size. A few cells from the centre of each colony were picked using a p10 Gilson pipette-tip and were expanded. Clones expressing the recombinant gene product of interest were grown in culture medium containing G418 ($500 \mu\text{g mL}^{-1}$, to maintain selection pressure).

2.5 Screening of clones for hERG1 expression

2.5.1 Real-time reverse transcription (RT RT) PCR

2.5.1.1 RNA extraction

Cells from each clone (in duplicate) were grown to 70% confluency in 6-well plates. Cells from one well of the duplicate were recovered and stored at -80°C until required. Cells from the other well were lysed for RNA extraction. Total RNA was extracted using the RNeasy mini-kit (Qiagen, USA) following the manufacturer's instructions. Briefly, cells were first lysed and homogenized, using a 20-gauge (0.9 mm) needle attached to a sterile plastic syringe, in the presence of a highly denaturing guanidine-thiocyanate-containing

buffer, which immediately inactivates RNases to ensure extraction of intact RNAs. An equal volume of ethanol (70% v/v) was then added to the lysate and the sample was applied to an RNeasy mini-spin column, where the total RNA binds to the membrane and contaminants can be washed away. Total RNA was eluted in 30 μL of nuclease-free water. All binding, washing, and elution steps were performed by centrifugation at room temperature.

Each RNA sample was incubated with 1 μL (2 units) DNase 1 enzyme (Ambion, Applied Biosystems, USA) at 37°C for 30 min to remove genomic DNA contamination. The RNA concentration was quantified by spectrophotometry (Gene Quant, Pharmacia Biotech), where an absorbance value of 1 corresponds to an RNA concentration of 40 $\mu\text{g mL}^{-1}$. RNA yields of 8-12 μg were produced from cells recovered from a single well. The quality of isolated RNA was assessed by running a fraction of each RNA sample on a 1% denaturing formaldehyde-agarose gel stained with ethidium bromide. A good quality RNA sample was defined as one that showed two well defined sharp 18S and 28S ribosomal RNA (rRNA) bands. Smear bands indicated RNA degradation and these samples were excluded and new RNA extracts prepared.

2.5.1.2 cDNA synthesis (reverse transcription)

The mRNA content of each sample was copied to cDNA by reverse transcription. 1 μg of total RNA was retro-transcribed by incubating at 37°C for 60 min with 1 μL (4 units) Omniscript reverse transcriptase (RT) (Qiagen, USA) in the presence of anchored oligo-dT primers (Abgene, UK), dNTP mix (5 mM of each nucleotide) and 1x reaction buffer. Oligo-dT primers are oligothymidine primers with one or two non-thymine bases in the 3'

end and only anneal (anchor) to the start of the poly-A tail junction of the mRNA template. Therefore, it eliminates transcription through the poly-A tail, providing more efficient cDNA synthesis. The cDNA obtained was stored at -20°C until required.

2.5.1.3 Checking the efficiency of cDNA synthesis by polymerase chain reaction (PCR)

PCR uses heat-stable DNA polymerase enzymes to extend a pair of primers annealed to complementary sites in the sense and the antisense strands of the template DNA. This allows a specific sequence of the template DNA to be copied and amplified via temperature cycling. First, a high temperature is applied to separate the strands of the DNA double helix (denaturation step). The temperature is then lowered to allow primers to specifically anneal to the template strands (annealing step). Finally, the temperature is set at that optimal for the polymerase to extend primers by incorporating nucleotide triphosphates (dNTPs) (extension step). This cycle is repeated many times to further amplify the specified product.

HEK-hERG cells are known to express large numbers of hERG1 channels and were used as a positive control for hERG1 mRNA RT-PCR. The cDNA from HEK-hERG cells was prepared as described above. PCR was then used to test HEK-hERG cDNA for hERG1 expression, which would confirm the success of both the RNA extraction and cDNA synthesis. cDNA from HEK-hERG cells was amplified using PfuTurbo DNA polymerase (Stratagene, CA, USA). The following primer sequences (reported by Pillozzi *et al.*, 2007) were used to amplify hERG1:

Forward GTGGAAATCGCCTTCTACCG

Reverse GCCCATCCTCGTTCTTCA

Glyceraldehyde 3-phosphate dehydrogenase (GAPDH) was used as a standard reference gene and as a loading control to verify that identical amounts of sample were added in each lane. Normalization of the target gene against this reference gene also eliminated errors resulting from variations in the amount of starting material between samples that could result in inaccurate RNA quantification. The primer sequences used to amplify GAPDH were as follows:

Forward AACAGCCTCAAGATCATCAGGAA

Reverse CAGTCTGGGTGGCAGTGAT

PCR reactions were performed on ice in 0.2 mm thin-walled plastic tubes as follows: 2 μ L (10-20 ng) of cDNA, 200 ng of each primer, 1x reaction buffer, 200 μ M dNTPs mix and 1.25 units of *PfuTurbo* DNA polymerase (Stratagene, CA, USA). These tubes were then transferred to the PCR machine (Techne, USA) and the following PCR cycling parameters were applied: a heated lid at 104°C, enzyme activation and DNA denaturation at 95°C for 2 min, thirty-three-step cycles of 95°C for 30 s, 56°C for 30 s and 72°C for 1 min, and a final cycle at 72°C for 10 min. The optimum annealing temperature depends on the melting temperatures of the pairs of primers chosen. A range of temperatures were tested and a temperature range of 56-60°C was found to be optimal for hERG1 amplification. WT hERG1 DNA in pCEP4 plasmid (10-50 ng) was used as a positive control. The following negative control samples were included in every PCR run:

1) No template control (NTC) where water instead of template cDNA is included in the reaction mixture. This checks for contamination of PCR components.

2) No reverse transcriptase (RT) and no RNA controls checks for the presence of genomic DNA contamination and contamination of the RT and PCR components.

The PCR products (81 bp for hERG1 and 138 bp for GAPDH) were run on 2.5% w/v agarose gel with $0.5 \mu\text{g mL}^{-1}$ ethidium bromide and visualized using UV light box relative to 100 bp DNA ladder (New England Biolabs, UK). The above-mentioned primers were also used in real-time RT-PCR reactions.

2.5.1.4 Quantification of relative hERG1 expression by real-time RT PCR

Quantitative real-time PCR (qPCR) is the most widely used method for accurate and sensitive quantification of relative gene expression. qPCR allows for detection of an amplified product in the early phases of DNA amplification and therefore, it is advantageous to conventional end-point PCR, which detects DNA amplification at the end of the reaction. A basic PCR reaction usually consists of three phases: the exponential phase, in which the amplified product accumulates exponentially and double with each amplification cycle, the retardation phase, in which the reaction is slowed because the reagents and DNA template are being consumed and the plateau, in which the reaction is stopped due to depletion of most PCR reagents. qPCR detects DNA amplification during the exponential phase. Consequently, this method is very sensitive and can detect minor differences of the target gene content in the starting samples. Conversely, conventional PCR detects the accumulation of the amplified product at the plateau (end-point) of the reaction and thereby cannot provide much information about the initial amounts of target molecules in the starting sample. At the end of the reaction the amount of the product does not only depend on the amount of the starting template molecules but also on changes in

the reaction conditions and the amounts of the limiting PCR components during the PCR reaction. Currently, traditional PCR is mainly used for qualitative detection of genes to distinguish positive from negative samples.

In real-time RT-PCR, the increase in double stranded DNA product with PCR amplification is detected by SYBR green fluorescence intensity. SYBR green is a dye that becomes fluorescent when it binds to double stranded DNA. As more double stranded amplicons are produced, the SYBR green fluorescence signal is increased. The fluorescence signal is measured every cycle as the product accumulates and this allow for monitoring the product amplification in “real time”. The difference in gene expression between samples is quantified by comparing the number of amplification cycles required for each sample to reach a particular threshold fluorescence signal set in the exponential phase of the PCR reaction. The number of cycles required to reach this fluorescence threshold is called the C_T value.

A major limitation of this method is that SYBR green binding is non-specific. SYBR green can bind to any double stranded DNA in the reaction including primer dimers and non-specific DNA products, which can lead to false increases in the fluorescence signal and inaccurate gene quantification. To control for this, a melting curve analysis is always applied to the final PCR products after the cycling protocol. The amplified products are subjected to gradually increasing temperatures and the fluorescence is measured as a function of temperature. When temperatures reach the melting temperature of the amplicon (T_m), its double strands separate and the SYBR green dye is released leading to a sharp decrease of the fluorescence signal, which appears as a characteristic peak in the melting

curve at that temperature. Primer dimers and amplification artefacts are usually of low molecular weight and their peaks appear at low melting temperatures in the melting curve.

Real time RT PCR reaction

Primers previously used for detection of hERG1 and GAPDH expression by conventional RT-PCR were also used for qPCR. Briefly, 25 μ L PCR reactions were prepared on ice in clear white 0.2 mL tubes as follows: 2 μ L (10-20 ng) of cDNA, 1.5 μ L of each primer (100 nM final concentrations), 7.5 μ L of nuclease-free water and 12.5 μ L of SYBR green master mix (Applied Biosystems, USA). No template controls (NTCs), containing no cDNA, were prepared for each primer pair and included in each qPCR run to monitor for contamination. These tubes were then transferred to PTC-200 thermal cycler (MJ Research, USA) and the following PCR cycling parameters were applied: 50°C for 2 min, 95°C for 10 min and thirty-two-step cycles (95°C for 15 s and 60°C for 60 s). The fluorescence signal was read after each cycle using an Opticon 2 fluorescence detector (Bio-Rad laboratories, CA, USA). After the cycling programme had finished, the temperature was increased from 55°C to 95°C in 1°C increments and the fluorescence signal read. Temperature programming and fluorescence measurement were controlled by Opticon monitor 3 software (Biorad, CA, USA), which was also used for off-line data analysis. Each clone was tested in duplicate and the assay was repeated for clones that gave positive hERG1 expression in the first run.

Data analysis

The $2^{-\Delta\Delta CT}$ method (Livak *et al.*, 2001) is one of the most commonly used methods for qPCR data analysis and the quantification of relative gene expression. In this method, the target gene content of the sample hERG1 is normalized to the internal reference gene

content of the same sample (GAPDH) and is expressed relative to the normalized target gene content of an external reference standard (the calibrator), which in this case was hERG1 in NIH-50 cells. This minimizes errors caused by variations in the input RNA content added to the reverse transcriptase reaction. This method assumes equal amplification efficiencies for both the target and the internal reference genes for each amplification cycle. It was essential to test this before adopting this method for data analysis. The efficiency of the PCR assay was estimated from a standard curve based on serial dilution of a standard. To test for an equal efficiency of hERG1 and GAPDH amplification, a serial dilution of cDNA derived from HEK-hERG cells was amplified in parallel to design a standard calibration curve for each gene. The C_T or the ΔC_T (C_T hERG1 - C_T GAPDH) values of the diluted standards were then plotted versus the logarithm of the standard dilution. The two standard curves should have the same slope and the absolute value of the slope of the ΔC_T standard curve should be less than 0.1 (Livak *et al.*, 2001).

The expression of hERG1 gene of each clone relative to the hERG1 gene content of NIH-50 cells was calculated as follows:

$$\text{Relative gene expression} = 2^{-\Delta\Delta C_T}$$

Where: $\Delta C_T = C_T \text{ hERG1} - C_T \text{ GAPDH}$

$$\Delta\Delta C_T = \Delta C_T \text{ clone} - \Delta C_T \text{ NIH-50}$$

2.5.2 [³H]dofetilide binding assay

Radioligand binding assays are widely used for the quantification of surface receptors that bind with high affinity to a radioligand. Cell membrane preparations are incubated with a

suitable radioligand for long enough for equilibrium binding to occur, unbound ligand is removed, usually by filtration or centrifugation, and the radioactivity bound to the receptor is determined by scintillation counting. However, the measured radioactivity value also includes an amount of radioligand that inevitably binds non-specifically to other components of the membrane preparation and therefore is referred to as the “total” binding. Non-specific binding is determined by repeating the assay in the presence of a non-radiolabelled ligand used at a concentration that completely occupies all specific binding sites and prevents the radioligand from binding to specific, but not non-specific sites. Specific binding is determined by subtracting non-specific binding from total binding and, if the radioligand concentration is sufficiently high, is a quantitative measure of the number of the receptors present.

Selective, high-affinity binding of [³H]dofetilide to hERG1 channels expressed in cardiac myocytes (Chadwick *et al.*, 1993), SH-SY5Y neuroblastoma cells (Finlayson *et al.*, 2001a) and mammalian cells transfected with hERG1 (Finlayson *et al.*, 2001a, Finlayson *et al.*, 2001b) has been reported previously.

2.5.2.1 Membrane preparation

Individual NIH-3T3 clones were grown in 2 flasks, each with average surface area of 175 cm². Culture medium was aspirated and discarded and cells washed with buffer A (10 mM HEPES, 0.9% w/v NaCl, 0.2% w/v EDTA, pH 7.4). Buffer A was then added and cells were incubated for 5 min at 37 °C to allow the cells to lift off the plastic substratum. Cells were transferred to a fresh tube and pelleted by centrifugation (25 xg, 5 min). The supernatant was discarded and cells were re-suspended in 5 mL of buffer B (50 mM

Tris/HCl, 1 mM EDTA, pH 7.4). Cells were homogenized using a Polytron (4 x 15 s bursts at near-maximal setting). The homogenate was centrifuged (40,000 xg, 20 min, 4°C) and the resulting pellet was re-suspended in buffer B, re-homogenized and re-centrifuged (40,000 xg, 20 min, 4°C). The recovered pellet was re-suspended and re-homogenized in 1 mL of assay buffer C (71.5 mM NaCl, 60 mM KCl, 1 mM CaCl₂, 2 mM MgCl₂, 10 mM HEPES, pH 7.4). The protein concentration was determined (Lowry protein assay; see below) and samples were stored at -80°C until required.

2.5.2.2 [³H]dofetilide saturation binding

In saturation binding assays, the concentration of [³H]dofetilide is increased until the specific binding approaches a maximum, defining the maximal specific binding (B_{\max}) value. [³H]dofetilide (specific activity 79 Ci mmol⁻¹) was a kind gift from Dr. Derek Trezise (GlaxoSmithKline, Harlow, UK). Total binding and non-specific binding was determined for [³H]dofetilide concentrations ranging from 1 to 55 nM. Unlabelled dofetilide (final concentration 10 μM) was used to determine non-specific binding. Briefly, 20 μL assay buffer (buffer C), ± dofetilide was incubated with 50 μL [³H]dofetilide and 50 μL of HEK-hERG membranes (stock: 1.5 mg mL⁻¹) for 2 h at room temperature. The assay was terminated by filtration onto GF/B glass filters (Whatman, UK; pre-soaked in 0.25% v/v polyethylimine (PEI; Sigma) for 1-2 h) using a sample manifold vacuum filtration system (Millipore, USA). Filter discs were washed three times with an ice-cold wash buffer (131.5 mM NaCl, 1 mM CaCl₂, 2 mM MgCl₂, 10 mM HEPES, pH 7.4) and then transferred to scintillation vials. 4.2 mL of Emulsifier Safe scintillation fluid (Lumac, Holland) was added to each vial. Radioactivity was determined using a liquid scintillation analyzer

(Packard Tri-Carb, Perkin Elmer, USA). Experiments were repeated at least 3 times and data analyzed by non-linear regression (single-site model) to determine the dissociation constant (K_D) of the radioligand and number of binding sites (B_{max}).

2.5.2.3 [^3H]dofetilide displacement assay

Competitive binding experiments were conducted to determine the binding affinity of a variety of hERG1 blockers. Stock solutions of dofetilide, terfenadine (Sigma) and E-4031 (Calbiochem) were prepared in DMSO at 10 mM concentration. Serial drug dilutions were prepared in assay buffer and each concentration was tested in duplicate in each experiment. 20 μL of each compound were incubated with 50 μL [^3H]dofetilide (final concentration ~ 12 nM) and 50 μL of the HEK-hERG membrane preparation (1.5 mg mL^{-1}) for 2 h at room temperature. Binding was terminated by rapid filtration and radioactivity was determined as described above. Data was analyzed by non-linear regression and IC_{50} values determined. The affinity for each hERG1 blocker (K_D value) was calculated using the Cheng-Prusoff equation (Cheng *et al.*, 1973):

$$K_D = \text{IC}_{50} / (1 + [\text{ligand}] / K_D)$$

Where IC_{50} is the concentration of the competing ligand (displacer) that gives 50% inhibition of [^3H]dofetilide specific binding (50% displacement); [ligand] is the concentration of [^3H]dofetilide used in the displacement assay; K_D is the dissociation constant determined in the [^3H]dofetilide-HEK-hERG1 saturation binding experiments (see above).

2.5.2.4 Screening of transfected NIH-3T3 clones

Unlabelled dofetilide (20 μL ; final concentration 10 μM) or assay buffer (20 μL) were incubated with 50 μL [^3H]dofetilide (~12 nM) and 50 μL of the clone membrane preparation (~1.5 mg mL^{-1}) for 2 h at room temperature. Three total binding and two non-specific binding values for [^3H]dofetilide binding were obtained for each clone membrane sample and three independent experiments were performed for each clone. Membranes prepared from HEK-hERG and NIH-VC cells were used as positive and negative controls, respectively.

2.5.3 Western blotting to analyze hERG1 protein expression

The Western blotting technique has been used here to detect expression of hERG1 proteins in stably transfected cells. Denatured proteins are separated on a polyacrylamide gel according to molecular mass. Proteins are then transferred to a nitrocellulose membrane for analysis. A primary antibody is used to bind specifically to the target protein. A secondary antibody conjugated to a reporter molecule is used to bind to the primary antibody and to produce a detectable, localized signal when a substrate is added.

2.5.3.1 Preparation of total cell extracts

Stably transfected cells were grown overnight to ~ 70% confluency in 6-well plates. Culture medium was aspirated and discarded. Cells in each well were then washed with 1 mL cold D-PBS and lysed with 200 μL ice-cold RIPA buffer (Sigma) supplemented with a protease inhibitor cocktail (Complete, Roche). After 10 min of incubation on ice on an orbital shaker, lysates were collected and homogenized by passing through 19G needles 5-6 times. Cell lysates were centrifuged (20,000 $\times g$, 4 min, 4°C) and supernatants were

transferred to fresh tubes. Protein concentrations of the cleared cell lysates were determined by Lowry protein assay. Total cell extracts were kept at -80°C and thawed on ice when used subsequently.

2.5.3.2 Lowry protein assay

This assay is widely used for measurement of total proteins in cell lysates. It involves two steps. First, proteins react with copper under alkaline conditions (Biuret reaction). Secondly, the copper-treated proteins produce a colour change on reduction of Folin reagent (Lowry *et al.*, 1951). Briefly, protein samples were diluted 1:25 in 0.1 M NaOH. Serial dilutions of a standard protein, BSA (1 mg mL^{-1}), were prepared to provide 0, 25, 50, 100, 200, 250 and $400\text{ }\mu\text{g mL}^{-1}$ protein concentrations. All samples and standards were made in duplicate. 1 mL of a solution containing (2 % w/v Na_2CO_3 /0.4 % w/v NaOH, 0.01 % w/v CuSO_4 and 0.02 % w/v Na^+/K^+ tartarate) was added to all standard and sample tubes, vortex-mixed and incubated for 10 min. $100\text{ }\mu\text{L}$ of Folin reagent (Sigma) diluted 1:3 in MilliQ water was added, vortex-mixed and left for a further 20 min. Absorbance was measured at 750 nm using a spectrophotometer (Shimadzu, Japan). Absorbance values for BSA standard samples were plotted against protein concentration and fitted with a linear regression to obtain a standard curve that was used to determine the protein concentration of the experimental samples.

2.5.3.3 hERG1 antibodies

Two anti-hERG1 antibodies custom-made for our lab (Invitrogen, UK) were used in this study to detect hERG1 expression. These were a rabbit anti-hERG1 antibody, raised against amino acids 883-901 of hERG1, and an affinity purified goat anti-hERG1 polyclonal

antibody, raised against amino acids 1145-1159 of hERG1. Both antibodies recognise C-terminal hERG1 epitopes. Initial experiments were performed to optimize the conditions of Western blotting using these antibodies.

2.5.3.4 Blotting

Cells were lysed and protein concentrations of cell lysates determined as described above. An appropriate amount of total protein from each sample was diluted with an equal volume of 2x Laemmli buffer (Sigma). Proteins were denatured by heating at 60°C for 2 min. Samples and a coloured molecular weight protein marker (Biolone, London) were then loaded onto 6% w/v sodium dodecylsulfate (SDS)-polyacrylamide gels and proteins resolved by electrophoresis (SDS-PAGE) at 150 V for 90 min. Proteins were transferred from the gel to a nitrocellulose membrane under semi-dry transfer conditions using a Trans-blot SD transfer cell (Biorad, CA, USA) for 20 min at 15 V. Protein transfer was confirmed by staining the membrane with Ponceau S solution (Sigma) which binds reversibly to protein bands. After washing with MilliQ water to remove Ponceau S stain, the membrane was then blocked for 1 h to decrease non-specific binding to the membrane in a blocking buffer consisting of 5% w/v Marvel milk powder in Tris/Tween-buffered saline (TTBS) containing 150 mM NaCl, 10 mM Trizma base and 0.1% v/v Tween-20, pH 8. The membrane was incubated overnight at 4°C with a 1:1000 dilution of rabbit or goat hERG1 antibody in the blocking buffer. The following day, the membrane was washed several times in TTBS and incubated for 1 h at room temperature with a 1:3000 dilution of anti-rabbit (Sigma) or anti-goat (R&D Systems, MN, USA) antibody, prepared in the blocking buffer. Secondary antibodies were conjugated to horseradish peroxidase (HRP) as a

reporter molecule. The membrane was washed several times with TTBS (0.1% v/v Tween-20) and proteins detected by treatment of the membrane with ECL-Plus reagent (Amersham). This reagent produces an enhanced chemiluminescent signal through a peroxidase-catalyzed oxidation of the Lumigen PS-3 acridan substrate and generation of an acridinium ester. Excess reagent was removed and the nitrocellulose exposed on an ECL Hyperfilm (Amersham) in a cassette, and developed using a hyperprocessor (Amersham). The chemiluminescence signal produced is proportional to the amount of target protein in each sample.

2.6 Migration assays

Metastatic cancer cells show an enhanced motility and increased migration into other tissues and thus changes in migration rate and pattern may be characteristics of a transformed phenotype. Migration was quantified in either scratch-wound assays, or using single-cell measurements of cell velocity monitored by time-lapse microscopy.

2.6.1 Scratch-wound assay

Scratch-wound assays are widely used to measure the migration rate of coherent groups of cells into a scratch/wound that is manually made in a confluent cell monolayer. Cells are plated in duplicate in normal culture medium at a density of 2×10^6 cells in 6 cm dishes overnight. During this time, the cells attached and form a near-confluent monolayer. A sterile pipette tip is used to form a scratch-wound within the cell monolayer. Culture medium is aspirated and the cells are washed with D-PBS to remove any floating/dead cells before adding fresh medium. The base of each dish is pre-marked with five transverse lines using a fine-tip permanent marker before returning the dishes to a humidified air:CO₂

incubator at 37°C. The diameter of the wound at the five marked points is recorded at time 0 and every 2 h up to 10 h using an eye graticule calibrated against a slide graticule. The rate of wound closure ($\mu\text{m h}^{-1}$) at each of these five different points on the plate is calculated as follows:

$$\text{Wound closure rate} = (\text{width at zero h} - \text{width after 10 h})/10$$

These values are averaged to obtain the mean wound closure rate for each condition/clone. This is repeated for the duplicate plate and both are averaged to obtain the final mean value of wound closure rate in one experiment. The experiment is repeated at least three times for each clone per condition and the mean (\pm SEM) values calculated.

During this research, the assay has been modified for use with imaging software to allow more precise data acquisition and analysis. 35 mm dishes were marked underneath with three transverse lines using a sharp razor blade. Each scratch wound was imaged at the 3 marked points of contact with the transverse lines using OpenLab nodular imaging software (Improvision, USA) that controls a digital camera integrated with a Nikon Eclipse TI-S inverted microscope (Nikon, Japan) and images taken at time zero and after 10 h of incubation at 37°C in an atmosphere of humidified air:5% CO₂. Acquired images were imported to ImageJ Software (**National Institutes of Health, USA**) and the surface areas calculated as the number of square pixels. The percentage closure of the wound at a single point was calculated as follows:

$$\text{Percentage wound closure (\%)} = [1 - (\text{SA after 10 h} / \text{SA at zero-time})] \times 100$$

Values from duplicate plates were averaged to obtain final mean values of percentage wound closure in one experiment. Experiments were repeated at least three times for each experimental condition.

2.6.2 Analysis of migration of single-cells using time-lapse microscopy

Malignant cell transformation is associated with acquisition of an enhanced migratory potential, which contributes to tumour invasion and metastasis (Hanahan *et al.*, 2000). Time-lapse microscopy is a useful technique to characterize the migratory phenotype of transformed cells (Rajah *et al.*, 1998). In this study, time-lapse microscopy has been used to investigate whether WT hERG1/hERG1 mutant expression affects the migratory behaviour of NIH-3T3 cells on different extracellular matrix (ECM) proteins. Migration of NIH-3T3 clones expressing WT hERG1 (NIH-50 and NIH-16), G628S hERG1 (NIH-C3 and NIH-C36), A561V hERG1 (NIH-C10 and NIH-C12), the mock-transfected (NIH-VC) and NIH-Ras cells on various ECMs was assessed.

35 mm dishes were coated with collagen type I ($30 \mu\text{g mL}^{-1}$; Cascade Biologics), fibronectin ($2 \mu\text{g mL}^{-1}$; Sigma) or laminin-I ($1 \mu\text{g mL}^{-1}$; R&D Systems, Minneapolis, USA) prepared in D-PBS. The dishes were incubated at 37°C for 30 min (collagen-1 and fibronectin) or overnight (laminin-1) according to the supplier's recommendations. The ECM protein-PBS solution was removed and dishes were washed with D-PBS. The density of seeded cells and the time-points chosen for measuring migration were determined based on optimization experiments using NIH-VC cells. Cells were initially plated at different densities (5 , 7.5 and 10×10^4) cells per 35 mm dishes. Only a density of 5×10^4 cells produced well-spaced cells when visualized in acquired images, which was important to

avoid contact inhibition of migration. NIH-VC cells were plated on tissue culture plates and the speed of migration was determined after 1, 2, 3, 4, 5, 6, 7, 8 or 14 h of initial plating. Cells (5×10^4) in 2.5 mL of the culture medium were added and dishes incubated at 37°C in a humidified air:5% CO₂ incubator. After 5, 6, 7 and 8 h of incubation, dishes were placed on a 37°C temperature-controlled stage of an inverted microscope (Eclipse TI-S, Nikon, Japan). Cells were visualized (20X objective) and a field of view containing an appropriate number (20-30) of well-spaced single cells chosen. Automated image acquisition of the selected field of view was performed by OpenLab modular imaging software (Improvision, USA), which controlled a digital CCD camera (Hamamatsu, Japan) mounted on the microscope. Images were recorded every 10 min over a period of 1 h in an automated fashion, resulting in a time-lapse sequence of seven images for the 1 h time-frame. Acquired digital images were saved to computer for off-line analysis.

2.6.2.1 Analysis of cell morphology and migration parameters

i. Speed of migration

The CCD camera and 20X objective resulted in digital images of 1344 x 1024 pixels (580 x 440 μm). The position of each individual cell in consecutive images was marked through manual tracking of its centroid (the central position of the cell). All visible, viable cells within the field of view were tracked. Excel measurement files were generated by OpenLab software, which were transferred to FileMaker Pro software (USA) for calculation of motility parameters for each cell including:

-Total cell displacement (μm): this represents the true distance travelled by the cell and is equal to the sum of cell-centroid translocations among successive images.

-Net displacement (μm): This represents the distance from initial cell position straight to the final position of the cell.

- True migration speed ($\mu\text{m min}^{-1}$): total cell displacement (μm)/recording time (60 min)

- Net migration speed ($\mu\text{m min}^{-1}$): net cell displacement (μm)/ recording time (60 min)

Individual cell data were used to calculate the mean values for the cell population in the field of view in every experiment. Each experiment was repeated at least three times.

ii. Migration directionality

Directional migration (persistence) refers to the ability of migrating cells continuously to move in one direction rather than moving randomly. It can be represented by the ratio of mean net cell displacement to total cell displacement (Friedl *et al.*, 1993). Cells moving persistently along one straight line in one direction would have a directionality value of 1 while cells moving randomly would have a directionality value approximating zero.

iii. Cell spreading

Cell transformation is characterized by decreased cell spreading. Ras-transformed fibroblasts exhibit a spindle-like morphology and a diminished transverse spreading (Gloushankova *et al.*, 1997, Kharitonova *et al.*, 2007). Cell spreading of hERG1-transfected NIH-3T3 was assessed by calculation of the mean SA of the cell population within each field of view. Briefly, images acquired at zero-time for each time-lapse microscopy experiment were transferred to ImageJ Software and the “freehand selection” tool was used to outline the circumference of individual cells. The SA of each cell (μm^2) was calculated and values averaged to get the mean SA of the cell population.

iv. Cell polarization

Transformed fibroblasts exhibit confined areas of protruding lamellae and increased cellular polarization. In addition, Ras transformation of epithelial cells causes loss of their non-polarized, discoid shape and induces cell polarization (Gloushankova *et al.*, 1995, Gloushankova *et al.*, 1997). To estimate the effect of hERG1 expression on cell polarization, the number of polarized cells was counted and divided by the total number of cells in the same field. A polarized cell was defined as one that has one localized lamellar protrusion at the leading edge, resulting in an asymmetric cell shape (Nobes *et al.*, 1999). Twelve values (3 experiments at each of 4 time-points) were obtained for each clone.

2.7 Analysis of β 1-integrin, β -actin and vinculin expression levels on culture plasticware and fibronectin by Western blotting

Low confluency lysates were generated by plating 2.5×10^5 cells in a 35 mm dish for 24 h in absence or presence of fibronectin ($2 \mu\text{g mL}^{-1}$) coating. Lysates were prepared and blotting performed as previously described (Section 1.5.3). Briefly, 20-60 μg of sample protein was loaded on 10% w/v SDS-polyacrylamide gel and resolved by electrophoresis. Gels were blotted onto nitrocellulose membranes, which were blocked by incubating in a blocking buffer and incubated with a primary antibody:

Mouse anti- β 1-integrin (BD Bioscience) diluted 1:1000

Monoclonal mouse anti- β -actin (Sigma) diluted 1:1000

Mouse monoclonal anti-vinculin (Sigma) diluted 1:10000

Primary antibody was incubated for 24 h at 4°C (anti- β 1-integrin antibody) or for 1 h at room temperature (anti- β -actin and anti-vinculin antibodies). Blots were washed in TTBS and incubated with a 1:3000 dilution of HRP-conjugated goat anti-mouse secondary antibody (Sigma) for 1 h at room temperature. Blots were then washed in TTBS and Immunoreactivity was visualized by ECL as described previously.

Band intensities were analyzed by densitometry using ImageJ Software (NIH, USA). The ratio of vinculin to β -actin immunoreactivity was determined for each sample, and the results were expressed **relative to vinculin expression from cells cultured on plastic**.

2.8 Immunocytochemistry

2.8.1 Vinculin and actin double-staining

Glass coverslips were treated with poly-L-lysine (20 mg mL⁻¹) (Sigma) or fibronectin (2 μ g mL⁻¹) as previously described. Cells were cultured for 8 h prior to removing the medium, washing twice in D-PBS and fixation. Cells were fixed in 4% w/v paraformaldehyde in PBS (Sigma) at room temperature for 15 min and coverslips then washed 3 times with D-PBS. Cells were then permeabilized by treatment with 0.2% v/v Triton X-100 in PBS (Sigma) for 4 min, blocked using 5% v/v goat serum in PBS for 20 min and washed with PBS. Coverslips were incubated for 1 h with a 1:100 dilution of mouse monoclonal anti-vinculin (Sigma) antibody in PBS containing 1% v/v goat serum before washing with PBS. Anti-mouse secondary antibody conjugated to Alexafluor 488 was added for 1 h at a 1:100 dilution in PBS containing 1% v/v goat serum; cells were washed and blocked with 0.1% w/v BSA in PBS for 30 min. To visualize actin, cells were treated with 100 μ L of a 1:250 dilution of Texas-Red-conjugated phalloidin (Molecular Probes) in 0.1% w/v BSA in PBS

for 30 min. The Alexafluor- and Texas-Red-conjugated reagents were incubated in the dark to minimize photobleaching. Coverslips were washed with 0.1% w/v BSA in PBS for 20 min and mounted using ProLong Gold antifade reagent (Molecular Probes). Vinculin and actin staining were visualized at excitation and emission wavelengths of 488 and 650 nm, respectively using a confocal laser-scanning microscope (Olympus Fluoview, Japan).

2.9 Proliferation assays

2.9.1 Saturation-density assay

Saturation-density assays measure the number of cells that can grow and be viable on a specific surface area. Therefore, it can measure the ability of confluent cells to grow over each other as a consequence of loss of contact inhibition. However, the assay does not take into consideration cell size, shape, or proliferation rate, which may vary from one clone to another. Briefly, cells were plated in duplicate in normal culture medium at a density of 2×10^6 cells per 6 cm dish. The medium was exchanged every day. On the 4th day, the medium was aspirated and cells washed with PBS, trypsinized to generate a cell suspension, and cells counted using a haemocytometer, in the presence of 0.4% w/v trypan blue. Experiments were repeated at least 3 times for each clone.

2.9.2 MTT proliferation assay

3-(4, 5-Dimethylthiazol-2-yl)-2, 5- diphenyltetrazolium bromide (MTT) is widely used to measure the proliferation and viability of cells (Mosmann, 1983). MTT is reduced to purple formazan crystals by mitochondrial enzymes in living cells. These crystals can be dissolved in a suitable solvent and the intensity of the colour can be measured by spectrophotometry.

NIH-3T3 clones were plated at a density of 4×10^4 cells in 1 mL of culture medium in 4 replicate wells in 24-well plates. Culture medium was replaced every 3 days. After 4-8 days, 100 μL of 5 mg mL^{-1} MTT solution in PBS was added to each well. The plates were rocked for 3 min on an orbital shaker at room temperature to mix the MTT and then incubated at 37°C for 2 h. The culture medium was then removed and 0.5 mL of dimethyl sulfoxide (DMSO, Sigma) added to each well and the plate rocked for 15 min. Absorbance at 570 nm was measured using a microplate reader (NOVOstar, BMG LABTECH, Germany). Wells without cells were used as a negative control. Absorbance values for 4 replicate wells for each clone were averaged to get a mean absorbance value for one experiment. Experiments were repeated at least three times.

In these experiments, cells were also counted at day 8 after plating to give an independent measure of cell viability. Culture medium (1 mL per well) was collected and the cells were washed with 0.5 mL D-PBS and this also collected. Cells were lifted using 0.5 mL trypsin-EDTA solution and all three volumes were collected together producing a total volume of 2 mL per sample. Viable cells in each sample were counted using a cell counter (CASY1, Scharfe system counter, Innovatis, Reutlingen, Germany).

WT NIH-3T3 cells were used to produce a standard curve of MTT absorbance over a range of cell densities. Cells were plated in quadruplicate in 24-well plates at a density of 0, 0.2, 0.4, 0.8, 1, 2, 3 or 5 ($\times 10^5$) cells per well and kept at 37°C for 5 h for the cells to attach. The MTT assay was performed as above and the absorbance values for different cell densities measured. Experiments were repeated at least 3 times and the mean (\pm SEM)

values plotted against cell number and fitted with a linear regression function to obtain a standard curve.

2.10 Statistical analysis of data

Data are expressed as mean \pm standard error of the mean (SEM) of different treatments/experimental conditions. Statistical comparisons of results were performed using one-way analysis of variance (ANOVA) or two-way ANOVA with repeated measures as appropriate. Following ANOVA, a suitable multiple comparison post-test was applied to identify significant differences between means. Dunnett's test of multiple comparisons has been used when means of groups are compared to the mean of a reference group (control). Bonferroni's post-test has been used when the number of groups was ≤ 5 , otherwise Tukey's post-test was used. A non-paired Student's *t*-test has been used to compare means of two datasets. A value of $p < 0.05$ was considered statistically significant. Prism 4.0 (GraphPad Prism Software, San Diego, USA) was used for statistical analyses and to present results graphically.

Chapter 3

Investigating the effects of extracellular matrix on the transforming properties of NIH-3T3 cells stably expressing hERG1

3.1 Introduction

The oncogenic potential of hERG1 is presently well characterized. Many studies have suggested roles of hERG1 in numerous aspects of tumour progression including proliferation, migration, angiogenesis, invasion and metastasis. Moreover, stable expression of wild-type (WT) hERG1 in NIH-3T3 cells confers some of the characteristics of a transformative phenotype, including enhanced cell migration, overgrowth at confluency and post-confluent changes in cell morphology (Pier, 2007).

The extracellular matrix (ECM) provides a physical scaffold for cellular adhesion. Moreover, cell-matrix adhesions, mainly mediated by integrins, generate signals that regulate many cellular processes, such as survival, proliferation, migration and differentiation. ECM also plays a pivotal role in tumour progression, and both pro- and anti-tumorigenic effects of tumour cell-ECM adhesion have been reported. Collagen-1 has been reported to inhibit proliferation of human melanoma cells (Henriet *et al.*, 2000). Integrin signalling can directly influence transformed cell characteristics and is involved in the invasive and metastatic phenotype of tumour cells (Hood *et al.*, 2002).

Interestingly, it has been shown that adhesion of hERG1-expressing tumour cells of neuronal and hemopoietic origins to components of ECM results in a short-term activation of hERG1 channels, associated with the induction of neurite extensions and cell differentiation (Arcangeli *et al.*, 1993, Arcangeli *et al.*, 1996, Hofmann *et al.*, 2001). Moreover, hERG1 co-

immunoprecipitates with β 1-integrins and its downstream signalling effectors, focal adhesion kinase (FAK), Src tyrosine kinase (Cayabyab *et al.*, 2002) and the small GTPase Rac1 (Cherubini *et al.*, 2005). It has been suggested that binding to ECM induces integrin-hERG1 coupling, and hERG1 channel activity modulates the downstream signalling of the integrin to influence tumour cell characteristics.

However, these data are derived from studies performed on hERG1-expressing cancer cell-lines and primary tumour cells. Given the complex nature of these cell systems, with a vast array of genes potentially being dys-regulated as a consequence of cumulative mutations occurring during tumorigenesis, it is difficult to conclude with confidence that hERG1-mediated effects in tumour cells are truly dependent upon or affected by adhesion to ECM components. An alternative approach is to investigate the effect of adhesion to ECM in NIH-3T3 cell-lines, previously generated in my lab, which stably express WT hERG1, and to investigate changes compared to cells transfected with an empty vector and lacking endogenous hERG1 expression. NIH-Ras cells, which express a constitutively-active V12-Ras mutant, were used as a positive control for a transformed phenotype.

In this Chapter, the effect of ECM on the transforming activity of hERG1 was studied by investigating over-growth capacity, cell morphology, migratory properties and cytoskeletal organization of two NIH-3T3 cell-lines stably expressing hERG1, namely NIH-50 and NIH-16, on different extracellular matrices as compared to vector control (NIH-VC) cells. The effect of modulation of hERG1 function and/or surface expression has also been studied.

3.2 Results

NIH-16 and NIH-50 are two NIH-3T3 cell-lines that stably express WT hERG1. It was first essential to test if these cells display the previously reported features of a transformed behaviour. The transforming behaviour of hERG1 expression in NIH-3T3 cells was evaluated by assessing saturation density, alterations in post-confluency cell morphology and enhancement of cell migration. Migration and loss of contact inhibition experiments were performed on hERG1-expressing cells and compared to vector-control NIH 3T3 (NIH-VC) cells.

3.2.1 hERG1 expression in NIH-3T3 cells allow over-growth and increased post-confluent cell density

To confirm the transforming activity of hERG1 expression, a saturation density assay was used. This assay measures cell number several days after the cells have formed a confluent monolayer. Non-transformed cells stop dividing and cease growing once a homogenous monolayer has formed. A feature of transformed cells is that they continue to divide and grow on top of each other (Johansen *et al.*, 1994). Thus, a plate can support larger numbers of transformed than non-transformed cells. NIH-3T3 cells were plated at 1×10^6 cells per 35-mm culture dish, a density sufficient to produce a near-confluent monolayer. After 4 days, there was an increase in the number of NIH-16 and NIH-50 cells and this increase was significantly higher than that observed in NIH-VC cells (Fig. 3.1A). The cell number of NIH-VC cells was $0.97 \times 10^6 \pm 0.9 \times 10^5$; whereas hERG1-expressing clones grew to greater cell densities. The cell density reached for NIH-16 cells was $1.77 \times 10^6 \pm 0.1 \times 10^5$ ($p < 0.01$ versus NIH-VC; $n=3$), while NIH-50 cells achieved a density of $1.57 \times 10^6 \pm 0.3 \times 10^5$ ($p < 0.01$ versus NIH-VC; $n=3$). The saturation density assay does not take into account changes in cell size or cell

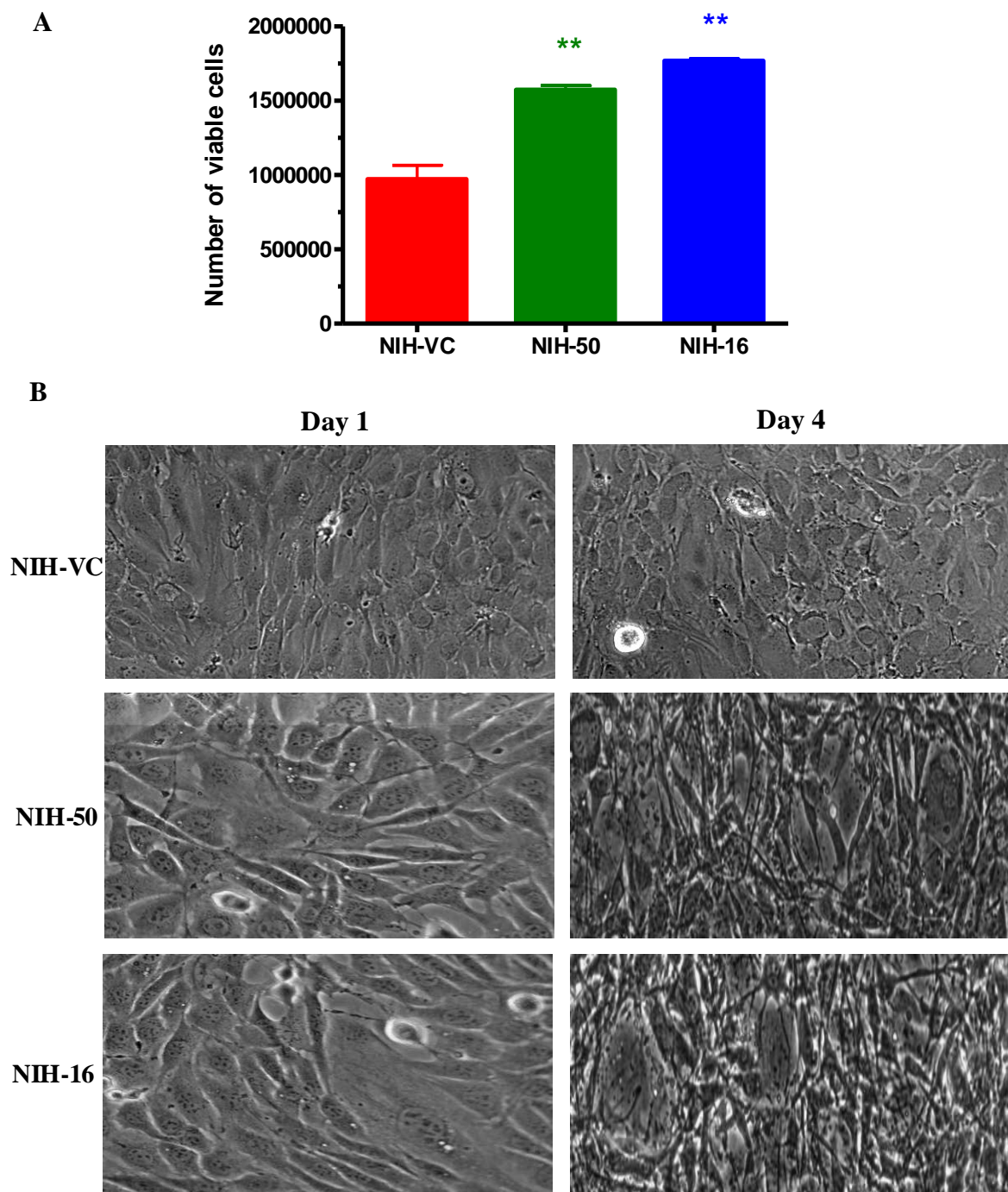


Figure 3.1 hERG1 expression results in an increase of post-confluency cell density. **A.** Number of viable cells counted on the 4th day after plating cells at a density of 1×10^6 cells per 35 mm dish. Data represent means \pm SEM of 3 experiments performed in duplicate. ** indicates significantly different results compared to NIH-VC ($p < 0.01$). **B.** Live images of NIH-3T3 cells taken one day (left) and four days (right) after cell plating at confluency.

shape; therefore, it was important to confirm that the increase in cell number seen in hERG1-expressing clones is due to over-growth. The high density of NIH-16 and NIH-50 cells could be due to changes in cell morphology that allow cells to pack more closely together. Post confluency images of the NIH-3T3 clones are shown in Fig. 3.1B. When NIH-VC cells become confluent, they stop dividing due to contact inhibition and showed a characteristic flattened ‘cobblestone’ morphology typical of NIH-3T3 fibroblasts. The NIH-16 and NIH-50 cells displayed changes in morphology post-confluency, where they become more elongated and spindle-like in appearance and gained the ability to grow on top of one another, possibly due to loss of contact inhibition.

3.2.2 hERG1 expression in NIH-3T3 cells enhances cell migration

A scratch-wound assay was used to compare migration rates of different NIH-3T3 clones. This assay involves measuring how fast cells migrate into an artificially made gap (wound) in a confluent cell monolayer. An example of cell migration into the wound is shown in Fig. 3.2. Photographs of the same point are shown just after the wound was made and 10 h later. The NIH-VC cells show a uniform pattern of wound closure compared to the more disorganized pattern observed with NIH-16 cells. It seems that hERG1-expressing cells move as individuals rather than the sheet-like collective migration seen in NIH-VC cells. The change from sheet-like to individual cell migration is seen in cancer cells (Friedl *et al.*, 2004). In collective migration, cells at the leading edge form lamellipodia, these ‘pull’ trailing cells behind them, maintaining cell-cell contacts and thereby allowing movement as a sheet in a direction perpendicular to the scratch. hERG1-expressing cells migrate in different directions and so do not maintain an organized wound edge. The faster movement of the leading cells

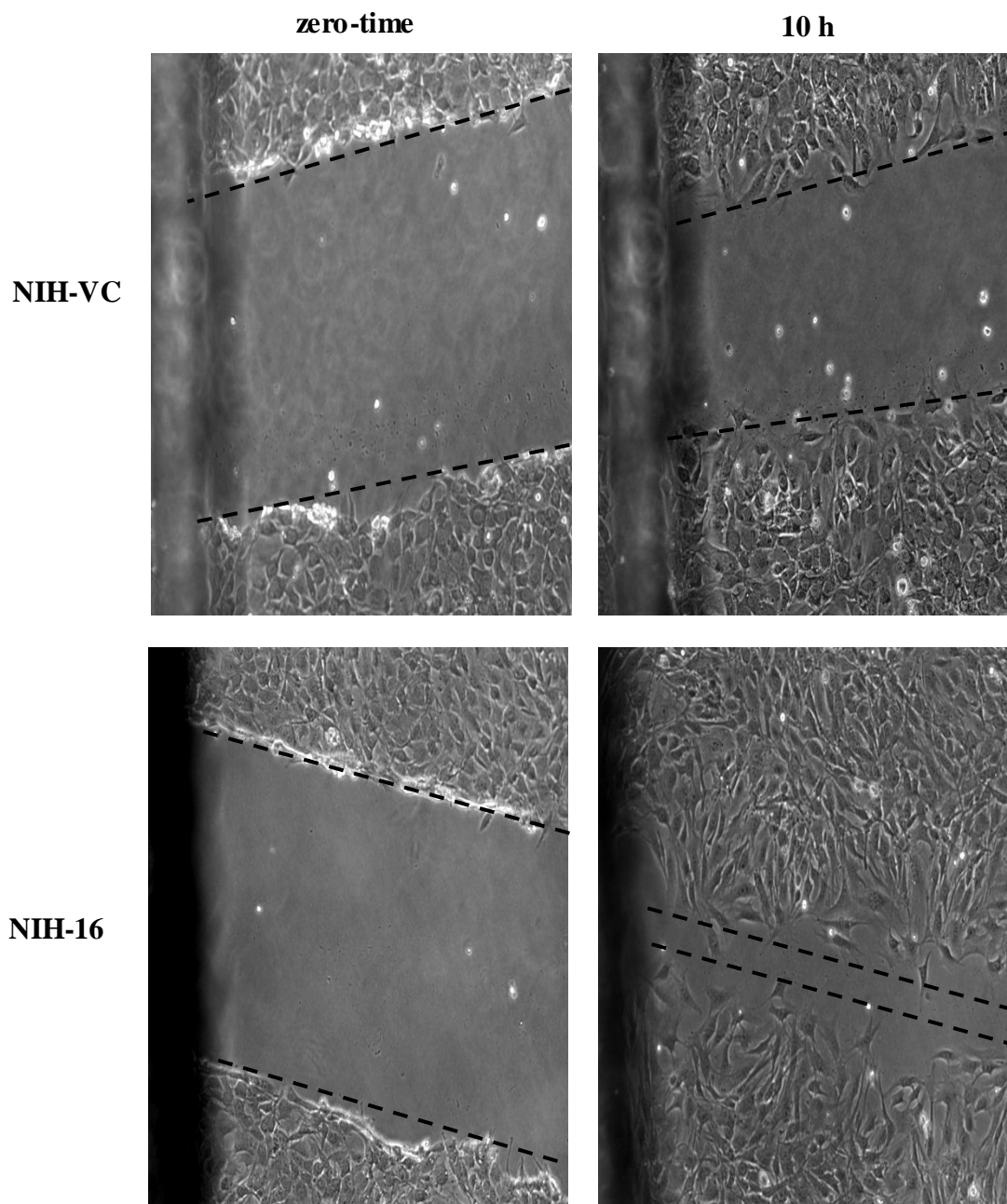


Figure 3.2 Images of wound closure in NIH-VC and NIH-16 cells.

Images were taken immediately after a scratch-wound was made in confluent monolayers of cells and again after 10 h. The images show a greater rate of wound closure in case of NIH-16 cells. NIH-16 cells seem to move individually rather than the collective, sheet-like migration seen for NIH-VC cells. Black dashed lines highlight the margin of wounds at the beginning and end of the experiment. Scale-bar, 50 μm .

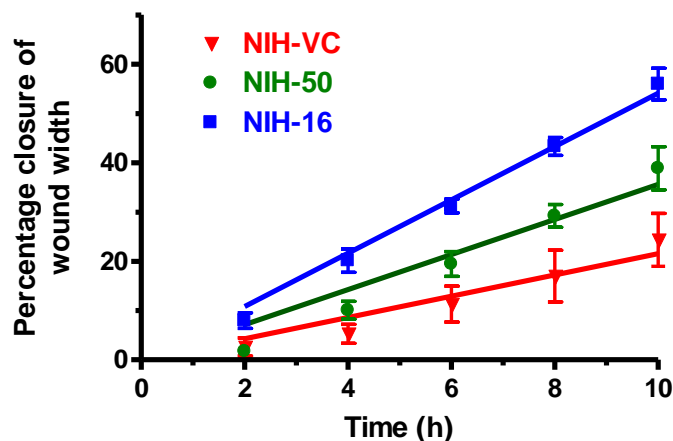
may allow other cells behind them to form lamellipodia, a behaviour also characteristic of a transformed phenotype (Friedl *et al.*, 2004).

To measure the rate of migration of NIH-3T3 clones, it was essential to confirm that wounds close linearly with time. The wound closure of NIH-3T3 clones was monitored by measuring wound width every 2 h over a total period of 10 h. The percentage decrease in wound width was calculated at each time-point and data obtained were fitted by a linear regression function (Fig. 3.3A). The correlation coefficient (r^2) values for NIH-VC, NIH-50 and NIH-16 regression curves were 0.979, 0.999 and 0.999, respectively, indicating a linear pattern of wound closure. The rate of wound closure at the end of each experiment (10 h after making the wound) was then determined. The closure of wounds at this time is primarily due to cell migration and can be minimally ascribed to proliferation of NIH-3T3 cells, since the mean doubling time for NIH-3T3 cells is reported to be ~ 24 h (Johansen *et al.*, 1994, Kuo *et al.*, 2000). Moreover, hERG1-expressing NIH-3T3 clones exhibited similar proliferation rates as WT NIH-3T3 and NIH-VC cells (Pier, 2007). Fig. 3.3B shows mean (\pm SEM) values from at least three experiments for relative rates of wound closure of NIH-3T3 clones. NIH-VC cells exhibited a rate of migration of $14.6 \pm 2.1 \mu\text{m h}^{-1}$. The NIH-16 and NIH-50 clones close wounds at faster rates (33.1 ± 1.8 and $26.4 \pm 1.5 \mu\text{m h}^{-1}$, respectively); the latter migration rates were significantly higher than that found for NIH-VC ($p < 0.01$; $n=5$).

3.2.3 Does ECM-mediated signalling influence the over-growth capacity of hERG1-expressing cells?

Adhesion of cells to the ECM is essential for proliferation (Guadagno *et al.*, 1993). The ability of transformed cells to over-grow each other is mediated through their capacity to overcome contact inhibition of growth due to dys-regulation of cell-cell adhesion mediated

A



B

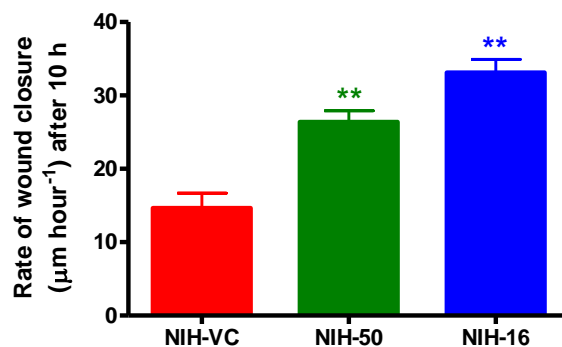


Figure 3.3 hERG1 expression increases the migration rate of NIH-3T3 cells.

A. The closure of wounds made in confluent monolayers of the NIH-3T3 cell-lines follow a linear pattern over a 10 h interval. The width of artificially-made wounds in confluent monolayers was measured over 10 h and the change in width normalized to the initially measured value. **B.** Rate of wound closure in NIH-3T3 clones. The rate of wound closure was calculated as follows: wound closure rate ($\mu\text{m h}^{-1}$) = (width (μm) after 10 h - width (μm) at zero-time)/10 (See Methods). In both panels **A**, **B**. Data represent means \pm SEM of at least 3 experiments performed in duplicate. ** indicates statistically significant values with reference to NIH-VC ($p < 0.01$).

by cadherin receptors. Several reports have indicated a potential role of integrin-dependent signalling in regulation of cadherin-dependent cell-cell adhesion (Braga *et al.*, 1997, Kuroda *et al.*, 1997, Takaishi *et al.*, 1997, Huttenlocher *et al.*, 1998). Dys-regulation of integrin-mediated signalling in transformed cells may cause disassembly of cell-cell contacts and over-growth, possibly through activation of MAP kinase pathways (Zhang *et al.*, 2002).

To test if ECM adhesion could affect the loss of contact inhibition of growth induced by hERG1-expression, saturation density assays were performed on different extracellular matrices and compared to cell density on tissue culture plastic as a source of non-integrin-mediated over-growth. The use of extracellular matrix-coated surfaces in this assay made it difficult to determine viable cell counts at the end of the assay by direct cell counting using traditional dye exclusion (trypan blue) methods because even non-viable cells remained attached to the culture surface. Therefore, the MTT viability assay was used. This assay indicates the viability of living cells through the ability of mitochondria to metabolize the MTT dye into a coloured salt, which can be easily quantified. The absorbance value measured directly correlates with the number of viable cells (Mosmann, 1983). To avoid errors that could result from differences in metabolic activity between the different NIH-3T3 cell-lines, a standard absorbance curve using a range of cell densities for each cell-line was determined (Fig. 3.4A). The correlation factor (r^2) for absorbance curves of NIH-VC, NIH-50, NIH-16 and NIH-Ras were 0.979, 0.956, 0.887 and 0.959, respectively, indicating a linear relationship. These curves were then used to determine viable cell number on each cell matrix 3 days after cells were plated at confluency (Fig. 3.4B). As shown previously, hERG1-expressing clones showed a higher cell density (2-3 fold) compared to NIH-VC cells. There was no significant effect of matrix adhesion on growth for any of the cell-lines tested, which might suggest that integrins are not involved in hERG1-induced cell over-growth.

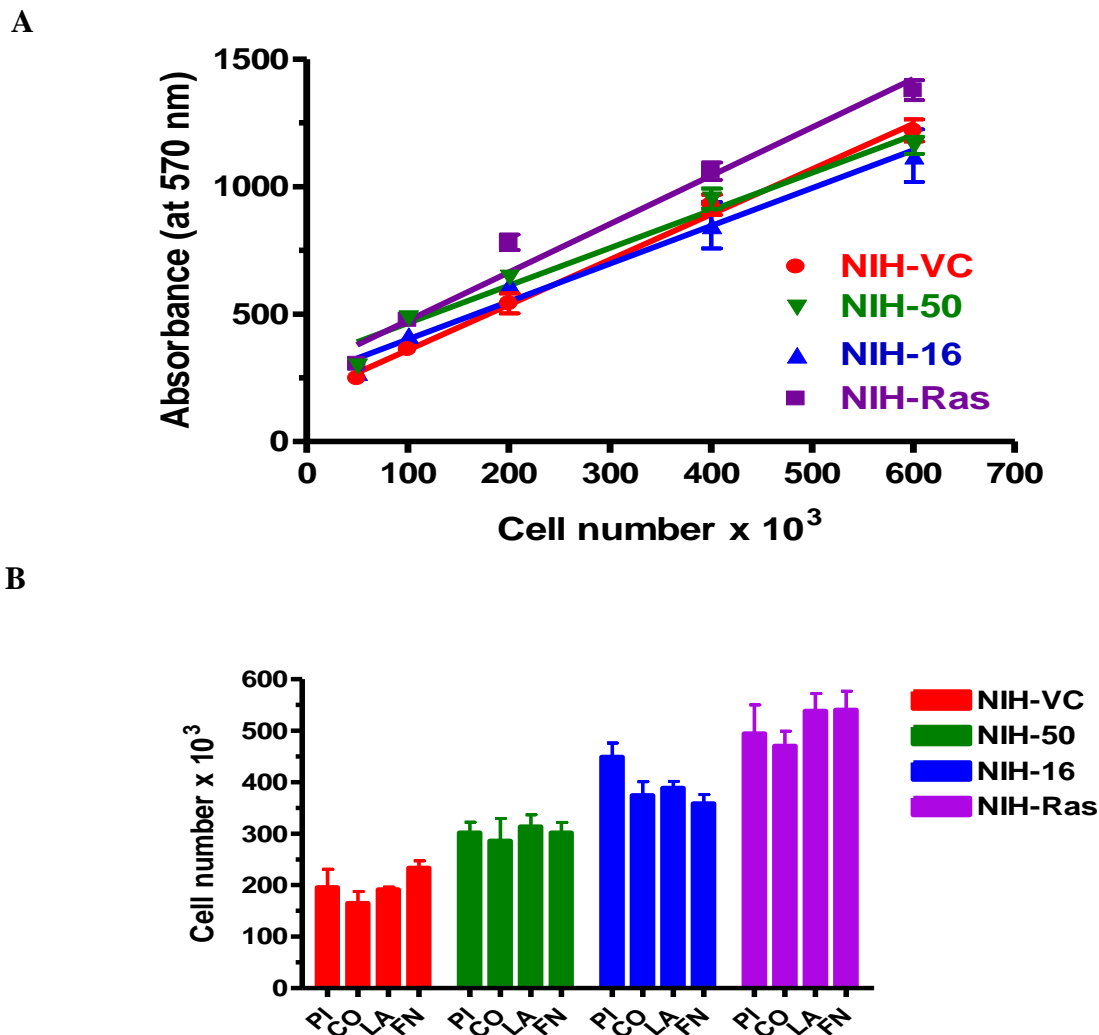


Figure 3.4 Effect of extracellular matrix adhesion on the over-growth capacity of hERG1-expressing cells. **A.** Different densities ($0.5\text{-}6 \times 10^5$) of each NIH-3T3 cell-line were plated and incubated with MTT (5 mg mL^{-1}) for 2 h before absorbance values at 570 nm were measured and data fitted with a linear regression function. **B.** Saturation density assay: 1.5×10^5 cells per 10 mm well for each cell-line were plated on either tissue culture plastic (PI), collagen-1 (CO, $30 \text{ }\mu\text{g mL}^{-1}$), laminin-1 (LA, $1 \text{ }\mu\text{g mL}^{-1}$) or fibronectin (FN, $2 \text{ }\mu\text{g mL}^{-1}$) and allowed to grow for 3 days before MTT was added and absorbance values measured. Viable cell numbers were determined by interpolation from the corresponding cell number-absorbance curves for each cell-line. For results shown in **A**, **B**. Data represent means \pm SEM values for at least 3 experiments, with each experiment obtained as an average of 4 replicate readings.

The effect of ECM-adhesion mediated-signalling on the over-growth potential of hERG1-expressing cells could have been masked by conditions used in the saturation density assays. First, the long experimental time required for over-growth of cells (3 days post-confluency) makes it difficult to avoid any deposition of endogenous ECM synthesized by the cells themselves. It has been shown that NIH-3T3 cells can deposit their own matrix after 5-9 days of growth (Beacham *et al.*, 2007). Moreover, to investigate the effect of integrin-mediated signalling on contact inhibition of growth, experiments should be performed under serum-free conditions to exclude the effect of growth factor-mediated signalling. However, previous investigations (Pier, 2007), and my own preliminary data, have indicated that hERG1-expressing cells lose the capacity for post-confluent over-growth in the absence of serum. Thus, alternative approaches for investigating integrin mediated signalling are needed to be used.

3.2.4 Effect of ECM adhesion on morphology and migration properties of NIH-3T3 cells expressing hERG1

Oncogenic transformation of epithelial cells (Gloushankova *et al.*, 1995) and fibroblasts (Dartsch *et al.*, 1994) is accompanied by changes in cell shape, cell-extracellular matrix interactions, motility and cytoskeletal organization. Cancer cell migration is regulated by components of the tumour microenvironment, including the extracellular matrix. hERG1-expressing NIH-3T3 cells displayed faster rates of migration than cells that do not express hERG1 (Fig. 3.3B) To determine if adhesion to components of ECM affects the migration properties of hERG1-expressing NIH-3T3 cells, time-lapse microscopy was used to study the migration of single cells on common extracellular matrices, including collagen-1, laminin-1 and fibronectin. Concentrations of coating matrices were chosen based on previous reports

and preliminary experiments. Time-lapse microscopy is commonly used for studying the mechanisms for migration of invading cancer cells, which often migrate individually (Rajah *et al.*, 1998, Wang *et al.*, 2002b). It can also provide insights into the mechanistic basis of ECM-mediated changes in cell shape and migratory pattern.

3.2.4.1 Tissue culture plasticware

Initially, the conditions for time-lapse microscopy of single cell migration were optimized. NIH-VC cells were plated on tissue culture plasticware and the time required for them to adhere and spread was observed. Cells began to spread after 1 h of adhesion. By 3 h of plating, NIH-VC cells were partially spread and after 5 h of plating, spreading was complete and cells showed the typical flattened fibroblast morphology with extended processes (Fig.3.5A). The speed of migration of NIH-VC cells was then studied. Cells were imaged at 10-min intervals over a 1-h experiment. The centroid (the central position) of each visible cell within the field of view was manually tracked after each cell translocation in consecutive images using cell-tracking software to generate the cell-track (trajectory), which can then be used to calculate the total path length, net distance and true speed (Fig. 3.5B). The mean true speed of the cell population from each experiment was then calculated. Spreading of NIH-VC cells was associated with an increase in cell migration from $0.264 \pm 0.017 \mu\text{m min}^{-1}$ (n=3) after 1 h of adhesion to $0.400 \pm 0.031 \mu\text{m min}^{-1}$ after 5 h. After that, cells maintained near constant speeds of migration of 0.439 ± 0.054 (n=5), 0.425 ± 0.032 (n=3) and $0.444 \pm 0.049 \mu\text{m min}^{-1}$ (n=3) after 6, 7 and 8 h of adhesion, respectively (Fig. 3.5C). Therefore, the time range of 5 - 8 h after cell plating was chosen to investigate cell migration in subsequent experiments; allowing a sufficient time-window to generate quadruplicate determinations within each experiment, each of which was performed on at least three separate occasions.

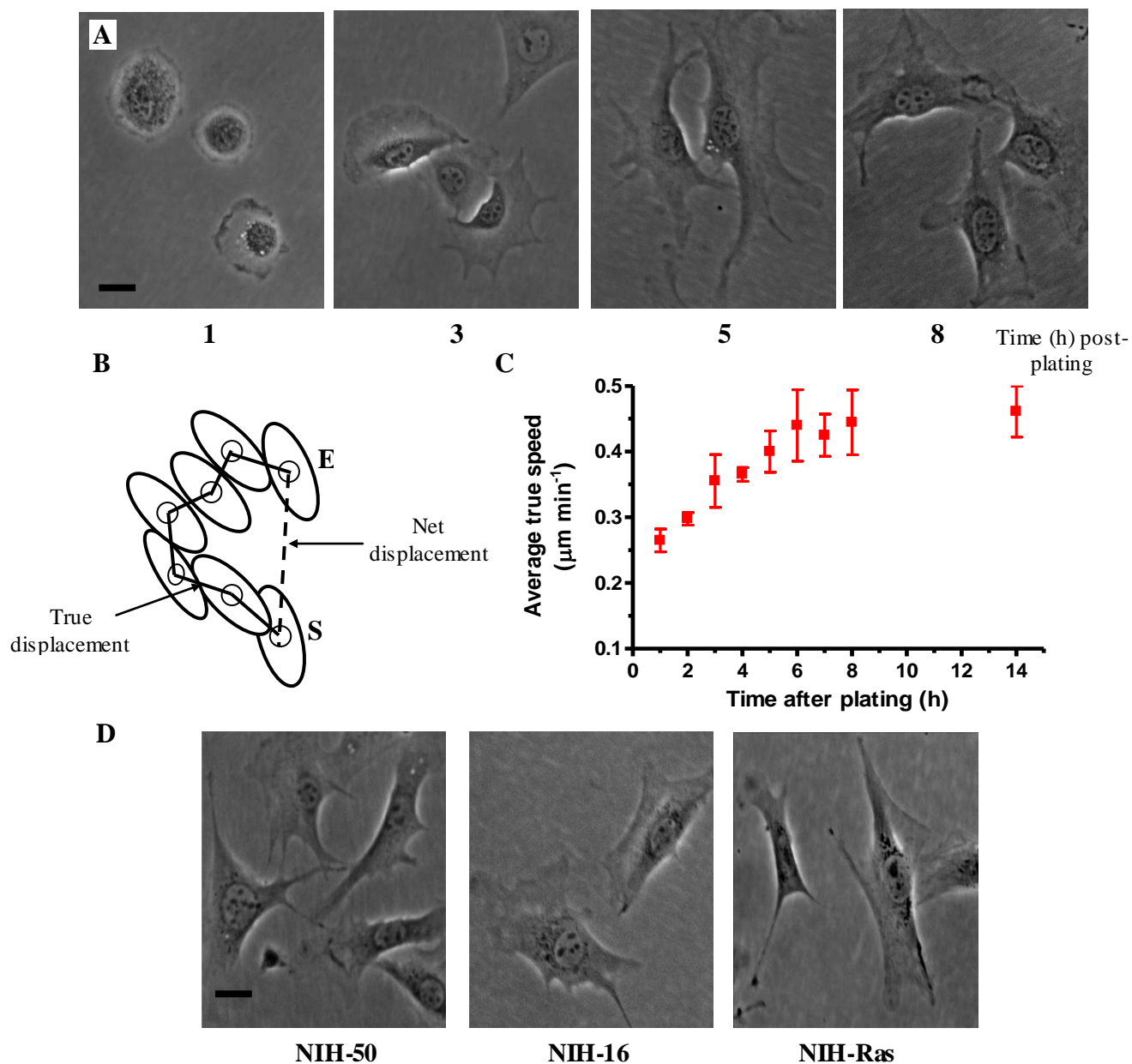


Figure 3.5 Optimizing time-lapse microscopy conditions for analysis of single-cell migration. **A.** Spreading of NIH-VC cells after indicated number of hours on tissue culture plasticware. **B.** Schematic representation of the tracking of a migrating cell. The cell centroid is marked in consecutive images taken at 10 min intervals for 1 h. The shortest distance from the start (S) to the end (E) position represents the net displacement, whereas the true displacement (the total path length) represents the sum of cell-centroid translocations. **C.** Average true speed of migration of NIH-VC cells. The mean speed of migration of the cell population was calculated over a 14 h period post-plating on tissue culture plasticware. Data are presented as means \pm SEM for at least 3 experiments. **D.** Morphology of different NIH-3T3 clones after 8 h of adhesion to tissue culture plasticware. **A, D.** Scale-bar, 20 μm .

Inspection of the morphology of hERG1-expressing (NIH-50 and NIH-16) cells that have adhered to culture plastic for 8 h revealed no substantial differences when compared to NIH-VC cells (Fig.3.5D), whereas NIH-Ras cells showed a range of transformed morphologies from spindle, elongated, polygonal and rounded appearances (Fig.3.5D).

The transformed behaviour of hERG1-expressing cells after adhesion to ECM proteins was assessed by characterizing changes in cell shape, cell spreading (as determined by calculating average cell-surface area), cell polarization, intrinsic persistence and migration speed (see Methods for a detailed description of the analysis parameters).

3.2.4.2 Migration of hERG1-expressing cells on collagen-1

The morphologies of hERG1-expressing cells after adhesion to collagen-1 were compared with those of NIH-VC and NIH-Ras cells (Fig. 3.6A). hERG1-expressing cells exhibited a similar cell shape to NIH-VC cells, having the typically flattened morphology of fibroblasts with extended lamellipodia around the whole cell margin. There were also no differences in spreading of NIH-VC, NIH-50 and NIH-16 cells, which assumed an average surface area of 2671 ± 102 , 2381 ± 103 and $2690 \pm 114 \mu\text{m}^2$, respectively (analyzed from 12 migration experiments for each cell-line) (Fig. 3.7A, right). Conversely, NIH-Ras showed a transformed cell shape, where cells were polygonal- or spindle-shaped with a polarized appearance conferred by a confined lamellipodium at the leading edge and a tail-like extension at the trailing edge (Fig. 3.6A). NIH-Ras cells showed a decreased cell spreading as indicated by an average cell-surface area of $1386 \pm 83 \mu\text{m}^2$ ($p < 0.01$ relative to NIH-VC; $n=12$).

Time-lapse microscopy experiments were performed 5 - 8 h post initial adhesion to collagen-1 and the speeds of migration calculated (Fig. 3.6B). hERG1 expression did not affect the migration speed of NIH-3T3 cells and there were no significant differences in their velocities

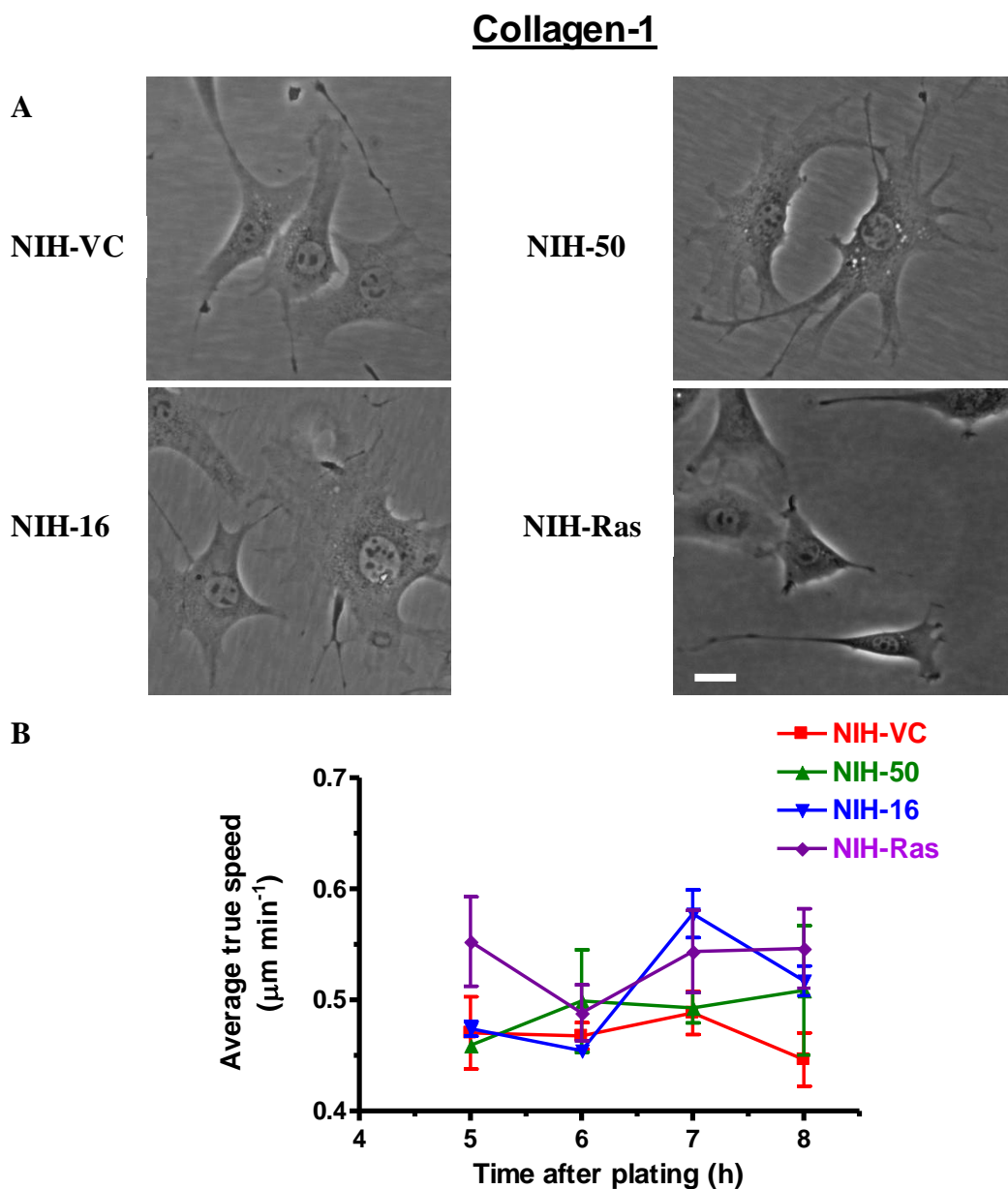
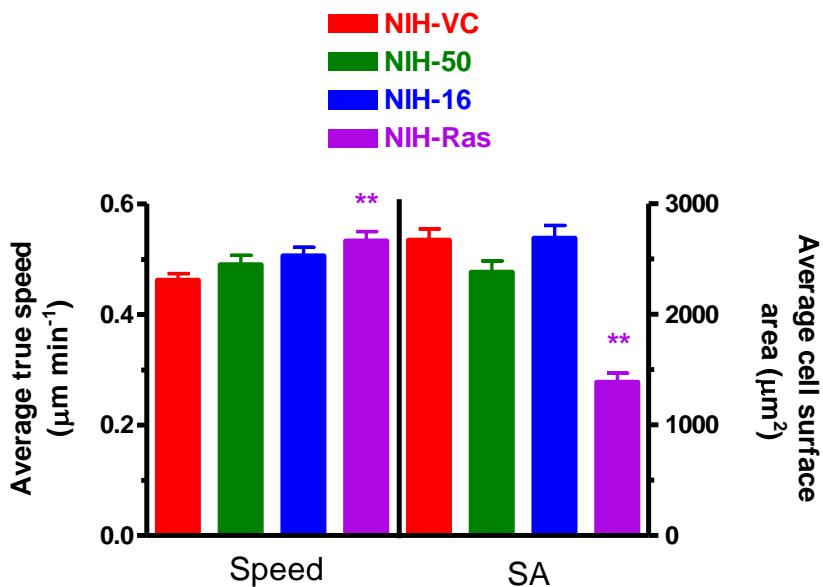


Figure 3.6 Migration of NIH-3T3 cells stably-expressing wild-type hERG1 on collagen-1 coated surfaces. **A.** Morphology of NIH-3T3 clones after 8 h adhesion to a collagen-1 (30 μg mL⁻¹) coated surface. Scale bar, 20 μm. **B.** Average true speed of NIH-3T3 cell-lines over the period 5-8 h after plating on collagen-coated dishes. NIH-3T3 cells were plated at a density of 5 x 10⁴ cells per 35 mm dish and imaged every 10 min for 1 h. Nuclei of single cells were tracked and the average speed of migration for the cell population (15-20 cells) in each experiment was calculated. Data represent means ± SEM for at least 3 experiments at each time-point.

Collagen-1

A



B

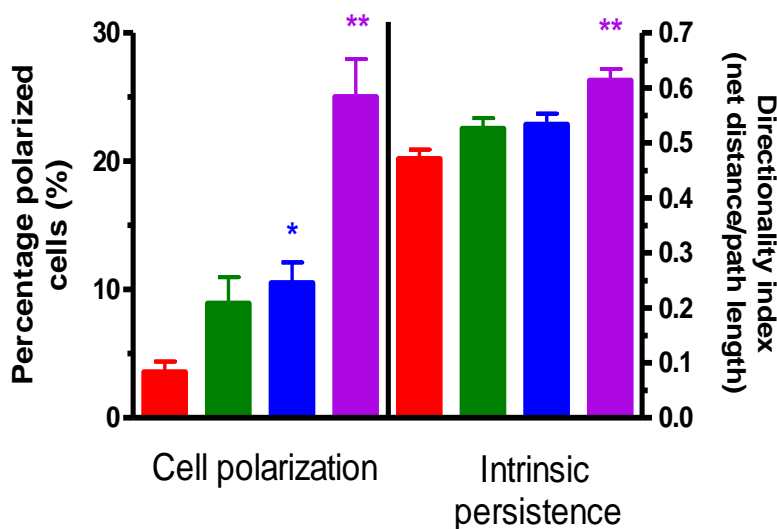


Figure 3.7 Analysis of the migratory behaviour of hERG1-expressing cells on collagen-coated surfaces. **A.** Average true speed (left) and average cell-surface area (SA, right) of NIH-3T3 cell-lines. **B.** Percentage polarized cells (left) and directionality index (right) of NIH-3T3 cell-lines. Analysis parameters were calculated as described in Methods. Data represent means \pm SEM for the analysis of at least 12 experiments, representing the pooled data from experiments performed at 5-8 h after adhesion to collagen-coated dishes. Statistical significance with reference to NIH-VC was as follows: * $p < 0.05$ and ** $p < 0.01$.

when compared to NIH-VC at any time-point. This finding was confirmed by the analysis of the pooled data (Fig. 3.7A, left). NIH-VC cells showed an average migration speed of 0.461 ± 0.012 (n=12) $\mu\text{m min}^{-1}$, whereas NIH-50 and NIH-16 cells showed similar migratory velocities of 0.489 ± 0.017 (n=12) and 0.505 ± 0.015 (n=12) $\mu\text{m min}^{-1}$, respectively ($p > 0.05$). NIH-Ras cells showed a significantly higher speed of migration of 0.532 ± 0.016 $\mu\text{m min}^{-1}$ ($p < 0.01$ relative to NIH-VC; n=12).

A polarized cell morphology, where cells develop a protrusive leading edge and a trailing edge, is a characteristic of cell transformation (Gloushankova *et al.*, 1995). The percentage-of polarized cells in the populations studied in the migration experiments was also determined (Fig. 3.7B, left). The NIH-VC cell population showed the occasional occurrence of a polarized phenotype ($3.5 \pm 0.8\%$), whereas NIH-50, NIH-16 and NIH-Ras cell populations exhibited higher percentages (8.9 ± 2.0 , 10.5 ± 1.6 ($p < 0.05$) and 25.0 ± 2.9 ($p < 0.01$), respectively).

Establishing a polarized cell morphology is a requirement for directional cell migration (induced by an external stimulus, such as a growth factor), or internal persistence (in the absence of exogenous chemotactic stimuli), where cells tend to move continuously in one direction without turning. Intrinsic persistence of cell migration was quantified by calculating a directionality index (the ratio of the net cell displacement to the total path-length travelled by the cell, see Fig. 3.7B, right). A directionality index close to 1 indicates the cells are travelling in a straight line. Low directionality index values indicate the cell is making little progress in a particular direction. NIH-VC and the hERG1-expressing NIH-50 and NIH-16 cells showed an essentially random cell movement, as indicated by directionality indices of 0.47 ± 0.01 (n=173), 0.52 ± 0.02 (n=159) and 0.53 ± 0.02 (n=148), respectively. In contrast,

NIH-Ras cells showed a higher intrinsic persistence (0.61 ± 0.02 ($p < 0.01$ versus NIH-VC; $n=142$). Overall, these data suggest that adhesion to collagen-1 did not affect the migratory behaviour of hERG1-expressing cells.

3.2.4.3 Migration of hERG1-expressing cells on laminin-1

Adhesion of hERG1-expressing cells to laminin-1 was associated with some alteration in cell shape, particularly after 8 h of adhesion (Fig. 3.8A). Some cells assumed a spindle-shaped, polarized appearance with anterior-posterior asymmetry and extended tail-like cellular processes. NIH-Ras cells exhibited a typical transformed, spindle-like morphology (Fig 3.8A). hERG1-expressing cells were also significantly less well spread when compared to NIH-VC cells ($p < 0.01$, $n=12$). The average surface area (SA) occupied by NIH-VC cells was $4456 \pm 297 \mu\text{m}^2$, whereas NIH-50, NIH-16 cell and NIH-Ras cells had an average SA of 2535 ± 164 , 1998 ± 86 and $1283 \pm 56 \mu\text{m}^2$, respectively (Fig. 3.9A, right panel).

Fig. 3.8B shows the speeds of migration of hERG1-expressing cells at different time-points after adhesion to laminin-1. NIH-16 cells attained their highest speed after 8 h of adhesion ($0.491 \pm 0.030 \mu\text{m min}^{-1}$; $n=3$), which was significantly greater ($p < 0.05$) compared to the speed of migration of NIH-VC at this time-point ($0.336 \pm 0.023 \mu\text{m min}^{-1}$; $n=3$). Analysis of pooled data comprising values of migration speeds at all time-points also revealed a significant difference between NIH-16, NIH-50 and NIH-VC cells.

Populations of the hERG1-expressing NIH-50 and NIH-16 cells examined by time-lapse microscopy showed higher percentages of polarized cells of $16.9 \pm 2.4\%$ and $19.6 \pm 4.7\%$, respectively. NIH-VC cells completely lacked a polarized morphology, while NIH-Ras cells exhibited a greater proportion ($25.9 \pm 1.6\%$) of polarized cells (Fig. 3.9B, left). NIH-50 and NIH-16 cells also showed more directional cell movement, as indicated by respective

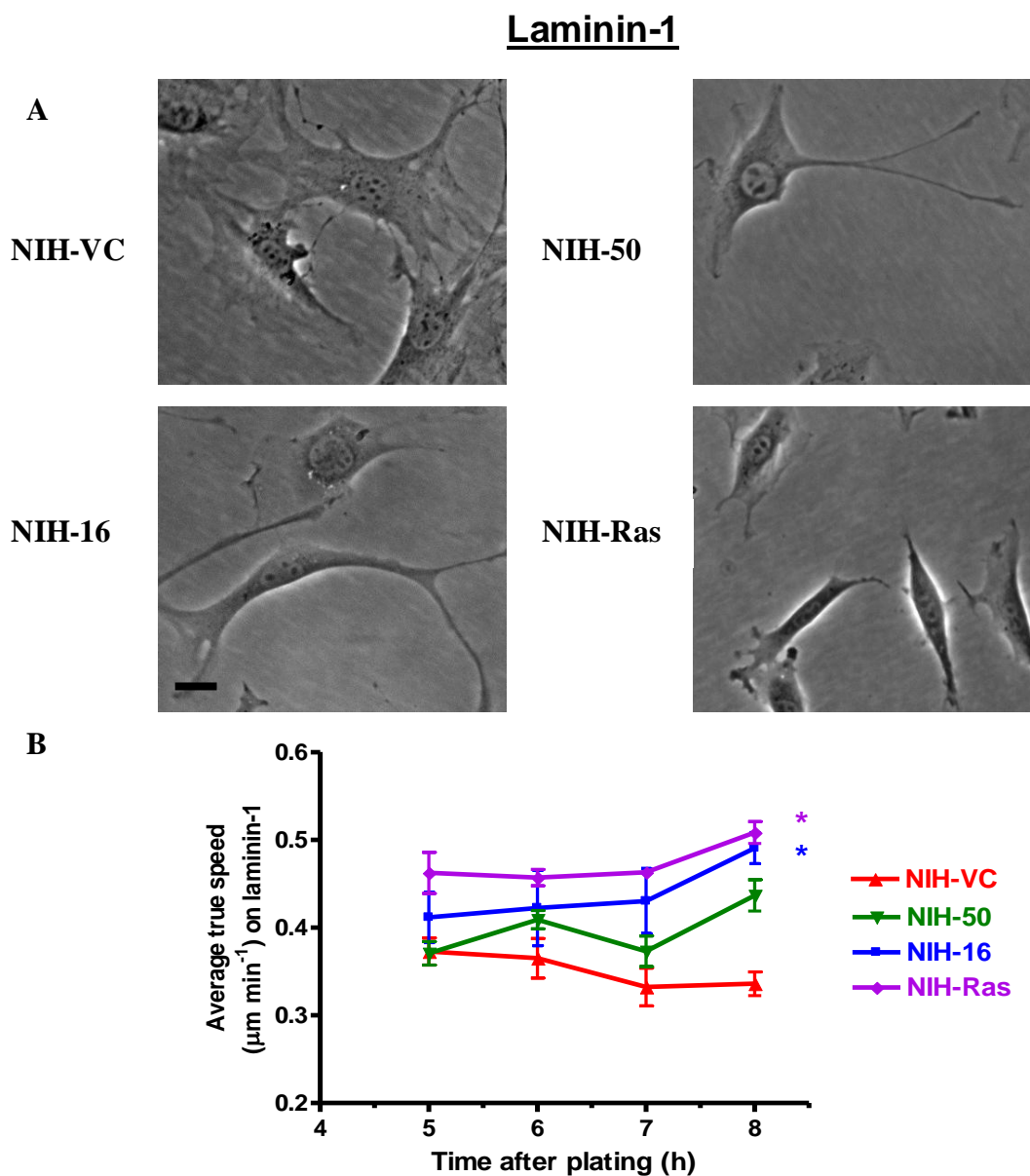


Figure 3.8 Migration of NIH-3T3 cells stably expressing WT hERG1 on laminin-1 coated surfaces. **A.** Morphology of NIH-VC, NIH-50, NIH-16 and NIH-Ras cells 8 h after plating on laminin-1 ($1 \mu\text{g mL}^{-1}$) coated surfaces. Scalebar, $20 \mu\text{m}$. **B.** Average true speed of NIH-3T3 cell-lines after 5-8 h of plating on laminin-1 ($1 \mu\text{g mL}^{-1}$) coated dishes. NIH-3T3 cells were plated at a density of 5×10^4 cells per 35 mm dish and imaged every 10 min for 1 h. Tracking was performed and analyzed as described in Methods. Data represent means \pm SEM for at least 3 experiments at each time-point. * indicates statistically significant values with reference to NIH-VC ($p < 0.05$).

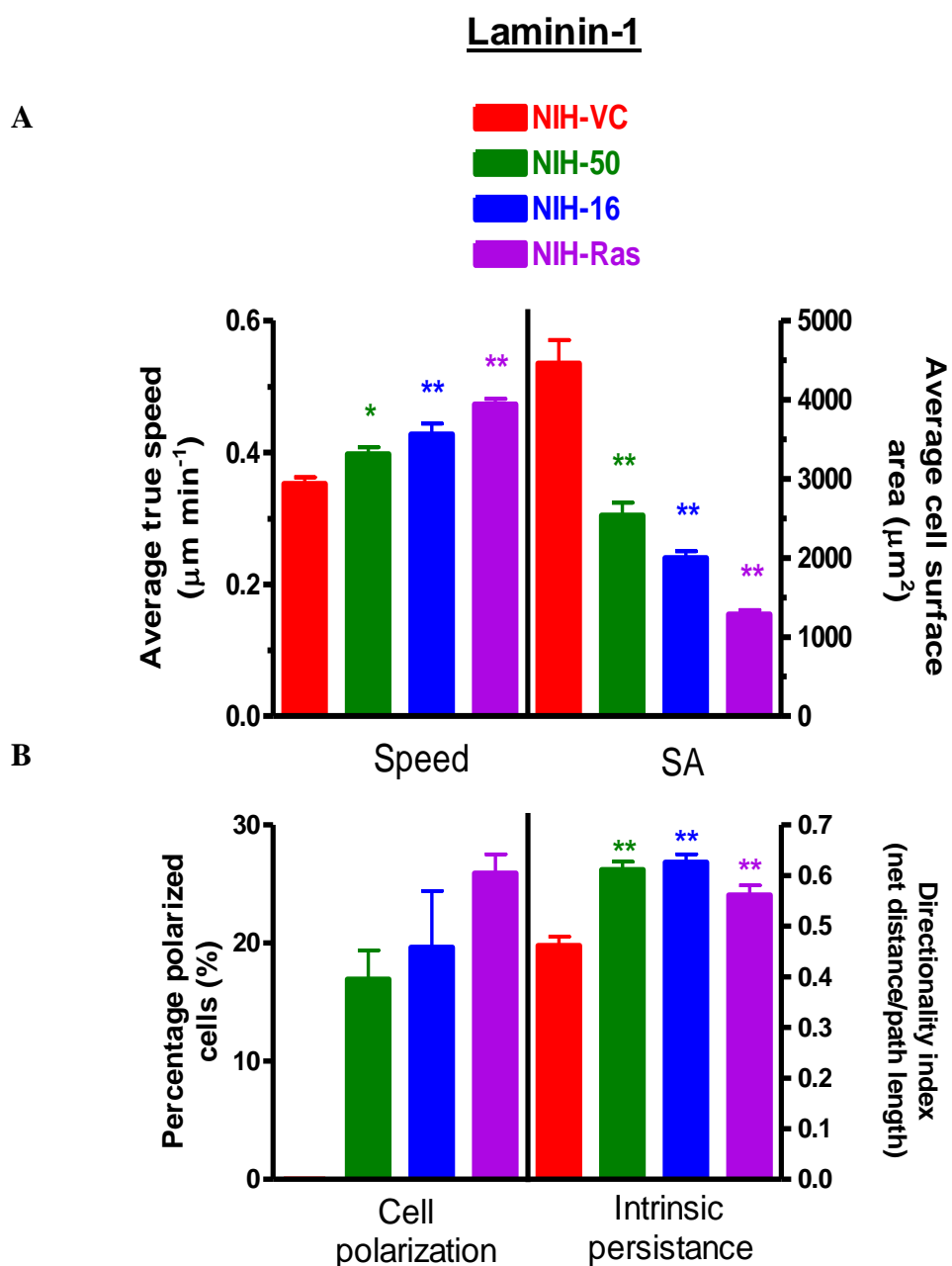


Figure 3.9 Analysis of the migratory behaviour of hERG1-expressing cells on laminin-1-coated surfaces. **A.** Average true speed (left) and average cell surface area (SA, right) of NIH-3T3 cell-lines. **B.** Percentage polarized cells (left) and directionality index (right) of NIH-3T3 cell-lines. Data represent means \pm SEM for at least 12 experiments, representing the pooled data from experiments performed at 5-8 h after adhesion to laminin-1 coated dishes. Statistical significance with reference to NIH-VC was as follows: * $p < 0.05$ and ** $p < 0.01$.

directionality indices of 0.61 ± 0.01 ($p < 0.01$; $n = 232$ cells) and 0.62 ± 0.01 ($p < 0.01$; $n = 208$ cells), compared to NIH-VC cells (0.46 ± 0.02 ; $n = 150$ cells). Collectively, it has been observed that adhesion of cells stably-expressing hERG1 to laminin-1 causes significant changes in cell behaviour, including cell shape changes, acquisition of a polarized appearance and enhanced directionality and speed of migration.

3.2.4.4 Migration of hERG1-expressing cells on fibronectin

When adhered to fibronectin, hERG1-expressing NIH-3T3 cells exhibited similar morphological features to Ras-transformed NIH-3T3 cells, including a spindle-shaped and elongated appearance with extended, elongated cellular processes at the trailing end of the cell (Fig. 3.10A). This altered phenotype was reflected by the significantly decreased ($p < 0.01$) surface area occupied by NIH-50 ($1906 \pm 68 \mu\text{m}^2$), NIH-16 ($1834 \pm 125 \mu\text{m}^2$) and NIH-Ras ($1276 \pm 72 \mu\text{m}^2$) cells compared to NIH-VC cells ($3344 \pm 210 \mu\text{m}^2$) (Fig. 3.11A). NIH-16 and NIH-Ras cells also exhibited higher significantly migration speeds on fibronectin compared to NIH-VC cells at all time-points investigated ($p < 0.05$), while the higher migration speed seen for NIH-50 cells did not attain statistical significance except 8 h after plating (Fig. 3.10B). Analysis of pooled data (Fig. 3.11A) confirmed statistically significant greater speeds exhibited by all clones relative to NIH-VC.

Analysis of cell polarity and persistence of cell migration is shown in Fig. 3.11B. hERG1-expressing NIH-50 and NIH-16 cells showed higher proportions of polarized cells ($41.8 \pm 3.1\%$ and $41.2 \pm 4.6\%$, respectively) compared to NIH-Ras ($23.0 \pm 1.0\%$) and NIH-VC ($3.8 \pm 1.0\%$) cells.

hERG1-expressing cells showed not only changes in migration speeds, but also displayed a distinct migratory phenotype on adhesion to fibronectin. An example of this difference is

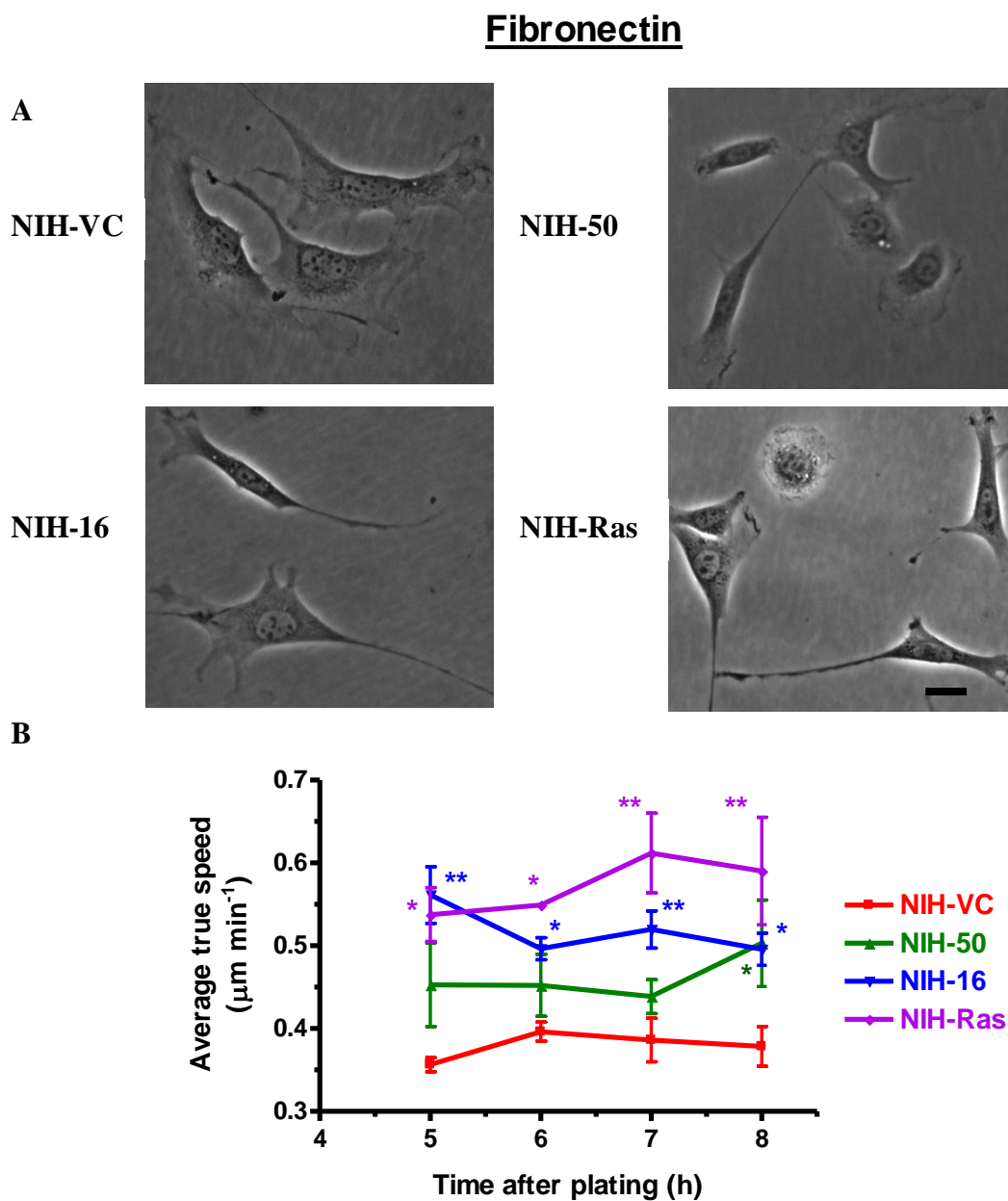


Figure 3.10 Migration of NIH-3T3 cells stably expressing WT hERG1 on fibronectin coated surfaces. **A.** Morphology of NIH-3T3 clones 8 h after adhesion to a fibronectin ($2 \mu\text{g mL}^{-1}$) coated surface. Scalebar, $20 \mu\text{m}$. **B.** Average true speed of NIH-3T3 cell-lines 5-8 h after plating on fibronectin coated dishes. Experiments were performed as described previously. Data represent means \pm SEM for at least 3 experiments at each time-point. Statistically significant values with reference to NIH-VC with * $p < 0.05$ and ** $p < 0.01$.

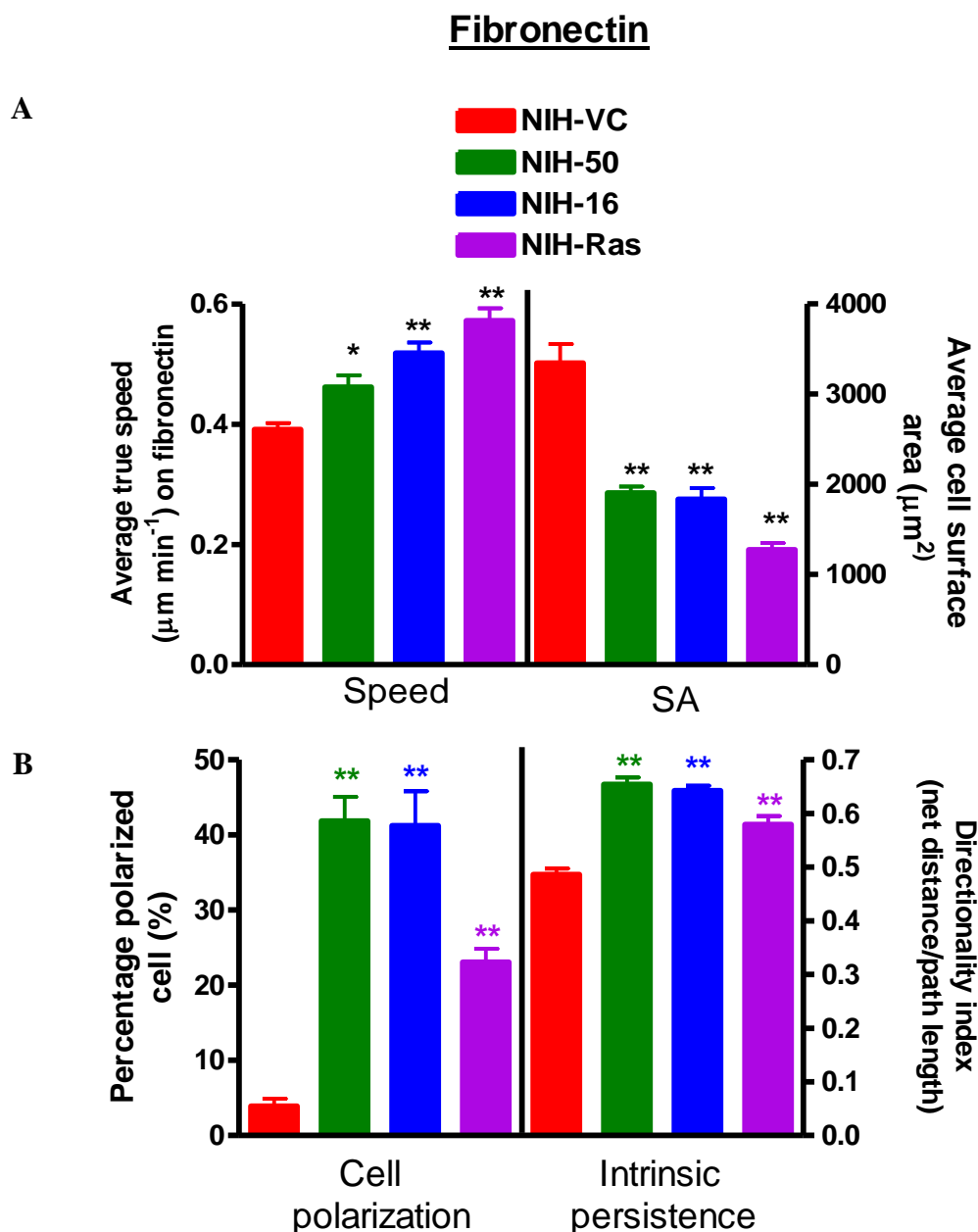


Figure 3.11 Analysis of the migratory behaviour of hERG1-expressing cells on fibronectin coated surfaces. **A.** Average true speed (left) and average cell-surface area (SA, right) of NIH-3T3 cell-lines. **B.** Percentage polarized cells (left) and directionality index (right) of NIH-3T3 cell-lines. Data are shown as means \pm SEM for at least 12 experiments, and represent the pooled data from experiments performed 5 - 8 h after adhesion to fibronectin coated dishes. Statistically significant values with reference to NIH-VC with * $p < 0.05$ and ** $p < 0.01$.

shown in Fig. 3.12. NIH-VC cells exhibited typical fibroblast motility, displaying large lamellipodia that ruffle around the cell causing short cell translocations and small net displacements (Fig. 3.12A). hERG1-expressing cells assumed a spindle-shaped, elongated morphology with small confined lamellipodia formed at the leading edge. hERG1-expressing cells also moved unidirectionally, with the cell body seeming to reduce adhesive contact and push against the front of the cell. Moreover, hERG1-expressing cells appeared to have difficulty in rear retraction, and the front of the cells seemed to pull against the rear-substrate adhesion, producing long tail-like extensions. At a certain point, rear substrate contacts are broken, eliciting a large forward displacement (Fig. 3.12B). This migratory phenotype was also observed, albeit less frequently, in NIH-Ras cells.

The migratory phenotype described for hERG1-expressing NIH-50 and NIH-16 cells suggests that they have a higher intrinsic persistence than NIH-VC cells, which was confirmed by observing trajectories of tracked cells during cell migration. Examples of cell tracking collected from one representative experiment for NIH-VC and NIH-16 cells are shown in Fig. 3.13A. Analysis of the frequency of directionality index values among the cell populations tested in migration experiments revealed that hERG1-expressing cells showed higher frequency of directionality index values (close to 1), indicating a persistent, directional cell movement. In contrast, NIH-VC cells exhibited a homogenous, uniform distribution of directionality index values (Fig. 3.13B).

3.2.5 Do hERG1-expressing cells exhibit altered levels of β 1-integrin, vinculin or actin proteins on adhesion to fibronectin?

The 'transformed' behaviour exhibited by hERG1-expressing NIH-3T3 cells induced by adhesion to fibronectin may be due to modulation of cellular integrin expression levels,

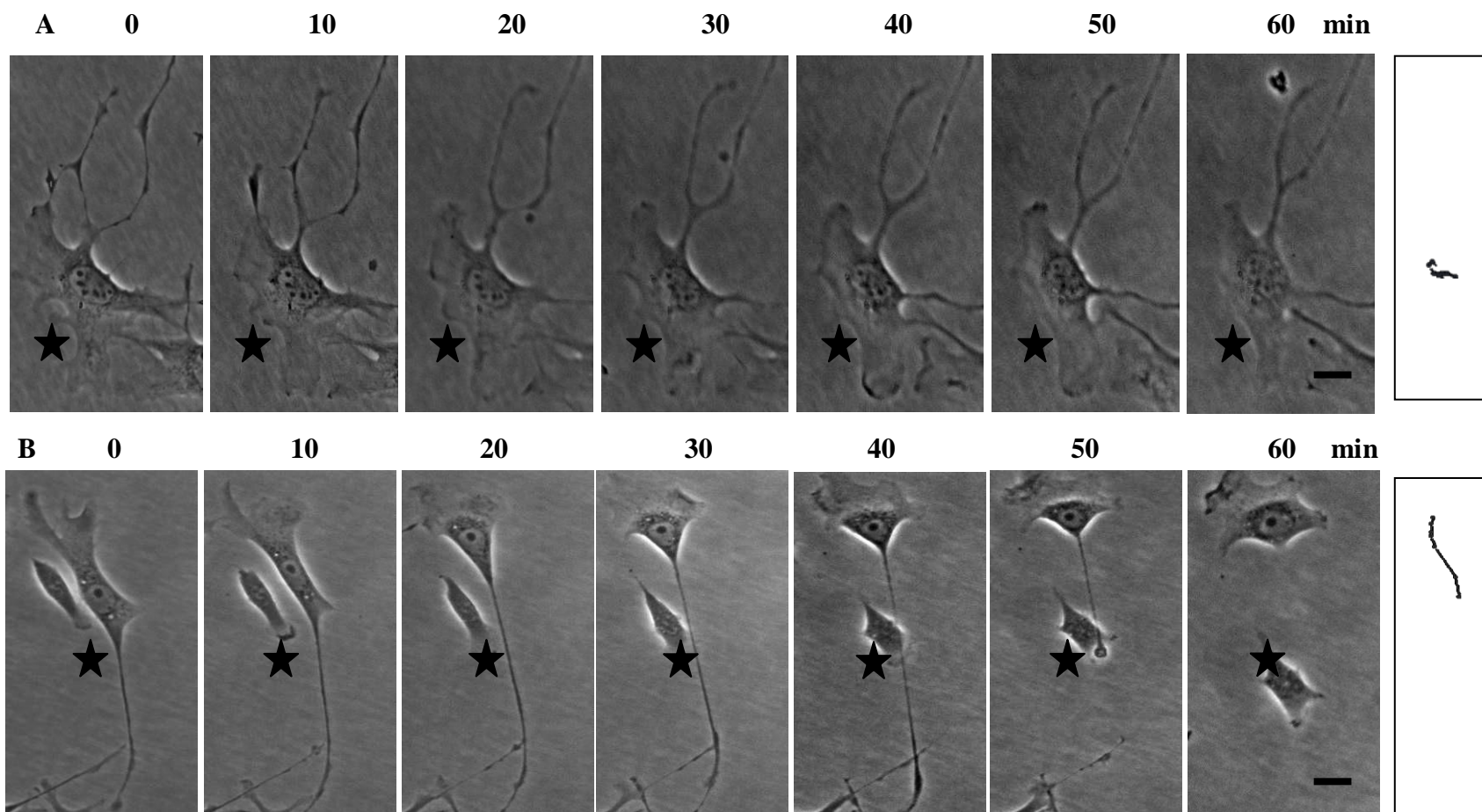


Figure 3.12 Patterns of migratory behaviour of NIH-VC (A) and NIH-16 (B) cells on fibronectin-coated surfaces. Cells were imaged at 10 min intervals for 60 min. Movements of individual cells were followed using cell-tracking software and represented as overlays of representative trajectories in boxes on the far right. The star represents a stationary reference point. All images are at the same magnification (20X) and equally cropped. Scalebars = 20 μ m.

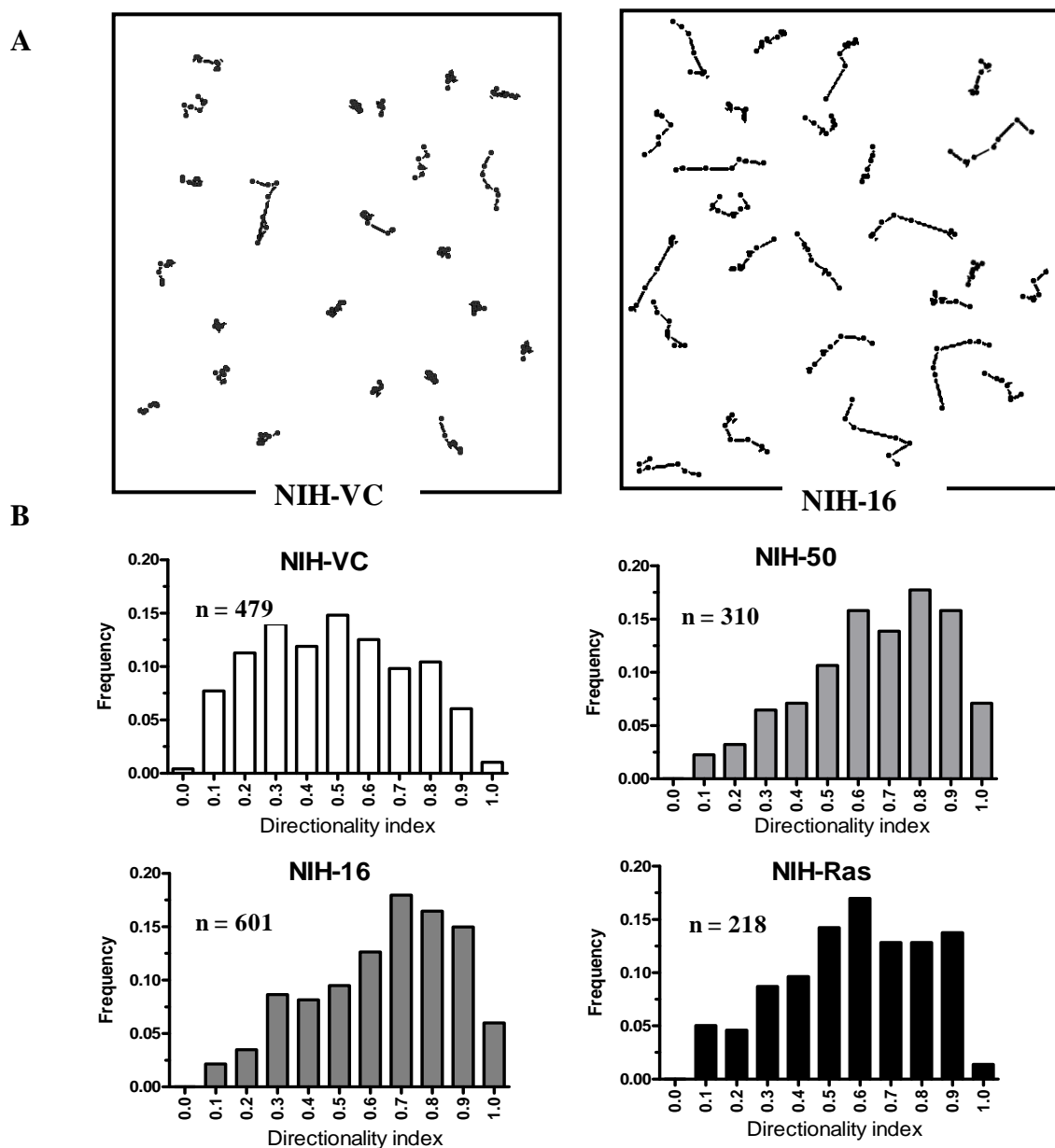
Fibronectin

Fig. 3.13 **hERG1-expressing cells exhibit intrinsic directional migration on fibronectin.** **A.** Representative migration tracks of NIH-VC and NIH-16 cells. Track blots were created by combining migration paths of individual cell movement from one experiment into a single figure to avoid empty spaces (Pankov *et al.*, 2005). **B.** Histograms showing relative frequency of cells with directionality index values binned in 0.1 unit increments. Note the skewing of histograms to high directionality index values for hERG1-expressing and Ras-transformed cells. The number of cells analyzed in each histogram is indicated.

producing the observed alterations in cell motility and morphology. It has been shown that hERG1 associates with β 1-integrin in tumour cells and heterologous expression systems (Cherubini *et al.*, 2005, Pillozzi *et al.*, 2007). The β 1-integrin subunit is expressed in NIH-3T3 cells (Dalton *et al.*, 1995, Whitfield *et al.*, 1999) and can combine with several integrin α -subunits to form receptors for the extracellular matrix proteins used in this study, such as collagen-binding (α 1 β 1 and α 2 β 1), laminin-1-binding (α 6 β 1) and fibronectin-binding (α 5 β 1) integrins. To determine if β 1-integrin expression is affected by adhesion to fibronectin in hERG1-expressing NIH-3T3 cells, the expression of β 1-integrin was assessed by immunoblotting. Cell lysates were prepared from NIH-3T3 cell-lines, which were seeded for 24 h at low confluency (50-60%) on either tissue culture plasticware or fibronectin, and β 1-integrin protein (MWt ~ 130 kDa) levels assessed (Fig. 3.14A, top). There were no apparent changes in β 1-integrin protein content of the hERG1-expressing cells on adhesion to fibronectin.

The loss of a typical flattened fibroblastic morphology and acquisition of a spindle-shaped-appearance by hERG1-expressing NIH-3T3 cells that adhere to fibronectin may be due to modulation of cytoskeletal protein levels, particularly actin and vinculin. To investigate this possibility, expression of these proteins was also investigated by immunoblotting. The expression levels of vinculin ((MWt ~ 120 kDa, Fig. 3.14A, middle) and β -actin ((MWt ~ 42 kDa, Fig. 3.14A, bottom) in cells plated on either tissue culture plasticware or fibronectin were examined. There was no significant change in the expression of β -actin in the different clones after attachment to fibronectin. However, hERG1-expressing cells showed an apparent reduction in vinculin levels on adhesion to fibronectin. To confirm this, densitometric analysis of vinculin protein band intensities was performed (Fig. 3.14B). To overcome any differences in total protein loading, the intensity of the vinculin band was normalized to the β -actin band

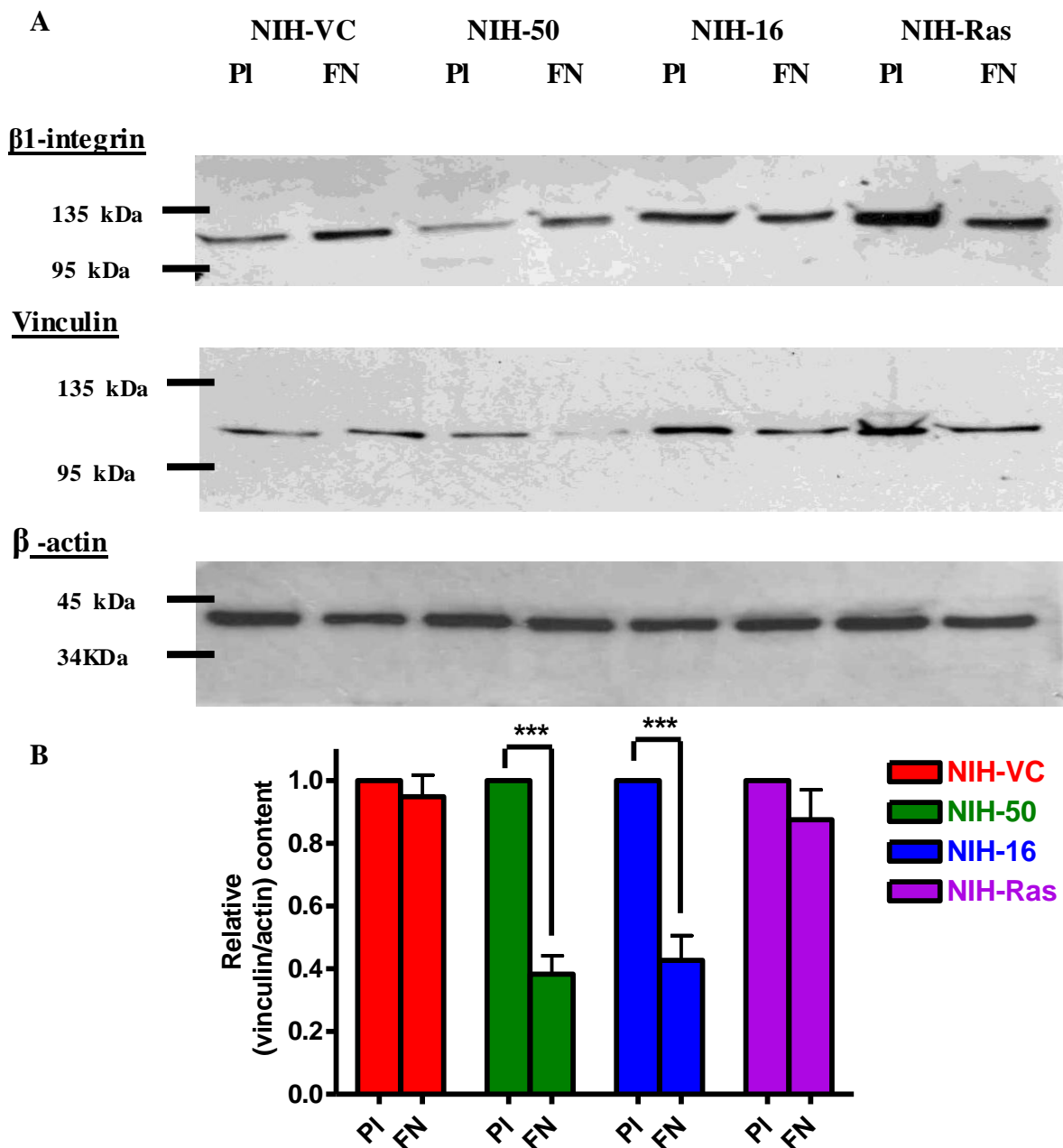


Figure 3.14 Effect of adhesion to fibronectin on expression of β 1-integrin, β -actin and vinculin in hERG1-expressing cells. **A.** Total cell lysates prepared from NIH-3T3 cell-lines plated on tissue culture plastic (PI) or fibronectin (FN) were separated by electrophoresis and probed with anti- β 1 integrin (top), anti-vinculin (middle) or anti- β -actin (bottom) antibodies. The blots shown are representative of at least 3 independent experiments. **B.** Densitometric analysis showing relative vinculin expression. Vinculin content was normalized to β -actin and expressed relative to vinculin expression from cells cultured on plastic. Data are presented as means \pm SEM for 3 experiments. *** indicates statistically significant values ($p < 0.001$).

intensity from the same sample. NIH-50 and NIH-16 cells showed reductions in vinculin expression of 62 ± 6 and $58 \pm 8\%$, respectively ($p < 0.001$ relative to corresponding expression on plastic; $n=3$); in contrast, no difference in the expression of this protein between growth substrata was observed in NIH-VC or NIH-Ras cell-lines (Fig. 3.14B).

3.2.6 Does adhesion to fibronectin induce cytoskeletal modulation in hERG1-expressing cells?

Among the structural components that determine the morphology of fibroblasts are the focal adhesions and actin microfilaments (Nigg *et al.*, 1986). Oncogene-induced transformation of fibroblasts is associated with disassembly of focal adhesions and stress fibres, a process associated with increased cell migration (Izawa *et al.*, 1998). Similarly, the apparent transformed morphology of hERG1-expressing cells plated on fibronectin may be related to alterations in actin cytoskeleton organization and assembly of cell-substrate adhesions. To investigate these possibilities, cells were plated either on poly-L-lysine or fibronectin, fixed and double-stained with phalloidin-Texas Red (to analyze the actin cytoskeleton, Fig. 3.15), and an anti-vinculin antibody (to visualize focal adhesions, Fig. 3.16). Cells adhere to poly-L-lysine-coated surfaces through a non-integrin-mediated mechanism (McKeehan *et al.*, 1976) and therefore this substratum was used as a control for integrin-mediated signalling.

NIH-VC cells plated on poly-L-lysine showed a flattened, square-like morphology with abundant well-formed stress fibres that extended across the cytoplasm. There was no change in actin cytoskeletal organization of NIH-VC cells when plated on fibronectin (Fig. 3.15, top panels). On the other hand, adhesion to fibronectin seemed to cause alterations in the actin cytoskeleton of hERG1-expressing cells. hERG1-expressing cells adhered to poly-L-lysine showed a similar appearance of stress fibres, although these appeared thinner than those seen

in NIH-VC. However, when hERG1-expressing cells were allowed to adhere to fibronectin, they exhibited a polarized, spindle-shaped morphology, which was associated with cytoskeletal reorganization. Actin staining was mostly diffuse in the cytoplasm and stress fibres were fine, thin and almost undetectable where they extended into lamellipodia (indicated by arrowheads in Fig. 3.15, second and third panel rows), suggesting a highly dynamic leading edge, which may explain the increased motility of hERG1-expressing cells on fibronectin. Ras-transformed fibroblasts showed a diffuse actin staining that was similar whether on fibronectin or not (Fig.3.15 bottom panel, Dartsch *et al.*, 1994, Khosravi-Far *et al.*, 1994).

Vinculin-stained focal adhesions were also examined (Fig. 3.16). NIH-VC cells plated on poly-L-lysine or fibronectin showed numerous, evenly stained, large focal adhesions located both centrally and at the cell periphery (Fig. 3.16, top panels). NIH-50 and NIH-16 cells showed a reduction in the number of focal adhesions on fibronectin; moreover, focal adhesions were smaller and localized primarily to the leading cell margin (Fig. 3.16, second and third right hand panels). Ras-transformed fibroblasts also showed few, sparse and less prominent focal adhesions (Fig. 3.16, bottom panels). Collectively, these data suggest that adhesion to fibronectin is associated with reorganization of the actin cytoskeleton and focal adhesions in hERG1-expressing cells.

3.2.7 Does modulation of hERG1 function and/or cell-surface expression influence the migration of hERG1-expressing cells on fibronectin?

It has been suggested that hERG1 channel activity is required to enhance cell migration of hERG1-expressing tumour cells (Pillozzi *et al.*, 2007). hERG1 has been shown to associate with components of focal adhesions (Cherubini *et al.*, 2005), which may suggest that hERG1

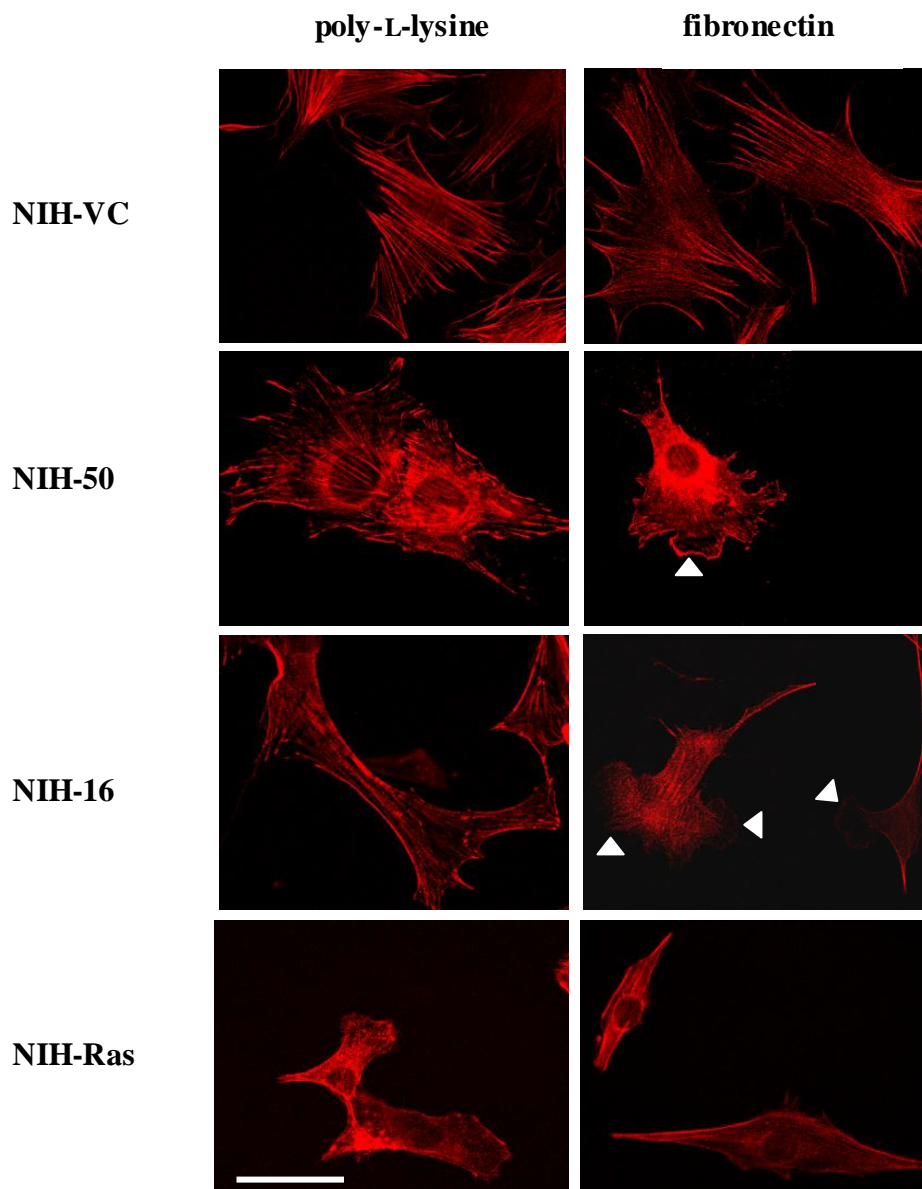


Figure 3.15 Adhesion to fibronectin induces cytoskeletal alterations in hERG1-expressing cells. NIH-3T3 cells were plated onto poly-L-lysine (left panels) or fibronectin (right panels) coated glass coverslips for 8 h. Cells were fixed, permeabilized and stained with Texas Red-conjugated phalloidin to reveal the actin cytoskeleton. Cell images were captured using a confocal microscope at 63x magnification. Arrow-heads indicate lamellipodia. All panels are similarly magnified: scale-bar indicates 100 μm .

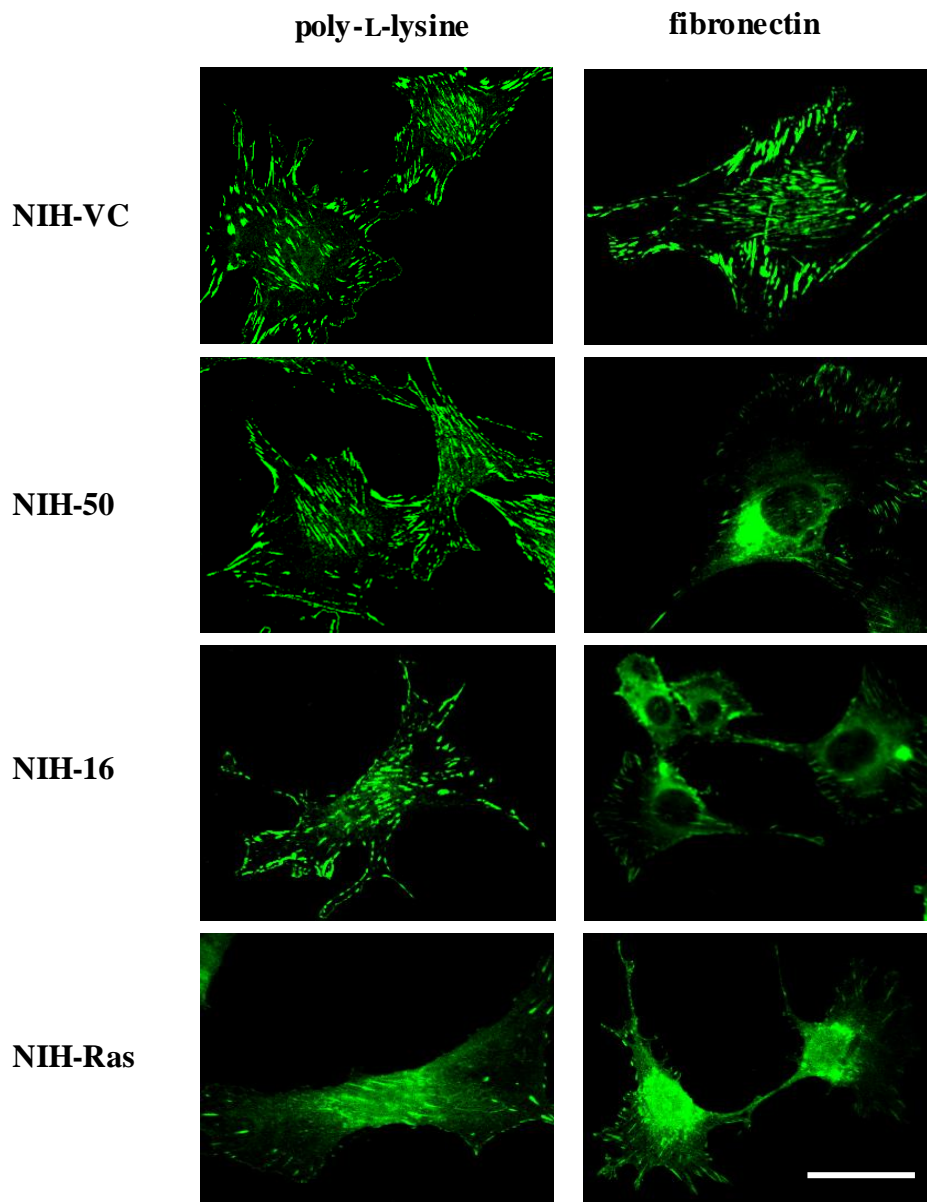


Figure 3.16 Effect of adhesion to fibronectin on focal adhesion formation in **hERG1-expressing cells**. NIH-3T3 cells were plated on poly-L-lysine (left panels) or fibronectin (right panels) coated glass coverslips for 8 h. Cells were fixed, permeabilized and stained with a monoclonal anti-vinculin antibody, which was detected using an Alexa fluor 488-labelled secondary antibody. Cell images were captured using a confocal microscope at 63x magnification. All panels are similarly magnified: scale-bar indicates 100 μm .

can modulate migration through direct interaction with signalling components regulating cellular motility. To test these possibilities, the involvement of the hERG1 current and/or hERG1 cell-surface expression in fibronectin-dependent cell migration of hERG1-expressing cells was investigated using different hERG1 channel modulators, including high (20 mM) extracellular $[K^+]_o$ concentration, the hERG1 channel activator, ICA-105574 (Gerlach *et al.*, 2010), the hERG1 channel blocker dofetilide, and the trafficking inhibitors, pentamidine and arsenic trioxide.

3.2.7.1 Effect of high $[K^+]_o$ and the hERG1 channel activator ICA-105574 on fibronectin-dependent cell migration in hERG1-expressing cells

hERG1 currents can be modulated by high $[K^+]_o$ (Sanguinetti *et al.*, 1995, Sturm *et al.*, 2005). In addition to altering the reversal potential of hERG1 current and also the resting membrane potential of cells, which tend to be governed by K^+ conductances, high K^+ also reduces hERG1 channel inactivation and so increases the open probability (P_o) of the channel. ICA-105574 is a recently described hERG1 channel activator that acts by suppressing hERG1 channel inactivation, while also having a minor effect on hERG1 activation kinetics at negative membrane potentials around -50 mV (Gerlach *et al.*, 2010). Initially, I tested if the high $[K^+]_o$ and ICA-105574 alone or in combination augment hERG1 channel conductance. A $[K^+]_o$ of 20 mM was chosen as at this concentration, the equilibrium potential for K^+ (E_K) is expected to shift to ~ -52 mV as predicted by Nernst equation, assuming an intracellular K^+ concentration of 140 mM, and results in a modest depolarization of the resting potential.

WT hERG1 was expressed in *Xenopus* oocytes, which were bathed in recording solutions containing 5 mM $[K^+]_o$, 20 mM $[K^+]_o$, 5 mM $[K^+]_o$ + 3 μ M ICA-105574, or 20 mM $[K^+]_o$ + 3 μ M ICA-105574. hERG1 currents were recorded under these conditions in each cell using the

voltage protocol shown in Fig. 3.17A. hERG1 currents were activated by 5 s depolarizing pulses applied in 10 mV increments from -60 to +50 mV followed by a final step to -120 mV. Upon depolarization, there was a slow increase of outward current caused by slow opening of hERG1 channel activation gate. Outward current amplitudes decreased at more depolarized potentials because of rapid channel inactivation (Fig. 3.17B, top left). Moderate increases in hERG1 outward current were observed in both 20 mM $[K^+]_o$ and 5 mM $[K^+]_o$ + 3 μ M ICA-105574 solutions. However, combining elevated $[K^+]_o$ and the pharmacological activator elicited a very large increase in outward hERG1 current (Fig. 3.17B, right). Peak outward current recorded under each condition was normalized to the highest current amplitude recorded under the control (5 mM $[K^+]_o$) condition (from the same cell) and plotted against membrane voltage (Fig. 3.17C) to determine the voltage dependence of hERG1 current augmentation. At +20 mV, hERG1 outward current increased from $0.22 \pm 0.02 \mu$ A in 5 mM $[K^+]_o$ to $0.45 \pm 0.04 \mu$ A in 20 mM $[K^+]_o$, $0.97 \pm 0.08 \mu$ A in 5 mM $[K^+]_o$ + 3 μ M ICA-105574 and $3.72 \pm 0.83 \mu$ A in 20 mM $[K^+]_o$ + 3 μ M ICA-105574 solutions ($p < 0.001$, compared to all other conditions; $n=4$; Fig. 3.17D).

Fig. 3.18A shows hERG1 tail currents (recorded at -120 mV, using the same protocol shown in Fig. 3.17A) under the same recording conditions. The hyperpolarizing pulse to -120 mV rapidly recovers the hERG1 channels from inactivation giving rise to the initial increase of inward current. The amplitude of the tail current depends on the number of channels that have activated during the preceding depolarization step and is also dependent on driving force for K^+ ($V_m - V_{reversal}$). The tail currents then slowly decay due to slow channel deactivation (Fig. 3.18A, top). A very large increase in inward hERG1 tail currents were observed in both 20 mM $[K^+]_o$ and 20 mM $[K^+]_o$ + 3 μ M ICA-105574 solutions, whereas 5 mM $[K^+]_o$ + 3 μ M ICA-105574 only caused a modest increase of hERG1 tail currents (Fig. 3.18A). The voltage

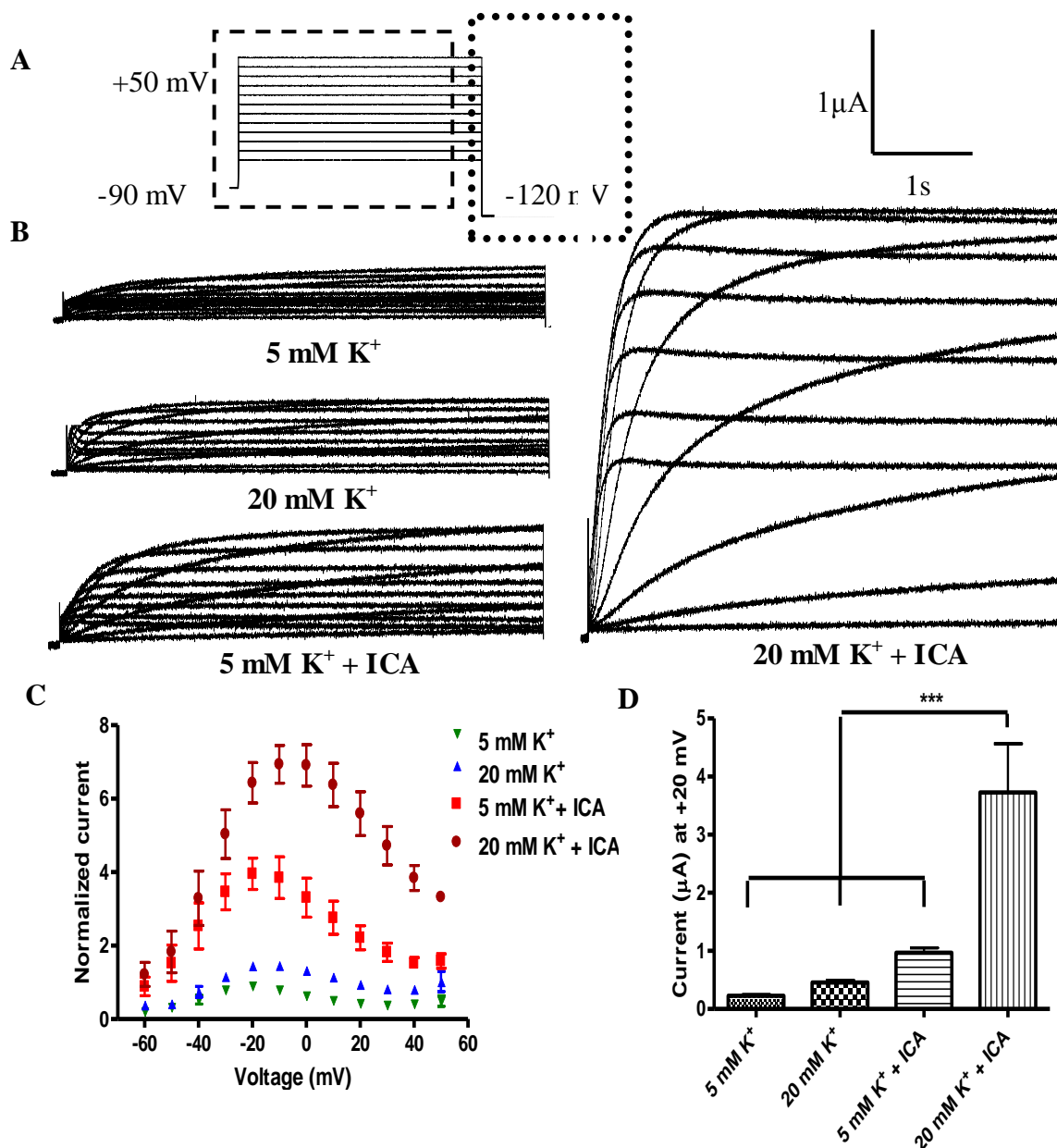


Figure 3.17 Effect of high extracellular K⁺ concentration and the hERG1 activator ICA-105574 on WT hERG1 currents expressed in *Xenopus* oocytes. **A**. Representation of the protocol used. The holding potential was -90 mV and a family of 5 s test pulses from -60 to +50 mV were applied followed by a final step to -120 mV. **B**. Representative current traces of hERG1 currents recorded from an oocyte perfused with 5 mM K⁺, 20 mM K⁺, 5 mM K⁺ + 3 μ M ICA-105574 or 20 mM K⁺ + 3 μ M ICA-105574 containing solutions. Only outward currents elicited by voltage pulses (marked by the dashed box in A) are shown. **C**. End of pulse currents are normalized to the highest current amplitude elicited in 5 mM K⁺ and plotted against the corresponding test potential. **D**. Comparison of end of pulse current amplitudes measured at +20 mV. Data represent means \pm SEM for recordings obtained from at least 5 oocytes. *** indicates statistically significant values ($p < 0.001$).

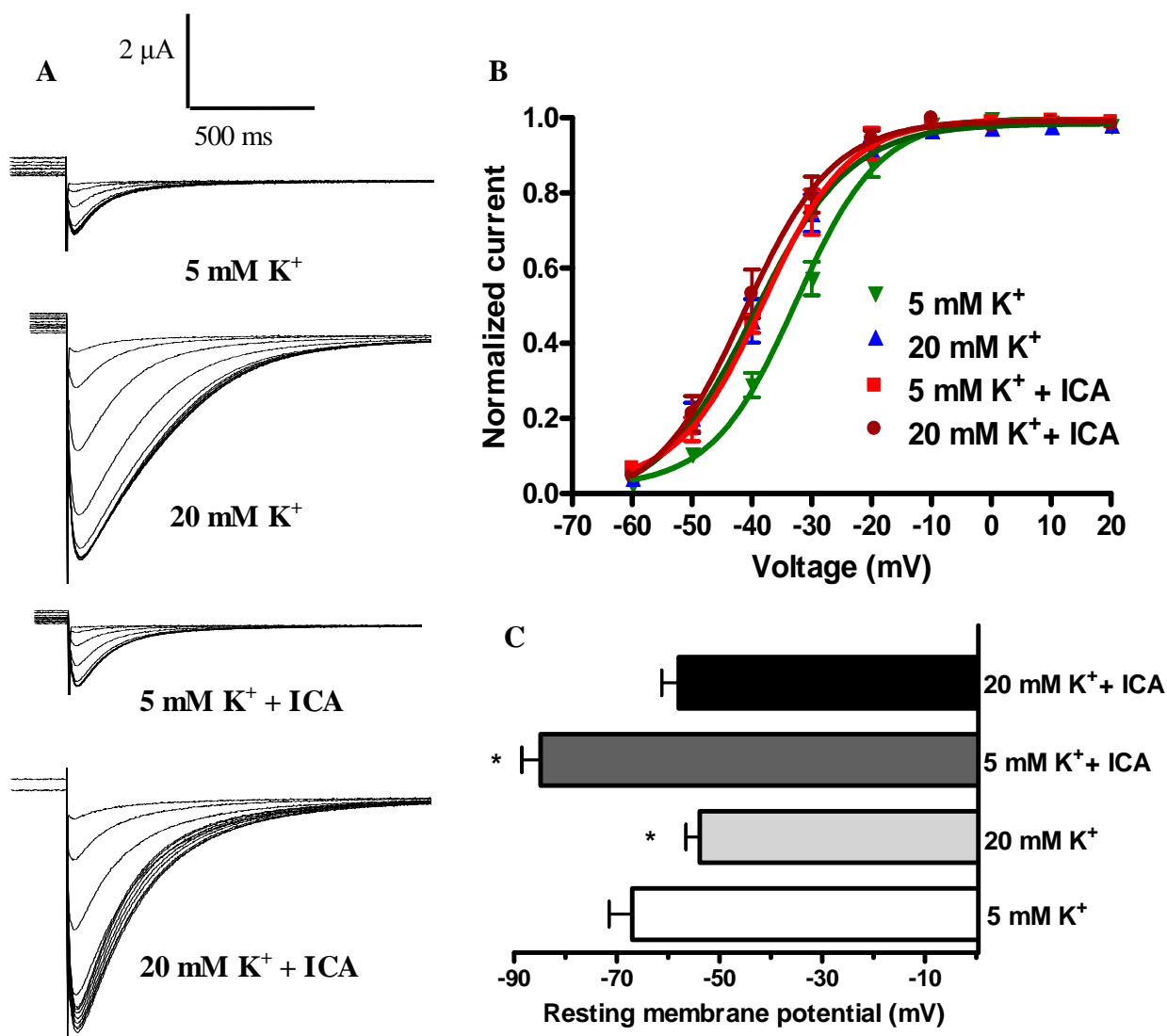


Figure 3.18 Effect of elevated K^+ concentration and the hERG1 activator ICA-105574 on the voltage dependence of activation of WT hERG1 currents expressed in *Xenopus oocytes*. **A**. Representative current traces of hERG1 currents recorded from oocytes perfused with 5 mM K^+ , 20 mM K^+ , 5 mM K^+ + 3 μ M ICA-105574 or 20 mM K^+ + 3 μ M ICA-105574 containing solutions. For clarity, only tail currents at -120mV are shown (as indicated by dotted box in Fig. 3.17A). **B**. Normalized to peak hERG1 tail currents calculated at -120 mV are plotted against the corresponding preceding test pulse and fitted with a Boltzmann function. **C**. Resting membrane potential of oocytes expressing hERG1 under the different recording conditions. Data represent means \pm SEM of recordings obtained from at least 5 oocytes. * indicates Statistical significance relative to 5 mM K^+ recording solution (* p <0.05).

dependence of hERG1 current activation was determined (Fig. 3.18B). Peak hERG1 tail currents were normalized to the maximum value and plotted against the preceding test pulse potential (Fig. 3.18B). Activation threshold was ~ -60 mV and increased with further depolarization to reach a maximum at $\sim +10$ mV. A negative shift of the activation curves was observed in solutions containing 20 mM $[K^+]_o$, 3 μ M ICA-105574 or 20 mM $[K^+]_o + 3$ μ M ICA-105574. The activation curves were fitted with a Boltzmann function and the $V_{0.5}$ values were determined. The mean value (\pm SEM) of the midpoint of activation ($V_{0.5}$) were -32 ± 1.7 mV ($n=4$) in 5 mM $[K^+]_o$, -40 ± 2.6 mV in 20 mM $[K^+]_o$ ($n=4$; $p<0.05$), -38 ± 1.8 mV in 5 mM $[K^+]_o + 3$ μ M ICA-105574 ($n=4$; $p>0.05$) and -41 ± 2.4 in 20 mM $[K^+]_o + 3$ μ M ICA-105574 solutions ($n=4$; $p<0.01$).

Oocyte resting membrane potential (V_{REST}) was also measured in the different recording solutions used (Fig. 3.18C). ICA-105574 (3 μ M) caused a highly significant hyperpolarization of V_{REST} from -67.0 ± 4.5 to 85.0 ± 3.7 mV ($p<0.01$; $n=6$). This is most likely due to the negative shift in the voltage dependence of activation by this compound. Increasing extracellular K^+ concentration $[K^+]_o$ to 20 mM depolarized the resting membrane potential of oocytes to -54.0 ± 2.7 mV ($p<0.05$; $n=6$) and -58.0 ± 3.3 ($p>0.05$; $n=6$) in the absence and presence of 3 μ M ICA-105574, respectively.

The effect of enhancing hERG1 channel conductance under these conditions on the migration of NIH-3T3 clones on fibronectin was investigated using the single-cell migration (Fig. 3.19A) and wound healing (Fig. 3.19B) assays. Wound healing assays were performed to provide a longer time-course experiment to observe any long-term effect of the elevated $[K^+]_o$ /hERG1 channel activator treatments. In both assays, the high glucose (25 mM) culture medium routinely used for maintenance of NIH-3T3 cells was exchanged for a lower glucose

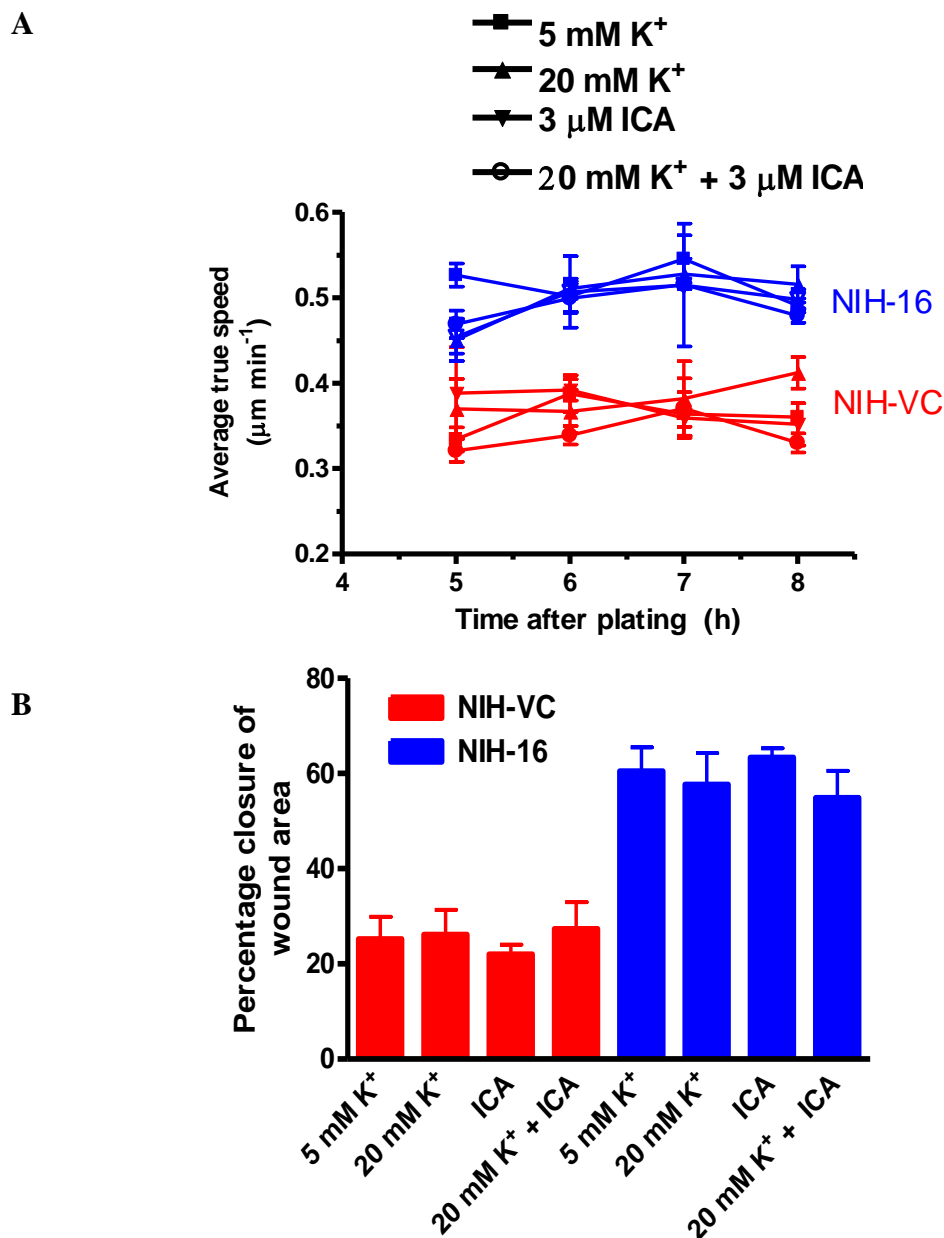


Figure 3.19 Altering hERG1 channel conduction and resting membrane potential does not modulate rates of migration by hERG1-expressing NIH-3T3 cells. **A.** Average true speed of NIH-3T3 cell-lines 5-8 h after plating on fibronectin ($2 \mu\text{g mL}^{-1}$). Data represent means \pm SEM of at least 3 experiments at each time-point. **B.** Wound-healing experiments for NIH-VC and NIH-16 cells plated on fibronectin. Cells were plated at a density of 1×10^6 cells per 35 mm dish. Wound diameter at 9 points per dish was measured at time 0 and after 10 h. Data represent means \pm SEM for at least 3 separate experiments.

medium (5 mM) of identical composition to compensate for osmotic changes caused by increasing $[K^+]_o$ to 20 mM. Cells adapted well to these conditions and no change in cell size was observed during the course of the experiments. Despite the predicted changes in V_{REST} and hERG1 P_0 , none of above treatments produced significant changes in migration of either NIH-VC or NIH-16 cells. These results may indicate that hERG1-induced effects on cell motility may be independent of K^+ ion conductance or changes in membrane potential. Alternatively, changes may need to be longer term in order to make significant changes to cellular properties.

3.2.7.2 Effect of hERG1 trafficking inhibitors on fibronectin-dependent migration of hERG1-expressing cells

The effect of hERG1 channels on NIH-3T3 cell migration on fibronectin may be dependent on hERG1 expression at the plasma membrane, through direct interaction of hERG1 protein domains with focal adhesion proteins regulating cytoskeletal organization and cell motility. To test the importance of cell-surface expression of hERG1 proteins, the effect of compounds linked to acquired long QT syndrome that inhibit hERG1 trafficking on the migration of hERG1-expressing cells was investigated. It has been shown that 24 h pre-incubation with arsenic trioxide (10 μ M), or pentamidine (10 μ M) reduces hERG1 protein trafficking to the plasma membrane and results in ~80% and ~40% reductions in hERG1 cell-surface expression, respectively (Ficker *et al.*, 2004, Cordes *et al.*, 2005, Kuryshev *et al.*, 2005). As described previously, migration speeds of NIH-16 and NIH-50 cells were faster than NIH-VC. Arsenic trioxide (10 μ M) and pentamidine (10 μ M) were added to the culture medium 24 h before measuring migration speeds. The reagents were also present in the migration assay media. Arsenic trioxide had no significant effect on migration speed of any of the NIH-3T3

clones (Fig. 3.20). Interestingly, pentamidine caused only a slight reduction of NIH-VC migration and no change to NIH-Ras migration; however, it caused a highly statistically significant decrease in cell migration of both the hERG1-expressing cell-lines. Following pre-incubation with 10 μM pentamidine, the migration speeds of NIH-50 and NIH-16 cells were reduced from 0.519 ± 0.017 and 0.471 ± 0.013 , respectively, to 0.332 ± 0.029 and 0.336 ± 0.034 , respectively ($p < 0.01$ relative to untreated cells; $n=3$; Fig. 3.20). Since effects were not observed on either NIH-VC or NIH-Ras cells it suggests the concentration used was not toxic under these experimental conditions.

The lack of effect of arsenic trioxide, which has been reported to have a greater ability to inhibit hERG1 trafficking, on the migration of hERG1-expressing cells means that we should not assume that the pentamidine-mediated reduction in migration speed is hERG1-specific. Thus, we need to be cautious in our interpretation of this result. Further experiments are required to determine the potential effects of trafficking inhibition on the motility of hERG1-expressing NIH-3T3 cells. Nevertheless, it is intriguing that pentamidine only inhibits migration of the hERG1-expressing clones.

3.2.7.3 Effect of acute and chronic hERG1 current inhibition on fibronectin-dependent migration of hERG1-expressing cells

To determine the contribution of hERG1 current to hERG1-induced changes in cell motility on fibronectin, dofetilide (1 μM) was added to the culture medium for 1 h before migration speeds were determined (Fig. 3.20). Short term application of dofetilide (1 μM) had no significant effect on the migration speeds of any of the clones.

The effect of chronic hERG1 current inhibition on cell migration was also investigated. NIH-VC cells and NIH-16 cells were maintained in culture medium containing 100 nM dofetilide

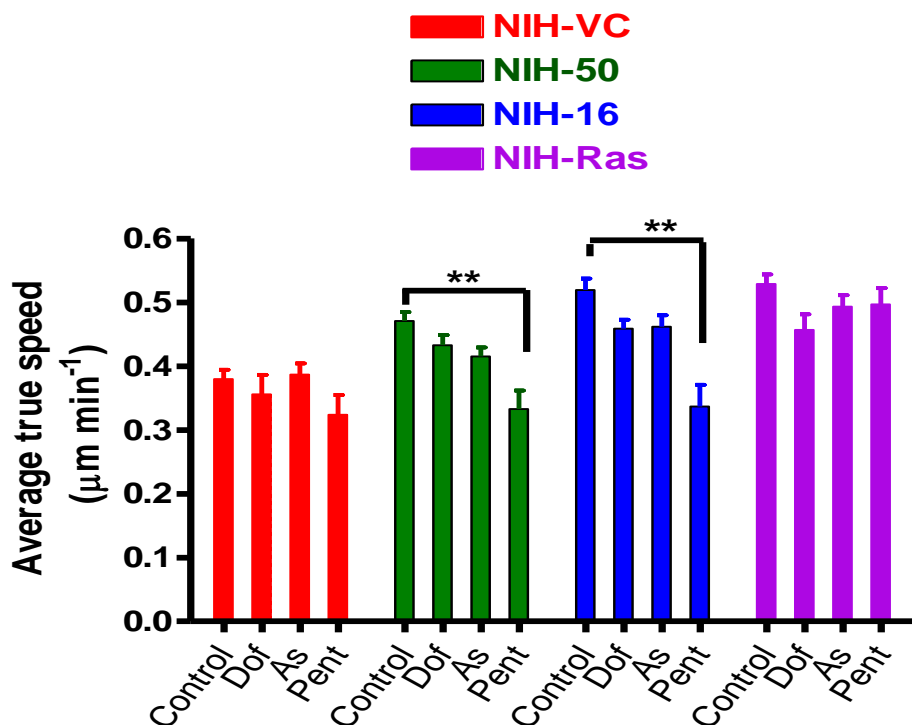


Figure 3.20 Effect of dofetilide (Dof), arsenic trioxide (As) or pentamidine (Pent) on migration of hERG1-expressing cells adhering to fibronectin. Cells were incubated for 24 h with arsenic trioxide (10 μM) or pentamidine (10 μM) before plating onto fibronectin (2 μg mL⁻¹) for 5 h and the migration speed (average true speed) determined. Dofetilide (1 μM) was added to culture medium 1 h before cell migration was assessed. Data represent means ± SEM for 3 experiments performed in duplicate. ** indicates statistical significance with reference to untreated conditions ($p < 0.01$).

and migration speeds on fibronectin were determined at 7, 14 and 21 days after dofetilide addition. A concentration of 100 nM dofetilide was chosen as this is at the lower end of concentrations that cause profound inhibition of hERG1 in these culture conditions (see Chapter 4). Dofetilide containing culture medium was exchanged every 3 days or when cells were split after reaching ~ 70% confluency.

As shown in Fig. 3.21A, NIH-16 cells treated with the blocker exhibited time-dependent decreases in migration speed, whereas NIH-VC cells maintained a constant speed of migration over the treatment period. Analysis of pooled data (Fig. 3.21B) showed that NIH-16 cells treated with dofetilide for 14 and 21 days had migration speeds of $0.442 \pm 0.016 \mu\text{m min}^{-1}$ and $0.408 \pm 0.010 \mu\text{m min}^{-1}$, which were not significantly different to the speed of migration of NIH-VC cells at the corresponding days ($0.413 \pm 0.010 \mu\text{m min}^{-1}$ and $0.397 \pm 0.008 \mu\text{m min}^{-1}$, respectively). Interestingly, NIH-16 cells appeared to also undergo changes in cell morphology following chronic dofetilide treatment. Cells gradually lost their spindle-shaped, 'transformed' appearance and reverted to a typical flattened fibroblastic morphology (Fig. 3.21C) similar to NIH-VC cells. The morphology of NIH-VC cells was unaffected by chronic dofetilide treatment (data not shown). These results suggest that experimental interventions that alter hERG1 current can alter the migration and morphology (transformed) properties of NIH-16, but importantly, these effects occur on relatively long time scales and short term inhibition has little effect.

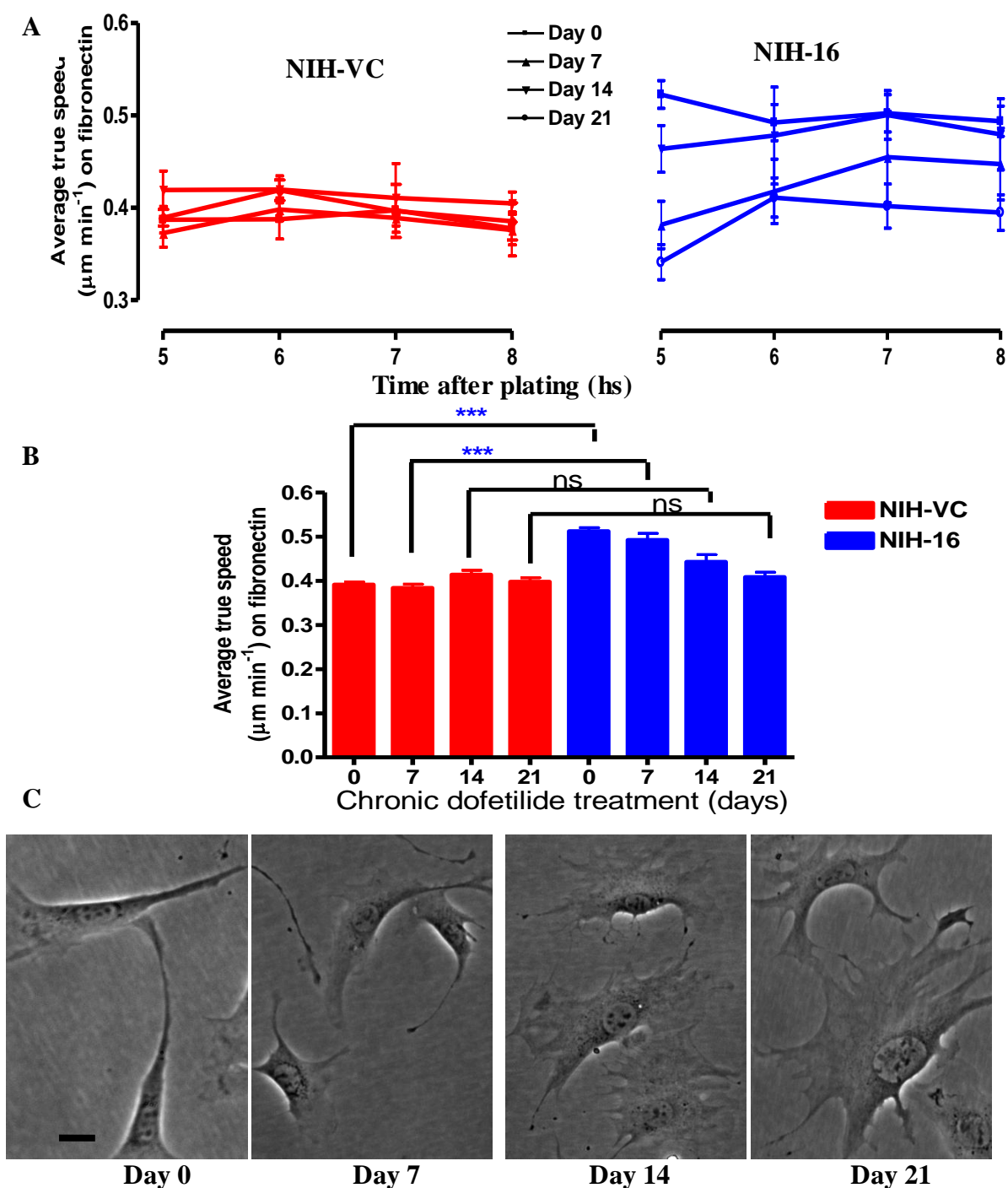


Figure 3.21 Effect of chronic hERG1 inhibition on the migration speed and morphology of hERG1-expressing NIH-3T3 cells plated on fibronectin. **A.** Average true speed of NIH-VC and NIH-16 cell-lines 5-8 h after plating onto fibronectin ($2 \mu\text{g mL}^{-1}$)-coated dishes. Cells were maintained in dofetilide (100 nM)-containing culture medium for 7, 14 or 21 days. Data represent means \pm SEM for 3 experiments at each time-point. **B.** Pooled data. Statistical significance was assessed using a two-way ANOVA with Bonferroni's post-test ($***p < 0.001$; ns, not significant). **C.** Morphology of NIH-16 cells on fibronectin after chronic dofetilide treatment.

3.3 Discussion

Results in this Chapter demonstrate that adhesion to extracellular matrix (ECM) proteins can induce a transformed phenotype in hERG1-expressing cells, characterized by changes in cell morphology, migration and cytoskeletal rearrangement, suggesting a potential cross-talk between ECM-mediated signalling and hERG1 in tumour cells. NIH-3T3 cells expressing hERG1 exhibited a spindle-like, elongated and polarized cell morphology when adhered to fibronectin or laminin-1, but not to collagen-1, which was associated with an enhanced directional motility. Adhesion of hERG1-expressing cells to fibronectin also elicited a reduced expression of the cytoskeletal protein vinculin, a decreased number of focal adhesions and alterations in the actin cytoskeleton. These effects may be dependent on the cell-surface location of hERG1, since pentamidine, a known hERG1 trafficking inhibitor, decreased the migration speed of a hERG1-expressing cell-line (NIH-16) on fibronectin. Moreover, prolonged inhibition of the hERG1 current may be required to reverse hERG1-induced effects observed on fibronectin. The main findings of this Chapter are discussed below.

3.3.1 hERG1-expressing cells exhibit changes in shape, spreading and migratory phenotype on adhesion to fibronectin and laminin-1

Upon adhesion to fibronectin or laminin-1, hERG1-expressing cells showed some morphological similarities to transformed NIH-Ras cells, in that they adopted a spindle-like, polarized morphology and exhibited an enhanced directional migration, indicating a ‘transformed’ phenotype that is enhanced by ECM adhesion.

The spindle-shaped appearance adopted by hERG1-expressing cells suggests that they form a reduced number of cell-substratum contacts, enhancing cell motility. Increased motility is a

common characteristic of transformed cells and is a critical step in the tumour cell metastatic cascade. It has been reported that polarized cell morphology may correlate with the invasive and metastatic potential of cancer cells. The less metastatic breast cancer MCF-7 cell-line typically displays ruffling activity over most or all of the cell perimeter, whereas the highly metastatic MDA cell-line tends to be more polarized with one, or a few distinct areas of the cell periphery undergoing active ruffling (Rajah *et al.*, 1998). Similarly, ruffling of well-defined regions of the cell membrane shows a good correlation with metastatic potential in various rat prostatic adenocarcinoma cell-lines (Partin *et al.*, 1988). Directed migration of cancer cells, in response to chemo-attractants, is also well-correlated with the ability to invade and metastasize (Wang *et al.*, 2002b). Invasion requires an enhancement of directional “chemotactic” cell migration stimulated by the protrusive activity of the cell membrane on attachment to ECM, which helps invading cells navigate through the ECM, to break-away from the invasive front and change from a collective to an individual migratory phenotype (Machesky, 2008).

Therefore, the polarity and persistence of migration of hERG1-expressing cells seen on ECM substrata support previous reports that suggested a role of hERG1 in tumour cell invasion and metastasis. Colon cancer cells expressing high levels of hERG1 display an enhanced migration through synthetic matrix-coated filters (Lastraioli *et al.*, 2004). Similarly, migration of HEK293 cells transfected with hERG1 cDNA was much greater than cells transfected with empty vector (Lastraioli *et al.*, 2004). The level of hERG1 mRNA/protein expression correlated well with the degree of tumour malignancy (Lastraioli *et al.*, 2004, Masi *et al.*, 2005). Collectively, these observations suggest that hERG1 contributes to the invasive / metastatic programme of tumour cells through acquisition of a directional migratory phenotype.

3.3.2 hERG1-expressing cells exhibit decreased vinculin expression on adhesion to fibronectin

Vinculin is a cytoskeletal adapter protein, which is recruited to focal adhesions on cell-substrate contact and anchors actin microfilaments to the ECM via focal adhesions. The decreased vinculin protein expression in hERG1-expressing cells on adhesion to fibronectin may explain hERG1 involvement in cell migration and metastasis. Vinculin expression has been linked to cell transformation and tumorigenesis. Transformation of fibroblast and epithelial cells often results in decreased vinculin expression (Rodriguez Fernandez *et al.*, 1992). Moreover, vinculin expression is reduced in highly metastatic melanoma cell-lines (Raz *et al.*, 1982, Lifschitz-Mercer *et al.*, 1997). Vinculin also regulates focal adhesion formation and turnover (Jockusch *et al.*, 1996, Humphries *et al.*, 2007). Suppression of vinculin expression in NIH-3T3 cells induces a transformed-like phenotype characterized by alterations in cell morphology, decreased number and size of focal adhesions and increased cell motility (Rodriguez Fernandez *et al.*, 1993). This has been confirmed by disruption of vinculin expression in other cell-types (Coll *et al.*, 1995, Volberg *et al.*, 1995, Xu *et al.*, 1998, Saunders *et al.*, 2006). Over-expression of vinculin in transformed cells suppresses the transformed phenotype and restores the normal architecture of the actin cytoskeleton (Rodriguez Fernandez *et al.*, 1992). Whether the changes observed in vinculin expression in hERG1-expressing cells plated on fibronectin are caused by altered rates of protein synthesis or turnover remains to be determined. It has been shown that vinculin synthesis in NIH-3T3 fibroblasts is sensitive to changes in cell shape induced by altering cell matrix adhesion, where cells that assume a spindle-like, elongated shape show decreased rates of vinculin synthesis compared to those showing a fibroblastic morphology (Ungar *et al.*, 1986). Therefore, it might be possible that hERG1 expression modulates integrin signalling

regulating cell shape, which affects vinculin synthesis. The regulation of gene expression by integrin-mediated signal transduction is well-established (Jones *et al.*, 1993).

3.3.3 hERG1-expressing cells exhibit alterations in cytoskeletal organization and focal adhesion formation following adhesion to fibronectin

On adhesion to fibronectin, hERG1-expressing NIH-3T3 cells showed clear differences in actin cytoskeleton structure and focal adhesions when compared to NIH-VC cells. hERG1-expressing cells exhibited reduced numbers of stress fibres, decreased abundance and size and altered distribution of focal adhesions, which were similar to the cytoskeletal rearrangements observed in NIH-Ras cells. These alterations are mediated through transduction of ECM extracellular signals, since hERG1 expressing cells plated on poly-L-lysine displayed a normal cytoskeletal architecture.

These cytoskeletal rearrangements may explain changes in cell shape, spreading and patterns of migration of hERG1-expressing cells seen on fibronectin. It is well established that cell transformation is associated with modulation of the actin cytoskeleton and focal adhesion assembly (Izawa *et al.*, 1998, Pritchard *et al.*, 2004). Focal adhesions are used as nucleation centres for the initial formation of stress fibres. Therefore, decreased numbers of focal adhesions reduce stress fibre formation, cause a loss of the flattened fibroblastic morphology and may provide a higher concentration of monomeric actin that can polymerize at the leading edge of the cell, enhancing forward cell movement (Wozniak *et al.*, 2004). Decreased focal adhesion size may also be indicative of a reduction in focal adhesion strength, which is a barrier to motility and invasion. Moreover, the localization of focal adhesions to the leading edge of hERG1-expressing cells may help stabilize lamellipodia producing the polarized protrusion activity and intrinsic persistent migratory phenotype of hERG1-expressing cells

observed on fibronectin. Taken together, hERG1 expression in NIH-3T3 cells may enhance cell migration by coordinating cytoskeletal changes with cell-matrix interactions.

3.3.4 hERG1-expressing cells display an integrin-dependent transformed phenotype

In contrast to NIH-Ras cells, hERG1-expressing cells exhibit a matrix-dependent cell transformation. Here I will discuss possible interactions of hERG1 with integrin signalling pathways that could mediate the transforming behaviour of hERG1-expressing cells.

hERG1 has been shown to co-immunoprecipitate with β 1-integrin in tumour cells and HEK-hERG cells (Cherubini *et al.*, 2002, Cherubini *et al.*, 2005, Pillozzi *et al.*, 2007). Moreover, β 1-integrin activation enhanced cell migration of hERG1-expressing AML cells through fibronectin-coated porous membranes (Pillozzi *et al.*, 2007). The cell behaviour induced by adhesion of hERG1-expressing NIH-3T3 cells to fibronectin was not due to alterations in the level of β 1-integrin expression (see Fig. 3.14). However, other changes in the integrin expression profile of these cells cannot be excluded. For example, adhesion of leukemic FLG 29.1 cells to fibronectin via β 1-integrins increased expression of another integrin, the vitronectin receptor $\alpha_v\beta_3$ (Hofmann *et al.*, 2001). Other possibilities include hERG1-induced alterations in integrin distribution and modulation of integrin-mediated signalling.

Integrin signalling depends on the recruitment and activation of signalling, cytoskeletal and kinase proteins at cell-matrix adhesion sites and the net signalling outcome is determined by the profile of signalling proteins recruited to focal adhesion sites (Hynes, 2002). The effect of fibronectin adhesion on the vinculin expression, cytoskeleton organization and focal adhesions in hERG1-expressing NIH-3T3 cells suggests that hERG1 influences focal adhesion signalling. hERG1 has been suggested to recruit, associate with and activate focal adhesion kinase (FAK) on fibronectin adhesion (Cherubini *et al.*, 2005). FAK regulates focal

adhesion turnover and cell migration (Katz *et al.*, 2003) and fibroblasts lacking FAK showed a decreased focal adhesion turnover and reduction in cell migration (Mitra *et al.*, 2005).

hERG1 has also been shown to associate with the small GTPase Rac1 (Cherubini *et al.*, 2005). Members of Rho GTPases regulate multiple aspects of actin organization, including membrane ruffling (Ridley *et al.*, 1992b), stress fibre formation and focal adhesion assembly (Ridley *et al.*, 1992a). Rho GTPases are also reported to determine cell polarity and persistence of cell migration (Nobes *et al.*, 1999, Srinivasan *et al.*, 2003, Vial *et al.*, 2003). The ability of fibroblasts to move unidirectionally with high persistence has been reported to be dependent on the degree of Rac1 activation downstream of the fibronectin receptor $\alpha 5 \beta 1$ integrin, and reducing Rac activity can switch cell migration mode from random to persistent (Pankov *et al.*, 2005). hERG1 current has been shown to be important for Rac1 activation (Cherubini *et al.*, 2005). Both $\beta 1$ -integrin and hERG1 are also reported to associate with caveolin-1 (Cherubini *et al.*, 2005), which has been shown to be required for the polarized and elongated morphology and intrinsic persistency of migration in fibroblasts by affecting Rho GTPase activation (Grande-Garcia *et al.*, 2007). One of the clear phenotype of NIH-16 and NIH-50 cells is a reduced ability to retract the trailing edge as cells migrate forwards. This results in long thin cellular processes. Failure of hERG1-expressing cells to re-tract might be due to defects in Rho GTPase signalling that regulate adhesive-protrusive activities of migrating cells.

NIH-Ras cells showed a matrix-independent transformed behaviour. This may be ascribed to the finding that these cells show constitutive dysregulation of the components of integrin downstream signalling. In normal cells, integrin-mediated signalling cross-talks with the Ras signalling pathway, since FAK, Ras and MAPK are activated on integrin activation

(Schlaepfer *et al.*, 1994, Morino *et al.*, 1995). Moreover, cells plated on fibronectin recruit components of the Ras signalling pathway, including Grb2 and mSOS1 to focal adhesion sites (Schlaepfer *et al.*, 1994), suggesting that the Ras/MAPK pathway could be regulated downstream of integrin signalling. Ras-induced cellular transformation may enable cells to bypass or disrupt integrin-mediated signal transduction. Supporting this notion, Ras-transformed cells show a constitutive ability to turnover focal adhesions via a net FAK dephosphorylation (Hall *et al.*, 1995), which enhances cell motility. Moreover, Rho GTPase activity may be dys-regulated in Ras-transformed cells (Qiu *et al.*, 1995a, Qiu *et al.*, 1995b, Zhong *et al.*, 1997, Izawa *et al.*, 1998).

3.3.5 Is hERG1 current required for integrin-mediated changes in the transforming behaviour of hERG1-expressing cells?

Enhancing hERG1 channel activity through the use of high external K^+ and/or the use of a hERG1 channel activator did not affect integrin-mediated migration of hERG1-expressing cells. Elevation of $[K^+]_o$ is sufficient to depolarize the membrane potential and open hERG1 channels, whereas ICA-105574 is expected to hyperpolarize the membrane potential as it enhances single channel conductance, removes channel inactivation and shifts the voltage dependence of activation to negative potentials (Gerlach *et al.*, 2010). Thus, $[K^+]_o$ and ICA-105574 have quite complex effect on channel gating. The largest effect on membrane potential was observed when ICA-105574 was added to the 5 mM $[K^+]_o$ medium. This resulted in a hyperpolarization of ~ 18 mV in oocytes, in which hERG1, as with NIH-16 and NIH-50 cells, is the major K^+ conductance regulating resting membrane potential. Resting membrane potential was only modestly depolarized in 20 mM $[K^+]_o$ compared to 5 mM $[K^+]_o$ containing media. Adding ICA-105574 to the 20 mM $[K^+]_o$ media had little effect on resting

potential, which is largely governed by E_K , but would cause a substantial increase of hERG1 P_0 . Thus, these interventions allowed us to independently regulate resting potential and hERG1 P_0 . Unfortunately, neither the high $[K^+]_o$ or ICA-105574 conditions influenced NIH-3T3 cell migration. Moreover, acute application of dofetilide (1 μ M) also failed to affect motility of hERG1-expressing cells on fibronectin. This may suggest that the integrin-dependent hERG1-phenotype may be independent of ion flux or bioelectrical effect on membrane potential. However, surprisingly, chronic hERG1 current inhibition removed the integrin-dependent enhancement of hERG1-expressing cell migration and restored a normal, flattened, fibroblastic morphology to NIH-16 cells, providing evidence for a role of ion conduction in the altered motility of hERG1-expressing cells. The reason for the requirement for such a prolonged incubation time with dofetilide to impair motility of hERG1-expressing cells is not clear and requires further investigation. It may be possible that hERG1-induced effects on the cell migratory phenotype are mediated via changes in expression levels of key signalling intermediates and therefore sufficient time is required to restore expression profiles of signalling molecules to those found in normal cells. This hypothesis may be supported by our finding that adhesion of hERG1-expressing cells to fibronectin was associated with a decrease in the cell content of the cytoskeletal protein vinculin.

A link between integrins and hERG1 current is suggested by several previous reports. Activation of β 1-integrin in human SH-SY5Y neuroblastoma, leukemic FLG29.1 and HEK-hERG cells through engagement with ECM ligands, or by using activating antibodies, was associated with an increase in hERG1 current density. This was subsequently shown to be critical for recruitment and activation of Rac1 and FAK (Arcangeli *et al.*, 1996, Hofmann *et al.*, 2001, Cherubini *et al.*, 2005). Adhesion to ECM also modulates oncogenic EAG currents and affects cytoskeletal organization of EAG-expressing CHO cells (Toral *et al.*, 2007).

Moreover, the electrophysiological properties of EAG are also affected by cytoskeletal modulations (Camacho *et al.*, 2000).

In conclusion, ECM adhesion modulates the characteristics of hERG1-expressing cells, possibly through association with integrins and activation of intracellular signalling cascades that are involved in modulation of cell morphology and cell migration through remodelling of the actin cytoskeleton. Elucidating the role of ECM in modulating hERG1-mediated effects in tumour cells may be important in determining potential therapeutic targets for impairment of metastasis of hERG1-expressing tumours.

Chapter 4

K⁺ channel function is required for the transforming potential of hERG1

4.1 Introduction

The contribution of hERG1 to tumorigenesis has now been investigated for several years. This ion channel appears to play roles in several aspects of cancer progression, including proliferation, migration, angiogenesis, and metastasis (Pillozzi *et al.*, 2002, Smith *et al.*, 2002a, Lastraioli *et al.*, 2004, Pillozzi *et al.*, 2007). Moreover, the expression of WT hERG1 in NIH-3T3 cells confers the cells with a transformed phenotype characterized by loss of contact inhibition, enhanced cell migration and extracellular matrix-dependent modulation of morphology and cytoskeletal organization (Chapter 3; Pier, 2007), further supporting the oncogenic potential of hERG1.

However, the mechanism remains elusive and whether hERG1-mediated oncogenic effects are solely dependent on ion conduction and the resulting changes in transmembrane potential, or whether it can directly modulate cancer cell signalling via direct coupling to intracellular signalling components remains to be determined. Most studies highlighting the oncogenic roles of hERG1 have utilized cancer cell-lines or primary tumours that express hERG1 and have investigated the effects of modulating hERG1 function using selective blockers. However, these blockers have been used at concentrations which are often orders of magnitude greater than the corresponding IC₅₀ value for hERG1 current block by the inhibitor. Moreover, hERG1 blockers failed to reverse the transformed phenotype induced by WT hERG1 expression in NIH-3T3 fibroblasts (Pier, 2007). On the other hand, there is evidence that hERG1 associates with several signalling proteins, including β 1-integrin, the

non-receptor tyrosine kinases FAK and Src, the small GTPase Rac1, scaffolding 14-3-3 proteins, vascular endothelial growth factor receptor 1 (VEGFR1) and the chemokine receptor CXCR4, which are linked to cancer progression (Cayabyab *et al.*, 2002, Kagan *et al.*, 2002, Cherubini *et al.*, 2005, Pillozzi *et al.*, 2007, Pillozzi *et al.*, 2010). Taken together, these observations may indicate a signalling activity for hERG1 in tumour cells that might accompany, or occur independently of, ion conduction.

Some ion channels act as bi-functional proteins, where in addition to regulating ion fluxes, they may also directly modulate intracellular signalling pathways. For example, the C-terminal domain of the L-type voltage-gated Ca^{2+} channel regulates transcription (Dolmetsch *et al.*, 2001). The β -subunits of voltage-gated sodium channels simultaneously modulate channel function and act as adhesion molecules (Malhotra *et al.*, 2000, Brackenbury *et al.*, 2008). Other examples include a member of the transient receptor potential (TRP) channels that contains a functional kinase domain (Runnels *et al.*, 2001) and EAG K^+ channels that bind and activate Ca^{2+} /calmodulin-dependent protein kinase II (CaMKII) (Sun *et al.*, 2004). Interestingly, the signalling activities of voltage-gated ion channels may be determined by channel gating. EAG-induced cell proliferation appears to be limited to the channel-closed conformation, since mutations that increase open probability no longer stimulate proliferation (Hegle *et al.*, 2006). Moreover, Ci-VSP, a protein which contains a voltage-sensor linked to a cytoplasmic phosphatase domain, homogenous to the tumour suppressor PTEN, displays a voltage-dependent enzymatic activity (Iwasaki *et al.*, 2008).

The role of ion conduction of K^+ channels involved in carcinogenesis has been investigated for EAG, a closely-related channel to hERG1 (Hegle *et al.*, 2006, Downie *et al.*, 2008) as

well as TASK-3 channels (Pei *et al.*, 2003). To elucidate the importance of hERG1 function with respect to its cell-transforming potential, here I stably expressed the dominant-negative non-functional hERG1 mutants G628S hERG1 and A561V hERG1 in NIH-3T3 cells and characterized cell transformation behaviours in relation to cells stably transfected with a hERG1-free (empty) vector (referred to as vector-control cells). G628S hERG1 is a mutant channel, whose subunits are correctly synthesized, properly folded and assembled, producing a protein that is processed and sorted to the plasma membrane as WT hERG1 channels, however, it contains a point mutation in the selectivity filter of the hERG1 channel pore, which causes a complete loss of channel function (Sanguinetti *et al.*, 1996, Zhou *et al.*, 1998a). A561V hERG1 has a mutation in the S5 domain that impairs hERG1 trafficking, causing its retention in the endoplasmic reticulum (Sanguinetti *et al.*, 1996, Ficker *et al.*, 2000, Kagan *et al.*, 2000).

NIH-3T3 cells are widely used to investigate oncogenic proteins (Jouanneau *et al.*, 1989, Pardo *et al.*, 1999, Kuo *et al.*, 2000, Hegle *et al.*, 2006) as they display a partially transformed phenotype, which makes them susceptible to oncogenic transformation. These cells are derived from mouse embryonic fibroblasts and display several valuable properties for assessing the cell biological properties of transformed cells, including contact inhibition of division on reaching confluency, a flattened, fibroblastic morphology and strong adherence to different substrata.

In this Chapter, the generation and characterization of NIH-3T3 cell-lines stably expressing A561V hERG1 and G628S hERG1 mutants is described.

4.2 Results

4.2.1 Is the biological activity of hERG1 channel blockers lost under cell culture conditions?

Previous studies that have investigated the importance of hERG1 channel function for tumour cell biology have used hERG1 blockers at concentrations many times (often orders of magnitude) higher than their IC_{50} for hERG1 current inhibition. For example, the IC_{50} for dofetilide blockade of hERG1 currents expressed in mammalian cells is approx. 12 nM (Snyders *et al.*, 1996). However, 1 μ M dofetilide was required to impair proliferation of hERG1-expressing SK-Br3 tumour cells (Lin *et al.*, 2007). Authors have justified the need for such high concentrations of hERG1 blockers as being due to the instability and degradation of blockers over the time-course of the experiment. Moreover, hERG1 channel blockers, such as dofetilide, did not reverse the transforming properties induced by WT hERG1 expression in NIH-3T3 cells even when used at a concentration >100-fold the IC_{50} for hERG1 blockade (Pier, 2007). It was necessary to confirm that these blockers maintain their activity and potency in the culture medium used for NIH-3T3 cell maintenance. *Xenopus* oocytes have been used for a large number of pharmacological studies in our laboratory and are an expedient method for testing the potency of compounds. The potencies of two blockers (terfenadine and dofetilide) were tested on hERG1 currents expressed in *Xenopus* oocytes. hERG1 currents were recorded using the voltage protocol shown in Fig. 4.1A. A depolarizing pulse to 0 mV from a holding potential of -90 mV caused hERG1 channels to activate and rapidly inactivate producing a small outward current. However, stepping to a hyperpolarizing potential of -120 mV causes hERG1 channels to recover from the inactivation state, eliciting a large inward tail current that

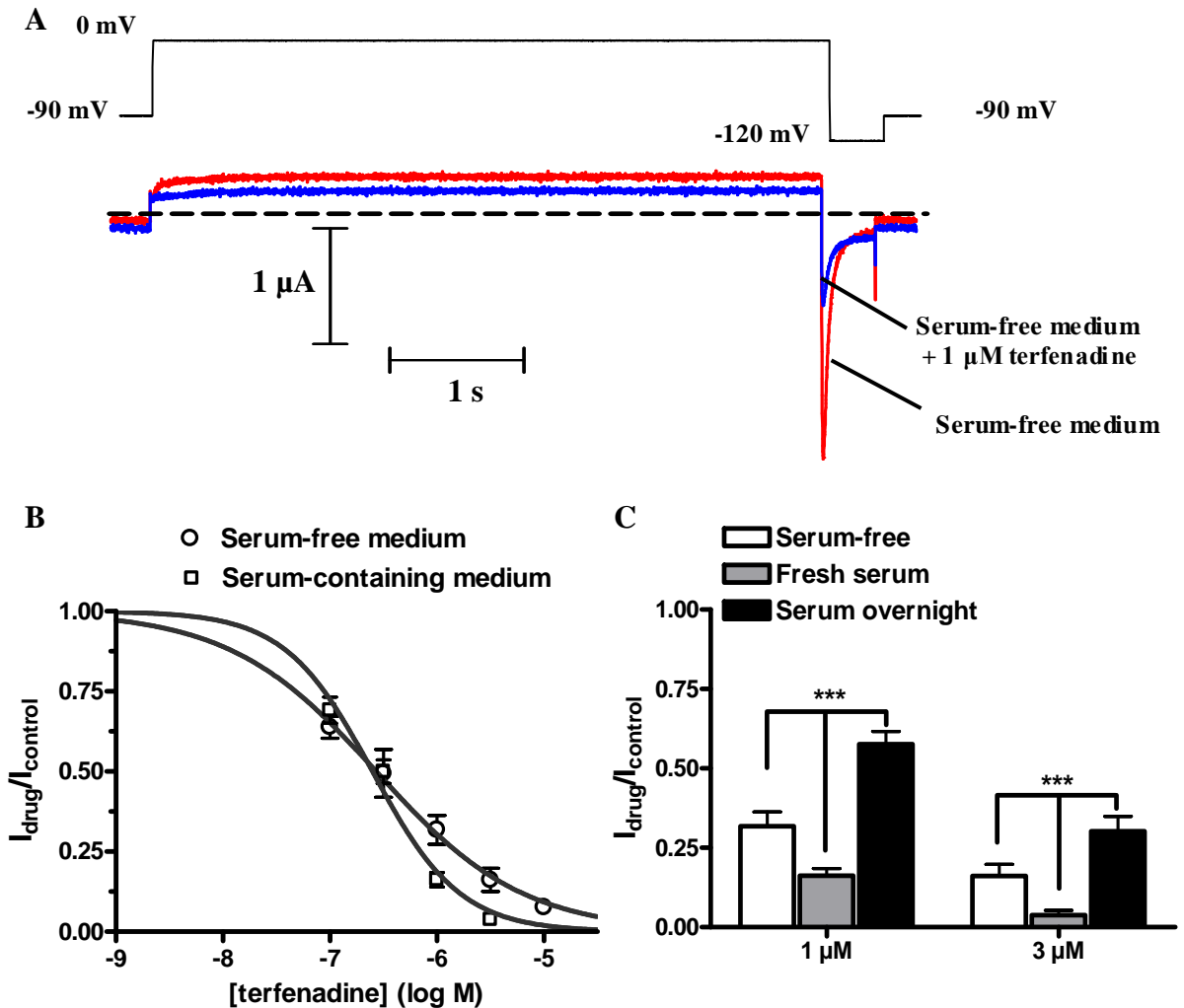


Figure 4.1 Evaluation of hERG1-blocking potency of terfenadine. **A.** top: Representation of the voltage protocol to elicit hERG1 currents. hERG1 currents are activated with 5 s voltage step to 0 mV and peak tail currents measured with a voltage step to -120 mV. **A.** bottom: Representative hERG1 current trace recorded from a *Xenopus* oocyte injected with WT hERG1 cRNA in serum-free medium in the absence (red) or presence (blue) of 1 μ M terfenadine. The dotted line represents the 0 current line. **B.** Concentration-response curves for terfenadine block of WT hERG1 peak tail currents recorded in either serum-free medium (open circles) or serum-containing medium (open rectangles). Steady-state peak tail current amplitudes at -120 mV for each concentration were normalized to control. Mean values were plotted against terfenadine concentration and fitted with a Hill function. Mean IC_{50} and Hill coefficient values were 291 ± 59 nM and -0.7 ± 0.07 ($n = 5$) in serum-free medium and 451 ± 78 nM and -1.1 ± 0.1 ($n = 4$) in serum-containing medium. **C.** Comparison of the effects of 1 and 3 μ M terfenadine on fractions of WT hERG1 current remaining in different media.

decayed during the pulse due to channel deactivation (Fig. 4.1A, red current trace). Application of hERG1 blockers (e.g. 1 μ M terfenadine) causes a decrease in the amplitude of outward current during depolarization and of the tail current during repolarization of hERG1 channels (Fig. 4.1A, blue current trace). The amplitude of the peak tail current was measured before and after blocker application to determine current inhibition.

I first tested if serum bound to or inactivated terfenadine by comparing concentration-response relationships in serum-free and 10% FCS-containing media. Terfenadine caused a concentration-dependent inhibition of hERG1 tail current under both serum-free and serum-containing conditions (Fig. 4.1B) with IC_{50} values of 292 ± 59 nM (n=5) and 452 ± 78 nM (n=4), respectively, and Hill coefficient values of 0.70 ± 0.07 and 1.10 ± 0.10 , respectively. These values are comparable to those previously reported by Suessbrich *et al.* (1996), who reported an IC_{50} value of 246 nM and a Hill coefficient of 1.09, and by Kamiya *et al.* (2008) who reported an IC_{50} value of 350 nM and a Hill coefficient of 0.89. The IC_{50} and Hill coefficient values for terfenadine-mediated inhibition of hERG1 current in serum-free and 10% FCS-containing media were not significantly different ($p > 0.05$). These data indicate that the presence of serum has minimal effects on the potency of terfenadine. I next tested whether conditioning medium for 24 h on NIH-3T3 cells altered the potency of terfenadine. Terfenadine was dissolved in fresh culture medium to a final concentration of 1 or 3 μ M. These concentrations were chosen as they are close to the steepest part of the concentration-response relationship enabling small reductions in potency to be detected. The terfenadine-containing media were incubated on NIH-16 cells overnight and their effects on hERG1 currents were measured the next day. Fresh unconditioned serum-containing medium was used as a control. The percentage inhibition

of hERG1 current by 1 μM terfenadine was reduced (Fig. 4.1C, left). The current remaining changed from $32 \pm 5\%$ ($n=5$) in serum-free medium and $16 \pm 2\%$ ($n=5$) in serum-containing medium to $58 \pm 4\%$ ($n=15$; $p<0.001$) after incubation overnight. Similarly, the blockade by 3 μM terfenadine increased the remaining hERG1 current from $16 \pm 4\%$ ($n=4$) in serum-free medium and $4 \pm 2\%$ ($n=5$) in serum-containing medium to $30 \pm 5\%$ ($n=6$; $p<0.001$) after incubation overnight (Fig. 4.1C, right). Although there is a significant decrease in terfenadine potency after incubation overnight, the change was not large and 3 μM terfenadine was still able to cause $\sim 70\%$ block of hERG1 current. As will be discussed later, it is also known that hERG1 blockers are more potent at channels expressed in mammalian cells than in oocytes.

The potency of hERG1 blockade by dofetilide was next studied. hERG1 currents were elicited using the same I-V protocol (Fig. 4.2A). DMSO-containing (0.01% v/v) conditioned culture medium did not affect hERG1 current (Fig. 4.2A, bottom), indicating that the compound solvent and other soluble serum factors did not have acute effects on hERG1 inhibition. Block of hERG1 currents by dofetilide was compared under the same three recording conditions. For dofetilide, 30 nM increased the remaining hERG1 current from $16 \pm 1\%$ ($n=6$) in serum-free medium and $29 \pm 5\%$ ($n=4$) in serum-containing medium to $70 \pm 6\%$ ($n=5$) after incubation in medium overnight (Fig. 4.2B). However, a higher concentration of 100 nM was able to manifest its activity under all conditions, producing $89 \pm 2.4\%$ ($n=4$), $94 \pm 2.1\%$ ($n=6$) and $92 \pm 2.6\%$ ($n=5$) hERG1 current inhibition in serum-free, serum-containing and conditioned culture media, respectively (Fig. 4.2B). These data suggest that dofetilide is stable in culture medium and maintains its hERG1-blocking activity when used at concentrations of ≥ 100 nM.

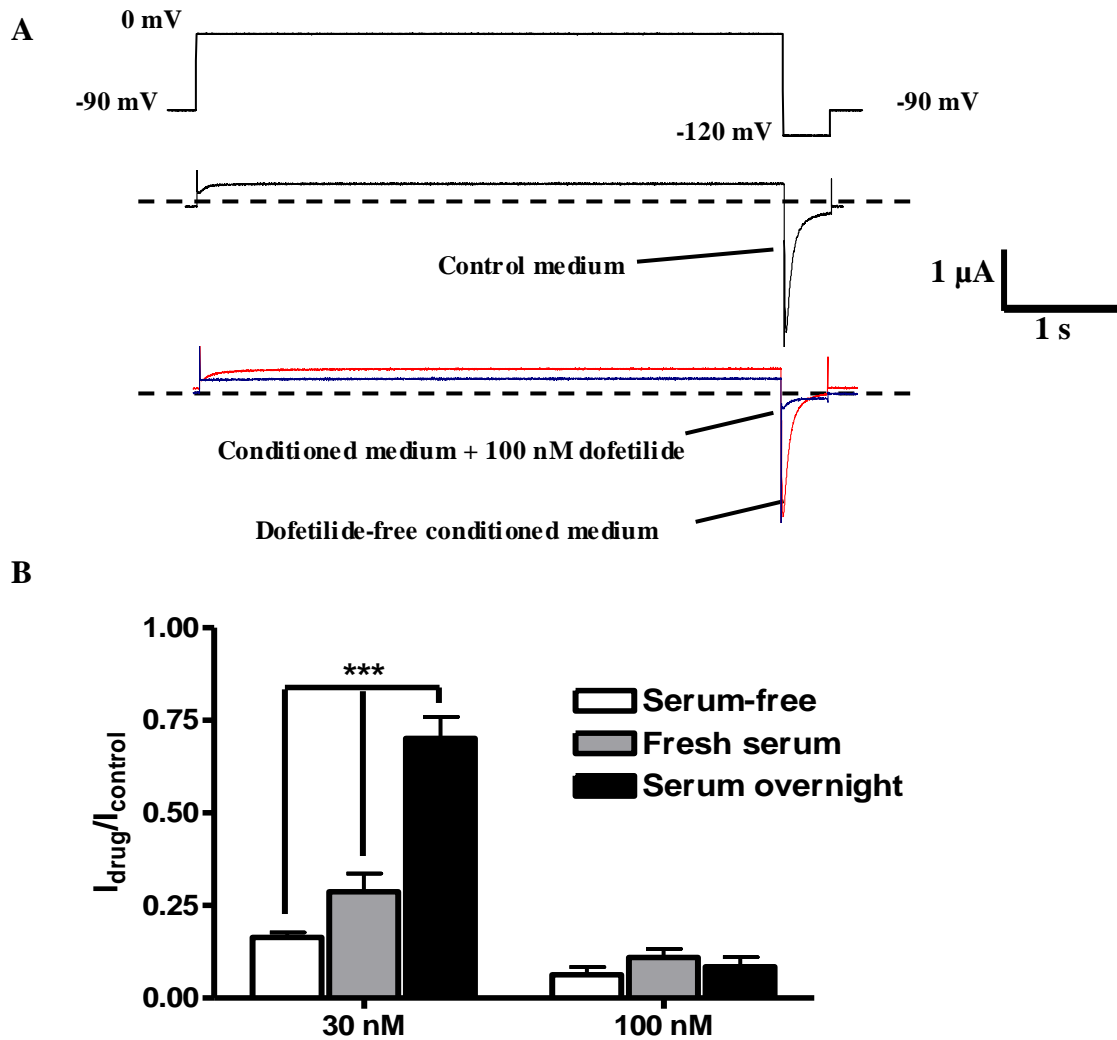


Figure 4.2 Dofetilide is a potent hERG1 blocker. **A.** top: Representation of the voltage protocol to elicit hERG1 currents. **A.** middle: Representative hERG1 current trace recorded from a *Xenopus* oocyte injected with WT hERG1 cRNA in serum-free medium. The dotted line represents 0 current line. **A.** bottom: Representative hERG1 current traces recorded from the same cell as in middle pane in the presence of dofetilide-free conditioned medium and a conditioned medium containing 100 nM dofetilide. **B.** Fractions of hERG1 currents remaining after inhibition by 30 and 100 nM dofetilide in different culture media. Steady-state peak tail current amplitudes at -120 mV were normalized to currents in compound-free medium. Recordings were obtained from at least 4 oocytes for each drug concentration. *** $p < 0.001$ indicates significantly different results compared to serum-free medium.

4.2.2 Do G628S hERG1 and A561V hERG1 exhibit a dominant-negative suppression of hERG1 current?

hERG1 blockers either have no effect on the transformation of cells by hERG1 expression, or the concentrations that are required are so high they may be causing non-specific actions on cells. As an alternative approach, we suppressed hERG1 currents by using a genetic approach using point-mutations that reduce hERG1 channel function. Dominant-negative suppression of function is a widely used approach to abolish the activity of a functional protein via co-expression of a non-functional dominant-negative mutant protein. Stable transfection of conduction-deficient, dominant-negative hERG1 mutants into NIH-3T3 cells is an approach that should allow us to study the contribution of K⁺ ion conduction to hERG1-mediated oncogenic effects and may also provide new insights into the mechanisms by which hERG1 effect tumour progression.

To confirm the dominant-negative behaviour of the two mutants, 10 ng WT hERG1 cRNA either alone or in a 1:1 ratio with G628S hERG1 or A561V hERG1 cRNAs was injected into *Xenopus* oocytes. Channel function was determined from analysis of hERG1 currents measured in response to a series of test potentials from -60 to +50 mV (Fig. 4.3A). Tail current amplitudes were measured at -70 mV. Fig. 4.3B shows typical voltage-activated K⁺ currents for WT hERG1 during this I-V protocol. During the depolarizing test pulses, small outward currents were observed, which corresponded to hERG1 channels opening and rapidly inactivating. On repolarization to -70 mV, the channels recover from inactivation and pass an outward current, whose amplitude depends on the number of channels that have opened (and inactivated) during the depolarization step. A561V hERG1 (Fig. 4.3C) and G628S hERG1 (Fig. 4.3D) -injected oocytes displayed tiny outward currents during

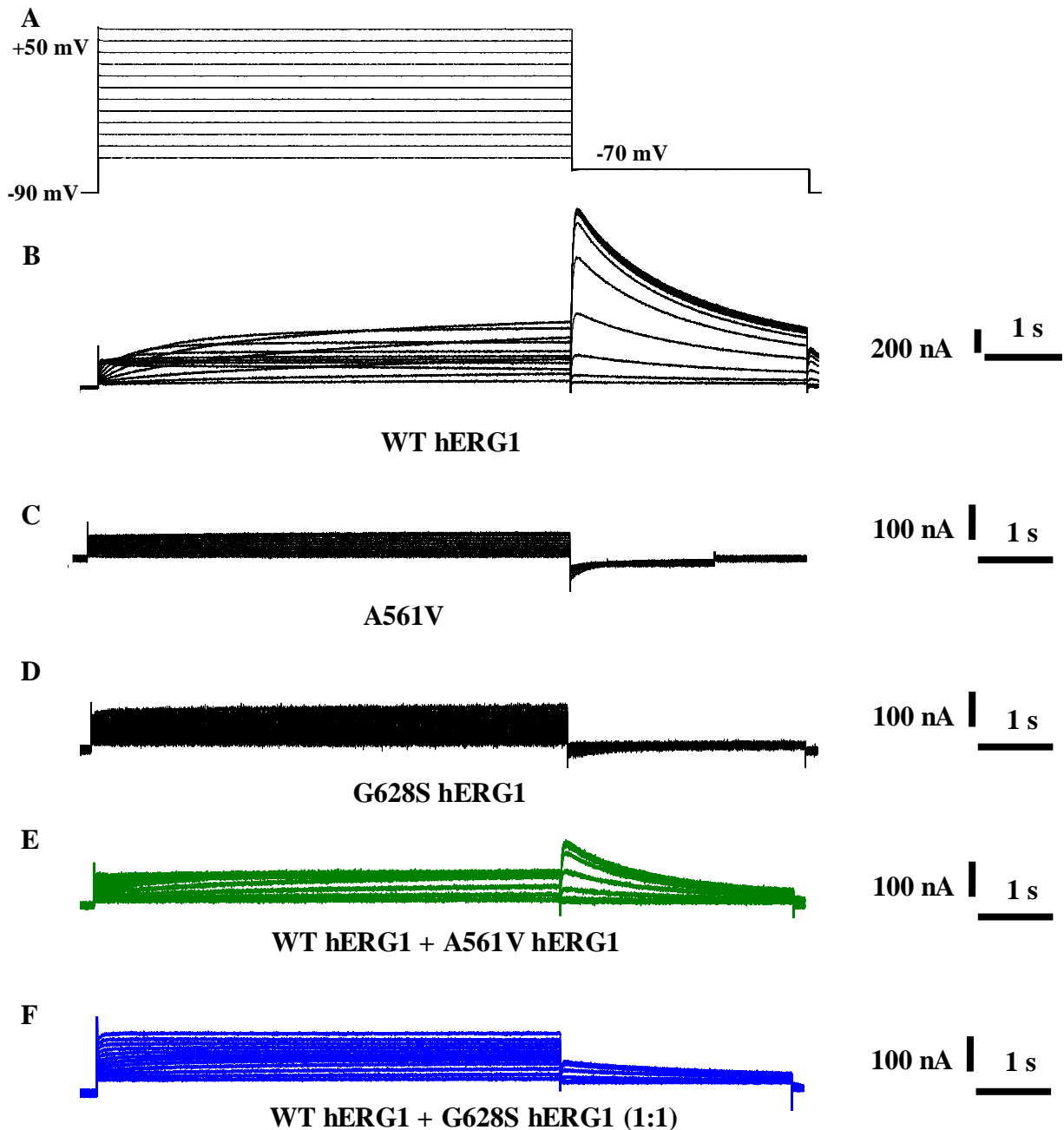


Figure 4.3 Co-expression of G628S hERG1 and A561V hERG1 mutants with WT hERG1 in *Xenopus* oocytes. **A.** Representation of the protocol used. Holding potential was -90 mV and a family of 5 s test pulses from -60 to +50 mV were applied followed by a final step to -70 mV. **B, C, D, E, F.** Representative current traces obtained using this protocol from oocytes expressing WT hERG1, A561V hERG1, G628S hERG1, WT hERG1 + A561V hERG1 (1:1 ratio) and WT hERG1 + G628S hERG1 (1:1 ratio), respectively. Note the different ordinate scale for WT hERG1 current amplitude in **B**.

depolarization, which might have been carried by leak K^+ channels endogenous to the oocytes. Moreover, no outward hERG1 tail currents were seen in A561V hERG1 (Fig. 4.3C) or G628S hERG1 (Fig. 4.3D) -injected oocytes. Oocytes injected with A561V hERG1 + WT hERG1 (Fig. 4.3E) or G628S hERG1 + WT hERG1 (Fig. 4.3F) showed substantially decreased outward hERG1 currents during depolarization and in hERG1 peak tail currents during repolarization. A maximal peak tail current of $\sim 1.5 \mu\text{A}$ was detected when WT hERG1 channels were activated by voltages positive to 0 mV. In contrast, maximal tail currents amplitudes of $\sim 0.2 \mu\text{A}$ and $0.1 \mu\text{A}$ were detected in A561V hERG1 + WT hERG1 or G628S hERG1 + WT hERG1-injected oocytes (Fig. 4.3E and F, respectively). The reduction of WT hERG1 current at all voltages by either mutant is graphically demonstrated by the mean voltage-dependence of activation curves (Fig. 4.4A). Peak tail current amplitudes are shown plotted against test pulse potential (Fig. 4.4A). Co-expression of either mutant with WT hERG1 caused substantial decreases in hERG1 current. At +20 mV, hERG1 tail current decreased from $1.50 \pm 0.14 \mu\text{A}$ in WT hERG1- to $0.20 \pm 0.03 \mu\text{A}$ in WT hERG1 + A561V hERG1- and $0.11 \pm 0.02 \mu\text{A}$ in WT hERG1+ G628S hERG1-injected oocytes ($p < 0.01$, Fig. 4.4B). To determine whether co-expression of these mutants affected the voltage-dependence of WT hERG1 activation, tail currents at each test potential were normalized to the maximum in each cell and the mean results plotted against test potential (Fig. 4.4C). The activation curve was slightly left-shifted for WT hERG1 + A561V hERG1, giving a $V_{0.5}$ for activation of $-37.1 \pm 3.5 \text{ mV}$ ($n=4$), which was significantly different to the value of $-28.0 \pm 1.5 \text{ mV}$ ($n=7$) for WT hERG1 currents ($p < 0.05$, Fig. 4.4D). These results show that A561V hERG1 and G628S hERG1 exhibit no functional current when expressed on their own. Moreover, the channel subunits are

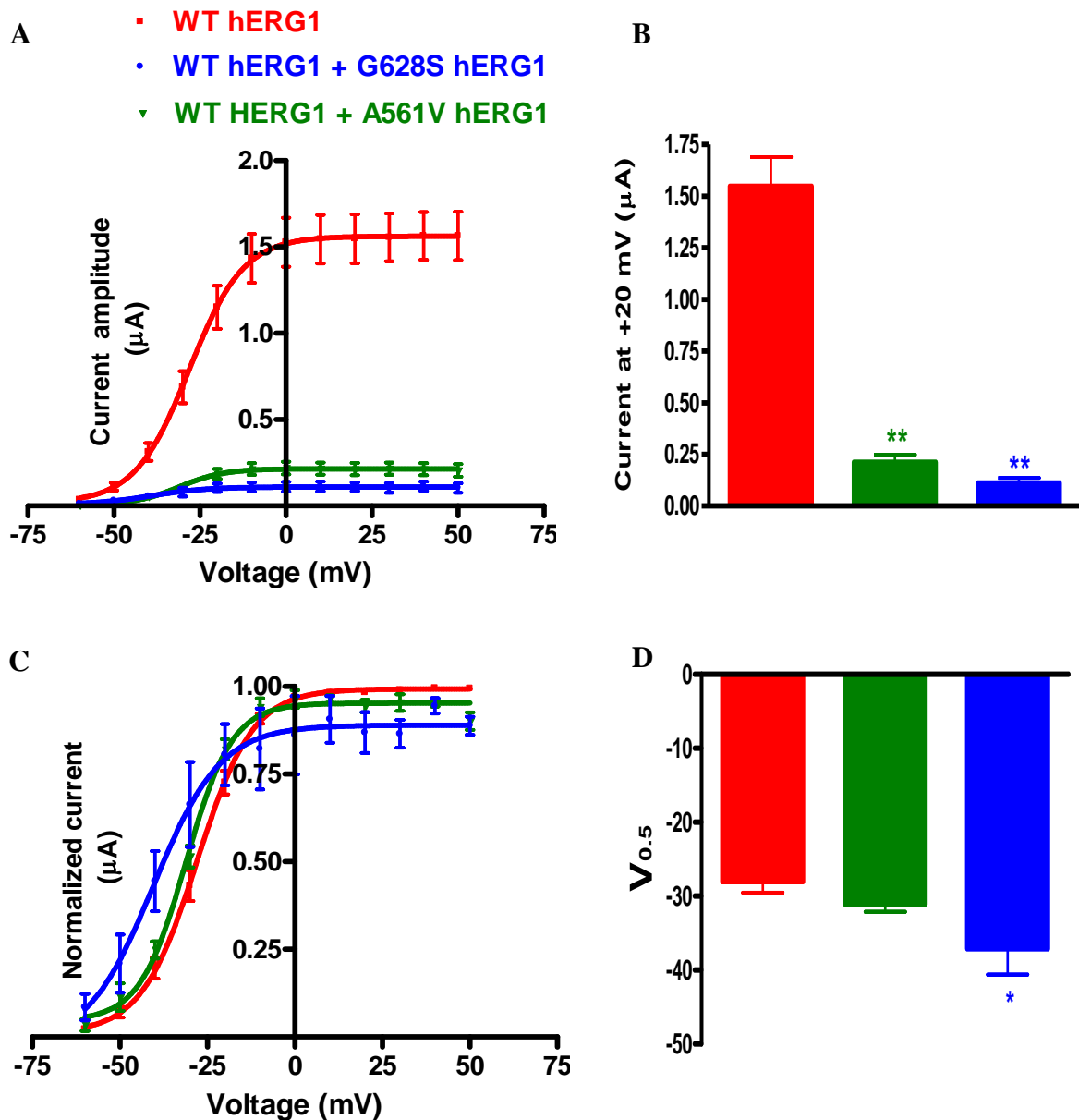


Figure 4.4 G628S hERG1 and A561V hERG1 mutants expressed in *Xenopus* oocytes produce a dominant-negative effect. **A.** Mean peak tail currents were plotted against the test pulse potential and fitted with Boltzmann function. **B.** Comparison of the maximal tail current amplitude measured following test pulse to +20 mV in oocytes expressing WT hERG1, WT hERG1 + A561V hERG1 (1:1 ratio) and WT hERG1 + G628S hERG1 (1:1 ratio). **C.** Normalized to peak hERG1 tail currents plotted against test pulse potential and fitted with Boltzmann function. **D.** Comparison of the $V_{0.5}$ of hERG1 current activation. Data points were obtained from at least 5 different oocytes. Statistically significant differences from WT hERG1-expressing oocytes are indicated as follows * p <0.05; ** p <0.01.

expressed, because they cause profound dominant-negative suppression of current when co-expressed with WT hERG1.

4.2.3 Generation of stable, WT and mutant hERG1 transfectants

NIH-3T3 cells were transfected with empty-vector, WT hERG1, A561V hERG1 or G628S hERG1 in pcDNA3. Stably-transfected cells were selected based on their resistance to a pre-optimized concentration of G418, which should only kill non-transfected cells. Clones were then selected from colonies that originated from single cells and were expanded (see Methods). Incorporation of the transfected DNA into the genome is a low probability event. Moreover, given the reputation of NIH-3T3 cells as a “difficult to transfect” cell-type, a large number (75-100) of clones were grown for each plasmid construct transfected. Therefore, it became necessary to develop rapid and effective screening methods to detect hERG1 expression in large numbers of transfected clones. We used real-time RT-PCR and [³H]dofetilide binding assays for this purpose.

4.2.3.1 Optimizing real-time reverse transcription PCR conditions for screening of NIH-3T3 clones

Real-time reverse transcription (RT-RT) PCR is the most common assay for estimation of relative gene expression in biological samples and *in vitro* cell cultures (Orlando *et al.*, 1998). It was previously used for quantification of hERG1 mRNA expression in blood samples from acute myeloid leukaemia (AML) patients (Pillozzi *et al.*, 2007) and gliomas (Patt *et al.*, 2004). I wanted to use real-time RT PCR for initial screening of NIH-3T3 clones for expression of hERG1/hERG1 mutants, as it allows screening of many clones in an assay that is relatively quick, accurate and highly-sensitive. Total RNA of each clone

was extracted and retro-transcribed into cDNA, which was used in the real-time RT PCR to detect hERG1 mRNA expression.

Low quality, impure or degraded RNA may interfere with the accuracy of gene expression evaluation by real-time RT PCR (Fleige *et al.*, 2006). Initially, integrity and quality of total RNA extracted from each clone was assessed using agarose gel electrophoresis. An example for RNA extracted from HEK-hERG, NIH-50 and NIH-16 cells is shown (Fig. 4.5A). As can be seen, RNA of each sample clearly showed two well-defined 18S and 28S rRNA bands characteristic of eukaryotic RNA. Moreover, no smearing or signs of degradation of these RNA bands was observed.

For accurate quantification of gene expression using real-time RT-PCR, the recommended methods of normalization were used (Huggett *et al.*, 2005). Total RNA of each clone was extracted from a cell monolayer grown to ~ 70% confluency in a 35 mm dish to ensure a similar sample size among clones. Normalization to cell number in each sample was not performed to avoid the use of chemical or enzymatic treatments of cells, which might affect gene expression. Other normalization strategies included assessing RNA quality (Fig. 4.5A), normalization to total RNA concentration and normalization relative to an internal reference gene, GAPDH, which controls for different RNA inputs used in reverse transcription reactions.

Next, I wanted to verify the success of both the RNA extraction and cDNA synthesis steps. To do this, a conventional PCR technique was used. RNA extracted from HEK293 cells stably expressing high levels of hERG1 (HEK-hERG cells), NIH-50 and NIH-16 were retro-transcribed and the cDNA products were used in the PCR reaction and amplified for hERG1. When the amplified PCR products were run on a gel, the correct product size (83

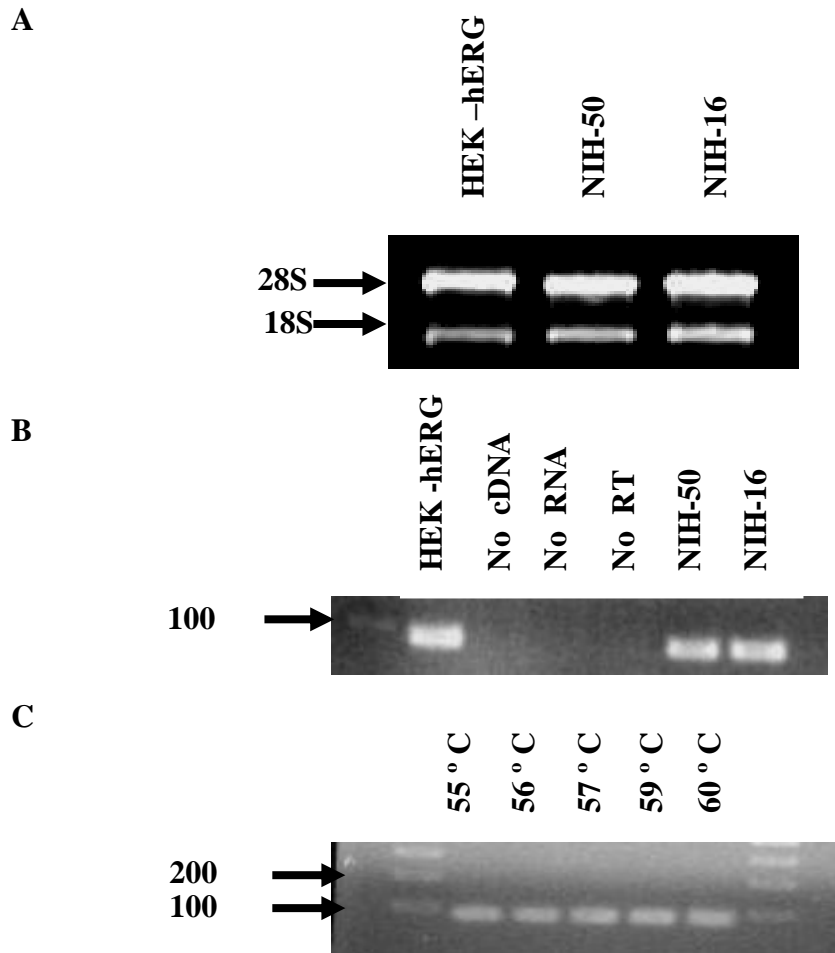


Figure 4.5 Optimization of conditions for real-time reverse transcription PCR to detect hERG1 expression in NIH-3T3 cells. **A.** Agarose gel electrophoresis of total RNA extracted from HEK-hERG, NIH-50 and NIH-16 cells. The quality of total RNA extracted from these cells was checked by electrophoresis of 1 μ g of each RNA preparation on a denaturing agarose gel. Each RNA sample shows two intact 18S and 28S ribosomal RNA bands. No degradation or smearing of RNA bands was seen. **B.** Representative conventional reverse transcription (RT) PCR for hERG1 (83 bp band) transcript. RNA extracted from HEK-hERG, NIH-50 and NIH-16 cells was retro-transcribed and amplified using hERG1 primers. Nuclease-free water (no cDNA) and a reverse transcriptase reaction lacking RNA (no RNA) or reverse transcriptase enzyme (no RT) were used as negative-controls. **C.** Representative conventional RT-PCR for hERG1 transcripts (83 bp band) performed at different primer annealing temperatures. RNA extracted from HEK-hERG cells was retro-transcribed and amplified for hERG1.

bp) was seen for HEK-hERG, NIH-50 and NIH-16 cDNAs, but not in the negative-control samples (no RT, no RNA and no cDNA, Fig. 4.5B). Overall, this confirms efficient RNA extraction, cDNA synthesis and an absence of contamination by genomic DNA or other sources of hERG1 DNA. Next, I optimized the PCR conditions to get a better yield. However, variation of the annealing temperature did not affect the amount of the amplified product (Fig. 4.5C). I next optimized conditions for testing for hERG1 and GAPDH expression using cDNA from HEK-hERG cells under real-time PCR conditions and using SYBR-green technology. SYBR-green is a dye that fluoresces when it binds to double-stranded DNA amplicons. Its fluorescence intensity is measured after each thermal cycle producing characteristic PCR amplification curves (Fig. 4.6A). No-template controls using either hERG1 or GAPDH primers showed insignificant peaks (Fig. 4.6A). The dotted-line represented a threshold fluorescence level set in the exponential region of amplification, which was used to calculate threshold cycle number (C_T) for each gene amplification (Fig. 4.6A). Each PCR run was followed by a melting curve analysis of the amplified products, which showed a single characteristic peak for each gene amplification. This was seen at each amplicon melting point (m.p), which for hERG1 product was at 79-80°C and for GAPDH was 82°C (Fig. 4.6B). This confirmed the absence of non-specific PCR amplification and excluded non-specific primer-dimer formation as a source of fluorescence signal. In order to ensure that the correct products are formed using the real-time RT PCR cycling protocol, PCR products were run on a gel against a DNA ladder of known molecular weights (Fig. 4.6C). The correct PCR product sizes were observed for hERG1 (83 bases, lanes 1 and 2) and GAPDH (138 bases, lanes 3 and 4), which confirmed that hERG1 and GAPDH are specifically amplified under these conditions. Conversely, no bands were detected in template DNA controls using hERG1 primers (lane 5) or GAPDH

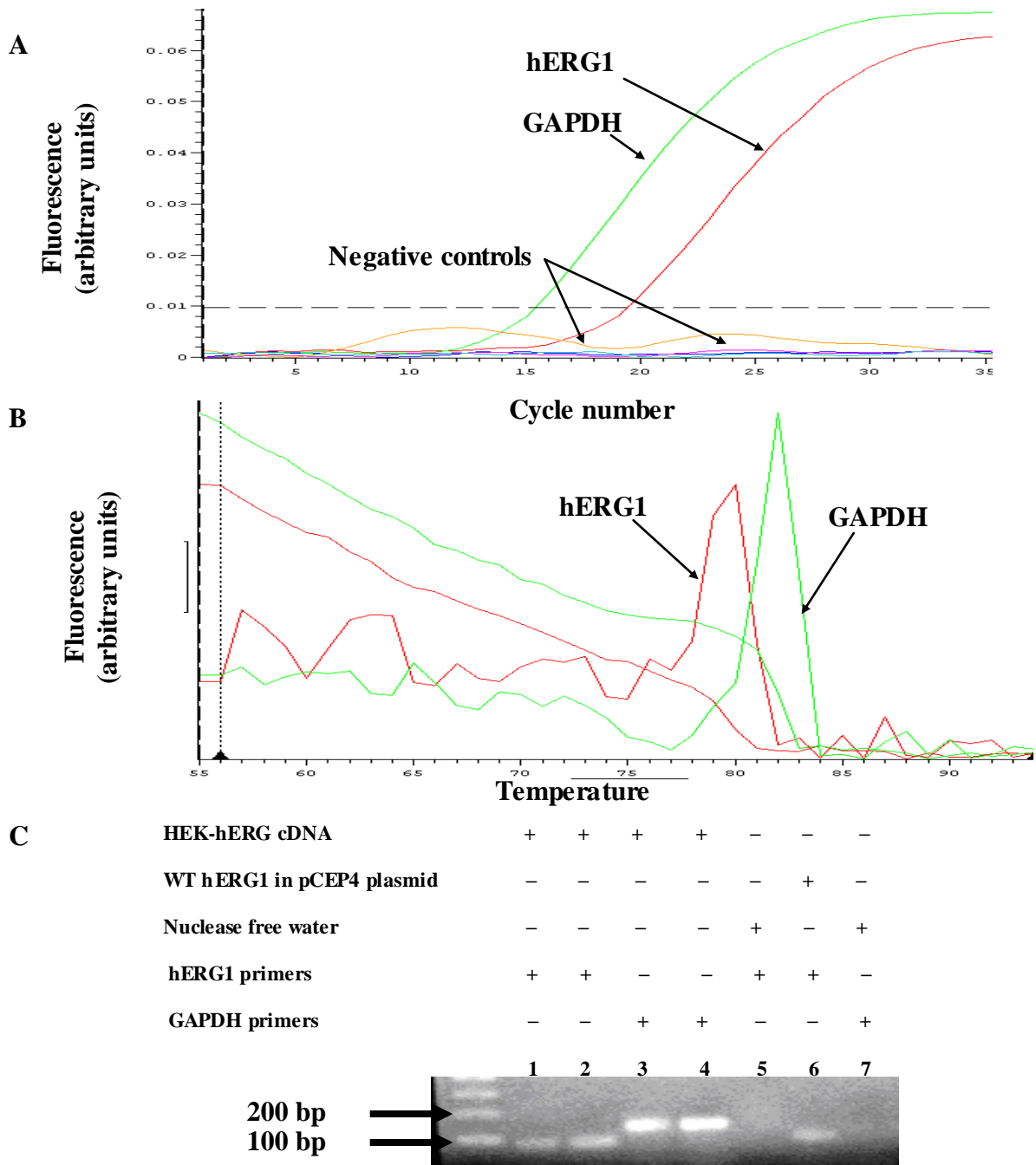


Figure 4.6 Real-time RT PCR is a reliable method for detecting hERG1 expression. **A.** A representative real-time RT PCR quantification curve. RNA extracted from HEK-hERG cells was retro-transcribed and amplified for hERG1 (red) and GAPDH (green). Nuclease-free water was used as negative-controls for hERG1 and GAPDH amplifications (brown and blue, respectively). The fluorescence signals elicited by SYBR-green-amplicon complexes in each sample are plotted versus the cycle number. **B.** Melting curve analysis for amplified real-time RT-PCR GAPDH (green) and hERG1 (red) products, respectively. **C.** Gel electrophoresis of hERG1 and GAPDH transcripts obtained from samples used in A.

primers (lane 7). Moreover, a positive-control pCEP4 plasmid expressing hERG1 also showed a PCR amplicon of the same size (lane 6). Overall, the data shown in Fig. 4.6C indicate that real-time PCR is a reliable method for quantification of hERG1 in transfected clones.

One of the most popular methods of real-time PCR data analysis is the $\Delta\Delta C_T$ method (Livak *et al.*, 2001). This method provides a target gene expression value, normalized to a reference gene, as a fold difference between the tested sample and an external calibrator sample (Livak *et al.*, 2001). In other words, it estimates the normalized target gene content of the sample relative to that of an external standard sample (calibrator) and hence does not require a standard curve in each run (c.f. absolute gene quantification), which also makes it more economic. However, for this method to be valid, it is necessary that the amplification efficiencies of the target gene and reference gene are similar. To test for the efficiencies of the primers used for hERG1 and GAPDH amplification, 10-fold serial dilutions of HEK-hERG cDNA were amplified by real-time RT PCR for hERG1 (Fig. 4.7A) and GAPDH (not shown). The C_T and ΔC_T (C_T hERG1 - C_T GAPDH) values were plotted versus the logarithm of the standard dilution and the curve was fitted using a linear regression function (Fig. 4.7B). Correlation coefficient (r^2) values for hERG1 and GAPDH standard curves were 0.96 and 0.87, respectively. The slopes for hERG1 and GAPDH curves were -3.49 ± 0.32 (n=4) and $(-3.35 \pm 0.18, n=4)$, respectively ($p>0.05$). Moreover, the slope of ΔC_T curve was -0.03 ± 0.16 (n=4), a value not different to zero. These data confirmed equal amplification efficiencies for the two pairs of primers and the suitability of the $\Delta\Delta C_T$ method for real-time PCR data analysis in this study.

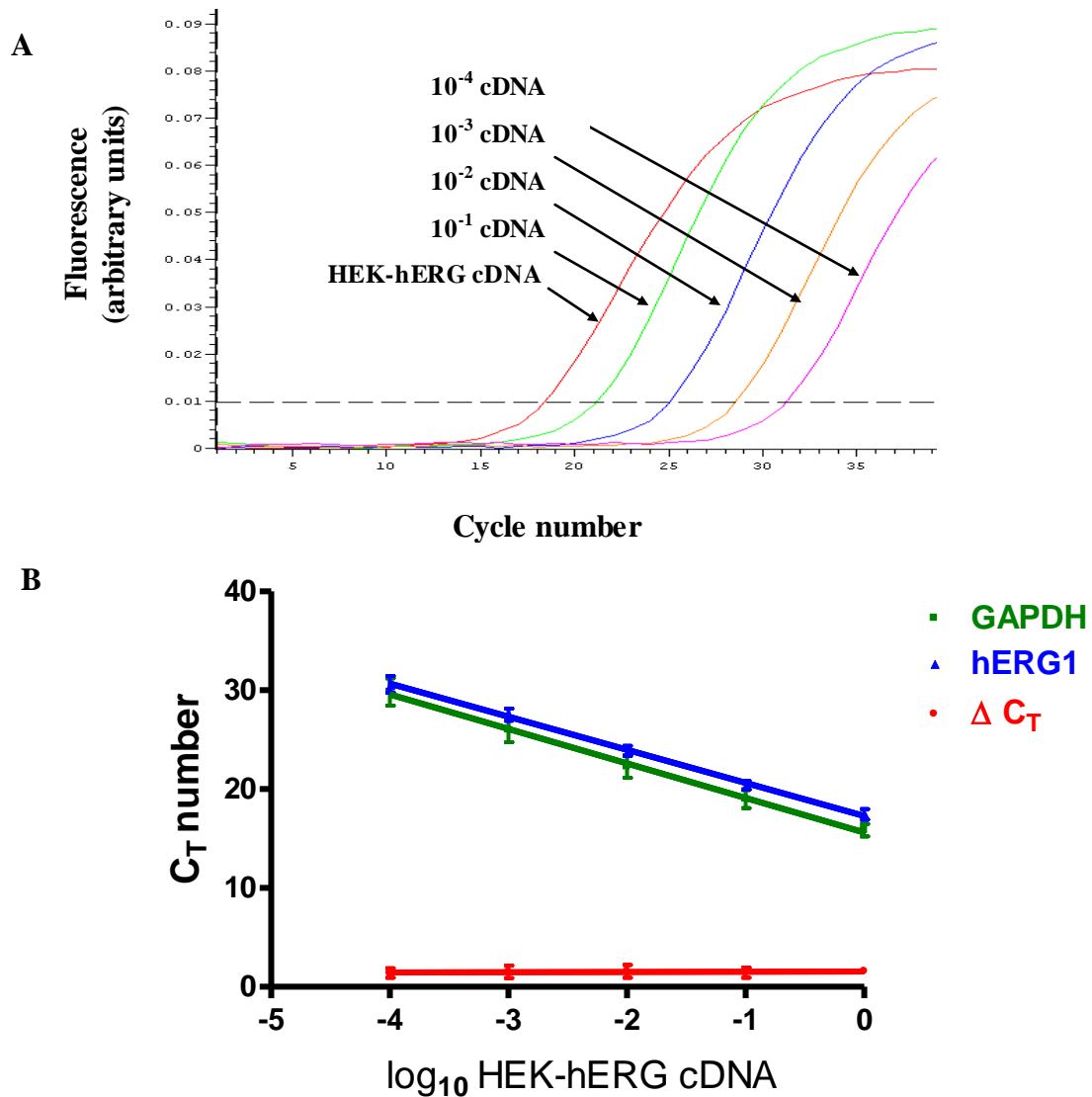


Figure 4.7 Validation of hERG1 and GAPDH amplification efficiencies. **A.** Representative of a real-time RT PCR quantification curve. Serial dilutions (10-fold) of a HEK-hERG cDNA sample were prepared and amplified for hERG1. The fluorescence signals of SYBR-green-amplicon complexes in each sample are plotted versus the cycle number. The dotted-line set at the exponential phase is used to determine the cycle threshold (C_T) for each sample. **B.** Real-time standard curves for amplification of hERG1 (blue) and GAPDH (green). The C_T values are plotted against the logarithm of the standard sample dilution. ΔC_T for each dilution = C_T hERG1- C_T GAPDH. Error bars denote SEM and results are from at least 3 experiments.

4.2.3.2 [³H]dofetilide binding assay

[³H]dofetilide binds to hERG1 with high affinity and has previously been used to quantify hERG1 expression in cardiac myocytes, ventricular homogenates, SH-SY5Y neuroblastomas and hERG1-transfected HEK293 cells (Chadwick *et al.*, 1993, Duff *et al.*, 1995, Finlayson *et al.*, 2001a, Finlayson *et al.*, 2001b). [³H]dofetilide binding has been used here to verify hERG1 protein expression in clones that showed positive hERG1 mRNA expression by the RT-RT PCR technique (see above).

The assay was optimized and validated using HEK-hERG membrane homogenates, which express relatively high levels of hERG1 protein. Saturation analysis (Fig. 4.8A) showed that increasing the [³H]dofetilide concentration added to HEK-hERG membranes (75 µg protein mL⁻¹) increased over the range 0-50 nM [³H]dofetilide allowed a full binding curve to be obtained. Specific (total-NSB) binding values were fitted by non-linear regression analysis (using a one site binding model), yielding a B_{max} value of 4.88 ± 0.60 pmol mg⁻¹ protein (n=4), and a K_D value of 15.4 ± 2.8 nM (n=4). These data indicate that [³H]dofetilide binds with high affinity (nM range) to hERG1 proteins in membranes, and this method can be used to quantify hERG1 protein expression. Based on these results we used a single concentration of 10 nM [³H]dofetilide in subsequent binding assays.

To characterize the specificity of [³H]dofetilide binding to hERG1, three hERG1 blockers were next assessed for their abilities to displace [³H]dofetilide from hERG1 using a competition binding assay (Fig. 4.8B). The hERG1 blockers each inhibited [³H]dofetilide binding in a concentration-dependent manner. pIC₅₀ (-log₁₀ concentration giving 50% inhibition of specific [³H]dofetilide binding) values and Hill coefficients were: dofetilide, 7.46 ± 0.04 and 1.13 ± 0.02 (n=3); E4031, 7.12 ± 0.09 and 1.11 ± 0.04 (n=3); terfenadine,

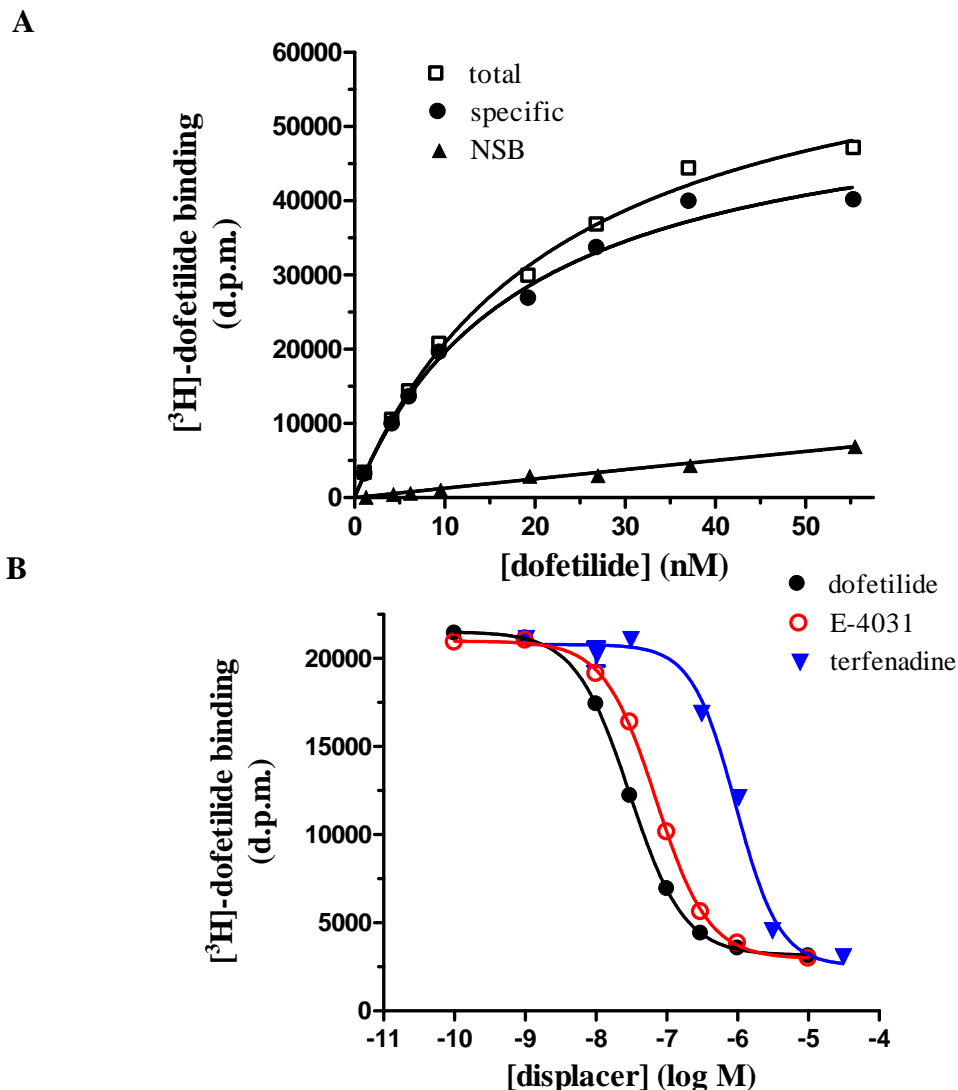


Figure 4.8 $[^3\text{H}]$ dofetilide binds specifically to hERG1 proteins in HEK-hERG membranes. **A.** Saturation analysis curve of $[^3\text{H}]$ dofetilide binding to HEK-hERG membranes. HEK-hERG membranes were treated with different concentrations of $[^3\text{H}]$ dofetilide in the absence and presence of unlabelled dofetilide and radioactivity was counted to determine total (open squares) and non-specific (NSB, closed triangles) binding, respectively. Specific (total-NSB) binding values were calculated (closed circles). B_{max} and K_D values were 4.88 ± 0.60 pmol mg^{-1} protein and 15.4 ± 2.8 nM, respectively. **B.** Inhibition of $[^3\text{H}]$ dofetilide binding in HEK-hERG membranes. HEK-hERG membranes were treated with $[^3\text{H}]$ dofetilide in the presence of increasing concentrations of dofetilide (closed circles), E-4031 (open circles) and terfenadine (closed triangles) and radioactivity was determined for each concentration. Data shown are representative saturation (**A**) and competition (**B**) curves from single experiments. At least 3 independent experiments were performed for each assay and mean \pm SEM values were used for statistical analysis.

6.04 ± 0.08 and 1.50 ± 0.05 ($n=3$). By using the Cheng-Prusoff correction (Cheng *et al.*, 1973) to these data, inhibitor affinity (K_i) values for dofetilide, E-4031 and terfenadine determined as 19 nM, 43 nM and 520 nM, respectively. These values are consistent with previous reports (Finlayson *et al.*, 2001b). Moreover, these data are in agreement with the rank order of potency for these inhibitors with respect to hERG1 channel blockade, as reported in previous electrophysiological studies (Roy *et al.*, 1996, Snyders *et al.*, 1996, Ficker *et al.*, 1998, Weerapura *et al.*, 2002, Kamiya *et al.*, 2008). The Hill coefficient values for these compounds approximated unity, providing evidence of competition for binding to a single population of binding sites in the membrane preparation.

4.2.3.3 Quantification of hERG1 expression in transfected clones

Real-time RT PCR was used to assess expression levels of hERG1 mRNA in transfected clones relative to hERG1 mRNA level in NIH-50 cells, a cell-line that stably expresses hERG1 and exhibits a transformed phenotype (Chapter 3; Pier, 2007). Clones that showed evidence of hERG1 mRNA expression were further assessed by [3 H]dofetilide binding to verify if hERG1 protein expression correlated with mRNA levels detected by RT-RT PCR. The screening results for some selected clones are illustrated in Fig. 4.9.

NIH-VC cells (NIH-3T3 cells transfected with an empty vector) were used as a negative-control in both assays. NIH-VC showed 0.12 ± 0.04 ($n=3$) fold hERG1 mRNA expression relative to NIH-50 cells and no specific binding in [3 H]dofetilide binding assay. On the other hand, NIH-16 and HEK-hERG cells were used as positive controls. The hERG1 mRNA level of NIH-16 was 4.76 ± 0.87 ($n=3$) fold higher than NIH-50, as calculated using $\Delta\Delta C_T$ method. Also, specific [3 H]dofetilide binding could be demonstrated in both NIH-16 and HEK-hERG membranes.

Among the many WT hERG1 transfectants tested, only a few clones showed any evidence of hERG1 mRNA expression. Moreover, many of these clones showed no specific binding to [³H]dofetilide. An example for the RT-RT PCR/[³H]dofetilide binding discrepancy is shown in Fig. 4.9. C68, a WT hERG1-transfected clone, which showed a $\Delta\Delta C_T$ value of 3.40 ± 0.46 (n=3) (Fig. 4.9A), exhibited no specific binding to [³H]dofetilide (Fig. 4.9B). Therefore, it has not proved possible to add additional WT hERG1-expressing NIH-3T3 cell-lines to the existing NIH-16 and NIH-50 clones.

The results for G628S hERG1 and A561V hERG1 clones were more promising. hERG1 mRNA and protein expression were confirmed in two G628S hERG1 transfectants (C3 and C36) and two A561V hERG1 transfectants (C12 and C10, Fig. 4.9). hERG1 mRNA expression levels in these clones, relative to NIH-50 cells, were 5.1 ± 2.8 , 3.1 ± 0.4 , 7.4 ± 1.9 and 5.5 ± 1.8 for C3, C36, C12 and C10, respectively (Fig. 4.9A, n=3). hERG1 protein expression in these clones was confirmed by [³H]dofetilide binding in 3 independent experiments. Representative data from a single [³H]dofetilide binding assay are shown in Fig. 4.9B. For these clones a difference was seen between total and non-specific binding, indicating specific dofetilide binding and hERG1 protein expression.

4.2.3.4 Detection of hERG1 expression in mutant hERG1 transfectants using Western blotting

The [³H]dofetilide binding assay is performed on a crude cell membrane preparation and therefore cannot distinguish between cell-surface (plasma membrane) and intracellular (ER, Golgi, etc.) localizations of hERG1 proteins. Therefore, it was important also to assess the localization of hERG1 protein by Western blotting. Two anti-hERG1 antibodies were characterized: rabbit anti-hERG1 (recognizes residues 833-901) and purified goat anti-

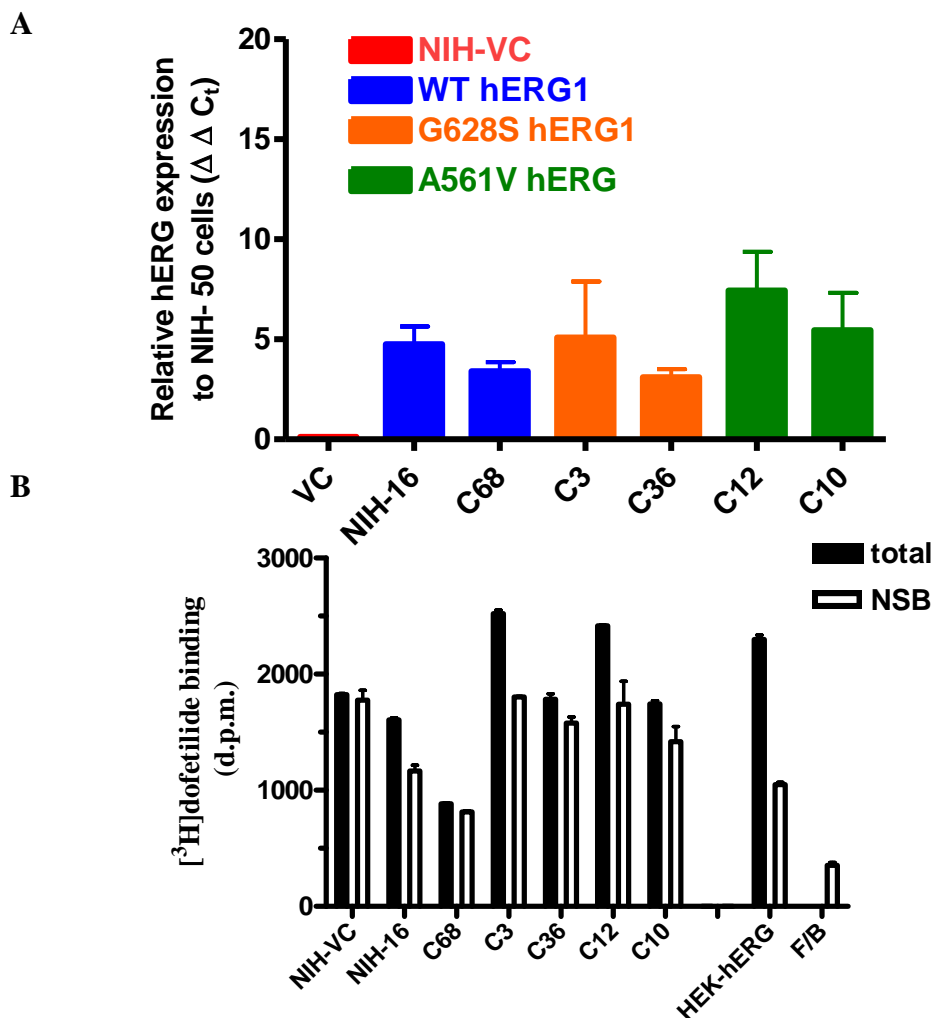


Figure 4.9 Quantification of hERG1 expression by real-time RT PCR and [³H]dofetilide binding. **A.** Real-time PCR quantification of hERG1 expression in NIH-3T3 clones. hERG1 gene expression of each clone was quantified relative to NIH-50 cells using the comparative C_T ($\Delta\Delta C_T$) method as described in the main text and Methods Chapter. Data represent means \pm SEM from 3 experiments. **B.** Membrane preparations of NIH-3T3 clones were incubated with [³H]dofetilide for 2 h and then filtered and washed. The bound ligand was determined by scintillation counting (total binding). Non-specific binding (NSB) was determined in the presence of 10 μ M unlabelled dofetilide. Filter blanks (F/B) measure the amount of filter-retained ligand in the absence of cell membranes. HEK-hERG membrane was used as a positive control for hERG1 protein expression. Data shown are from a single representative assay done in duplicate. The assay was repeated three times for each clone.

hERG1 (recognizes residues 1145-1159). HEK-hERG cell lysates were used to characterize these antibodies and optimize the conditions for their use for hERG1 protein detection by Western blotting. hERG1 proteins run as two bands, which correspond to a partially-glycosylated (core-glycosylated), immature protein (MWt 135 kDa) that is likely to be localized to the ER and Golgi apparatus, and a fully glycosylated, mature form (MWt 155 kDa), which is likely to be found at the plasma membrane (Zhou *et al.*, 1998b). As shown in Fig. 4.10A, Western blotting using the rabbit anti-hERG1 antibody at a dilution of 1:1000 (left) or 1:3000 (right) showed a strong band at 135 kDa and a more diffuse immunoreactivity at ~150 kDa in HEK-hERG preparations. No bands were detected at 135 or 155 kDa for WT HEK293 lysates, indicating antibody specificity at the relevant MWts. However, all samples showed immunoreactivity to a non-hERG1 band at MWt ~165 kDa (Fig. 4.10A). To determine the sensitivity of this antibody for hERG1 protein detection, Western blotting was repeated in samples following two-fold serial dilution of the HEK-hERG cell lysate (Fig. 4.10B). Detection of the mature, fully-glycosylated hERG1 protein (155 kDa band) was lost when only 5 μ g protein was loaded and both the core-glycosylated (135 kDa) and mature form (150 kDa) bands were no longer visible when 2.5 μ g protein was loaded, indicating that this antibody is not especially sensitive for detection of low levels of hERG1 protein expression. Using the purified goat antibody (Fig. 4.10C) at a dilution of 1:1000 (left) and 1:3000 (right), only the core-glycosylated form of hERG1 protein was detected in HEK-hERG samples. Although no bands were detected in WT HEK293 cell lysates, this antibody failed to visualize the 150 kDa form of hERG1. The insensitivity of this antibody to recognize the mature, glycosylated form of hERG1 protein might be due to post-translational protein modifications interfering with binding of the antibody to its primary sequence epitope.

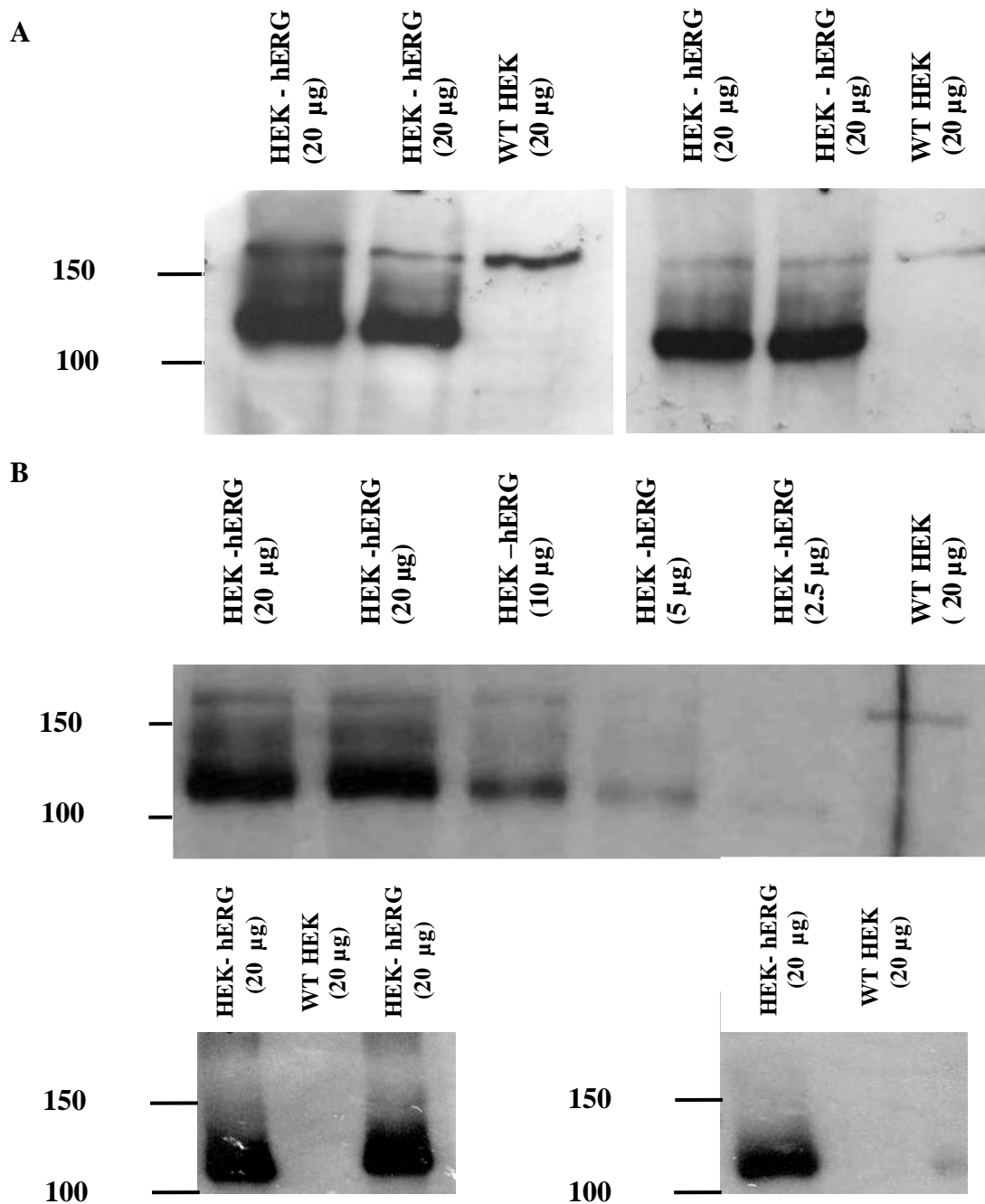


Figure 4.10 Optimization of Western blotting conditions for detection of hERG1 protein expression using anti-hERG1 antibodies. **A**, **C**. Optimization of the concentration of rabbit (**A**) and goat (**C**) anti-hERG1 antibody. 20 µg of HEK-hERG or WT HEK cell proteins were resolved on 6% SDS-PAGE gels and probed with either 1:1000 (left) or 1:3000 (right) anti-hERG1 antibody. **B**. Determination of the sensitivity of rabbit anti-hERG1 antibody for quantitative detection of hERG protein expression. Two-fold serial dilutions of HEK-hERG total cell extracts were probed with 1:1000 rabbit anti-hERG1 antibody.

Given the low sensitivity of these anti-hERG1 antibodies and the low hERG1 expression level of hERG1 proteins in transfected clones, we increased the gel loading to 100 µg protein for each clone sample assayed by Western blotting (Fig. 4.11). Using rabbit-anti-hERG1 antibody (Fig. 4.11A), C3 showed the hERG1 135 and 150 kDa bands, strongly suggesting that these cells expressed the non-conducting mutant G628S hERG1 protein at the cell-surface. Conversely, C12 showed only the immature hERG1 protein band, which is consistent with these cells expressing the trafficking-deficient A561V hERG1 protein, which has previously been shown not to be fully glycosylated and to fail to reach the cell-surface. No bands were detected in NIH-VC cell lysate (100 µg protein), confirming the specificity of the hERG1 protein labelling seen in the samples from transfected clones. hERG1 protein expression in these clones was further supported by Western blotting using the purified goat anti-hERG1 antibody (Fig. 4.11B), using lysates of the hERG1-expressing HEK-hERG and NIH-50 cells as positive controls.

Overall, the combined results from RT-RT PCR, [³H]dofetilide binding and Western blot assays strongly suggest hERG1 expression in C3 and C36 (G628S hERG1) and C12 and C10 (A561V hERG1) clones.

4.2.4 Do G628S hERG1 and A561V hERG1 transfectants exhibit a transformed phenotype?

Clones were characterized for properties of a transformed phenotype. NIH-16 cells, which express WT hERG1, were used as a positive control for hERG1 expression. Moreover, NIH-Ras was also used as a control for oncogene-transformed cells.

Increased cell proliferation and loss of contact inhibition of growth are characteristics of cell transformation (Pardo *et al.*, 1999). To test if stable mutant hERG1 expression

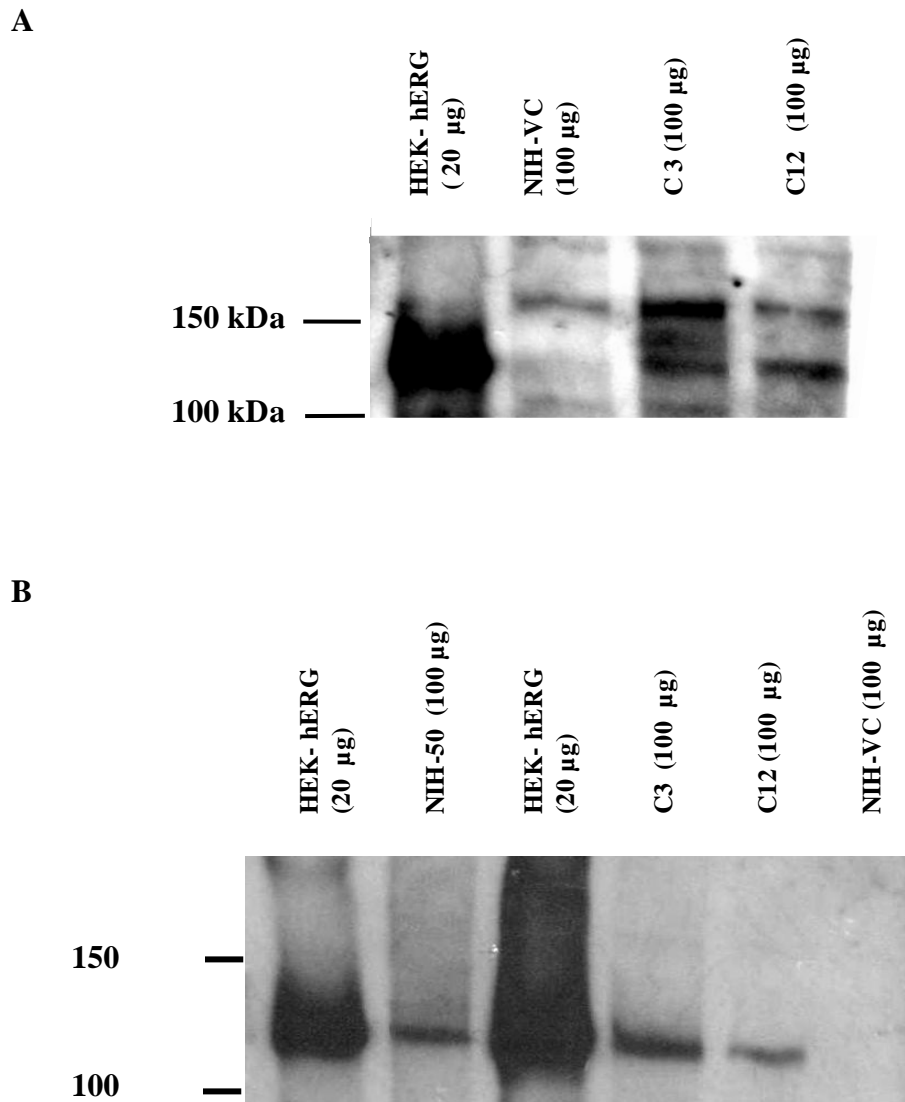


Figure 4.11 Detection of hERG1 protein expression in NIH-3T3 clones. Representative Western blots probed with 1:1000 rabbit (A) or 1:1000 goat (B) anti-hERG1 antibodies.

conferred these properties to NIH-3T3 cells, an MTT cell proliferation assay was used (Mosmann, 1983), which has been used previously to assess the proliferative properties of transformed cells (Pardo *et al.*, 1999).

Initially, the relationship between WT NIH 3T3 cell number and absorbance signal was established (Fig. 4.12A). Data obtained were fitted using a linear regression function ($r^2 = 0.984$), indicating a linear correlation over the range of cell number at plating tested ($0-5 \times 10^5$ cells per 16 mm well). Given that the MTT assay indirectly assesses cell proliferation as a function of metabolic activity and that transformed cells may have higher metabolic rates, it was essential to determine whether stable transfection of NIH-3T3 cells affected their metabolic rates. To do so, the metabolic activities of transfected NIH-3T3 clones, measured by MTT assay, were evaluated. The MTT assay was performed on a fixed cell number (2×10^5 per 16 mm well) of each cell-line and absorbance values compared. For most clones, the absorbance values were not significantly different from WT or vector-control NIH-3T3 cells, however, NIH-Ras cells showed a higher metabolic rate than the other clones (Fig. 4.12B; absorbance at 570 nm: 722 ± 38 ($n=3$) versus 504 ± 24 for NIH-VC; $p < 0.05$). These data indicate that with the notable exception of NIH-Ras cells hERG1-expressing clones had similar capacities to transform MTT to formazan product to NIH-3T3 and NIH-VC cells.

The MTT assay was then used to investigate the proliferation of hERG1-transfected NIH-3T3 cell-lines. Cells were plated at a sub-confluent cell density (0.4×10^5 cells per 16 mm well) and allowed to grow for 8 days. By day 3, all clones had formed a confluent monolayer that covered the culture plate surface and MTT assay at this point indicated similar cell numbers (data not shown). Data from MTT assays performed 4-8 days after

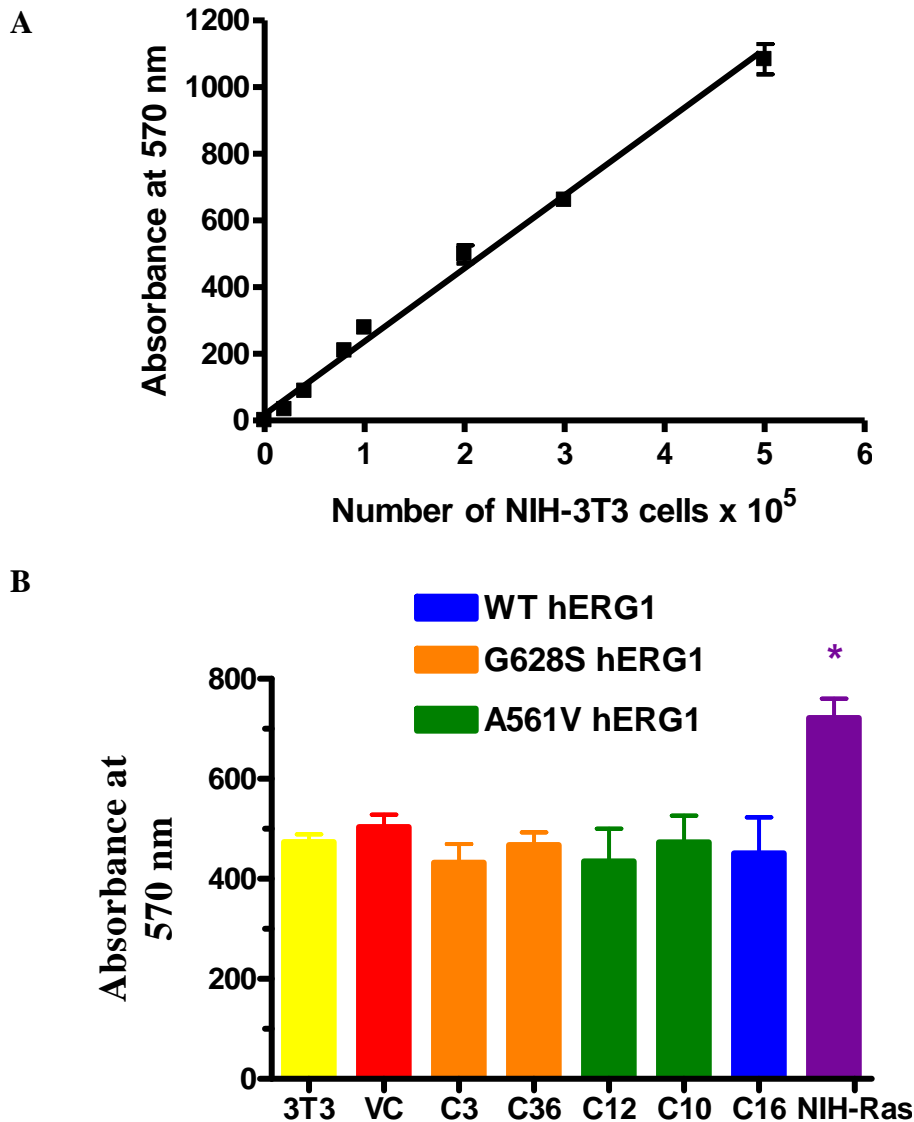


Figure 4.12 Validation of MTT cell proliferation assay. **A.** Different densities (0 - 5 x 10⁵) of WT NIH-3T3 cells were plated in 16 mm wells and allowed to react with MTT (5 mg mL⁻¹) for 2 h. Absorbance values at 570 nm was measured and fitted with a linear regression function ($r^2 = 0.984$). **B.** Evaluation of transfected clone metabolic activity. 2 x 10⁵ cells of each transfected cell clone were incubated with MTT (5 mg mL⁻¹) for 2 h and absorbance was measured. **A, B.** Absorbance values represent means \pm SEM values from at least 3 experiments, each of which is an average of 4 replicate readings. * $p < 0.05$ indicates statistically significant difference results compared to NIH-VC.

initial cell plating (Fig. 4.13A) should indicate the ability of cells to overcome contact inhibition and overgrow each other, a feature of cell transformation that is induced by WT hERG1 transfection (Chapter 3). As expected, MTT absorbance values for NIH-16 at days 5-8 were significantly higher than those of NIH-VC on the corresponding days. In contrast, G628S hERG1- (C3 and C36) and A561V hERG1-transfected clones exhibited insignificantly different MTT absorbance values from NIH-VC ($p > 0.05$). NIH-Ras showed significantly higher values at 4-8 days of growth (Fig. 4.13A).

To confirm the results of this assay and to provide an independent measure of proliferation, viable cells from parallel-performed experiments were counted at day 8 using a cell counter. Viable cell numbers from 3 independent experiments are shown in Fig. 4.13B. For NIH-VC this was $(1.53 \pm 0.04) \times 10^5$ and was not statistically significantly different for the G628S hERG1- and A561V hERG1-expressing clones ($p > 0.05$; $n=3$). The cell count was significantly larger for NIH-16 ($(3.64 \pm 0.25) \times 10^5$; $p < 0.01$) and for NIH-Ras ($(9.30 \pm 0.76) \times 10^5$; $p < 0.01$). In contrast to WT hERG1-expressing NIH-16 cells (Chapter 3, Fig 3.1), inspection of post-confluent cell morphology of G628S hERG1- and A561V hERG1-transfected cells showed that these clones formed a single confluent monolayer with no signs of overgrowth (images not shown). Overall, the data from Figs. 4.12 and 4.13 indicate that cells expressing non-conducting or non-trafficking hERG1 mutants lack the ability to grow over each other, a property induced by WT hERG1 expression.

WT hERG1-transfected cells displayed a change in morphology and an enhanced single-cell migration compared to NIH-VC cells when allowed to adhere to fibronectin-coated surfaces (Chapter 3). However, G628S hERG1- and A561V hERG1-transfected cells showed a similar morphology to NIH-VC cells, displaying the characteristic flattened

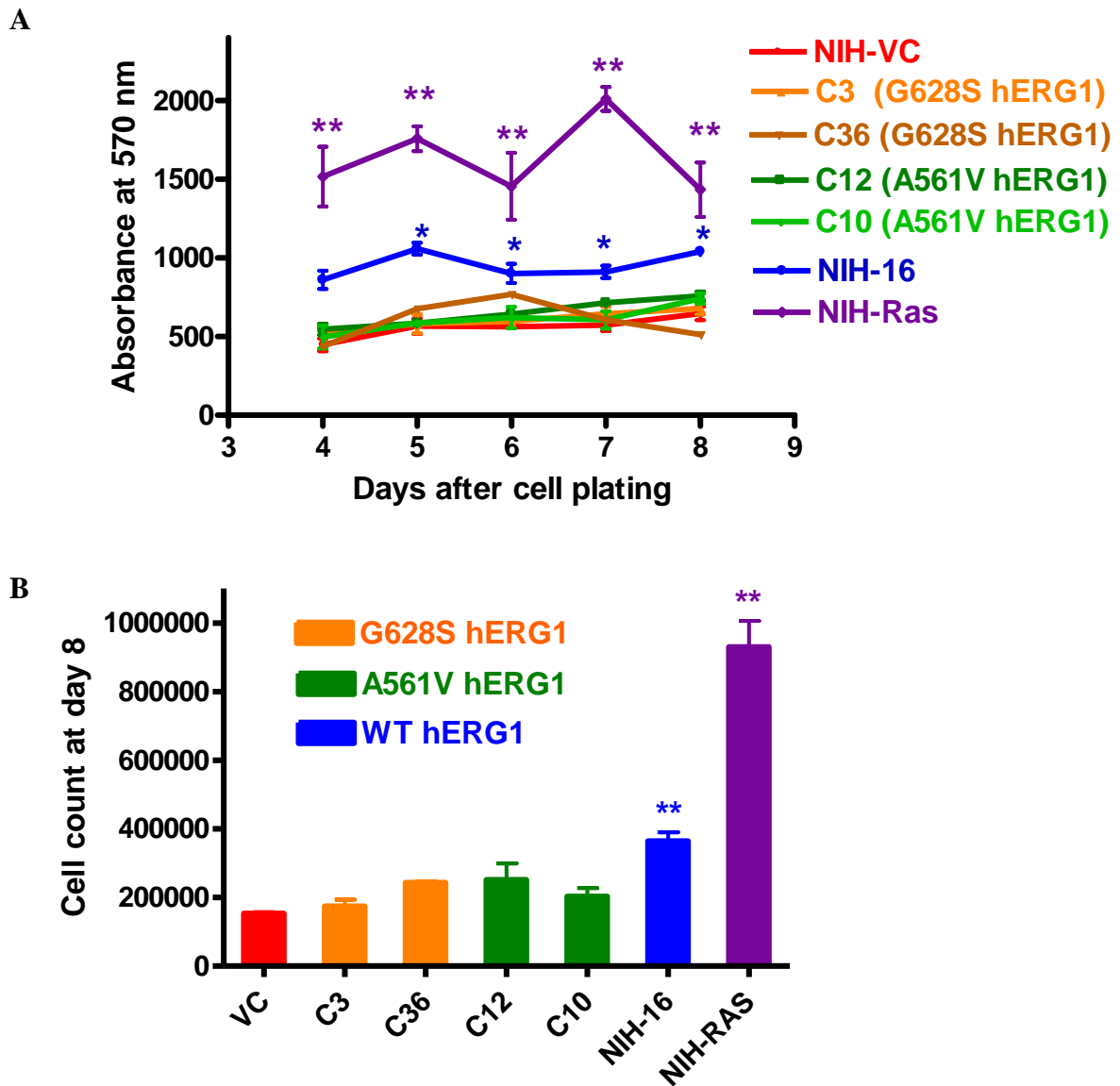


Figure 4.13 Effect of stable expression of functionally-inactive hERG1 mutants on the proliferation of NIH-3T3 cells. **A.** 0.4×10^5 cells of each cell-line were plated in 4 replicate wells of 24-well plates. Absorbance values at 570 nm were measured after 2 h-incubation with MTT (5 mg mL^{-1}) at days 4-8 after plating the cells. **B.** 0.4×10^5 cells of each cell-line were plated in 4 replicate wells of 24-well plates, allowed to grow for 8 days and viable cell numbers were determined. **A, B.** Data represent means \pm SEM values of at least 3 measurements, each of which is an average of 4 replicate readings. Statistically significant values with reference to NIH-VC are shown as $*p < 0.05$; $**p < 0.01$.

morphology of fibroblasts, in contrast to the transformed NIH-16 and NIH-Ras cells, which showed a spindle-shape and polarized cell morphology (Fig. 4.14). The migration speed of G628S hERG1 and A561V hERG1 transfected cells were also not significantly different from NIH-VC cells, whereas NIH-16 cells had higher migration speeds that were comparable to NIH-Ras cells (Fig. 4.15A). For example, after 5 h of attachment to fibronectin, the speed of migration of NIH-VC was $0.36 \pm 0.02 \mu\text{m min}^{-1}$, which was not different to that for each clone (C3, 0.38 ± 0.05 ; C36, 0.35 ± 0.02 ; C12, 0.40 ± 0.02 ; C10, $0.35 \pm 0.01 \mu\text{m min}^{-1}$). Migration speeds for NIH-16 and NIH-Ras were considerably faster (0.54 ± 0.02 and $0.58 \pm 0.01 \mu\text{m min}^{-1}$, respectively; $p < 0.01$).

Similar trends were also observed in wound healing assays (Fig. 4.15B), which measures the speed of collective cell migration. Migration of G628S hERG1-transfected cells caused closure of the wound surface area after 10 h by $31.5 \pm 2.2\%$ ($n=4$) and $29.3 \pm 4.4\%$ ($n=3$) for C3 and C36 clones, respectively. Similarly, A561V hERG1-transfected C12 and C10 cells showed wound reductions of $32.0 \pm 2.0\%$ ($n=3$) and $28.3 \pm 9.5\%$ ($n=3$), respectively. These values are comparable to the percentage closure of wound area seen for NIH-VC cells ($30.9 \pm 4.2\%$; $n=3$). In contrast, NIH-16 and NIH-Ras cells migrated more rapidly causing a decrease of wound surface area by $62.3 \pm 4.0\%$ and $83.5 \pm 2.9\%$ (both $p < 0.01$ relative to NIH-VC, $n=3$), respectively.

Taken together, these results strongly suggest that transfection of functionally-inactive G628S hERG1 and A561V hERG1 does not influence the growth, morphology or migratory behaviours of NIH-3T3 cells. Thus, these data suggest that hERG1 function and/or cell-surface expression of hERG1 is required for the altered properties observed in WT hERG1-expressing cells.

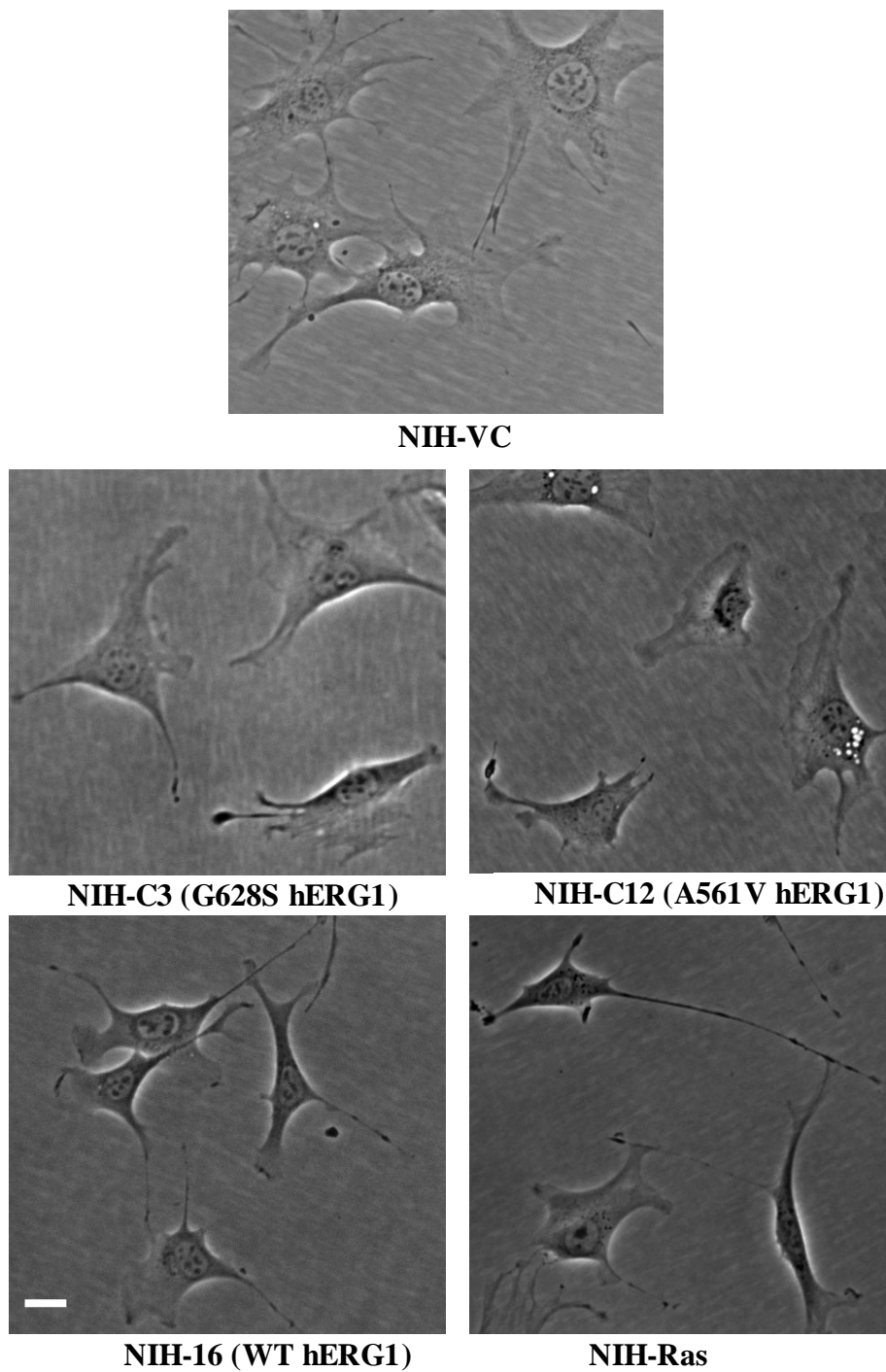


Figure 4.14 Morphology of transfected NIH-3T3 cells on a fibronectin matrix. Images were taken 5 h after plating on fibronectin-coated ($2 \mu\text{g mL}^{-1}$) surfaces. Scale-bar, 20 μm .

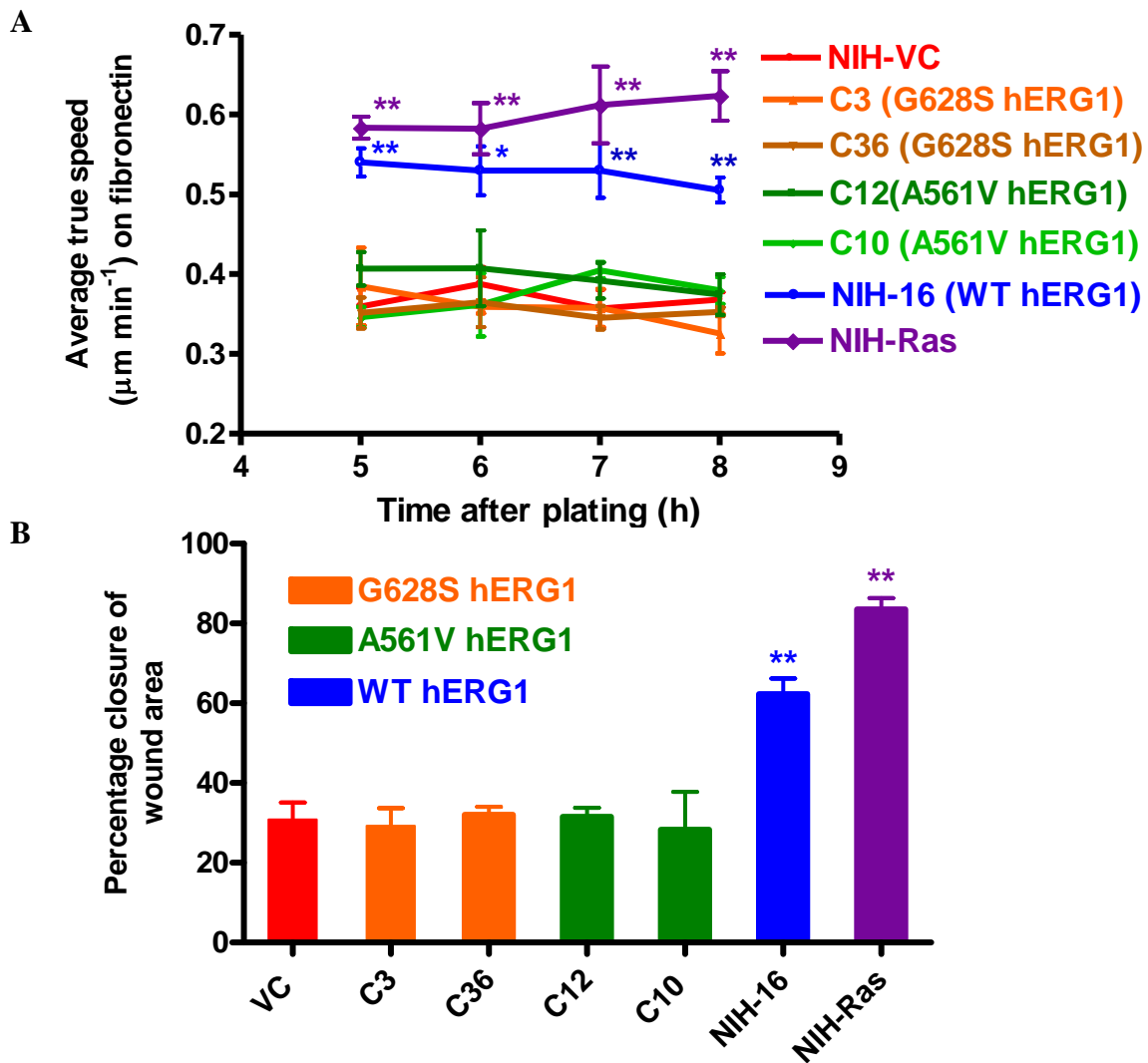


Figure 4.15 Effect of stable expression of non-conducting or trafficking-deficient hERG1 mutants on the migration of NIH-3T3 cells. **A.** Average true speed of NIH-3T3 cell-lines after 5-8 h of plating on fibronectin-coated ($2 \mu\text{g mL}^{-1}$) surfaces. Data represent means \pm SEM of 3 experiments at each time-point. **B.** Wound-healing cell migration experiment. Percentage closure of wound areas were calculated after 10 h. Data represent means \pm SEM of at least 3 experiments performed in duplicate. **A, B:** * $p < 0.05$; ** $p < 0.01$.

4.3 Discussion

In this Chapter, I have attempted to identify potential mechanisms by which WT hERG1 channels contribute to cell transformation. Stable transfection of NIH-3T3 cells with either G628S hERG1, a mutation that eliminates ion permeation, or A561V hERG1, that impairs hERG1 trafficking to the cell-surface, failed to induce a cell-transforming-behaviour in a similar way to cells transfected with WT hERG1. My data suggest that hERG1 channel function and cell-surface expression are required for its oncogenic effect. This finding is consistent with previous studies that showed hERG1-oncogenic effects can be inhibited by selective hERG-channel blockers, albeit at super-saturating concentrations (Pillozzi *et al.*, 2002, Smith *et al.*, 2002a, Lastraioli *et al.*, 2004, Masi *et al.*, 2005, Shao *et al.*, 2005, Pillozzi *et al.*, 2007). The main results of this Chapter are discussed below.

4.3.1 Biological activity of hERG1 channel blockers is not lost under culture conditions

hERG1 blockade by terfenadine and dofetilide was investigated under cell culture conditions used to maintain hERG1-expressing NIH-3T3 cells. hERG1 blockade by dofetilide (100 nM) was unaffected by the presence of serum, or incubation in conditioned medium of NIH-16 cells overnight. Although there was a significant decrease in terfenadine potency after incubation overnight, the change was not large and 3 μ M terfenadine was still able to cause $\geq 70\%$ block of hERG1 current. It is also known that hERG1 blockers are more potent in mammalian versus oocyte expression systems. Thus, previous reports have compared drug blockade of hERG1 currents in different expression systems (Thomas *et al.*, 2001, Thomas *et al.*, 2004, Dupuis *et al.*, 2005, Jo *et al.*, 2008). For example, the α_1 -adrenoceptor antagonists, prazosin, doxazosin, and terazosin, blocked

hERG1 currents in *Xenopus* oocytes with IC₅₀ values of 10, 18 and 113 μ M, respectively; in contrast, IC₅₀ values for hERG1 channel inhibition by these drugs in human HEK293 cells were 1.5, 0.6 and 18 μ M, respectively (Thomas *et al.*, 2004). In addition, 100 μ M propranolol blocked hERG1 channels expressed in HEK293 cells by ~75% relative to only a ~50% blockade in oocytes (Dupuis *et al.*, 2005). The more potent effects of hERG1 blockers on channels expressed in mammalian cells compared to oocytes may be related to the lipophilic nature of the yolk sac in the oocytes that can sequester hydrophobic drugs and hence reduce the actual 'free' concentration of drugs at the cell membrane (Dupuis *et al.*, 2005). Other possibilities include differential glycosylation of hERG1 channel proteins in the different expression systems, or different effects of endogenous proteins (Anantharam *et al.*, 2003). The reported binding of terfenadine to serum proteins (~99% bound), relative to dofetilide (~62% bound), might also account for compound-specific differences in the effect of conditioned culture medium on hERG1-blocking potency (Margulis *et al.*, 2010). Overall, these data show that hERG1 blockers, dofetilide and terfenadine, preserved their hERG1-blocking activity in serum-containing culture medium and after overnight incubation in conditioned culture medium. These results provide evidence that any absence of effect of hERG1 blockers in hERG1-expressing clones is unlikely to be due to a loss of activity of these drugs.

4.3.2 G628S hERG1 and A561V hERG1 exhibit dominant-negative suppression on the WT hERG1 current

A561V hERG1 and G628S hERG1 mutants can exert a dominant-negative suppression of current when these subunits are co-expressed with WT hERG1. The dominant-negative effect of A561V hERG1 on WT hERG1 current has previously been reported (Ficker *et al.*,

2000, Kagan *et al.*, 2000, Li *et al.*, 2007b). A561V hERG1 is a trafficking-deficient mutant that is retained in the ER and hence exists only as in a core-glycosylated 135 kDa form (Ficker *et al.*, 2000). There is controversy over the dominant-negative mechanism of A561V hERG1. It was initially thought that co-assembly of A561V hERG1 with WT hERG1 subunits occurs very early in de novo synthesis resulting in misfolding of assembling tetramers, increasing degradation, leading to a decrease in the full length WT hERG1 protein at the cell-surface (Kagan *et al.*, 2000). However, it has been shown that the trafficking of WT hERG1 is strongly inhibited by co-assembly with A561V hERG1 (Ficker *et al.*, 2000). Although the electrophysiological data showed that a single mutant subunit is most likely sufficient to reduce functional expression, Western blots showed that the reduction in the mature, glycosylated form at the plasma membrane did not parallel the electrophysiological experiments; that is, more hERG1 protein was found to be fully glycosylated than would have been expected from the electrophysiological data. HEK293 cell co-transfected with a 10:1 ratio of WT hERG1 + A561V hERG1 cDNA mixture displayed 54% suppression of hERG1 current, but only a 9% reduction in the fully glycosylated form, while co-transfection of 1:1 ratio produced 90% current reduction and an 80% decrease in the mature form (Ficker *et al.*, 2000). These data might imply that multimeric channel complexes (3 x WT / 1 x A561V hERG1) may still be able to exit the ER, be processed through the Golgi apparatus and reach the plasma membrane. These [3 x WT / 1 x A561V hERG1] channel complexes are probably entirely non-functional or conduct little current (Ficker *et al.*, 2000). This may explain the experimental data reported here, where more current is observed in (WT hERG1 / A561V hERG1)-injected oocytes (approx. 13% of current observed in WT hERG1-injected oocytes). Channel tetramers with two or more mutant subunits are more likely to be retained in the ER (Ficker *et al.*, 2000).

This is also in agreement with data reported by Sanguinetti *et al.* (1996) who showed that co-expression of the A561V mutant with WT hERG1 at a 1:1 ratio in *Xenopus* oocytes resulted in a current that was about 20% of the WT hERG1 current. The same authors suggested that some of the channel complexes that result from co-assembly of A561V hERG1 with WT hERG1 may produce a functional current (Sanguinetti *et al.*, 1996).

WT hERG1 protein is initially synthesized in the ER as ~132 kDa polypeptide, which then undergoes *N*-linked core glycosylation to produce an immature precursor (135 kDa). This precursor is further processed in the Golgi apparatus by addition of complex oligosaccharides to achieve the mature form (~155 kDa). The mature form of hERG1 is then transported to the cell-surface membrane resulting in functional hERG1 channels (Zhou *et al.*, 1998b, Gong *et al.*, 2002). The G628S hERG1 mutation produces a channel protein that is processed similarly to WT hERG1, but fails to produce a functional ion channel. This mutation is within the selectivity filter of the channel pore and disrupts K⁺ ion permeation (Zhou *et al.*, 1998a). Since hERG1 proteins form tetrameric channels, the expression of the G628S hERG1 mutation with WT hERG1 subunits produced a dominant-negative suppression of hERG1 current through to co-assembly. In my experiments, WT hERG1 current decreased to approx. 1/16th when co-expressed with the G628S hERG1 mutant. This is in agreement with Sanguinetti *et al.* (1996) who showed that one mutant subunit per tetrameric channel is sufficient to block conduction. Moreover, the dominant-negative effect of G628S hERG1 on I_{Kr} has also been demonstrated *in vivo* in transgenic mice (Babij *et al.*, 1998).

4.3.3 Differences between hERG1 mRNA and protein levels in screened clones

Screening of transfected NIH-3T3 clones for hERG1 expression revealed differences between levels of hERG1 mRNAs detected by real-time RT PCR and hERG1 protein levels detected by [³H]dofetilide binding assay. Several studies have shown that mRNA levels do not necessarily reflect the amount of protein produced by the cell (Anderson *et al.*, 1997, Gygi *et al.*, 1999, Greenbaum *et al.*, 2003). The level of protein expression is determined by several factors, including mRNA stability, transcription levels, post-transcriptional and post-translational modifications and protein turnover (Greenbaum *et al.*, 2003). Quality control mechanisms ensure that any misfolded or incompletely assembled hERG1 protein is retained in the ER to be targeted towards proteasomal degradation. Moreover, *N*-linked glycosylation, a post-translational processing of hERG1 protein, has been shown to increase hERG1 stability and decrease channel turnover (Gong *et al.*, 2002).

4.3.4 The link between hERG1 channel conduction and transformation

Our findings are in agreement with previous studies investigating mechanisms of transformation of other K⁺ channels. Over-expression of WT TASK3 in mouse embryonic fibroblasts induces oncogenic behaviour consisting of an increased cell proliferation in low serum, resistance to TNF-induced apoptosis and tumour formation when TASK3-expressing cells are injected into nude mice (Mu *et al.*, 2003). None of these properties was observed in cells over-expressing the dominant-negative, non-conducting mutant G95E TASK3 (Pei *et al.*, 2003). Moreover, co-expression of G95E TASK3 in WT TASK3 co-transfected cells abolished the tumour-promoting activity of these cells (Pei *et al.*, 2003).

Although it remains controversial, the oncogenic potential of EAG channels appears to be, at least partly, dependent on K⁺ permeation. Treatment of animals with a monoclonal

antibody that specifically blocks EAG current by ~40% is able to inhibit *in vivo* tumour growth by 30-40 % (Gomez-Varela *et al.*, 2007). Likewise, oral administration of the EAG blocker, astemizole, reduces *in vivo* tumour growth induced by subcutaneous implantation of EAG-expressing CHO cells in immuno-deficient mice, although it caused no inhibition of growth of smaller tumours induced by subcutaneous injection of WT CHO cells (Downie *et al.*, 2008). Moreover, implantation of NIH-3T3 and CHO cells stably expressing G440S EAG, a mutation in the signature sequence of the pore region that abolishes ion permeation, produced tumours of smaller size than WT EAG-induced tumours (Downie *et al.*, 2008), suggesting that ion permeation is important, but not an absolute requirement, for the oncogenic properties of EAG.

As discussed in Chapter 1, K⁺ channels may contribute to tumour cell progression via their abilities to regulate cell volume, membrane potential and voltage-dependent processes (e.g. Ca²⁺ influx and Na⁺-dependent membrane transport). hERG1 channels have been shown to be involved in volume regulation of MCF-7 cancer cells (Roy *et al.*, 2008), since E-4031 inhibited the ability of these cells to undergo a regulatory volume decrease after an initial swelling response. Cell volume regulation has also been suggested to be important for cell cycle progression (Rouzaine-Dubois *et al.*, 1998, Rouzaine-Dubois *et al.*, 2004) and cell migration (Schwab *et al.*, 1999b, Pedersen *et al.*, 2001). hERG1 channel conduction might indirectly influence many signalling and homeostatic processes by modulating membrane potential. hERG1 channels have been shown to contribute to the resting membrane potential of many tumour cell-lines (Bianchi *et al.*, 1998), which is reported to be relatively depolarized in tumour cells (Binggeli *et al.*, 1980) and may be important for cell DNA synthesis and cell proliferation. K⁺ efflux through hERG1 channels hyperpolarizes the cell.

However, hERG1 channels display a rapid, hyperpolarization-dependent inactivation and thus produce only a limited hyperpolarizing effect compared with other inwardly-rectifying K^+ channels, which helps maintain the depolarized membrane potential seen in tumour cells (Arcangeli *et al.*, 1995). This relatively depolarized membrane potential may allow Ca^{2+} entry through voltage-dependent channels (Wonderlin *et al.*, 1996). The role of intracellular Ca^{2+} in tumour cell signalling is well-established. $[Ca^{2+}]_i$ levels contribute to the control of cell cycle checkpoints and regulate other processes such as cell motility (Patel *et al.*, 1999). However, ‘clamping’ the membrane potential of tumour cells to a depolarized potential by hERG1 channels is an over-simplified hypothesis. Several reports showed that oscillations in membrane potential of tumour cells occur during cell cycle progression (Blackiston *et al.*, 2009). It may be possible that transient hyperpolarization currents carried by hERG1 channels play roles in tumour cell progression by increasing the driving force for Ca^{2+} entry (Nilius *et al.*, 1993), or by enhancing Na^+ -dependent transport of metabolic substrates across the membrane (Mummery *et al.*, 1982). It has been hypothesized that a transient hyperpolarization may be enough to cause G1 progression if it produces a threshold shift in membrane potential regardless of the final value of membrane voltage (Wonderlin *et al.*, 1996).

It remains to be determined why only certain K^+ channels can induce cell transformation or affect the behaviour of tumour cells. If oncogenic effects are merely dependent on modulating membrane potential, it should be expected that over-expression of many different types of K^+ channel would induce cell transformation. This is certainly not the case. Over-expression of either EAG or $K_v1.4$ in CHO cells alters the resting membrane potential, but only EAG is capable of inducing a transformed phenotype (Pardo *et al.*,

1999), indicating that tumorigenesis is K⁺ channel type-specific and does not depend on increased transmembrane K⁺ conductance *per se*. A possible explanation for this conundrum is that oncogenic K⁺ channels might be regulated by endogenous signalling pathways to produce only a transient shift of membrane potential synchronized to (or coupled to) certain cellular events, such as bypassing G1 phase during tumour cell proliferation, or transiently affecting Ca²⁺-influx in migrating cancer cells. There is some experimental support for this hypothesis: regulation of expression and activity of EAG (Bruggemann *et al.*, 1997, Meyer *et al.*, 1998, Pardo *et al.*, 1998, Camacho *et al.*, 2000, Gavrilova-Ruch *et al.*, 2002) and hERG1 (Arcangeli *et al.*, 1995, Crociani *et al.*, 2003) channels by the cell cycle has been reported. Moreover, adhesion of hERG1-expressing cells to extracellular matrix, which influences several cellular processes including cell migration, causes a short-term hERG1 current activation and membrane hyperpolarization (Arcangeli *et al.*, 1993, Arcangeli *et al.*, 1996, Cherubini *et al.*, 2005). Modulation of EAG currents by cytoskeletal interaction (Camacho *et al.*, 2000) and extracellular matrix adhesion (Torralba *et al.*, 2007) has also been reported. These findings are an indication of regulation of channel activity that might be important for their oncogenic roles.

The results presented in this Chapter do not eliminate the possibility that hERG1 can directly influence tumour cell signalling. Cancer development is a complicated process that involves the accumulation of gene mutations producing continuous changes in the intracellular milieu (Hanahan *et al.*, 2000). Given the fact that intracellular signalling pathways usually have several possible roles, the final signalling outcome at any tumour developmental stage will depend on cell context and crosstalk between signalling pathways. Therefore, although hERG1 ion function might be required to initiate

oncogenesis, it might also be possible that hERG1 could directly affect cancer cell signalling at later stages of malignant transformation, particularly angiogenesis, invasion and metastasis. In fact, hERG1 has been shown to associate with many tumorigenesis-related proteins, including β 1-integrin, TNF α , FAK, Rac1 and Src (Cayabyab *et al.*, 2002, Wang *et al.*, 2002a, Cherubini *et al.*, 2005, Pillozzi *et al.*, 2007). Interestingly, channel gating may play a role in its signalling activity through a voltage-dependent conformational coupling or enzymatic activity. For example, the phosphatidylinositol phosphatase activity of Ci-VSP, a member of the PTEN family, is voltage-dependent (Iwasaki *et al.*, 2008). EAG-induced proliferation has also been suggested to be membrane potential-sensitive and channel conformation-dependent. Transfection of NIH-3T3 cells with ^{F456A}EAG, a mutation in the EAG selectivity filter that abolishes EAG current, increases proliferation to a similar extent to WT EAG, whereas mutations that increase the probability of EAG channels being in an open conformation at resting potential inhibits EAG-mediated cell proliferation, even when the pore is non-conducting (Hegle *et al.*, 2006). hERG1 expression has different effects on cell function to EAG, suggesting different signalling pathways for mediating these effects. A direct measurement of gating currents from G628S hERG1 has not been yet reported, however, it is likely that G628S hERG1 is voltage-sensitive and responds to membrane depolarization indistinguishably to WT hERG1 channels. Future investigations are required to elucidate if the voltage-dependence of hERG1 and its state-dependent conformation(s) are determinants of hERG1-mediated effects on cell phenotype.

4.3.5 Why are high concentrations of hERG1 inhibitors required to block cell transformation?

The reason(s) for the requirement to use many-fold higher concentrations of hERG1 channel inhibitors to impair hERG1-mediated oncogenic effects compared to those needed to inhibit hERG1 channel function have yet to be established. WAY-123,398 at 40 μM was required to reduce proliferation of leukemic FLG 29.1 cells (Pillozzi *et al.*, 2002), or to impair the migration of colon cancer cells (Lastraioli *et al.*, 2004), although 1 μM WAY-123,398 was able to inhibit completely hERG1 currents in the both cancer cell-types. E-4031 (1 μM), which abolished hERG1 current in leukemic K562 cells, reduced the proliferation of these cells by <20% (Smith *et al.*, 2002a). Investigators have justified this apparent paradox on the basis of differences in experimental conditions used in cell proliferation, migration and invasion assays and those used for electrophysiological recordings of hERG1 current.

Serum might interfere with the mechanisms by which ion channel blockers influence tumour cell proliferation or migration. In agreement with this, serum inhibited the anti-proliferative effect of charybydotoxin (ChTx) on blood mononuclear cells without affecting its K^+ channel blocking activity, an effect which might be attributed to serum interference in the ability of ChTx to inhibit interleukin-2 release (Price *et al.*, 1989, Freedman *et al.*, 1992). Moreover, most hERG1 blockers used in previous studies are open channel blockers and therefore exhibit a voltage-dependent block, which necessitates that inhibition of hERG1 currents is measured at normal resting membrane potential of hERG1-expressing tumour cells. The IC_{50} for inhibition of EAG current by imipramine measured at -30 mV, a

typical resting voltage of melanoma cells, was 5-fold higher than the corresponding IC_{50} at +50 mV (Gavrilova-Ruch *et al.*, 2002).

If hERG1-mediated effects occur via transient changes of membrane potential that take place at certain time-points in tumour cell progression, then acute application of hERG1 blockers might only affect the population of cells undergoing transient hERG1 activation and higher drug concentrations might be needed to produce a longer-term hERG1-inhibition. This may also be explained in the pharmacological context of “spare receptor” theory (Ruffolo, 1982), whereby the concentration of an antagonist required to inhibit a certain response will be higher than its affinity for the receptor if sub-maximal occupancy of the receptor can produce a maximal functional effect. Some tumour cells over-express hERG1 channels. If the oncogenic effects of hERG1 channels are dependent on its ion conduction and the resulting membrane hyperpolarization, this may require, depending on resting membrane potential of tumour cells and the required voltage change to elicit a cellular effect, that only a fraction of the expressed hERG1 channels open to produce the necessary hyperpolarizing threshold, while other channels represent a “spare” channel reserve. Accordingly, higher concentrations of hERG1 blockers will be required to inhibit a majority of available hERG1 channels in order to interfere with hERG1-mediated oncogenic effects.

In summary, results in this Chapter suggest that the transforming potential of hERG1 is dependent on its primary function as an ion-conducting channel.

Chapter 5

Does transient transfection of hERG1 and the splice-variant hERG1b induce cellular transformation?

5.1 Introduction

Several splice-variants of hERG1 have been described (London *et al.*, 1997, Kupershmidt *et al.*, 1998, Guasti *et al.*, 2008, Huffaker *et al.*, 2009). Among these, hERG1b lacks most of the *N*-terminus (residues 2-376) relative to hERG1 and has instead a unique 36-residue *N*-terminus that is encoded by a specific exon not present in hERG1, suggesting that it is an alternative transcript (see Chapter 1, Fig. 1.5). The *N*-terminus is known to be important for the slow deactivation properties of hERG1 (Schonherr *et al.*, 1996, Morais Cabral *et al.*, 1998, Wang *et al.*, 1998, Muskett *et al.*, 2010), therefore, it is not surprising that currents elicited by the hERG1b isoform have faster deactivation kinetics (Lees-Miller *et al.*, 1997, London *et al.*, 1997, Larsen *et al.*, 2008). hERG1b is expressed in the heart (Jones *et al.*, 2004) and appears to contribute to the cardiac I_{Kr} current through co-assembly with hERG1 (Jones *et al.*, 2004, Larsen *et al.*, 2008, Larsen *et al.*, 2010). Thus, it might provide an explanation of the difference in gating properties of I_{Kr} compared to hERG1 currents.

hERG1b is expressed in primary acute myeloid leukaemia (AML) and some cancer cell-lines, including neuroblastoma SH-SY5Y and leukaemic FLG 29.1 and K562 cells (Pillozzi *et al.*, 2002, Crociani *et al.*, 2003, Pillozzi *et al.*, 2007). Interestingly, the extent of hERG1b expression is both tumour-specific and cell cycle-dependent. Moreover, hERG1 and hERG1b co-assemble at the cell membrane of tumour cells (Crociani *et al.*, 2003, Cavarra *et al.*, 2007). In addition to having altered gating kinetics, hERG1b-containing channels are

also differentially regulated by intracellular cues, including cyclic GMP, thyrotropin-releasing hormone (TRH) and cell acidosis (Kirchberger *et al.*, 2006, Mewe *et al.*, 2010, Du *et al.*, 2011). However, the role of hERG1b in tumorigenesis has not been fully explored. Does hERG1b play a role in oncogenesis? Does it regulate hERG1 properties and thus facilitate hERG1-oncogenic effects?

To address these questions, I investigated the effect of hERG1b expression on cell properties. Initially, I designed and generated a bicistronic plasmid that allows co-expression of both hERG1 and hERG1b isoforms from a single mRNA. This decreases cell-to-cell variability, which can be associated with co-transfection of hERG1b and hERG1 cDNAs (Larsen *et al.*, 2008). Moreover, such a plasmid ensured the same stoichiometric ratio of subunits, which in turn determines the subunit composition of cell-surface hERG channels and the biophysical properties of the hERG current. A further aim was to investigate whether the oncogenic properties of hERG1 occurred with short-term, transient expression. Up to now I have always used stable cell-lines, but this is time-consuming and challenging. Transient transfection has been used previously to investigate the oncogenic mechanisms of EAG K⁺ channels (Hegle *et al.*, 2006, Downie *et al.*, 2008). Therefore, the transient transfection approach has been utilized to investigate the effect of expression of hERG1, hERG1b and hERG1/hERG1b co-expression on cell migration and proliferation. One disadvantage of transient transfection is that only a proportion of the cells take up and express the plasmid(s). This is problematic when interpreting the results of multicellular studies. To mitigate against this we co-transfected cells with enhanced green fluorescent protein (eGFP) vectors and used this to sort and enrich cells most likely

to be expressing the plasmid(s) of interest. This approach has been routinely used to identify cells expressing ion channels in electrophysiological studies.

In this Chapter, the generation and characterization of bicistronic vectors that allow co-expression of hERG1 and hERG1b isoforms are described and the effects of both hERG isoforms on cell migratory and proliferative properties studied.

5.2 Methods

5.2.1 Generation of bicistronic cDNA constructs encoding hERG1 and hERG1b

Molecular biological techniques were used to create two cDNA constructs for dual expression of hERG1 and hERG1b in mammalian cells. These approaches involved generating an intermediate vector, which contained hERG1b, preceded by an internal ribosome entry site (IRES), or a cytomegalovirus (CMV) promoter. The nucleotide sequences encoding pIRES-hERG1b and pCMV-hERG1b were excised from the corresponding intermediate vectors and sub-cloned into a pcDNA3 expression vector containing hERG1. This generated two expression vectors containing either hERG1-pIRES-hERG1b (referred to here as C1) or hERG1-pCMV-hERG1b (C2) cloned to pcDNA3. A brief description of the protocols used for generation of these constructs is given below.

5.2.1.1 Site-directed mutagenesis for correction of a point-mutation in hERG1b-pcDNA3

hERG1b complementary DNA (cDNA) (Crociani *et al.*, 2003) in pcDNA3 (Fig. 5.1A) was a generous gift from Prof. Annarosa Arcangeli (University of Firenze, Italy). Sequencing of the hERG1b gene revealed a point-mutation (T793A) in the protein C-terminus. It was essential to correct this mutation before performing any cloning steps. This was achieved through site-directed mutagenesis using the Stratagene QuikChange[®] mutagenesis kit (Stratagene, USA). Forward (CAAGAAGGCCCCACCACGACGCCTCTC) and reverse (GAGAGGCGTCGTGTGTGGGGCCTTCTTG) primers containing the desired mutation (in bold and underlined) were 26 bases long, with melting temperature of 71.1°C and 65.4%

GC content. Primers were extended by a PCR amplification of hERG1b-pcDNA3 to generate a mutated plasmid containing staggered nicks. The restriction enzyme *DpnI* was added to the PCR reaction to digest parental template DNA. The remaining mutation-containing plasmid was then transformed into competent cells. The PCR reaction, *DpnI* digestion and bacterial transformation were performed as described in the earlier Methods Chapter.

5.2.1.2 Generation of the hERG1- pIRES- hERG1b (C1) cDNA construct

pIRES-eGFP (Clontech, USA) is a mammalian expression vector that allows the concurrent expression of eGFP and a gene of interest from a single bicistronic mRNA transcript. This vector contains an encephalomyocarditis virus (ECMV) internal ribosome entry site (IRES) flanked by a multiple cloning site (used for gene cloning) and the eGFP-coding region. The IRES segment drives the translation of the downstream eGFP-coding region independently of the cap-dependent initiation of translation of the 5'-end of the mRNA molecule and thus both proteins can be produced in the cell. However, the IRES sequence in eGFP-pIRES vector is partially disabled, which decreases the expression of the gene located downstream of the IRES (eGFP) relative to that located upstream (gene of interest) (Jang *et al.*, 1988, Rees *et al.*, 1996). A strategy was designed to insert the IRES sequence between the open reading frames of hERG1 and hERG1b to allow their concurrent expression. However, an equal (or nearly equal) expression of hERG1 and hERG1b in mammalian cells was desired. The IRES sequence in the pIRES-eGFP vector (kindly provided by Dr. D. Lodwick, Cardiovascular Sciences, University of Leicester) was manipulated to restore its activity and allow an equal expression of both genes. Four PCR primers were designed to amplify the coding region of IRES and the 5'-end of hERG1b from pIRES-eGFP and hERG1b-

pcDNA3 cDNAs. Two primers, IRSB1 (5'-TCAGTCGGATCCGCCCTCTCCCT-3') and IRSB-2 (5'-TGGGGCCGCCATATTATCATCGTGTTTTTCAAAGGA-3') flank the coding region of IRES, with IRSB-2 containing an overhang complementary to the 5'-end of hERG1b. IRSB-3 (5'-CACGATGATAATATGGCGGCCCCAGCCG-3') binds to the 5' start of hERG1b coding sequence and contains an overhang sequence that is complementary to the 3'-end of IRES, whereas IRSB4 (5'-CGAGTACAGCCGCTGGATG-3') is located within hERG1b and contains a unique *Nhe*-I restriction site. PCR amplification of pIRES-eGFP cDNA using IRSB-1 and IRSB-2 primers yielded a 599 bp product (see Fig. 5.1Ci), corresponding to the IRES sequence and the 5'-end (24 bp) of hERG1b. Amplification of hERG1b-pcDNA3 using IRSB-3 and IRSB-4 primers produced 1 kb product (see Fig. 5.1Cii), which corresponds to the 5' region of hERG1b and includes an overlap region with the first IRES PCR product. The two PCR products were combined with IRSB-1 and IRSB-4 primers in a PCR reaction to generate 1.6 kb product (Fig. 5.1Ciii) by overlap extension PCR amplification. The resulting overlap PCR product was further amplified by repeating the PCR reaction several times, purified from an agarose gel and digested with *Bam*HI/*Nhe*I restriction enzymes (NEB, USA). The final purified product of 1518 bp was ligated into hERG1b-pcDNA3 that was pre-digested with *Bam*HI/*Nhe*I restriction enzymes to produce an intermediate vector pIRES-hERG1b-pcDNA3 (Fig. 5.1D). Finally, the pIRES-hERG1b-pcDNA3 plasmid was digested with *Bam*HI/*Xba*I restriction enzymes to excise a 3 kb fragment, corresponding to IRES-hERG1b, which was sub-cloned into the hERG1-pcDNA3 vector (Fig. 5.1E) at *Bam*HI and *Xba*I restriction sites, producing hERG1-pIRES-hERG1b (Fig. 5.1F). Recombinants were amplified by transformation into competent bacteria and checked by restriction digestion and sequencing using appropriate sequencing primers.

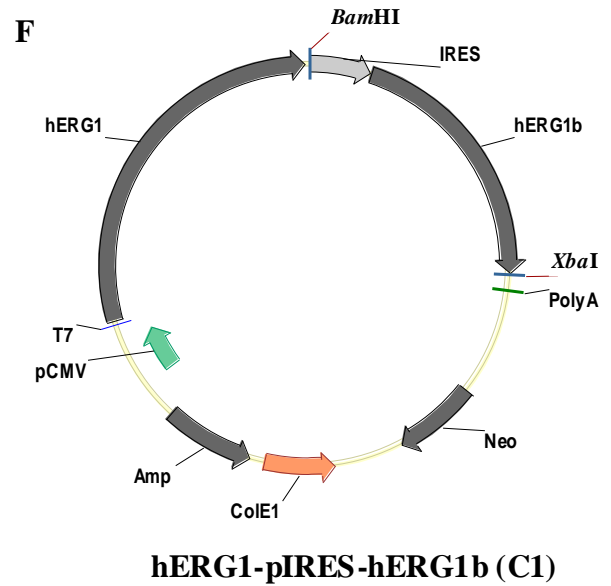
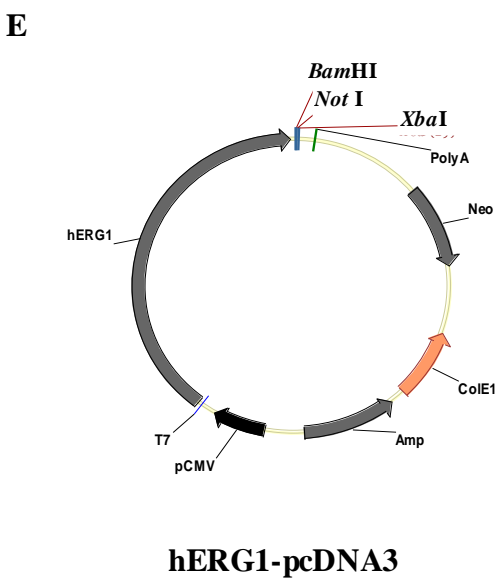
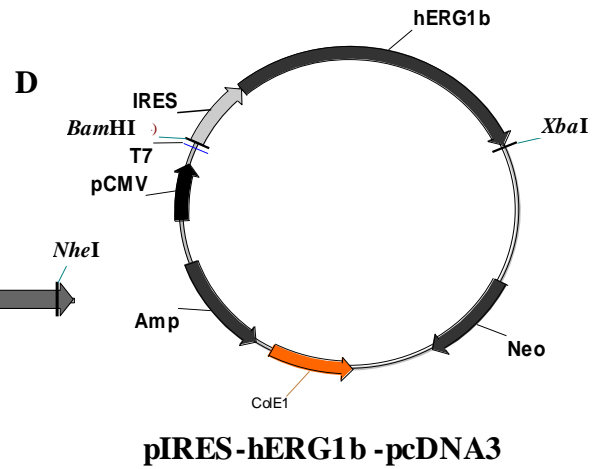
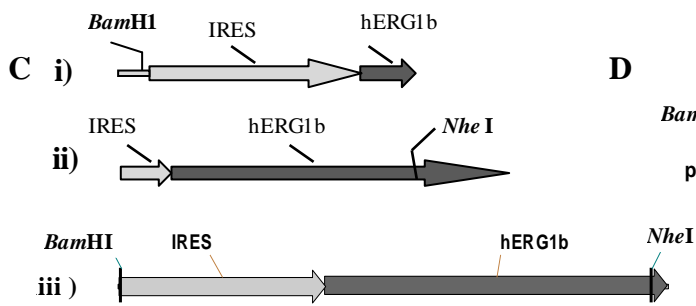
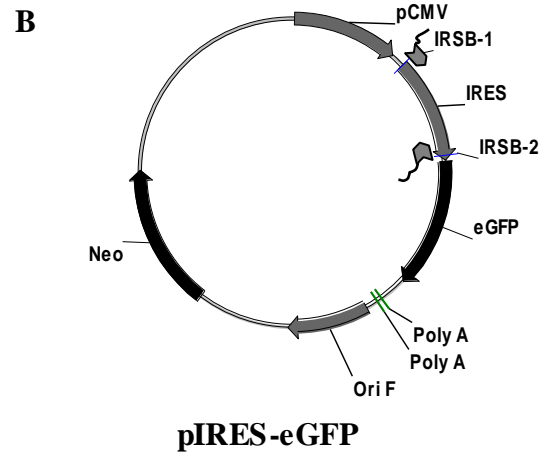
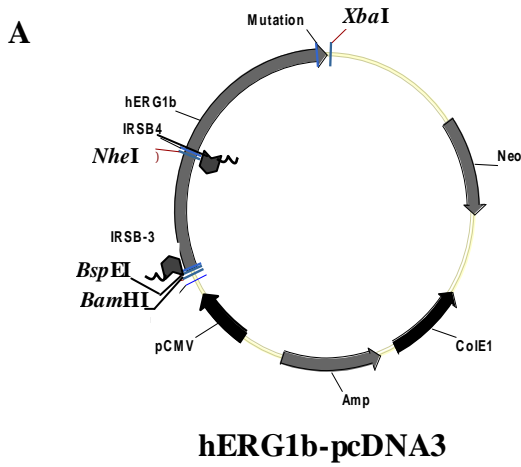


Figure 5.1 Diagrammatic overview of cloning events for generation of hERG1-pIRES-hERG1b (C1) construct. **A.** Map of hERG1b-pcDNA3. Sequencing revealed a point mutation (labelled on 3' end), which was corrected by site-directed mutagenesis (see Chapter 5, Methods). Binding sites for IRSB-3 and IRSB-4 PCR primers and restriction sites for *Bam*H1, *Nhe*-I, *Xba*-I and *Bsp*E1 enzymes are indicated. **B.** Map of pIRES-eGFP expression vector. The vector has an internal ribosome entry site (IRES) flanked by a 5' multiple cloning site and a 3' eGFP-coding sequence. Binding sites for IRSB-1 and IRSB-2 PCR primers are indicated. **C. i)** A PCR fragment (599 bp) was amplified from pIRES-EGFP using IRSB1 and IRSB2 primers. **ii)** A PCR fragment (996 bp) was amplified from hERG1b-pcDNA3 using IRSB3 and IRSB4 primers. **iii)** An overlap PCR product (1572 bp) was generated by an overlap extension PCR reaction using DNA fragments (shown in **Ci** and **Cii**) and IRSB1 and IRSB4 primers. **D.** Structure of the recombinant plasmid pIRES-hERG1b-pcDNA. The overlap PCR product (shown in **Ciii**) was digested with *Nhe*I and *Bam*H1 enzymes and ligated into hERG1b-pcDNA3 (shown in **A**), generating an intermediate recombinant pIRES-hERG1b-pcDNA. **E.** Map of hERG1-pcDNA3 DNA. Restriction sites for *Bam*H1, *Xba*I and *Not*I enzymes are indicated. **F.** Schematic representation of hERG1-pIRES-hERG1b (C1). hERG1b-pIRES-pcDNA (shown in **D**) was digested with *Xba*I and *Bam*H1 enzymes to excise the coding sequence for IRES-hERG1b, which was ligated into hERG1-pcDNA3 (shown in **E**), producing hERG1-IRES-hERG1b. hERG1 and hERG1b sequences are indicated. The IRES sequence enables the two genes to be expressed simultaneously, where a CMV promoter drives the translation of the two open reading frames from a single bicistronic mRNA transcript. The vector also contains ampicillin (Amp^r) and neomycin (Neo^r) resistance genes, which allow the use of for ampicillin and G418 for prokaryotic and eukaryotic selection, respectively.

5.2.1.3 Generation of the hERG1-pCMV-hERG1b (C2) cDNA construct

An alternative approach for simultaneous expression of both hERG1 and hERG1b in mammalian cells was to design a plasmid that expresses both genes from separate, but identical CMV promoters (the immediate/early promoter enhancer of cytomegalovirus). The CMV promoter is widely used for driving gene expression in mammalian cells, including NIH-3T3 cells (Mattingly *et al.*, 1994, Tu *et al.*, 2006), due its strong promoter activity. The choice of identical promoters was to minimize variations in cellular expression of the two genes.

Briefly, a pAd Track-CMV plasmid (Fig. 5.2A), kindly donated by Dr. D. Lodwick (Cardiovascular Sciences, University of Leicester), was digested with *Bgl*III and *Age*I restriction enzymes to excise a 974 bp fragment, which includes pCMV. This fragment was sub-cloned into hERG1b-pcDNA3 (Fig. 5.1A) at *Bam*HI and *Bsp*E1 restriction sites, producing an intermediate plasmid, pCMV-hERG1b-pcDNA3 (Fig. 5.2B). This intermediate plasmid was then digested with *Not*I to excise the pCMV-hERG1b fragment, which was gel-purified and re-inserted into hERG1-pcDNA3 (Fig. 5.1E) to generate hERG1-pCMV-hERG1b (C2; Fig. 5.2C), a construct that places both hERG1 and hERG1b sequences under the transcriptional control of CMV promoters. After transformation into competent bacteria, clones were selected and amplified and hERG1-pCMV-hERG1b recombinants (Fig. 5.2C) selected based on restriction digestion (to check for correct cloning and orientation of inserted fragment) and DNA sequencing.

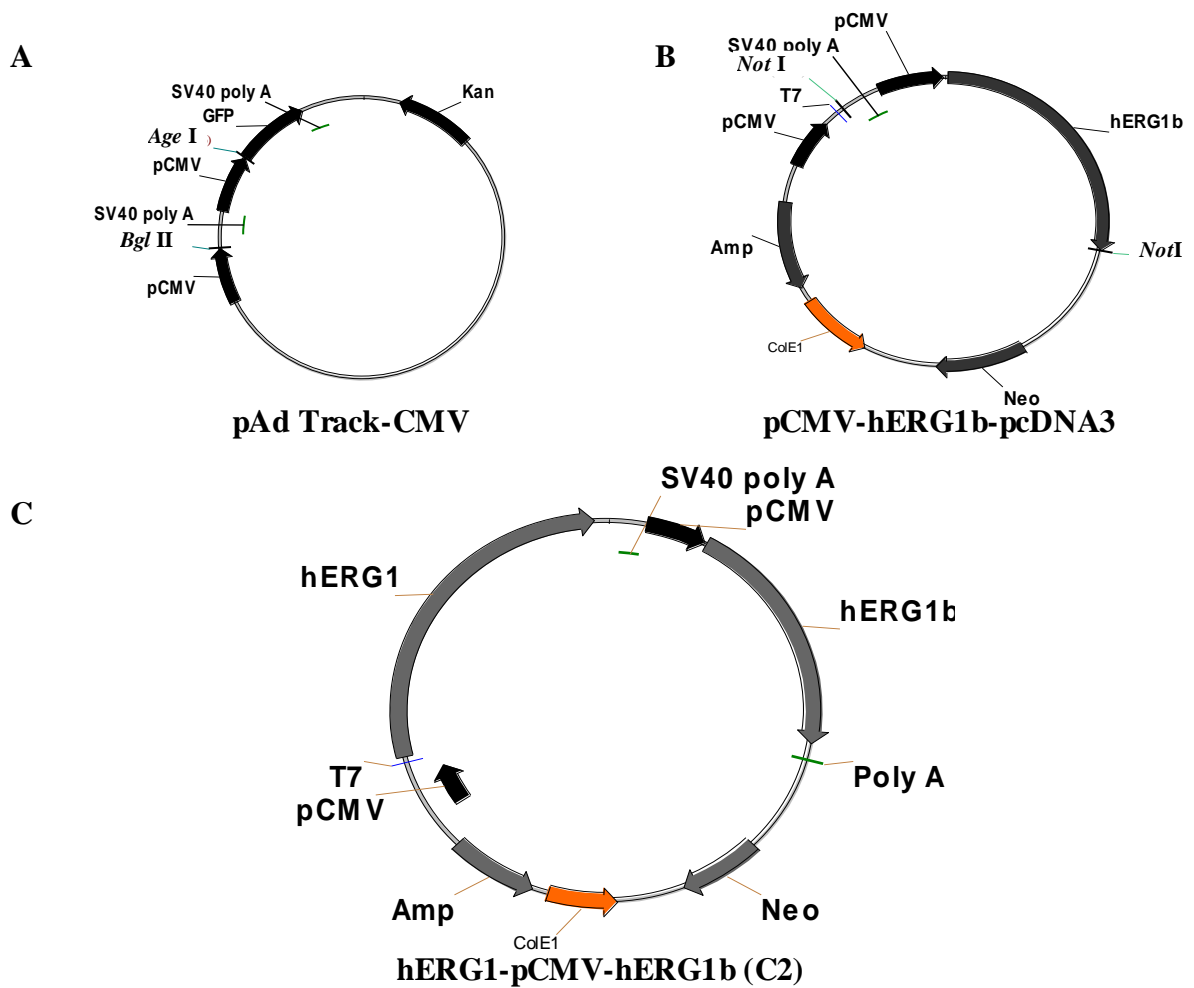


Figure 5.2 Diagrammatic overview of cloning events for generation of hERG1-pCMV-hERG1b (C2) DNA construct. **A.** Map of pAd Track-CMV plasmid. Restriction sites for *AgeI* and *Bgl*-II enzymes are indicated. **B.** Structure of the recombinant pCMV-hERG1b-pcDNA3. pAd Track-CMV plasmid (shown in **A**) was digested with *AgeI* and *Bgl*-II enzymes to excise the pCMV sequence, which was ligated into hERG1b-pcDNA3 (shown in Fig. 5.1A) at *Bam*H1 and *Bsp*E1 restriction sites. **C.** Schematic representation of hERG1-pCMV-hERG1b (C2). pCMV-hERG1b-pcDNA3 (shown in **B**) was digested with *NotI* enzyme to excise the coding sequence for pCMV-hERG1b, which was ligated into hERG1-pcDNA3 (shown in Fig. 5.1E) at the *NotI* restriction site, producing hERG1-pCMV-hERG1b. hERG1 and hERG1b sequences are indicated. A CMV promoter drives the translation of both genes from separate mRNA transcripts. The vector also contains ampicillin (Amp^r) and neomycin (Neo^r) resistance genes which allow the use of ampicillin and G418 for prokaryotic and eukaryotic selection, respectively.

5.2.2 Characterization of hERG currents expressed by C1 and C2 constructs by voltage clamp recording

Constructs were characterized in *Xenopus* oocytes as described in Chapter 2, or in WT HEK293 cells by patch clamp as follows. HEK cells were cultured in 35 mm dishes to 60-70% confluency and transiently transfected with a total of 3 μ g of WT hERG1, C1 or C2 cDNAs using LipofectAMINE2000 (Invitrogen). 24 h after transfection, cells were lifted using an enzyme-free cell dissociation buffer (Gibco, UK), gently pelleted and re-suspended in D-PBS. Cells were placed in the recording chamber of an inverted microscope (Eclipse, TE300, Nikon, Surrey) and allowed to adhere for 20 min. Borosilicate glass microelectrodes were pulled using a P-87 micropipette puller (Sutter Instrument Co, USA) to give a resistance of 3-5 M Ω and filled with an internal solution containing (in mM) 130 KCl, 5 MgATP, and 10 HEPES (pH 7.2). A Tyrode's solution containing (in mM) 140 NaCl, 1 MgCl₂, 4 KCl, 10 glucose, 5 HEPES, 2 CaCl₂ (pH 7.4) was used as the extracellular solution. Recordings were performed at room temperature using the whole cell patch clamp configuration using an Axopatch200B amplifier (Molecular devices, USA). Data acquisition and analysis were performed as described in Chapter 2.

5.2.3 Transient transfection

A strategy was adopted of co-transfecting cells with hERG constructs and an eGFP vector, and selecting transfected cells on the basis of eGFP expression using fluorescence-activated cell sorting (FACS). The first stage was to optimize the transfection conditions.

Commercial transfection reagents from different suppliers (Lipofectamine 2000 (Invitrogen), FuGENE HD (Roche), GeneJuice (Novagen), TurboFect (Fermentas) were tested for efficiency in transfection of NIH-3T3 cells following the manufacturers'

instructions. Lipofectamine 2000 was also used for optimization of the amount of eGFP cDNA required for subsequent co-transfection experiments. Briefly, 2.5×10^5 NIH-3T3 cells were grown overnight in 6-well plates in 3 mL culture medium to give ~70-80% confluency the following day. An eGFP-containing plasmid DNA was diluted in 300 μ L serum-free culture medium. The transfection reagent was then added to the solution at the recommended DNA:transfection reagent ratio (1:2 for TurboFect and FuGENE HD, 1:3 for Lipofectamine 2000 and GeneJuice) and allowed to complex with DNA for 15-20 min at room temperature. The transfection complexes were then added drop-wise to the cells and the plate was rocked to ensure uniform distribution of complexes over the cells. Plates were then incubated at 37°C. 4-5 h later, the culture medium was exchanged for fresh culture medium. 24 h after transfection, cells were harvested and analyzed for green fluorescence by flow cytometry. For co-transfection experiments, 7 μ L Turbofect was used to transfect cells in a 6-well plate with 3 μ g of plasmid DNA and 0.5 μ g of eGFP pcDNA3 as described above. 24 h after transfection, cells were harvested and the population of cells emitting green fluorescence was enriched by FACS. In some experiments, cells were co-transfected with monomeric red fluorescent protein (mRFP) plasmid DNA so that a voltage-sensitive fluorescent indicator, which emits in the green spectrum, could be used.

5.2.4 Flow cytometry analysis and fluorescence-activated cell sorting (FACS)

24 h after transfection, eGFP (or mRFP) -transfected NIH-3T3 cells were harvested using 0.5 mL trypsin/EDTA, centrifuged and re-suspended in 2 mL of culture medium prior to flow cytometry. Non-transfected WT NIH-3T3 cells were used as a control. Flow cytometry analysis and cell sorting were performed using FACSCanto II and FACSAria II flow cytometers, respectively (BD Biosciences, USA). The emitted GFP fluorescence was

collected between 515-545 nm and mRFP fluorescence between 650-670 nm. For analysis, data were collected from at least 10,000 events using CELLQuest ProSoftware (BD Biosciences). Sorted cells were used in migration and proliferation assays and also in experiments investigating membrane potential changes on hERG1 expression.

5.2.5 Detection of hERG1 expression by measurement of membrane potential changes

NIH-3T3 cells transiently co-transfected with mRFP and hERG1 (or an empty vector) were sorted for red fluorescence as described above. Sorted cells were grown overnight on glass coverslips in normal culture medium. The next day, cells were loaded with the potentiometric dye Di-8-ANEPPS (4-[2-[6-(dioctylamino)-2-naphthalenyl]ethenyl]-1-(3-sulfopropyl)-pyridinium; 5 μ M) for 20 min at room temperature. Coverslips were washed with Krebs-Henseleit buffer containing (in mM): 118 NaCl, 4.7 KCl, 1.3 CaCl₂, 1.2 KH₂PO₄, 1.2 MgSO₄, 25 Na HCO₃, 5 HEPES, 10 glucose, pH 7.4. Coverslips were then placed in the recording chamber of a laser scanning confocal microscope (Olympus FV500, Olympus, Japan). mRFP-expressing cells were identified by exciting cells using a 543 nm helium-neon laser and collecting emissions at 660 nm. A field of view of 3-7 mRFP-transfected cells was chosen. Cells were continuously perfused with Krebs-Henseleit buffer at 37°C. A high [K⁺] Krebs-Henseleit buffer (containing (in mM): 125 KCl, 1.3 CaCl₂, 1.2 KH₂PO₄, 1.2 MgSO₄, 25 Na HCO₃, 5 HEPES, 10 glucose, pH 7.4) was applied for around 200 s to cause depolarization. Cells were excited at 488 nm and emissions from Di-8-ANEPPS collected at 505-560 and >610 nm, respectively. Changes in signal were measured as a ratio of emissions at 505-560 nm/>610 nm; an increase in ratio being indicative of membrane depolarization.

5.2.6 Cell culture-based assays

Cell migration and proliferation assays were modified to be performed on the relatively low numbers of cells yielded by the sorting protocols. Cells were sorted 24 h after transfection. Data acquisition and analysis were as carried out previously described in Chapter 2.

5.2.6.1 Wound healing and single-cell migration assays

Experiments were performed as described previously, except for the following modifications:

For wound healing assays: sorted cells were seeded at a density of 1×10^5 cells in triplicate in 48-well plates, which were marked underneath with three transverse lines, and grown overnight to form a confluent cell monolayer. The following day, a single scratch was made in the cell monolayer and the scratch was imaged at the 3 marked points of contact with the transverse lines at time 0 and after 10 h.

For single-cell measurements of speed: sorted cells were plated at a density of 5,000 cells in 100 μL of D-PBS in 35-mm dishes, pre-coated with $2 \mu\text{g mL}^{-1}$ fibronectin. Cells were left to attach to the dish surface for 15 min at 37°C and more culture medium was then added to the cells. Migration was monitored by time-lapse microscopy as previously described.

5.2.6.2 Cell proliferation and saturation density assays

Sorted cells were seeded at a sub-confluent (10^4 cells), or nearly confluent (4×10^4 cells) density in 100 μL of culture medium in quadruplicate in 96-well plates and incubated at 37°C in humidified air:5% CO_2 . After 1-2 days, 10 μL of 5 mg mL^{-1} MTT solution was added to each well and incubated at 37°C for 2 h. The culture medium was then removed, crystals dissolved in 50 μL DMSO and the absorbance at 570 nm measured.

5.3 Results

5.3.1 Functional expression of hERG1 and hERG1b in *Xenopus* oocytes

Co-expression of hERG1b and hERG1 results in hERG currents with altered biophysical properties compared to homomeric hERG1 or hERG1b currents (London *et al.*, 1997). To test the relative expression of both subunits generated from hERG1-pIRES-hERG1b, this plasmid was expressed in *Xenopus* oocytes and currents compared to currents elicited in oocytes expressing hERG1, hERG1b or hERG1+hERG1b (1:1 ratio of cRNA). Co-expression of hERG1 and hERG1b was achieved by injection of oocytes with equal amounts of cRNAs, where protein expression is assumed to correlate with the amount of injected cRNA. Expression of hERG1b alone produced no currents other than endogenous currents seen in non-injected oocytes (data not shown). This finding is consistent with previous reports showing that homomeric hERG1b channels are poorly expressed and are not trafficked to the plasma membrane (London *et al.*, 1997, Phartiyal *et al.*, 2008).

The major functional effect of co-expressing hERG1 and hERG1b is a change in deactivation kinetics. We used this parameter to assess if hERG1b expression occurred using the hERG1-pIRES-hERG1b construct. The deactivation kinetics were investigated by recording the tail currents at potentials ranging from -150 to -60 mV after an activating step to +40 mV using the FA-IV protocol (Fig. 5.3A). Typical current traces for each recording condition are illustrated in Fig. 5.3B. During the activation step to +40 mV, WT hERG1 currents show a small outward current. The channels are fully activated, but rapidly inactivate, resulting in suppression of the observed outward current. On stepping to repolarizing or hyperpolarizing potentials, large tail currents are elicited by a rapid recovery of channels from inactivation. The direction of tail currents is determined by the

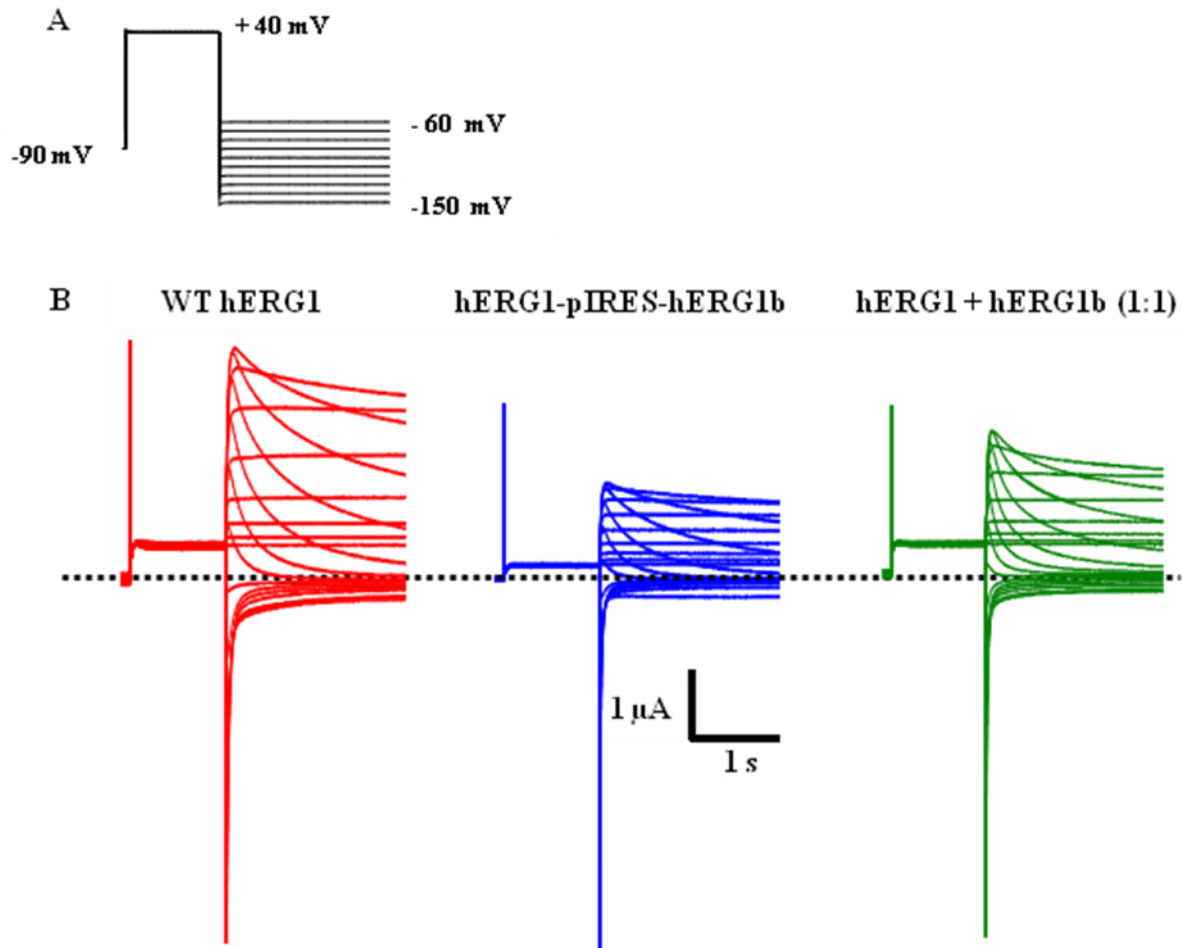


Figure 5.3 Characterization of hERG1-pIRES-hERG1b (C1) in *Xenopus* oocytes.

A. Representation of the voltage protocol. The holding potential was -90 mV; currents were activated by a depolarizing step to +40 mV, followed by a family of 5 s test pulses to potentials from -150 to -60 mV. **B.** Representative current traces from oocytes injected with hERG1, hERG1-pIRES-hERG1b (C1) and hERG1 + hERG1b (1:1). For clarity only the +40 mV step and the first 2 s of the test pulses are shown.

electrochemical gradient. These tail currents slowly decay due to slow deactivation. Tail currents recorded from hERG1-pIRES-hERG1b and hERG1+hERG1b (1:1) appeared to show a faster decay than WT hERG1. This is clearly shown by normalizing the tail currents to the same peak amplitude and comparing the time-course for channel deactivation at a single test potential of -70 mV (Fig. 5.4A). The hERG1-pIRES-hERG1b currents showed an intermediate rate of deactivation compared to WT hERG1 and hERG1+hERG1b (1:1) currents.

The deactivating current traces were best fitted to a double-exponential function (Fig. 5.4B). The time constants of the fast and slow components of deactivation were determined and plotted against the membrane potential (Fig. 5.5A). hERG1+hERG1b (1:1) showed faster deactivation rates compared to WT hERG1 at all test potentials. However, the increased deactivation rate observed for hERG1/hERG1b isoformic co-expression from the hERG1-pIRES-hERG1b plasmid was most evident at hyperpolarizing potentials. Deactivation time constants at a hyperpolarizing potential of -120 mV and a physiologically-relevant voltage of -60 mV are shown in Fig. 5.5B. The relative contribution of the fast component of deactivation for hERG1+hERG1b (1:1) (0.53 ± 0.01 ms; n=5) was significantly different ($p < 0.001$) to hERG1-pIRES-hERG1b (0.31 ± 0.02 ms; n=15) and hERG1 (0.33 ± 0.03 ms; n=5) injected oocytes when measured at -60 mV, whereas similar relative contributions were apparent at -120 mV (Fig. 5.5C).

hERG1/hERG1b heteromeric channels have also been reported to activate more rapidly than hERG1 and show a negative shift in the voltage-dependence of activation (Larsen *et al.*, 2008). Thus, the activation kinetics were studied by applying a standard I-V protocol with test pulses from -60 mV to +50 mV in 10 mV increments from a holding potential of

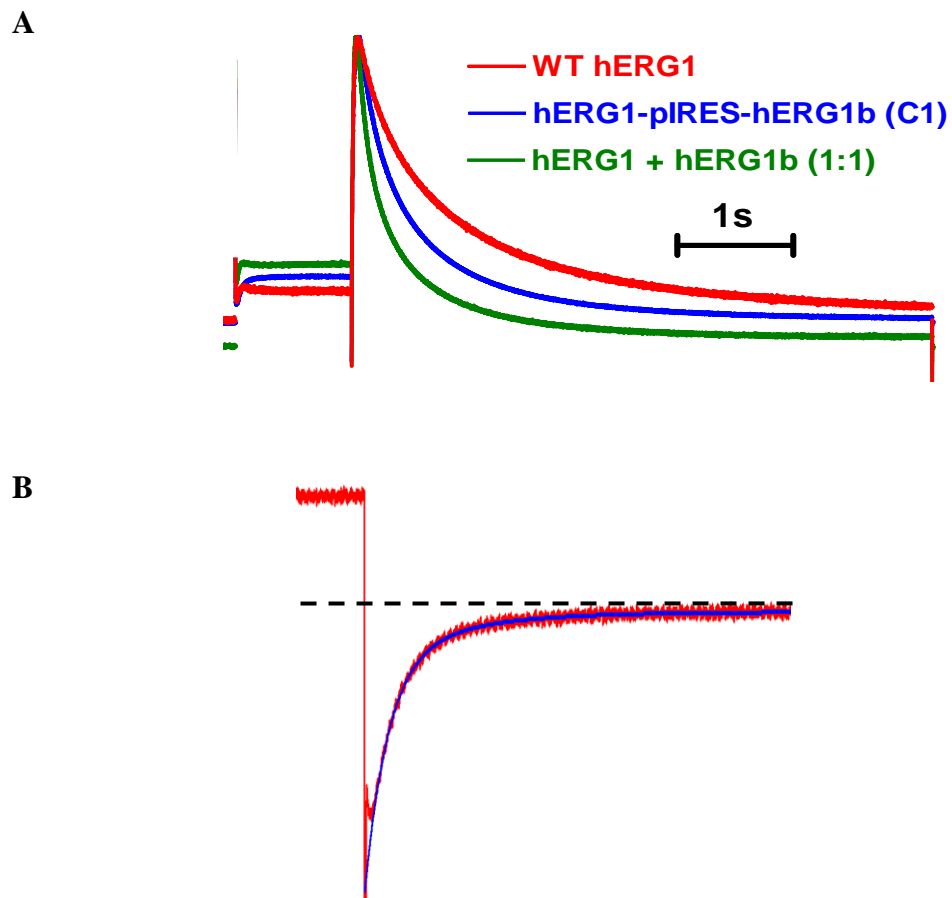


Figure 5.4 Effects of hERG1b co-expression on hERG current deactivation.

A. Tail currents at -70 mV are normalized to the peak amplitude and overlaid to show differences in rates of deactivation. **B.** Example of a double exponential fit (in blue) of hERG1 tail current (in red) at -120 mV. Dashed line indicates zero current line.

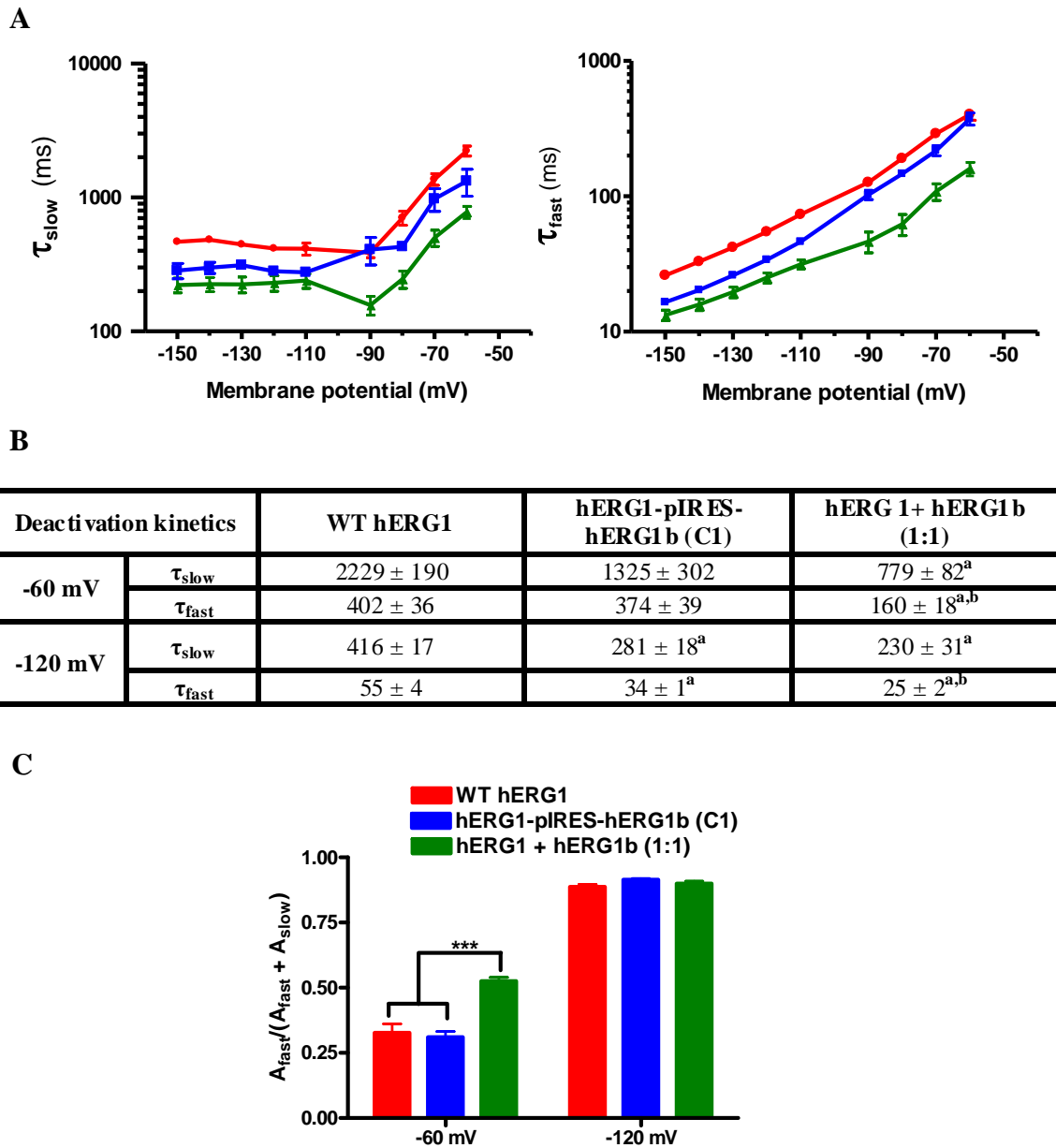


Figure 5.5 Deactivation kinetics of hERG1-pIRES-hERG1b currents expressed in *Xenopus oocytes*. **A.** Slow (right) and fast (left) time-constants for deactivation at various membrane voltages in oocytes injected with hERG1 (red), hERG1-pIRES-hERG1b (C1, blue) or hERG1 + hERG1b (1:1) (green). Values are shown as means ± SEM of records from at least 5 cells. **B.** Table of deactivation kinetics of hERG1 (n=5), hERG1-pIRES-hERG1 (n=15) and hERG1+hERG1b (1:1) (n=5) currents. Values are means ± SEM. ^a indicates a significant difference compared to wild-type hERG1 ($p < 0.05$) and ^b indicates a significant difference compared to hERG1-pIRES-hERG1b ($p < 0.05$). **C.** Relative contribution of the fast component of deactivation at -60 and -120 mV (*** $p < 0.001$).

-90 mV. Tail currents were measured at -70 mV. Representative current traces from oocytes injected with hERG1, hERG1+hERG1b (1:1) or hERG1-pIRES-hERG1b cRNAs are shown in Fig. 5.6A. Peak tail currents were normalized to the maximum and plotted against the test potential to construct conductance-voltage relationships that were fitted to a Boltzmann function to determine $V_{0.5}$ for activation (Fig. 5.6B). There was a significant difference ($p < 0.001$) in the voltage at which half-maximal activation of hERG1+hERG1b (1:1) currents (-25.3 ± 0.6 mV; $n=5$), but not hERG1-pIRES-hERG1b currents (-17.0 ± 0.8 mV; $n=6$) was observed compared to WT hERG1 (-16.5 ± 1.3 mV; $n=5$) (Fig. 5.6C).

Collectively, the data shown in Figs. 5.3-5.6 suggest that transfection with hERG1-pIRES-hERG1b does result in the expression of both hERG1b and hERG1 subunits, however, the relative expression of hERG1b appears to be at a (much) lower level than hERG1.

5.3.2 Functional expression of hERG1, hERG1-pIRES-hERG1b (C1) and hERG1-pCMV-hERG1b (C2) in mammalian cells

It was important to characterize the expression of hERG1-pIRES-hERG1b (C1) and hERG1-pCMV-hERG1b (C2) in mammalian cells. Differences in protein expression in mammalian and *Xenopus* oocyte expression systems may result from vector-dependent changes in protein expression, RNA stability or post-translational modifications. Moreover, the efficiency of protein translation in *Xenopus* oocytes from an IRES sequence, utilized in C1, is not known. Therefore, both C1 and C2 were transiently expressed in HEK293 cells and the deactivation properties of hERG currents were compared to WT hERG1-transfected cells.

Currents were recorded using the previously described FA-IV protocol. Representative current traces and the voltage protocol are shown in Fig. 5.7A. Deactivating tail currents

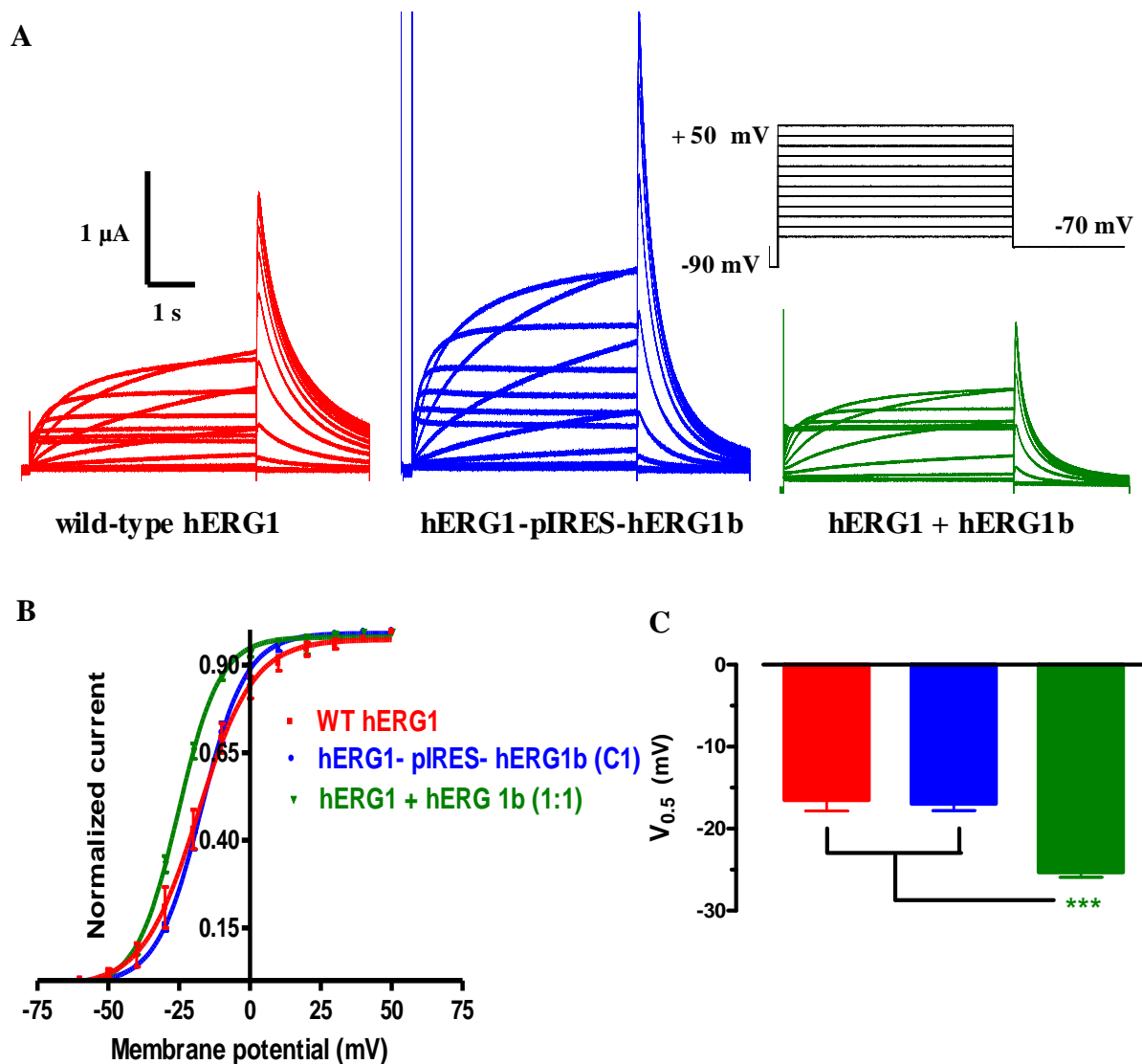


Figure 5.6 Activation kinetics of hERG1 and hERG1/hERG1b currents expressed in *Xenopus* oocytes. **A.** Currents activated by 5 s test pulses from -60 to +50 mV and peak tail currents recorded with a step to -70 mV. The voltage protocol is shown in the inset. **B.** Normalized conductance-voltage relationships. Peak tail currents at -70 mV recorded from oocytes injected with hERG1 (red), hERG1 + hERG1b (1:1) (green) and hERG1-pIRES-hERG1b (C1, blue) were normalized to the maximum in each cell and plotted against the preceding test potential. Solid lines represent the fitted Boltzmann function. Data represent means \pm SEM of recordings obtained from at least 5 different oocytes. **C.** Comparison of $V_{0.5}$ of activation of hERG currents (***) $p < 0.001$.

were fit using a double-exponential function and the fast and slow components of deactivation were determined and plotted at different voltages (Fig. 5.7B). Both C1 and C2 currents appeared to exhibit a modest decrease in the slow time constant relative to WT hERG1. However, the fast component of current deactivation elicited by both hERG1b-containing constructs was significantly faster than WT hERG1 at almost all voltages. For example, at -50 mV the fast time constants of deactivation for C1 and C2 were 185 ± 19 ms ($n=6$) and 186 ± 32 ms ($n=3$), respectively, which were significantly different ($p<0.05$) when compared to that of WT hERG1 (504 ± 110 ms; $n=5$; Fig. 5.7C). Moreover, the relative contributions of the fast component of deactivation for C1 and C2 at -50 mV were 0.57 ± 0.03 , ($n=6$; $p<0.05$) and 0.51 ± 0.03 ($n=3$), respectively compared to WT hERG1 (0.45 ± 0.03 ; $n=5$; Fig. 5.7D). These data suggest that transfection of either C1 or C2 plasmids results in expression of hERG1 and hERG1b subunits in HEK cells, resulting in hERG1/hERG1b currents with faster deactivation kinetics than WT hERG1.

5.3.3 Detection of hERG1 and hERG1b expression levels in NIH-3T3 cells by Western blotting

Western blotting was used to assess hERG1 and hERG1b expression levels in C1 or C2 cDNA-transfected NIH-3T3 cells. Goat and rabbit anti-hERG1 antibodies, previously characterized in Chapter 4, label epitopes located in the C-terminal domain shared by hERG1 and hERG1b and thus should be able to detect either isoform. Fig. 5.8A shows typical Western blots obtained using goat (left) and rabbit (right) anti-hERG1 antibodies. As previously mentioned, the goat anti-hERG1 antibody only recognized immaturely glycosylated forms of hERG1 (lane 2, ~135 kDa) and hERG1b (lane 3, ~ 85 kDa). Two bands can be seen at ~135 and 85 kDa for C1 (lane 4) and C2 (lane 5), confirming the

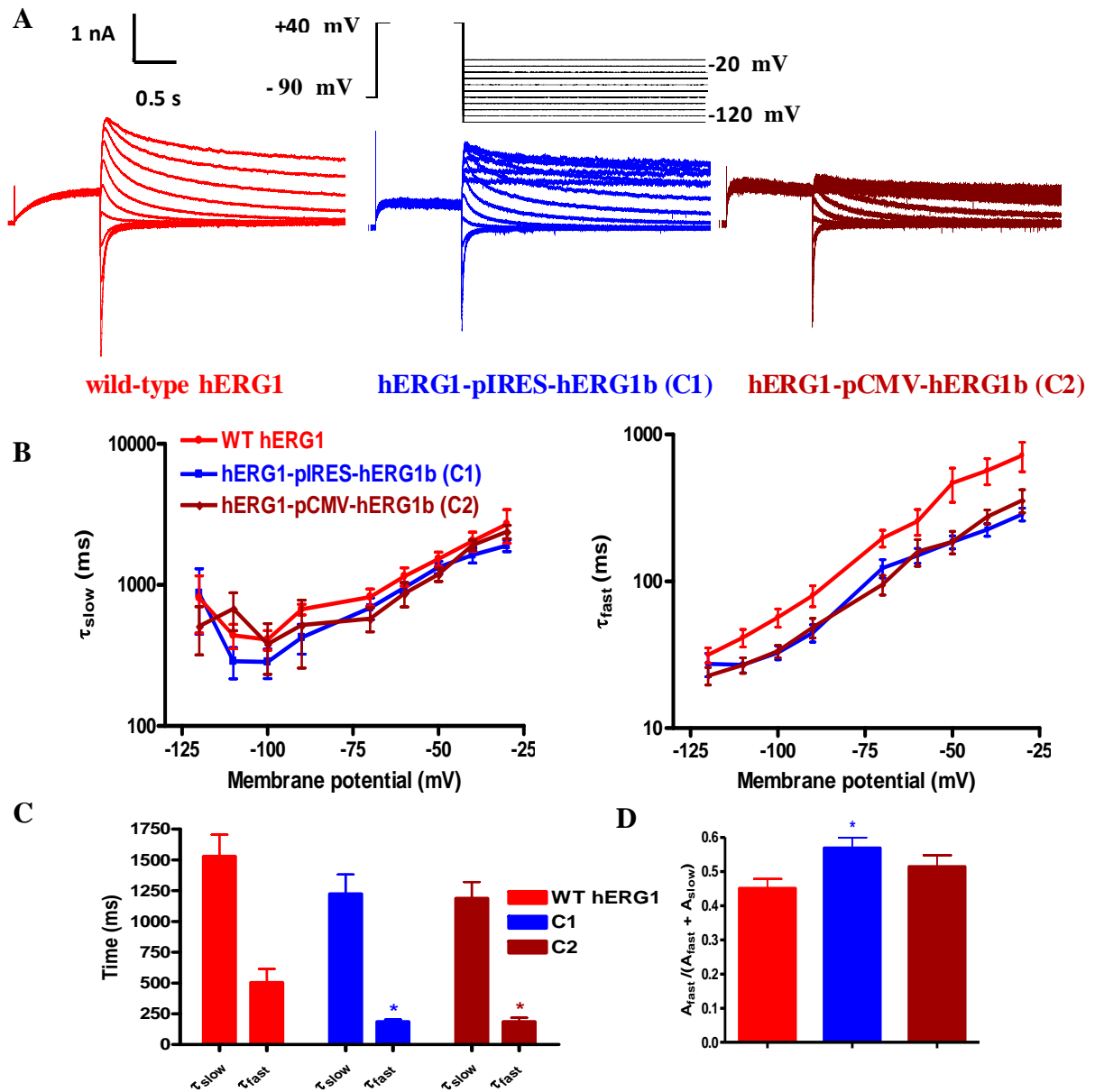


Figure 5.7 Deactivation kinetics of hERG current elicited by expression of hERG1-pIRES-hERG1b (C1) or hERG1-pCMV-hERG1b (C2) in HEK293 cells. **A.** Representative current traces recorded from cells transfected with hERG1 (red), hERG1-pIRES-hERG1b (C1, blue) or hERG1-pCMV-hERG1b (C2, brown). The voltage protocol is shown. For clarity only the activating +40 mV step and the first 4 s of the test potentials are shown. **B.** Slow (right) and fast (left) deactivation time-constants at various membrane voltages. **C.** Comparison of deactivation time-constants of hERG1 (n=5), hERG1-pIRES-hERG1b (n=6) or hERG1-pCMV-hERG1b (n=3) currents at -50 mV. **D.** Relative contribution of the fast component of deactivation at -50 mV. **C, D.** Values shown are means \pm SEM from at least 3 cells; * indicates a significant difference compared to hERG1 ($p < 0.05$).

expression of both subunits from these constructs. To confirm cell-surface expression of hERG1b from C1 or C2 cDNAs, the rabbit anti-hERG1 antibody was used. For C1 (lane 4) and C2 (lane 5) cDNA transfection, this antibody recognized one band for hERG1 (at ~135 kDa) and three bands at ~ 80, 87 and 95 kDa. These band sizes are consistent with those previously described for hERG1b expression in mammalian cells (Pond *et al.*, 2000, Crociani *et al.*, 2003, Jones *et al.*, 2004), where the 95 kDa band likely represents the mature glycosylated form of hERG1b, the 85 kDa band represents the core-glycosylated ER-retained form and the 80 kDa form represents non-glycosylated protein (Jones *et al.*, 2004). However, two bands of similar sizes (~ 80 and 87 kDa) were also detected in hERG1-transfected NIH-3T3 (lane 2). These could be partially degraded hERG1 subunit fragments in this protein sample. Moreover, the 95 kDa band is only detected in C1 and C2 lanes, suggesting cell-surface expression of hERG1b is achieved from these constructs.

The ratio of hERG1b to hERG1 expression from the C1 and C2 was also determined by densitometry analysis of hERG1 and hERG1b band intensities (Fig. 5.8C) from 3 Western blots (as in Fig. 5.8A). C1 showed a relatively higher, but not significant hERG1b/hERG1 expression ratio (0.77 ± 0.10) compared C2 (0.58 ± 0.04). These ratios have to be interpreted with caution since we cannot be certain that the epitopes are equally accessible on the two subunits despite the primary amino acid sequences of the C-termini being identical. Overall, characterization of both C1 and C2 by electrophysiological recording (Fig. 5.3-5.7) and Western blotting (Fig. 5.8) confirms that both constructs can result in functional expression of hERG1b and hERG1 proteins. The hERG1-pIRES- hERG1b (C1) construct was used in subsequent experiments.

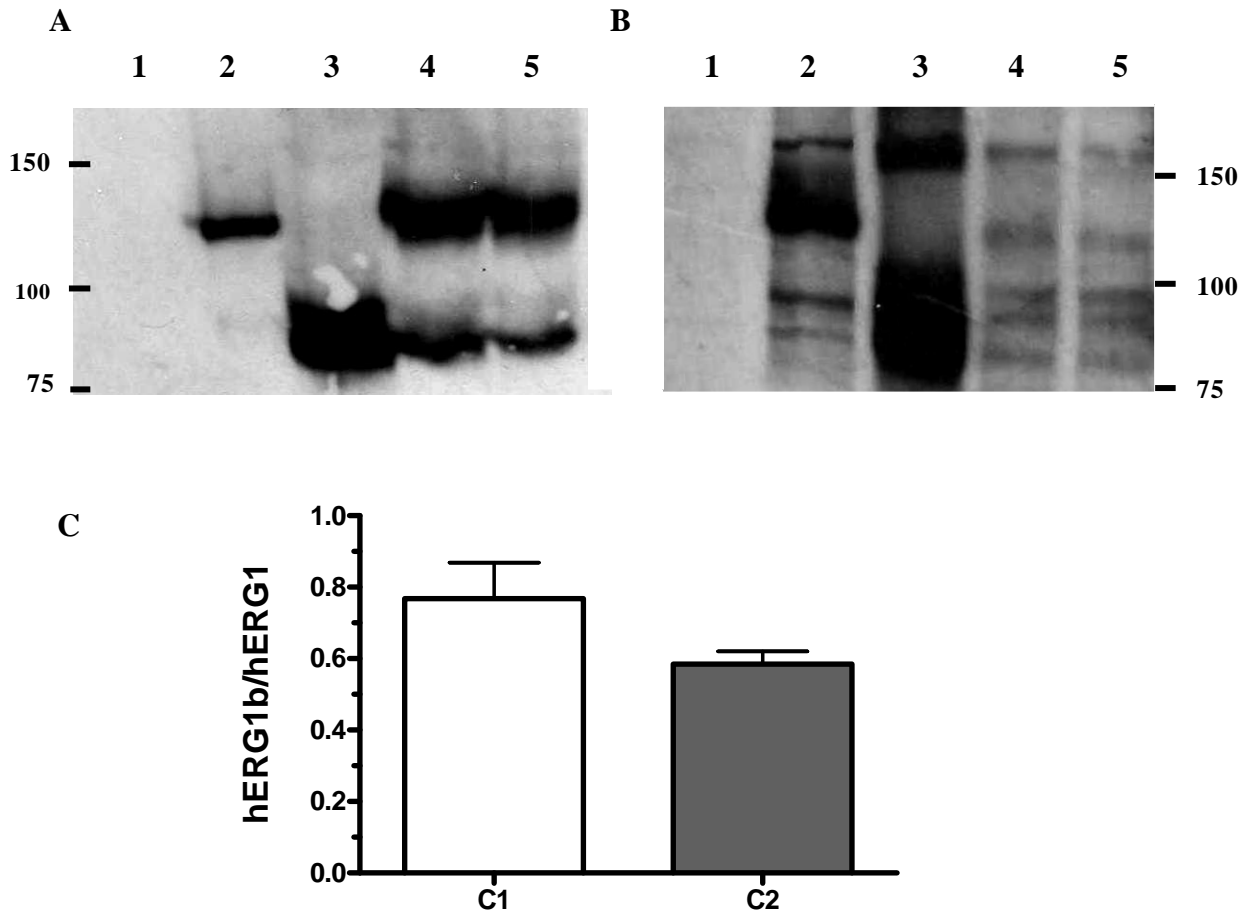


Figure 5.8 hERG1 and hERG1b proteins are expressed after transient transfection of bicistronic C1 and C2 DNA constructs. **A, B.** NIH-3T3 cells were transiently transfected with hERG1 (lane 2), hERG1b (lane 3), hERG-pIRES-hERG1b (C1, lane 4) or hERG1-pCMV-hERG1b (C2, lane 5). Total cell extracts were prepared and 60 μ g protein of each cell extract loaded and resolved on 6% SDS-PAGE gels. Proteins were probed with goat (**A**) or rabbit (**B**) anti-hERG1 antibody. Total extract of non-transfected NIH-3T3 cells (lane 1) was used as a negative-control. **C.** Densitometric analysis of relative hERG1b/hERG1 expression from C1 and C2 constructs. Band intensities were evaluated and background corrected using ImageJ Software. Data represent means \pm SEM of 3 independent experiments.

5.3.4 Optimization of transient transfection conditions

A major drawback of transient transfection is that the plasmid DNA introduced is usually not inserted into the nuclear genome, and therefore the foreign DNA is lost and diluted as the cells undergo mitosis. To determine the time-frame for hERG1 expression after transient transfection in NIH-3T3 cells, cell lysates were prepared at days 1, 2 and 3 after transfection and hERG1 expression levels assayed by Western blotting using the rabbit anti-hERG1 antibody. Cells transfected with an empty-vector (VC) served as a negative-control (Fig. 5.9 A). As shown, there was a significant decrease in hERG1 expression levels at days 2 and 3 of transfection compared to levels expressed at 24 h post-transfection. To quantify these decreases, the relative hERG1 expression was determined by densitometric analysis of blots obtained from 3 independent experiments (Fig. 5.9B). hERG1 expression levels at days 2 and 3 were $72 \pm 4\%$ and $37 \pm 9\%$ of levels expressed 24 h after transfection. Even at day 3 levels of hERG1 expression were as great, or greater than those seen in the stable hERG1-expressing NIH-16 and NIH-50 cells. A time-frame of three days was chosen for performing experiments assessing cell migration and proliferation properties after hERG1/hERG1b transient transfection.

Another potential drawback of transient transfection, particularly for NIH-3T3 cells, is a low efficiency of transfection and therefore many cells in the study population will not be expressing the gene of interest. Consequently, the contribution of transgene expression might go unobserved. Co-transfection of mammalian cells with a gene of interest and the fluorescent reporter eGFP has been routinely used to select cells expressing a target gene. This technique is also used to identify cells transiently expressing ion channels for patch clamp recordings. However, a balance of the quantities of eGFP and transgene DNA is

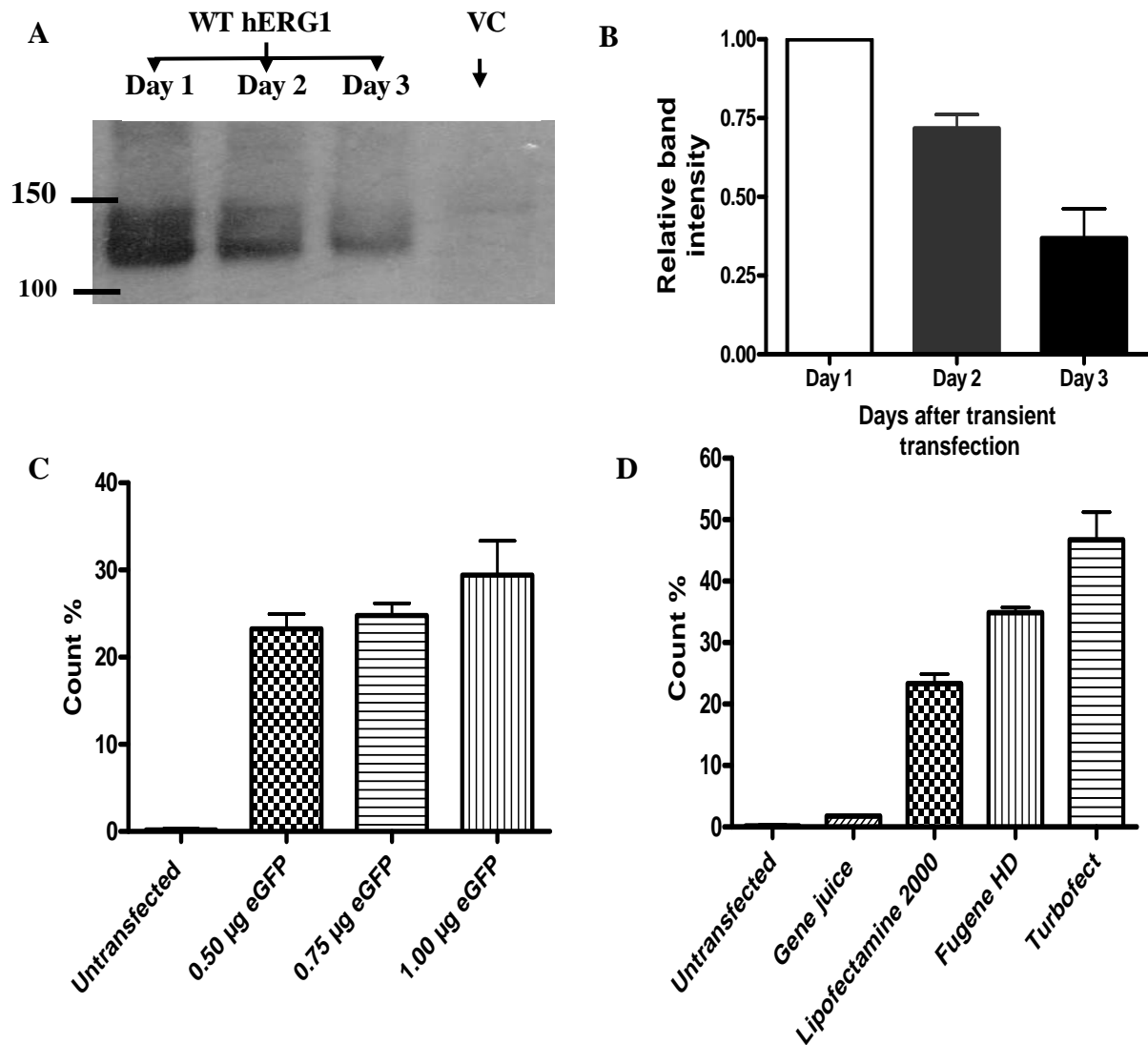


Figure 5.9 Optimization of conditions for transient transfection of NIH-3T3 cells.

A. hERG1 protein expression in NIH-3T3 cells after 1-3 days of transient transfection. NIH-3T3 cells were transiently transfected with a vector-control plasmid or wild-type hERG1. Total cell extracts were prepared at 1, 2 and 3 days post-transfection and 50 µg protein loaded and resolved on 6% SDS-PAGE gels. Blots were probed with rabbit anti-hERG antibody. **D.** Densitometric analysis of wild-type hERG1 relative to expression at 24 h post-transfection. Band intensities were assessed and background corrected using ImageJ Software. Data represent means \pm SEM of 3 independent experiments. **C.** NIH-3T3 cells were transfected with 0.5, 0.75 or 1.0 µg eGFP-cDNA using Lipofectamine 2000 and cells emitting green fluorescence were analyzed by flow cytometry. **D.** NIH-3T3 cells were transfected with 0.5 µg eGFP-cDNA using different transfection reagents. Cells were lifted and the % of cells exhibiting green fluorescence measured by flow cytometry. Untransfected NIH-3T3 cells were used as controls and data presented as means \pm SEM of 3 experiments performed in duplicate.

necessary. The use of a higher ratio of transgene-to-eGFP cDNAs in transient expression systems is required to compensate for a potentially greater translation of eGFP. To determine the minimum amount of eGFP required to produce a detectable level of expression after transient transfection, different quantities (0.5, 0.75 and 1 μ g) of eGFP plasmid DNA were incubated with cells plated in 6-well plates. The efficiency of transfection using the Lipofectamine 2000 transfection reagent was determined to be 23 ± 2 , 25 ± 1 and $29 \pm 4\%$, respectively using flow cytometry (Fig. 5.9C). A quantity of 0.5 μ g of eGFP per well was utilized in subsequent co-transfection experiments.

The efficiency of transfection of eGFP into NIH-3T3 cells was tested using different transfection reagents following the manufacturers' guidelines (Fig 5.9D). The order of transfection efficiency (from highest to lowest) was TurboFect ($47 \pm 5\%$; n=4), FuGENE HD ($35 \pm 1\%$; n=3), Lipofectamine 2000 ($23 \pm 2\%$; n=6), GeneJuice ($2 \pm 0\%$; n=3). Therefore, TurboFect was selected for use in co-transfection experiments.

5.3.5 Membrane potential changes in a sorted cell population transiently transfected with hERG1

Optical recording of membrane potential using the ratiometric voltage-sensitive fluorescent dye Di-8-ANEPPS is a useful non-invasive approach that can rapidly and conveniently measure membrane potential in individual cells or cell populations (Knisley *et al.*, 2000, Kao *et al.*, 2001, Hardy *et al.*, 2006). The dye was loaded into cells and excited at 460-500 nm and emissions assessed at 560 and 620 nm. The ratio of fluorescence emission correlates with the potential difference across the cell membrane and a change in the ratio indicates a membrane potential change. Ratiometric measurement decreases errors resulting from changes in cell size, morphology, or dye concentration.

This method was adapted to measure the contribution of hERG1 channels to resting membrane potential of single cells and to confirm that hERG1 is expressed during co-transfection studies. Changes in membrane potential were measured before and after treatment with the selective hERG1 blocker dofetilide in NIH-3T3 cells that have been co-transfected with mRFP and hERG1, and sorted based on red fluorescence. Dofetilide selectively blocks hERG1 channels causing a membrane depolarization that can be detected by the potentiometric dye. mRFP was utilized in these experiments, instead of eGFP, due to the overlap of the excitation and emission spectra of eGFP and Di-8-ANEPPS.

The fluorescence ratio was measured from a group of 3-7 mRFP-expressing cells perfused with 5 mM K⁺ Tyrode solution. After ~100 sec, 125 mM K⁺ was added to the external solution for 200 s. This decreases the K⁺ concentration gradient across the cell membrane causing cell depolarization. This was indicated by a fluorescence change in both vector-control and WT hERG1-transfected cells (Fig. 5.10A, B). The fluorescence ratio during perfusion with 5 mM K⁺ Tyrode solution (between points A and B in Fig. 5.10A, B) was subtracted from mean fluorescence ratio during perfusion with 125 mM K⁺ (between points C and D in Fig. 5.10A, B). WT hERG1-transfectants showed a greater fluorescence change than vector-control cells, suggesting a greater resting conductance to K⁺. On washing the cells with 5 mM K⁺ Tyrode solution, the fluorescence signal rapidly returned to a new baseline value. Application of dofetilide (5 μM), to block selectively hERG1 channels, had essentially no effect on vector-control cells (see Fig. 5.10C), while causing an increase in fluorescence ratio in hERG1-transfected cells (Fig. 5.10A, B). The change in fluorescence ratio produced by dofetilide was referenced to that induced by 125 mM K⁺. Dofetilide caused a fluorescence change $35 \pm 7\%$ of that induced by switching to the high K⁺ medium,

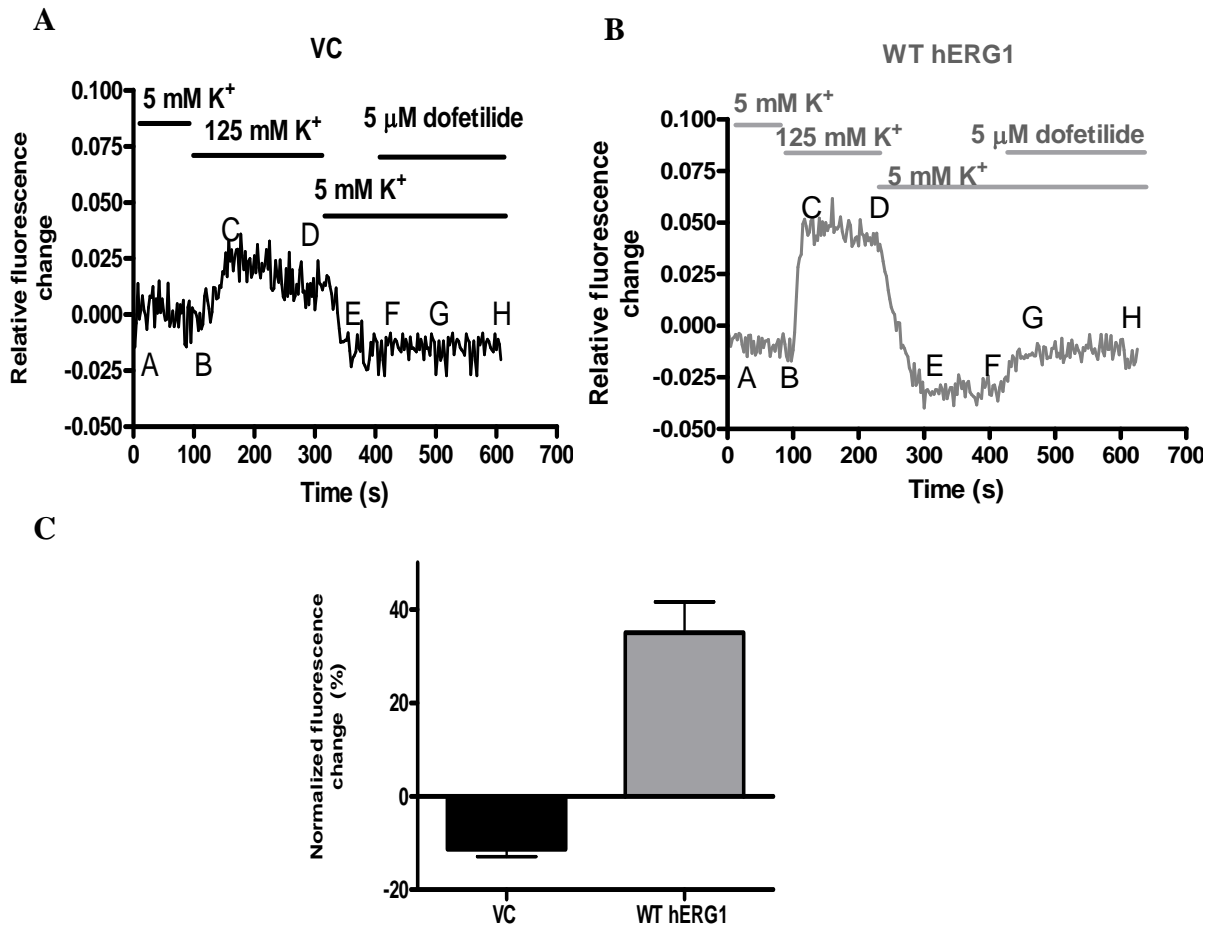


Figure 5.10 Effect of blocking hERG1 current on resting membrane potential. NIH-3T3 cells were transiently co-transfected with either a vector-control (VC) plasmid and RFP (A), or hERG1 and RFP (B). Cells emitting red fluorescence were sorted by flow cytometry and grown on cover-slips for 24 h. Cells were loaded with Di-8-ANEPPS dye (see Methods) and the change in fluorescence induced in response to 125 mM K^+ or 5 μ M dofetilide measured. A and B show representative recordings of fluorescence. Cells were superfused with 5 mM K^+ Tyrode solution. After 100 s, 125 mM K^+ was added to the external solution for 200 s before washing with 5 mM K^+ Tyrode solution. 5 μ M dofetilide was then added in 5 mM K^+ Tyrode solution for 200 s. The fluorescence ratio was baseline subtracted at the beginning of each experiment. C. Change in fluorescence ratio produced by 5 μ M dofetilide normalized to that induced by 125 mM K^+ (see Methods for details). Data presented as means \pm SEM of 6 experiments.

indicating a substantial depolarization (Fig. 5.10C). These data suggest that cell sorting based on a co-transfected fluorescent indicator is a reliable method for selecting cells transiently expressing hERG channels.

5.3.6 Effect of transient expression of hERG1b, hERG1 or hERG1/1b on cell migration, proliferation and overgrowth

Cell migration of hERG-transfected NIH-3T3 cells was quantified in either wound-healing assays, or using time-lapse microscopy for single-cell measurements of speed on fibronectin-coated surfaces. After adhesion to fibronectin, transiently transfected NIH-3T3 cells retained a flattened, fibroblastic morphology (Fig. 5.11A). Interestingly, a small proportion of cells transfected with hERG1 or hERG1+hERG1b had a spindle-shaped, polarized morphology (indicated by arrows, Fig. 5.11A) as previously described for cells stably-expressing hERG1 (Chapter 3, Fig. 3.10). The percentage of cells exhibiting this ‘transformed’ morphology was $14 \pm 3\%$ for hERG1 and $7 \pm 2\%$ for hERG1+hERG1b transfected cells. There was also a trend for the single cell migration speeds to be higher for these cells, however, these differences were not significant compared to empty vector-transfected cells (vector-control, 0.453 ± 0.013 ; hERG1, 0.499 ± 0.018 ; hERG1b, 0.417 ± 0.017 ; hERG1+hERG1b, $0.493 \pm 0.017 \mu\text{m min}^{-1}$; Fig. 5.11B). In wound-healing experiments, WT hERG1-transfected cells appeared to have a greater ability to close wounds than other transfectants, however, this varied from experiment to experiment resulting in no significant differences (vector-control, $44 \pm 4\%$ (n=5); hERG1, $59 \pm 12\%$ (n=3); hERG1b, $33 \pm 2\%$ (n=3); hERG1+hERG1b, $49 \pm 2\%$ (n=3); Fig. 5.11C). Interestingly, hERG1b-transfected cells showed no changes in morphology and consistently migrated more slowly than vector-control NIH-3T3 cells.

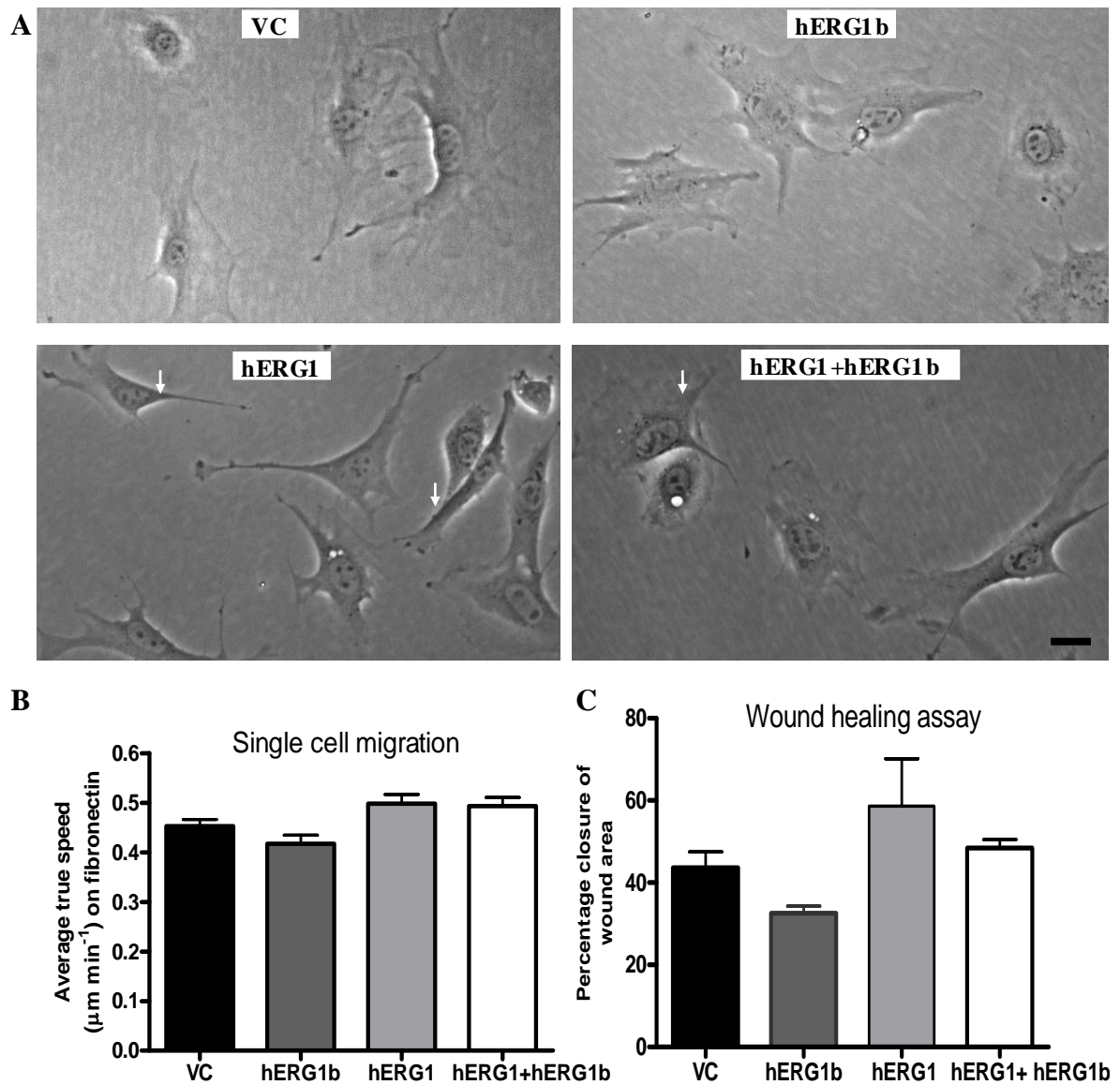


Figure 5.11 Effects of transient expression of hERG1b and/or hERG1 on migration of NIH-3T3 cells. NIH-3T3 cells were transiently co-transfected with a vector-control (VC) plasmid, hERG1b, hERG1 or hERG1-pIRES-hERG1b and eGFP. 24 h later, cells emitting green fluorescence were sorted and cell migration rates investigated as described in Chapter 5 Methods. **A.** Morphology of transfected NIH-3T3 cells after 8 h of adhesion to fibronectin. Arrows indicate cells showing a polarized morphology. Scale-bar, 20 μm . **B.** Average true speed of transiently-transfected NIH-3T3 cells on fibronectin. **C.** Rate of wound closure in transiently transfected NIH-3T3 cells. Data are presented as means \pm SEM for at least 3 experiments.

To study cell proliferation, transiently-transfected cells were plated at a density of 1×10^4 cells per well and absorbance following incubation with MTT measured at 0, 1 or 2 days after cell seeding (Fig. 5.12A). At day 0 all NIH-3T3 cell transfectants exhibited similar absorbance values, indicating a lack of effect of transgene expression on their metabolic activity. Interestingly, hERG1+hERG1b cells exhibited significantly higher ($p < 0.01$) absorbance values (534 ± 16) after 2 days, when compared to hERG1 (418 ± 17), hERG1b (382 ± 16) or vector (355 ± 35) -transfected cells. This suggests that hERG1+hERG1b expression may enhance cell proliferative rates. However, further experiments need to be performed to confirm this finding. Preliminary experiments were conducted to analyze cell cycle distribution by flow cytometry after propidium iodide staining of cells fixed with paraformaldehyde. However, the protocol involved cell permeabilization, which caused loss of eGFP expression, making it hard to identify transfected cells. Future optimization of conditions, or use of alternative dye for DNA labelling of living cells will be necessary.

The assay was also adapted to investigate the ability of cells to overgrow after reaching confluency. Transiently transfected cells were seeded at a density of 4×10^4 , which gave a near confluent monolayer of cells in each well. The MTT assay was performed 2 days after plating. There were no significant differences in MTT absorbance values (Fig. 5.12B), suggesting that these transfectants exhibit contact inhibition of growth. It is likely that longer time-frames might be required to observe a loss of contact inhibition, but this was not feasible because of the loss of hERG channel expression following transient transfection.

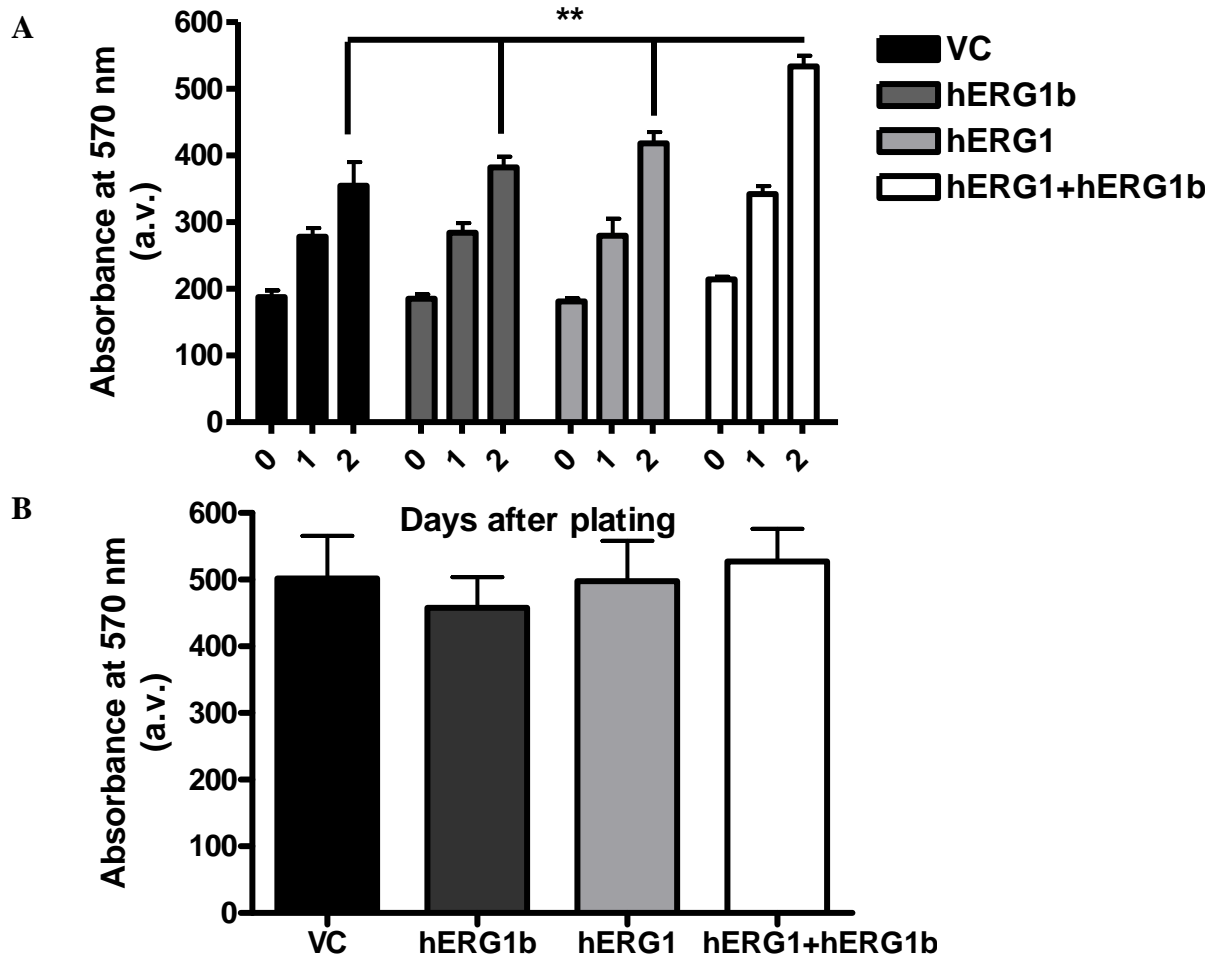


Figure 5.12 Effect of transient expression of hERG1b, hERG1 or hERG1+hERG1b on cell proliferation and overgrowth of NIH-3T3 cells. NIH-3T3 cells were transiently co-transfected with vector-control (VC) plasmid, hERG1b, hERG1 or hERG1-pIRES-hERG1b and eGFP. 24 h later, cells emitting green fluorescence were sorted and seeded in quadruplicate onto 96-well plates at a density of 1×10^4 (A), or 4×10^4 (B) cells. **A.** MTT absorbance values measured at 0, 1 or 2 days after plating. **B.** MTT absorbance values measured at day 2 after plating at a confluent cell density. Data are presented as means \pm SEM for 3 experiments (** $p < 0.01$).

5.4 Discussion

5.4.1 Characterization of hERG1-pIRES-hERG1b (C1) and hERG1-pCMV-hERG1b (C2)

In the present study, two DNA constructs have been designed and generated for dual expression of hERG1 and hERG1b subunits in different expression systems, hERG1-pIRES-hERG1b (C1) and hERG1-pCMV-hERG1b (C2). These were characterized by studying the electrophysiological properties of hERG currents expressed in *Xenopus* oocytes and mammalian cells and characterizing hERG1 and hERG1b protein expression by Western blotting.

Initially C1 was injected into *Xenopus* oocytes and properties of hERG currents compared to hERG1 and hERG1+hERG1b (1:1) co-injected oocytes. hERG1-pIRES-hERG1b currents appeared to show an intermediate rate of deactivation compared to WT hERG1 and hERG1:hERG1b (1:1) currents. The effect on deactivation was more evident at hyperpolarized potentials. Furthermore, hERG1-pIRES-hERG1b currents did not affect the voltage-dependence of activation in contrast to hERG1+hERG1b (1:1) currents which showed a negative shift in the activation curve. This might suggest that at least a 1:1 expression ratio of hERG1 and hERG1b may be necessary to affect hERG1 activation kinetics. Consistent with this concept, Sale *et al.* (2008) reported that expression of hERG1 and hERG1b in a 2:1 ratio did not affect hERG1 activation (Sale *et al.*, 2008), whereas others have reported that a 1:1 ratio of expression caused a negative shift of activation (Larsen *et al.*, 2008). However, the efficiency of protein translation using an IRES sequence in *Xenopus* oocytes expression systems has not been tested. A low efficiency of this sequence in *Xenopus* oocytes might be responsible for relatively low hERG1b

expression from hERG1-pIRES-hERG1b and thus the observed modest effect on hERG1 deactivation as compared to currents in hERG1+hERG1b (1:1) injected oocytes.

Both C1 and C2 plasmids were also transfected into mammalian cells. hERG currents from both constructs exhibited a modest effect on the slow component of deactivation relative to hERG1 currents. The fast component of deactivation was greatly enhanced and the effect was significant at physiologically-relevant potentials. Moreover, western blotting confirmed the expression of hERG1 and hERG1b protein by both constructs. The ratios of hERG1b: hERG1 expression from C1 and C2 were ~ 77% and 58%, respectively. However, it has been reported that expression of relatively low amounts of hERG1b is sufficient to cause substantial functional change in the properties of hERG1 channels (Larsen *et al.*, 2008). The expression of hERG1b may favour the formation of heteromeric channels and the proportion of hERG1b expressed in functional channel complexes at the plasma membrane might be higher than expected from the hERG1 protein levels detected here.

hERG1-pIRES-hERG1b, rather than hERG1-pCMV-hERG1b, was used in transient transfection experiments investigating the effect of hERG1/hERG1b co-expression on cell properties. This construct showed a relatively higher hERG1b:hERG1 expression ratio than hERG1-pCMV-hERG1b. Moreover, it expresses both hERG1 and hERG1b subunits from a bicistronic mRNA transcript and thus ensures their concurrent expression in every transfected cell. Furthermore, both subunits will be expressed stoichiometrically, which determines the biophysical properties of hERG currents expressed in the cell (Larsen *et al.*, 2008, Sale *et al.*, 2008). hERG1- pCMV-hERG1b expresses hERG1 and hERG1b cDNAs using separate CMV promoters, which may compete for available transcription factors, so

the expression of each cDNA will be lower than if expressed on their own. Moreover, a similar ratio of hERG1b: hERG1 expression in all transfected cells is not guaranteed.

5.4.2 Transient expression of hERG1 does not affect NIH-3T3 cell migration or growth properties

In contrast to stable hERG1 expression, transient expression of hERG1 in NIH-3T3 cells did not induce a ‘transforming’ behaviour. This may suggest a continuous, long-term expression of hERG1 is required to affect cell properties. This is consistent with findings reported in Chapter 3, where chronic inhibition of hERG1 current was necessary to inhibit the hERG1-dependent enhancement of cell migration (Chapter 3, Fig. 3.21). The ability of hERG1-transformed cells to migrate faster and to over-grow a confluent monolayer is potentially associated with modulation of cytoskeletal organization and cell-cell interactions. These are processes that may be induced by changes in gene expression of integrin and cadherin adhesion receptors, or other downstream components of intracellular signalling pathways (Braga *et al.*, 1997, Zhang *et al.*, 2002). A continuous hERG1 expression may then be necessary to induce changes in gene expression contributing to cell transformation. Another possibility is that a certain threshold of hERG1 expression is required to transform cells. Transiently transfected cells may have different expression levels of hERG1 and therefore only some transfected cells, which express the necessary number of hERG1 channels, exhibit a ‘transformed’ phenotype. This assumption may explain why a few hERG1-transfected NIH-3T3 cells exhibited a more transformed morphology, identical to that of cells stably-expressing hERG1 (Fig. 5.11A).

5.4.3 Transient expression of hERG1 and hERG1b enhances NIH-3T3 cell proliferation

NIH-3T3 cells transiently expressing hERG1+hERG1b subunits showed an increase in cell proliferation, as compared to cells expressing an empty vector, hERG1b or hERG1 alone. The contribution of K⁺ channels to cell proliferation has been ascribed to a modulation of membrane potential, which regulates cell cycle progression (Wonderlin *et al.*, 1996). A membrane hyperpolarization during G1 phase and a depolarization during S phase may be required to enhance progression through these cell cycle phases (Arcangeli *et al.*, 1995, Wonderlin *et al.*, 1996). Moreover, tumour cells often have depolarized membrane potentials (Redmann *et al.*, 1972, Smith *et al.*, 1975, Arcangeli *et al.*, 1995, Wonderlin *et al.*, 1996). hERG1 channels deactivate at relatively depolarized membrane potentials compared to the inward-rectifier K⁺ currents normally involved in regulating resting potential. This may help maintain the depolarized membrane potential reported in cancer cells (Arcangeli *et al.*, 1995). Currents carried by hERG1+hERG1b heteromeric channels deactivate faster than hERG1 homomeric channels and therefore may contribute to a more depolarized resting membrane potential, although resting potential is probably more dependent on the voltage-dependence of channel activation than the kinetics of channel deactivation.

Modulation of hERG1-expressing tumour cell membrane potential might be dependent on the expressed ratios of hERG1 and hERG1b isoforms. hERG1b expression is under the control of its own promoter (Luo *et al.*, 2008) and therefore could be subject to independent transcriptional regulation in tumour cells to alter hERG1/hERG1b stoichiometry under certain pro-proliferative conditions. It is tempting to speculate that regulation of hERG1b

expression in tumour cells might be responsible for modulating hERG1 channel properties, causing an increase in cell proliferation. Supporting this hypothesis, the expression of the hERG1b isoform in human neuroblastoma SH-SY5Y cells is cell cycle-dependent and is up-regulated during S phase (Crociani *et al.*, 2003).

hERG1b-transfected cells did not show an increase in cell proliferation. This may suggest that this isoform is regulating hERG1 properties to affect other tumour cell characteristics. This is supported by previous reports showing that hERG1b proteins expressed alone are largely retained in the endoplasmic reticulum (ER) due to an *N*-terminal RXR ER retention signal, resulting in poor functional expression of homomeric hERG1b currents (Phartiyal *et al.*, 2008). Moreover, it has been suggested that co-expression of hERG1 promotes hERG1b trafficking and maturation by overcoming the RXR-mediated retention and in this way regulates subunit composition of hERG cell-surface channels (Phartiyal *et al.*, 2008). Heteromeric association of hERG1 and hERG1b subunits occurs in the ER during ion channel biogenesis through direct interactions of the *N*-termini and this process increases the number of hERG1b channels incorporated at the plasma membrane (Phartiyal *et al.*, 2007). It remains unclear why the hERG1b isoform is expressed in a higher ratio than hERG1 in some tumour cell-lines (Crociani *et al.*, 2003). One possible explanation is that the expression of a higher hERG1b proportion in these cells may favour the formation of heteromeric hERG1/hERG1b channels, which modulate membrane potential and enhance cell proliferation.

Chapter 6

hERG1 expression does not affect survival of Chinese hamster ovary cells at low oxygen tension

6.1 Introduction

Maintenance of oxygen homeostasis is critical for eukaryotic cells. Molecular oxygen functions as the terminal electron acceptor in the mitochondrial respiratory chain, which efficiently generates energy necessary for cellular functions in the form of ATP. Impaired tissue oxygenation is involved in the pathophysiology of several diseases, such as myocardial infarction, stroke, fibrosis and cancer.

Cells can sense inadequate oxygen availability and as a consequence undergo adaptive changes in gene expression that either promote oxygen delivery, or support survival in an hypoxic environment. Specialized cells located in chemosensory organs, such as the carotid body and pulmonary artery smooth muscle cells, sense reduced oxygen availability and undergo changes in cell excitability in the form of increased contractility or secretory activity, which eventually lead to an increased rate of ventilation and improving oxygen delivery to tissues. A different kind of adaptive response, which can occur in all cell-types, involves fuelling cellular activities by oxygen-independent, energy-producing mechanisms and reducing ATP consumption (Gonzalez *et al.*, 2009).

Solid tumours inevitably develop areas of hypoxia (Vaupel *et al.*, 1989, Koh *et al.*, 1992). Oxygen can only diffuse ~100 µm from the nearest microvessel to cells before it is metabolized. The rapid growth of tumour cell mass and the distorted architecture of newly formed tumour blood vessels result in a decrease of oxygen delivery to tumour cells, which

produces a microenvironment with a reduced oxygen tension. Tumour cells develop many adaptive mechanisms that help them survive and grow in this hypoxic microenvironment, including switching to a glycolytic metabolism, promoting cell proliferation, evading apoptosis, inducing angiogenesis, invasion and metastasis and obtaining unlimited replication potential and genomic instability (Ruan *et al.*, 2009). Tumour hypoxia has also been shown to increase resistance to chemotherapy and radiotherapy (Teicher *et al.*, 1981, Gatenby *et al.*, 1988), and is thought to contribute to disease relapse, possibly through promoting selection of cancer cells with defective apoptotic regulators (Graeber *et al.*, 1996). Therefore, understanding the behaviour of hypoxic tumour cells may help develop better therapeutic strategies to target this potentially dangerous tumour cell population.

Components of the hypoxic response pathway include hypoxia inducible factor-1 (HIF-1) and potassium channels. HIF-1 is a transcription factor complex that is activated by hypoxic stress and facilitates cell survival under conditions of oxygen deprivation. HIF-1 trans-activates a diversity of genes involved in iron metabolism (e.g. erythropoietin), vasomotor control, cell proliferation, angiogenesis, glucose metabolism and apoptosis (Kaelin *et al.*, 2008). HIF-1 also plays a central role in tumour cell adaptation to hypoxic conditions by regulating transcription of genes involved in almost all aspects of cancer progression (Semenza, 2007, Ruan *et al.*, 2009).

Potassium channels, including hERG1, have been suggested to act as oxygen sensors and contribute to the cellular response to hypoxia under normal and pathological conditions (Kemp *et al.*, 2009). ERG1 currents in the rabbit carotid body regulate resting membrane potential. Blocking ERG currents with dofetilide depolarized resting membrane potential, increased $[Ca^{2+}]_i$ and mimicked the effect of hypoxia on the carotid sinus nerve (Overholt *et*

al., 2000). Moreover, hERG1 currents are modulated by prolonged hypoxia in normal and tumour cells (Fontana *et al.*, 2001, Nanduri *et al.*, 2009). hERG1 also contains a PAS domain in its *N*-terminus (see Chapter 1). PAS domains are found in a variety of different proteins, can bind haem, and confer sensitivity to oxygen (Gilles-Gonzalez *et al.*, 2004), although there is no direct evidence for this role in hERG1. Moreover, the closely-related PAS-containing EAG channels have been suggested to play roles in adaptation of HEK cells to mild hypoxic conditions (Downie *et al.*, 2008). However, so far, there is no conclusive evidence for a direct involvement of hERG1 in mediating an adaptive response of normal or tumour cells to hypoxia.

To investigate the effect of hERG1 on the cellular response to hypoxia, CHO cells expressing hERG1 (CHO-hERG), or an empty-vector-transfected control cell-line (CHO-VC) were subject to reduced oxygen levels and cell survival, apoptosis and cell cycle distribution compared.

6.2 Methods

6.2.1 CHO-VC and CHO-hERG cells

Chinese hamster ovary (CHO) cells have been used in several studies for investigation of hypoxia signalling pathways (Murphy *et al.*, 1991, Wood *et al.*, 1998) and mechanisms of hypoxia-induced apoptosis and cell death (Bruick, 2000). CHO cell-lines stably transfected with an empty-vector (CHO-VC) or WT hERG1 (CHO-hERG) had been previously generated in the lab. They were maintained in minimum essential medium (MEM) without nucleosides, supplemented with 10% fetal bovine serum, 50 U mL⁻¹ penicillin, 50 µg mL⁻¹ streptomycin and 500 µg mL⁻¹ G418. Cells were maintained at 37°C in an atmosphere of humidified air:5% CO₂. Cells were grown in 25 cm² flasks and split at a ratio of 1:10 every 3-4 days.

6.2.2 Exposure of CHO cells to low oxygen tension

Cells were grown overnight at a starting density of 2×10^5 cells per well of a 6-well plate. The following day, plates were incubated for 24-48 h at 37°C in an atmosphere where O₂ was decreased from 21 to 5%. Alternatively, culture medium was exchanged for a medium that had been pre-gassed with 95% N₂:5% CO₂ for 20 min to remove dissolved oxygen (Newby *et al.*, 2005). Plates were then placed in a modular hypoxia chamber (Billups-Rothenberg, USA) and purged with 95% N₂ and 5% CO₂ for another 20 min. The chamber was tightly sealed and incubated at 37°C in an atmosphere of 5% CO₂. Previous reports using similar hypoxic treatments have achieved O₂ levels of <1% (Dubinsky *et al.*, 1995). Exposure to hypoxia varied in duration from 8 to 36 h. Replicate aerobic control plates were maintained under normal culture conditions. At the end of the exposure period, cell

survival was assessed using the MTT assay, or cells were stained with propidium iodide for analysis of apoptosis and cell cycle parameters of surviving cells by flow cytometry.

6.2.3 MTT viability assay

The viability of CHO cells exposed to hypoxia was evaluated by an MTT test as previously described. Absorbance values have been presented as a percentage of those of time-matched control plates maintained under normal oxygen (~21%) conditions as follows:

$$\% \text{ viable cells} = \frac{\text{Mean absorbance value for CHO cells under hypoxia}}{\text{Mean absorbance value for CHO cells under normoxia}} \times 100$$

6.2.4 Analysis of apoptosis and cell cycle distribution by flow cytometry

Care was taken to collect all cells (viable and non-viable) for analysis. Culture medium from each well was collected into a fresh tube. Cells were washed with 1 mL phosphate-buffered saline (PBS). Cells were then collected by trypsinization (0.5 mL for each well) and washed with 1 mL ice-cold PBS. Cells were recovered by centrifugation (200 $\times g$, 5 min). The cell pellet was washed with 1 mL PBS and re-centrifuged. Cells were then resuspended in cold 70% (v/v) ethanol and fixed for at least 24 h at -20°C . After ethanol fixation, the cells were washed again with cold PBS and finally resuspended in a staining buffer containing 50 $\mu\text{g mL}^{-1}$ propidium iodide (Sigma) and 100 $\mu\text{g mL}^{-1}$ RNase A (Sigma) in PBS. Tubes were incubated at 37°C in the dark for 1 h. The suspension was then analyzed using a flow cytometer (FACSCanto II, BD Biosciences, USA). Fluorescence was collected at >600 nm. Data were collected from at least 10,000 events using BD CELLQuest ProSoftware (BD Biosciences).

6.2.5 Flow cytometry acquisition parameters and data analysis

Propidium iodide is a fluorochrome that binds to nucleic acid and emits fluorescence (after being excited) that is proportional to the DNA content of the cell. Labelling of DNA can be used to discriminate between apoptotic and surviving cells and to analyze cell cycle distribution of viable cells (Riccardi *et al.*, 2006). However, a careful setting of acquisition parameters is initially required for accurate data analysis. A dot plot of fluorescence width (PE-W) against fluorescence area (PE-A) is used to gate single cells. PE-W is indicative of the transit time of the particle through the exciting laser beam and is low for debris and single cells, and high for doublets and aggregates. PE-A is indicative of total fluorescence emitted by the particle. Cell and nuclear debris are gated off by their low fluorescence and low transit time. Aggregates are recognized by high DNA labelling and long transit times. A collection gate is set to recognize single cells (see Fig. 6.1A). DNA fluorescence histograms can then be used for determining SubG1, G1, S and G2/M fractions. Apoptotic cells have partially degraded DNA and therefore apoptotic nuclei have lower DNA content and appear as a broad region (sub-G1) before the sharp peak of G1. The G2/M region is set at double the fluorescence of in G1. The S region lies between the G1 and G2/M peaks (Fig. 6.1B). Chronic exposure of cells to hypoxia induces apoptosis and cell death, which results in an increase in the percentage of cells in the sub-G1 region (Fig. 6.1C).

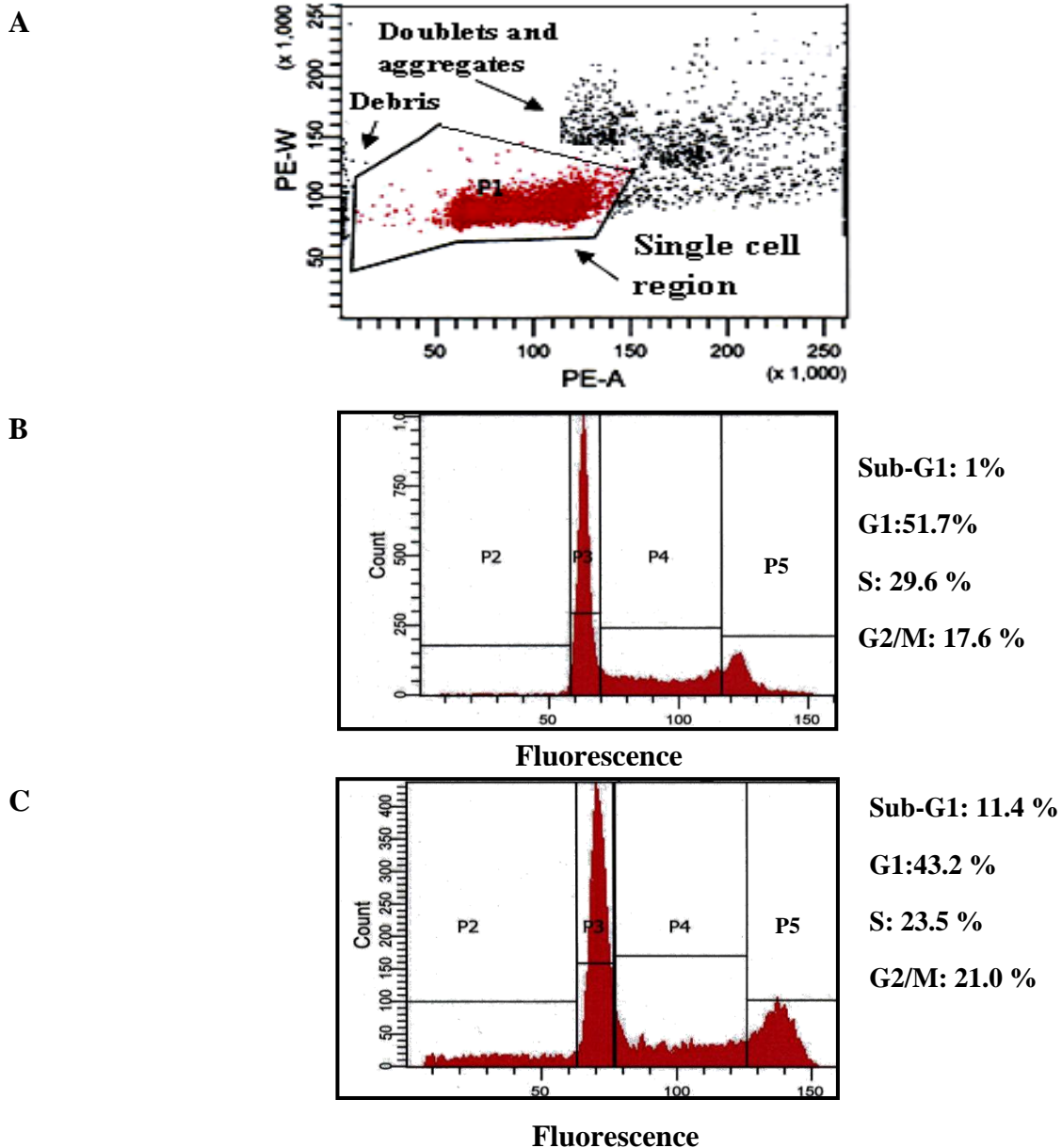


Figure 6.1 Analysis of apoptosis and cell cycle distribution. A. Representative dot-plot of pulse width (PE-W) versus area (PE-A) showing the analysis parameters from a single flow cytometry experiment on vector-control CHO cells under normoxic (~20% O₂) conditions. Each dot represents an event acquisition by the flow cytometer. Cell and nuclear debris and cell doublets and aggregates are gated-off by eliminating the corresponding regions. B. DNA fluorescence histogram. Gated single cells (P1 region in A) were analyzed for DNA content. Apoptotic cells can be recognized by a reduced DNA fluorescence in the sub-G1 (P2) region. Peaks in the P3 and P5 regions denote cells in G1 and G2/M, respectively. The P4 region indicates cells undergoing DNA synthesis (S phase). C. DNA fluorescence histogram of vector-control CHO cells after 24 h exposure to hypoxic conditions. Note the increase in % of cells in the sub-G1 (P2) region.

6.3 Results and Discussion

6.3.1 hERG1 expression in CHO-hERG cells

CHO-hERG cells are Chinese hamster ovary cells that stably express WT hERG1 channels. This cell-line was generated in the Mitcheson lab during a previous PhD project. It was important to validate hERG1 expression in these cells and confirm that hERG1 expression had not been lost on prolonged storage. To confirm the cell-surface expression and functionality of hERG1 channels in CHO-hERG cells, hERG1 currents were recorded by conventional whole-cell patch clamping (Fig. 6.2A) using a standard I-V protocol. Depolarizations from a holding potential of -90 mV to +40 mV in 10 mV increments elicited outward currents characteristic of hERG1 currents, exhibiting rectification at positive potentials. CHO-hERG cells showed a mean tail current amplitude at +40 mV of 101 ± 18 pA (n=3). The current amplitudes were small compared to HEK-hERG cells, but comparable to those recorded in NIH-16 and NIH-50 clones. A plot of normalized peak tail currents against preceding pulse potentials (Fig. 6.2B) shows that CHO-hERG cells activate at approx. -40 mV and have a potential for half-maximal activation ($V_{0.5}$) of -10.6 ± 1.4 mV (n=3). These results confirm functional hERG1 expression in CHO-hERG cells.

6.3.2 Response of CHO-VC and CHO-hERG cells to 5% oxygen levels

Several reports have suggested that signalling of hypoxia can be varied depending on the level of oxygen tension applied. For example, EAG-expressing cells showed a high HIF-1 α protein expression under mild (5% O₂) hypoxia, whereas HIF-1 α protein content was low in EAG-expressing cells exposed to 1% O₂ (Downie *et al.*, 2008). In the current study, CHO cells were subjected to two levels of reduced oxygen: 5% and <1 % O₂ as described in Methods.

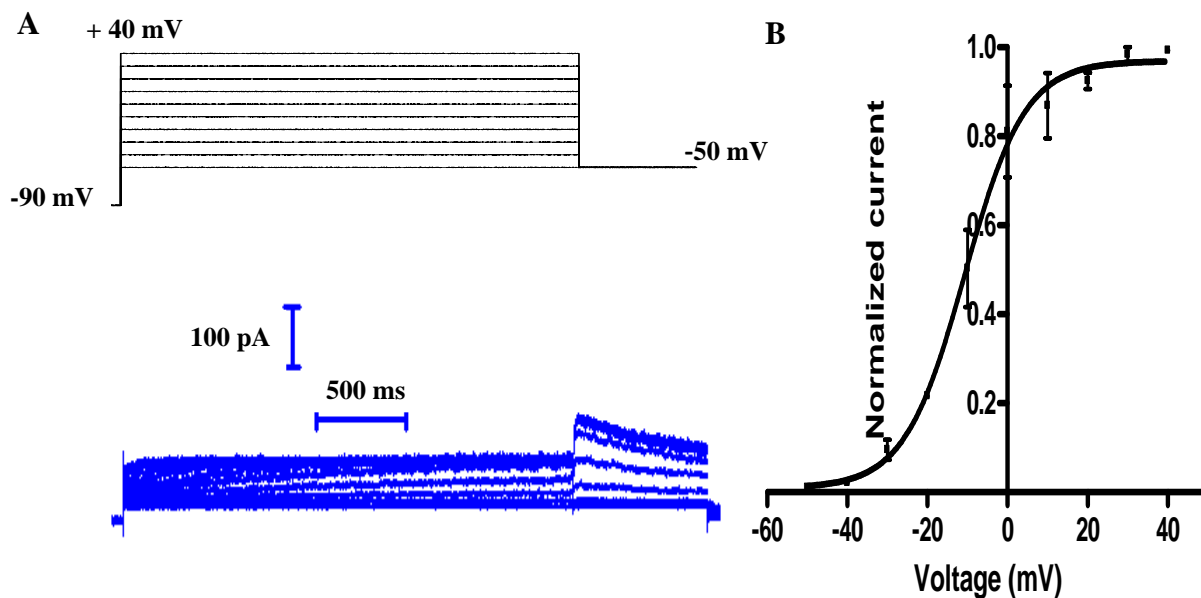


Figure 6.2 hERG1 currents measured in the CHO-hERG stable cell-line. A. Representative recording of hERG1 currents (blue) in response to I-V protocol shown above. B. Peak tail current-voltage for hERG1 currents in CHO-hERG cells. Peak tail current amplitudes were normalized, plotted against the corresponding test pulse potential and fitted with a Boltzmann function ($n=3$).

Both CHO-VC and CHO-hERG cell-lines exhibited similar cell cycle distributions at 21% O₂ and after 24 and 48 h of exposure to 5% O₂ (Fig. 6.3A, B). Moreover, both cell-lines adapted well to this mildly hypoxic condition and showed only low levels of apoptosis. The percentage of CHO-VC cells in the sub-G1 region were $5.1 \pm 2.3\%$ (n=3) and $8.1 \pm 2.4\%$ (n=3) after 24 h and 48 h of exposure to 5% O₂, respectively. For CHO-hERG cells, the comparable sub-G1 fractions were $6.0 \pm 4.9\%$ (n=3) and $4.3 \pm 1.3\%$ (n=3), respectively ($p > 0.05$ relative to CHO-VC at corresponding exposure times). Moreover, the percentage of apoptotic cells for both cell-lines after 24 or 48 h of exposure to 5% O₂ were indistinguishable from levels observed in control cells maintained under normal atmospheric (21% O₂) conditions (2.4 ± 0.9 and 1.8 ± 0.33 for CHO-VC and CHO-hERG, respectively). This may be explained by reports suggesting that 5% O₂ is in fact a physiologically-relevant O₂ level (Atkuri *et al.*, 2007, Li *et al.*, 2010). Moreover, it has been suggested that cell culture ambient O₂ levels are in fact hyperoxic and may alter cellular phenotype over time (Milosevic *et al.*, 2005, Atkuri *et al.*, 2007).

6.3.3 Response of CHO-VC and CHO-hERG cells to severe hypoxia (<1% O₂)

The effect of oxygen deprivation on survival of the CHO-VC and CHO-hERG cell-lines was next studied. Cells were exposed to low O₂ levels for 8-36 h and cell survival was assayed by MTT (Fig. 6.4A) and flow cytometry assays (Fig. 6.4 B, C). Both assays showed a similar pattern of cell death over time in both cell-lines with a dramatic deterioration observed between 30 and 36 h of hypoxia. There were no significant differences between CHO-VC and CHO-hERG cells in the susceptibility to hypoxia-induced toxicity or the cell cycle parameters. After 16 and until 30 h of exposure, apoptotic bodies could be observed when hypoxic cells were inspected by microscopic examination.

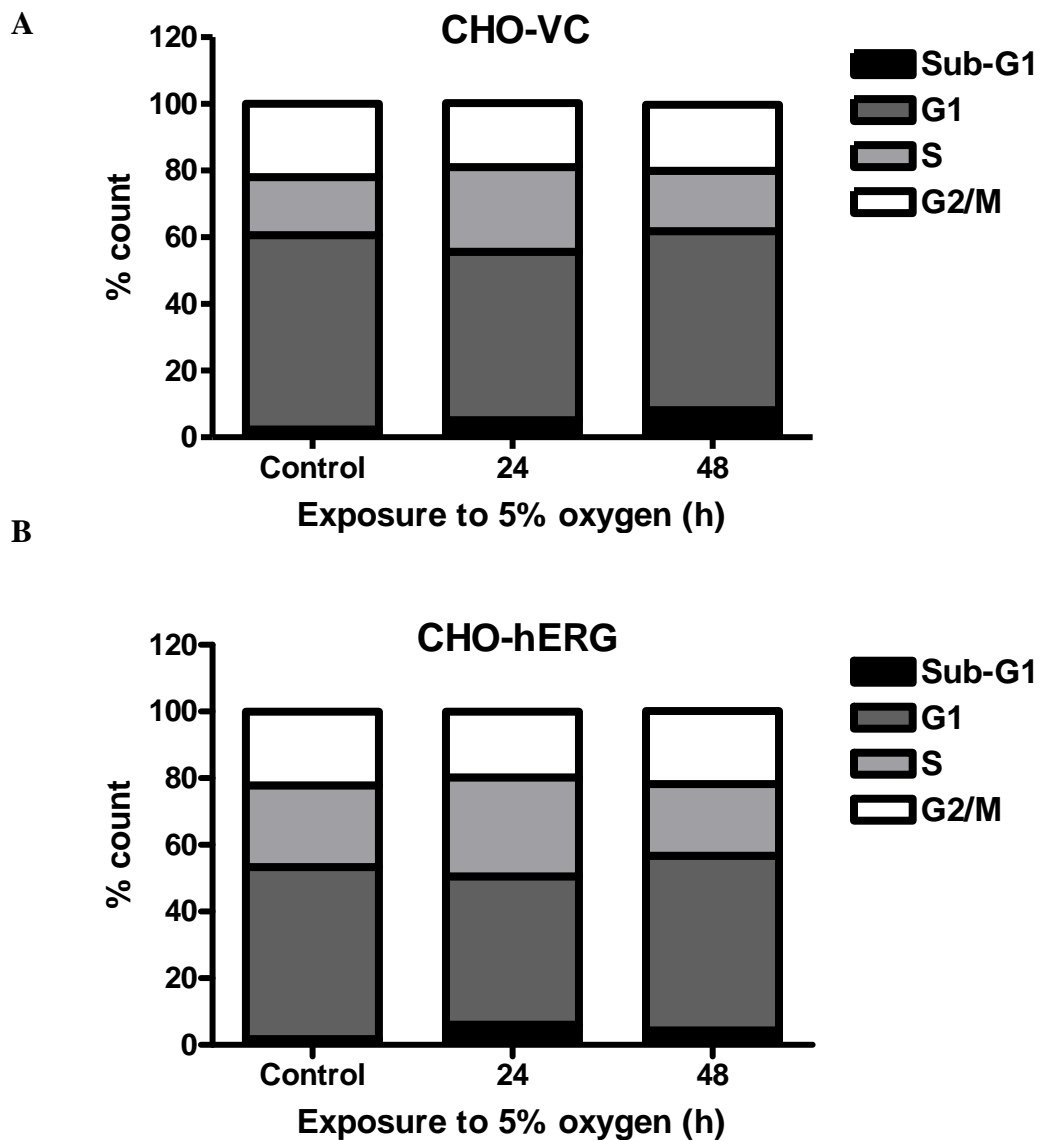


Figure 6.3 Response of vector-control CHO and CHO-hERG cells to incubation in 5% O₂. Cell cycle analysis of vector-control CHO (CHO-VC, A) and CHO-hERG (B) cells after incubation for 24 or 48 h in 5% O₂. Control cells were maintained in 21% O₂. Cells were then fixed and stained with propidium iodide (PI). Cellular DNA content was evaluated by flow cytometry. Data represent means of 3 independent experiments performed in triplicate. For clarity, error bars are not shown.

Further hypoxic exposure (36-48 h) caused cell necrosis (images not shown). This was confirmed by results from the MTT assay. After 36 h of hypoxic exposure, CHO-VC and CHO-hERG cells showed relative MTT absorbances of $17 \pm 3\%$ and $24 \pm 3\%$ compared to matched normoxic populations ($n=3$; $p>0.05$). In the flow cytometry assay, the sub-G1 fractions in CHO-VC and CHO-hERG cell populations were $88 \pm 10\%$ and $93 \pm 1\%$, respectively. Overall, these results suggest that hERG1 expression did not provide any growth/survival advantage to CHO cells under hypoxic conditions.

The relatively long times required to induce apoptosis and cell death by hypoxia is likely mediated by adaptive cellular mechanisms, which facilitate cell survival under conditions of oxygen deprivation. A prolonged exposure to hypoxia can cause the protective response to fail and lead to the activation of apoptotic genes (Bruick, 2000). The tumour suppressor p53, a mediator of stress-induced apoptosis, is stabilized under hypoxic conditions leading to its accumulation. However, p53 only induces apoptosis under conditions of prolonged exposure to severe hypoxia, possibly in association with nutrient deprivation and acidosis (Koumenis *et al.*, 2001, Achison *et al.*, 2003).

Several studies have shown that hERG1 currents are regulated by hypoxia. Exposure of HEK-hERG cells to prolonged hypoxia decreased hERG1 current density and cell-surface protein expression; an effect ascribed to inhibition of hERG1 trafficking by reactive oxygen species (ROS) generated during hypoxia (Nanduri *et al.*, 2009). Acute oxidative stress decreased hERG1 function through an acceleration of hERG1 deactivation (Kolbe *et al.*, 2010). ERG1 channels may also contribute to regulation of resting membrane of rabbit carotid body type-I cells, since the ERG1 blocker dofetilide produced membrane depolarization and increased $[Ca^{2+}]_i$, mimicking the effects of hypoxia (Overholt *et al.*,

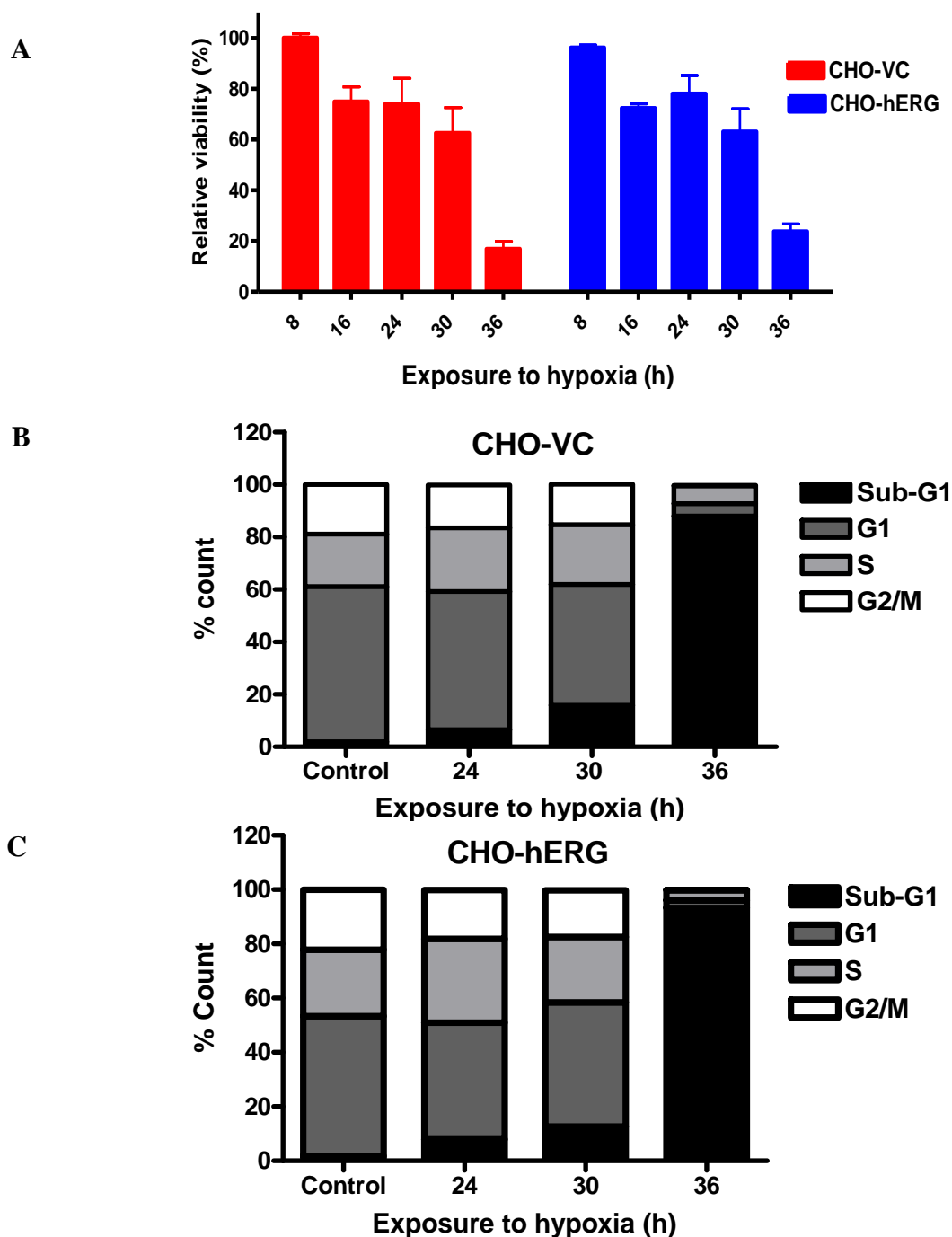


Figure 6.4 Lack of effect of hERG1 expression on adaptive responses of CHO cells to hypoxia. A. Cells were exposed to hypoxia (<1% O₂) for 8-36 h. At the end of this time, cell viability was assessed using MTT assay. Absorbance values were normalized to those of time-matched control cells maintained under normoxic conditions. B, C. Cell cycle analysis of vector-control CHO (CHO-VC; B) and CHO-hERG (C) cells after 24-36 h hypoxia. Control cells were maintained at ambient 21% O₂. Data represent means of 3 independent experiments performed in triplicate. For clarity, error bars are not shown.

2000). hERG1 currents in SH-SY5Y cells are modulated by chronic exposure to hypoxia, which produces a slowing in deactivation kinetics and a negative shift in the voltage-dependence of activation (Fontana *et al.*, 2001). Taken together, these reports may suggest the involvement of hERG1 channels in oxygen-sensing in normal and tumour cells.

HIF-1 mediates hypoxia-induced apoptosis in CHO cells (Wood *et al.*, 1998) and cancer cell-lines (An *et al.*, 1998, Sowter *et al.*, 2001). Tumour cells can develop various mechanisms to escape HIF-1-induced apoptosis through up-regulation of pro-survival and anti-apoptotic signals by HIF-1-dependent and -independent mechanisms (Dong *et al.*, 2001, Schmid *et al.*, 2004, Zhang *et al.*, 2004, Kaidi *et al.*, 2007). Cross-talk between HIF-1 and potassium channels has been suggested. Expression of EAG K⁺ channels has been shown to increase HIF-1 α expression and enhance VEGF secretion and tumour vascularization (Downie *et al.*, 2008). K_{Ca} channels are up-regulated in the IGR-1 melanoma cell-line after exposure to chronic hypoxia via a HIF-1-dependent mechanism (Tajima *et al.*, 2006). Moreover, blockade of K_{Ca} channel activity reduced hypoxia-induced cell proliferation of melanoma cells, suggesting a contribution of K_{Ca} to HIF-1-mediated hypoxic adaptive responses (Tajima *et al.*, 2006).

However, in the present study, hERG1 expression did not affect the survival of CHO cells at mild or severe levels of hypoxia. Future experiments investigating hERG1 role in hypoxia in other cell-lines/primary cultures are required to confirm these results, since the oxygen sensitivity of ion channels is thought to be both tissue-specific and species-dependent (Kemp *et al.*, 2009). Moreover, it may be possible that hERG1 is involved in other cell responses to hypoxia that were not investigated in this study. Adaptation of tumour cells to hypoxia involves the expression of genes involved in angiogenesis, invasion

and metastasis, and hERG1 has been shown to play roles in these processes (Masi *et al.*, 2005, Pillozzi *et al.*, 2007). hERG1 expression is involved in VEGF secretion by tumour cells (Masi *et al.*, 2005); whether this occurs via HIF-1-dependent mechanisms needs to be elucidated.

Chapter 7

Concluding Discussion

It has been shown that the expression of hERG1 channels in non-excitabile cells give rise to a transformed phenotype (Pier, 2007) and that hERG1 expression is also able to induce tumorigenesis in mouse models (the Mitcheson lab, unpublished data), suggesting that hERG1 expression in many primary tumours can contribute to the initiation and progression of tumours, rather than being expressed simply as a consequence of cancer development.

The aim of the present study was to investigate the mechanisms underlying cellular transformation induced by hERG1 expression in model cell backgrounds. Initially, I investigated whether the properties of hERG1-expressing cells are influenced by integrin-mediated signalling. The effect of adhesion to the extracellular matrix on cell morphology, cytoskeletal organization, cell motility and contact inhibition of NIH-3T3 cells stably expressing WT hERG1 channels was investigated. Moreover, the importance of K^+ conductance and/or cell-surface expression of hERG1 channels in mediating their oncogenic potential has been explored using (i) pharmacological approaches, which included the use of the hERG1 blocker dofetilide, hERG1 channel trafficking inhibitors, the hERG1 channel activator, ICA-105574, and high extracellular K^+ concentration, and (ii) molecular biological approaches by characterizing the effect of stable expression of dominant-negative, non-functional hERG1 mutants in NIH-3T3 cells. A transient transfection approach was also used to investigate whether short-term expression of WT hERG1 can elicit a transformed phenotype and to investigate the effect of hERG1b and hERG1/hERG1b co-expression on cellular properties. Finally, CHO cells stably expressing

WT hERG1 channels were utilized to investigate if hERG1 expression conferred any pro-survival advantage to cells under mild and severe hypoxic conditions.

7.1 Technical considerations

A few technical considerations regarding the methodology in the current study are discussed below.

7.1.1 Use of antibiotics in cell culture media

The antibiotics streptomycin and penicillin were added to the culture medium used for maintenance of hERG1-expressing cells in the present study. A concern has been raised that these antibiotics might affect hERG1 channel activity. It has been demonstrated that streptomycin can inhibit several types of ion channels Shen *et al.*, (2003). However, hERG1 current inhibition by penicillin and streptomycin has not been reported. Moreover, hERG1 currents have been routinely recorded from cells maintained in streptomycin/penicillin-containing culture media in numerous studies (e.g. Roy *et al.*, 2008). Nevertheless, a direct measurement of hERG1 currents in the presence and absence of these antibiotics is required to rule this possibility out.

7.1.2 Western blotting

7.1.2.1 Anti-hERG1 antibodies

Two newly purified and previously uncharacterised anti-hERG1 antibodies were used in the present study (Chapter 4, Fig. 4.10). These antibodies were raised against epitopes that have been used by other laboratories (Roti *et al.*, 2002, Zhou *et al.*, 1998), which have been thoroughly tested and characterized. In the current study, we confirmed the specificity of our antibodies in lysates of HEK-hERG cells and WT HEK cells. Blots showed the protein

bands at the expected molecular size for hERG1 protein in lysates of HEK-hERG cells, while these bands were absent WT HEK cells. Although we are confident that our anti-hERG1 antibodies are specific for hERG1 proteins, this could have been confirmed via additional negative controls including performing Western blotting after pre-incubation of antibodies with an excess of control antigens or using lysates from cells in which hERG1 expression was knocked down using selective siRNA against hERG1.

7.1.2.2 Densitometric analysis of Western blots

Quantitative densitometry of Western blots was used to assess relative vinculin/ β -actin (Fig. 3.14) and hERG1b/hERG1 (Fig. 5.8) protein expression. The quantification procedure consists of 3 steps: visualizing reactive bands on an X-ray film using a chemiluminescence development system, image acquisition using a scanner and determination of band optical density using appropriate software. Care was taken to load the minimum amount of protein to avoid saturation of the signal on the film and thus ensure a linear protein concentration-optical density relationship. However, the linearity of detection of protein expression could have been further confirmed using a serial dilution of standard protein to determine the linear dynamic range of this densitometry technique (Bromage *et al.*, 2007).

7.1.3 Normalization to a single reference gene in real time RT PCR

Normalizing the target gene content of RNA samples relative to multiple reference genes rather than to a single reference gene is the most robust method for accurate gene quantification by real time RT PCR (Huggett *et al.*, 2005). However, in the present study, this was not possible due to the large number of clones tested and the resulting economic considerations. Therefore, real time RT PCR was essentially used as a high throughput and

quick method for initial screening of transfected clones. hERG1 expression in positive clones was further confirmed using [³H]-dofetilide binding and Western blotting.

7.2 Extracellular matrix-dependent signalling is important for hERG1-mediated oncogenic effects

I have shown that hERG1-expressing cells exhibited an extracellular matrix (ECM) - dependent transformative activity characterized by a ‘transformed’ cell morphology, cytoskeletal re-organization, changes in vinculin protein content, increased cell migratory activity and a modulation of the migratory phenotype. My study provides some of the first evidence for an involvement of ECM-mediated signalling in the oncogenic effects of hERG1 expression in a heterologous cell system, rather than hERG1-expressing cancer cell-lines, where the observed transformed phenotype has been directly linked to hERG1 expression.

These findings support previous studies suggesting a link between hERG1 and integrin-mediated signalling in tumour cells (Cherubini *et al.*, 2005, Pillozzi *et al.*, 2007). The increased cell motility, polarized cell morphology and directional cell migration observed in hERG1-expressing NIH-3T3 cells grown on fibronectin suggests that hERG1 modulates integrin signalling to regulate the cell motility machinery to induce a migratory/invasive behaviour akin to that seen in cancer cells. In fact, hERG1 expression in primary tumour tissues correlates with an aggressive, highly metastatic phenotype. The level of hERG1 mRNA/protein expression also correlated well with the degree of tumour malignancy (Lastraioli *et al.*, 2004, Masi *et al.*, 2005), and colon cancer cells expressing high levels of hERG1 display enhanced migration through synthetic matrix-coated filters (Lastraioli *et al.*, 2004).

Adhesion of hERG1-expressing cells to fibronectin was also associated with a decrease in the cell content of the cytoskeletal protein vinculin. This may explain the mechanism underlying cytoskeletal rearrangements, increased cell motility and metastasis of hERG1-expressing tumour cells. Highly metastatic melanoma cell-lines exhibit a reduced vinculin expression (Raz *et al.*, 1982, Lifschitz-Mercer *et al.*, 1997). Suppression of vinculin expression in NIH-3T3 cells induces a transformed phenotype similar to that seen in hERG1-expressing cells adhering to fibronectin (Rodriguez Fernandez *et al.*, 1993). Oncogenic transformation and an acquisition of metastatic potential are often associated with loss of focal adhesion structures. v-Src-induced transformation has been shown to reduce the expression of the focal adhesion and vinculin-binding protein, vinexin, and increase cell migration (Umemoto *et al.*, 2009). The mechanism mediating the change in vinculin in hERG1-expressing cells needs further investigation to determine whether it occurs through a reduction in transcription/translation, through acceleration of vinculin degradation, or via both mechanisms.

Understanding the mechanisms of hERG1 modulation of ECM-mediated signalling in cancer cells may be of therapeutic benefit. Several reports suggested “a two-way” interaction between the extracellular matrix and hERG1 channels. Adhesion of neuroblastoma cells and leukaemic FLG 29.1 cells to ECM elicits an increase in hERG1 current density and a membrane hyperpolarization associated with cell differentiation; these effects are mediated through engagement of β 1-integrins, which associate with and activate hERG1 channels (Arcangeli *et al.*, 1993, Arcangeli *et al.*, 1996, Hofmann *et al.*, 2001, Cherubini *et al.*, 2005). Moreover, effectors downstream to integrin signalling including c-Src and members of the Rho-GTPase family can regulate hERG1 activity (Cayabyab *et al.*, 2002, Miranda *et al.*, 2005). On the other hand, hERG1 channel activity appears to be

required for recruitment and activation of integrin downstream signalling proteins, such as Rac1 and focal adhesion kinase (Cherubini *et al.*, 2005), and thus can influence cellular activities regulated through integrin signalling. This speculation needs to be confirmed through appropriate experimental approaches. Most of the suggested hERG1 associations with signalling proteins have been shown by co-immunoprecipitation experiments, which do not prove direct protein-protein interactions since other components of immunoprecipitated multi-protein complexes can link the two protein together. However, if this is the case, then a strategy based on dissociating hERG1 from hERG1- β 1-integrins complexes, possibly by using peptides that compete at the interaction domain(s) which mediate these physical interactions, may provide a novel therapeutic approach that avoids the need to use hERG1 blockers with their associated risk of cardiac arrhythmias (Arcangeli *et al.*, 2009).

The contribution of K^+ channels to cell migration may be mediated by spatially regulated changes in cell volume or membrane potential caused by a polarized channel distribution, or a localized activation of ion channels, which allows a regional change in the migratory machinery of the cell (Reinhardt *et al.*, 1998, Schwab *et al.*, 2006, deHart *et al.*, 2008). Whether these mechanisms are operating in the hERG1-expressing cells investigated in the present study is unknown. Cell polarization, seen in hERG1-expressing cells, may require a localized change in concentration or activation of signalling molecules, such as the phospholipid phosphatidylinositol 3,4,5-trisphosphate and Cdc42 GTPase, which are involved in stabilizing F-actin polymerization at the leading edge and inducing directional cell migration (Wu, 2005).

The present study has been performed using two-dimensional (2D) culture systems. Several studies have shown that results for cell migration experiments differ between 2D and 3D systems. Reduced vinculin expression is associated with increased cell motility on 2D collagen-coated substrates. However, vinculin expression correlates with enhanced cell invasion into 3D collagen matrices (Mierke *et al.*, 2010). Therefore, future studies investigating migration of hERG1-expressing cells in 3D culture systems is likely to be essential to gain a full understanding of mechanisms of cell migration *in vivo* of hERG1-expressing tumour cells, and the possible roles of hERG1 in remodelling of ECM itself during the invasion process. Moreover, it is also important to investigate the cell migratory and invasive mechanisms of hERG1-expressing primary tumour cells. Tumour microenvironment cannot be precisely simulated by *in vitro* cell migration studies. Many components found in the extracellular environment of tumours can modulate hERG1-mediated transformation. For example, the chemokine stromal cell-derived factor-1 (SDF-1) has been shown to enhance hERG1 currents and the hERG1 blocker, E4031, has been reported to impair SDF-1-induced migration of leukaemic cells (Li *et al.*, 2009).

7.3 hERG1 channel conductance and cell-surface localization are necessary for hERG1-induced cell transformation

Results obtained in the present study suggest that cell-surface expression of functional hERG1 channels is important to induce cellular transformation. Stable expression of mutant hERG1 channels that cannot be trafficked to the cell-surface (A561V hERG1), or that are expressed at the cell-surface, but fail to conduct K⁺ ions (G628S hERG1) did not induce a ‘transformed’ phenotype in NIH-3T3 cells. Therefore, the changes in contact inhibition and cell motility behaviours in WT hERG1-expressing NIH-3T3 cells appear to be dependent

on ion flux through the channel and/or the associated hyperpolarization of transmembrane potential. Regulation of cell volume through K^+ efflux has been shown to be important for cell migration (Schwab *et al.*, 1999b) and proliferation (Rouzai-Dubois *et al.*, 1998, Rouzai-Dubois *et al.*, 2000, Rouzai-Dubois *et al.*, 2004). Moreover, a hyperpolarization of membrane potential increases the driving force for Ca^{2+} influx, which plays a central role in the signal transduction mechanisms involved in cell migration (Schwab *et al.*, 1997) and proliferation (Nilius *et al.*, 1992, Nilius *et al.*, 1993). It has been suggested that some of the cellular activities mediated by ion channels are dependent on the gating conformation of the channel rather than the ion flux itself. $K_v1.3$ channels expressed in T lymphocytes and melanoma cells associate with $\beta 1$ -integrins in a conformation-dependent manner, even when the channels are non-conducting (Levite *et al.*, 2000, Artym *et al.*, 2002). EAG-induced oncogenic effects have also been reported to be membrane potential-sensitive and channel conformation-dependent (Hegle *et al.*, 2006). However, it is most likely that G628S hERG1, investigated in the present study, responds to membrane depolarization indistinguishably from WT hERG1 channels. Future investigations are required to determine if hERG1-mediated effects on cell phenotype are dependent purely on ion conductance, or a channel conformation dependency can also be discerned.

hERG1 channel activity has been shown to be crucial for association with $\beta 1$ -integrin, focal adhesion kinase and Rac1 (Cherubini *et al.*, 2005), the type 1 VEGF receptor (Pillozzi *et al.*, 2007) and the CXCR4 chemokine receptor (Pillozzi *et al.*, 2010). An interesting possibility is that ion channel effects on cell signalling are not always mediated through, or not entirely dependent on, ion flux itself, but through modulation of V_{REST} and induction of a voltage-dependent conformational coupling with other membrane receptors and/or downstream signalling effectors. We investigated the effects of independently regulating

resting potential and hERG1 channel open probability (P_0) on ECM-mediated signalling in hERG1-expressing cells by using high $[K^+]_o$ (20 mM), the hERG1 channel activator, ICA-105574, or a combination of these treatments. The effects of these treatments on hERG1 currents and V_{REST} were tested in *Xenopus* oocytes expressing WT hERG1 channels. Elevating $[K^+]_o$ to 20 mM produced a modest membrane depolarization and opened hERG1 channels, whereas ICA-105574 enhanced hERG1 P_0 , causing a hyperpolarization. Combining ICA-105574 and elevated $[K^+]_o$ had little effect on resting potential, but caused a substantial increase of hERG1 P_0 . However, none of these manipulations influenced the migration of hERG1-expressing cells on fibronectin. It is possible that these manipulations need to be applied longer-term in order to affect integrin-dependent cellular activities. Whether hERG1 channel association with transmembrane and cytoplasmic proteins occurs in a voltage-dependent or voltage-independent manner remains to be determined.

An involvement of hERG1 in direct interactions with other signalling proteins in hERG1-mediated oncogenic effects has been previously suggested (Cherubini *et al.*, 2005, Pillozzi *et al.*, 2007, Pillozzi *et al.*, 2010). This would infer that removal of hERG1 channels from the cell membrane should impair the transforming behaviour seen on hERG1 expression. Some of the results in the present study support this idea. Stable expression of trafficking-deficient A561V hERG1 in NIH-3T3 cells did not cause a transforming behaviour. Moreover, the hERG1 trafficking inhibitor pentamidine inhibited fibronectin-dependent migration of hERG1-expressing cells. However, another compound, arsenic trioxide, which should also impair trafficking of hERG1 to the cell-surface, did not produce this effect. This discrepancy may be due to an ineffective inhibition of hERG1 trafficking by the later compound being achieved. Future work investigating the effect of both compounds on cell-surface hERG1 expression in the NIH-16 and NIH-50 cell-lines by cell

fractionation and Western blotting may be warranted. It is also difficult to infer if hERG1 mediates some of its oncogenic effect via direct protein-protein interactions since the above-mentioned interventions interfering with hERG1 cell-surface expression, would also inevitably inhibit hERG1 conduction.

An interesting and important finding in this project was that long-term inhibition of hERG1 current may be necessary to impair hERG1-induced cell transformation. Acute application of dofetilide (at a concentration of 1 μM) failed to affect cell motility of hERG1-expressing cells grown on fibronectin, whereas the chronic use of dofetilide (at 100 nM) for 14 days was able to inhibit fibronectin-dependent cell migration of hERG1-expressing cells and restore normal fibroblastic morphology. This might explain previous findings showing that hERG1 channel blockers acutely applied at concentrations that should fully block hERG channel conductance either failed to inhibit, or only partially impaired hERG1-mediated effects (Smith *et al.*, 2002a, Pier, 2007). The reason for a requirement for such a prolonged exposure time to dofetilide to observe impaired cell motility of hERG1-expressing cells is unclear. A possible explanation is that hERG1-induced cellular transformation is associated with changes in expression levels of key signalling intermediates, and therefore sufficient time is needed to restore expression profiles of signalling intermediates to those found in normal cells.

hERG1 channels may represent a therapeutic target for future cancer treatments. A blockade of hERG1 channel function, or a reduction in hERG1 cell-surface expression may be of therapeutic benefit. A major concern with blockade of hERG1 channels as a therapeutic approach for treatment of cancer is the confounding blockade of channels within cardiac tissues, which may induce serious cardiac adverse effects. However, chronic

administration of therapeutically-tolerated concentrations of hERG1 blockers may interfere with tumour progression without accompanying drug-inducing long QT syndrome. Future studies are required to investigate if these results can be extrapolated to hERG1-expressing primary tumours. The activity of ion channels in primary tumour cells may vary from that seen in cultured cells (Kunzelmann, 2005). Moreover, the activity/expression of ion channels may be differentially regulated throughout the progression of tumour or even through cell cycle.

7.4 Co-expression of hERG1 and hERG1b enhances cell proliferation

Another set of experiments reported here have provided preliminary evidence suggesting that hERG channels incorporating hERG1b subunits may play roles in tumour cell proliferation. NIH-3T3 cells transiently co-transfected with hERG1 and hERG1b exhibited enhanced cell proliferation relative to cells transfected either subunit alone. Although my findings need to be confirmed, they are supported by the observation that hERG1 channel blockers impair cell proliferation in tumour cells that express hERG1b together with hERG1, such as neuroblastoma (Crociani *et al.*, 2003) and leukaemia (Pillozzi *et al.*, 2002, Smith *et al.*, 2002a, Pillozzi *et al.*, 2007) cell-types. hERG1b may modify biophysical channel properties differentially to regulate the resting membrane potential in a way that favours cell proliferation. Currents elicited by hERG1+hERG1b heteromeric channels deactivate faster than hERG1 homomeric channels and therefore may contribute to a more depolarized resting membrane potential, which is thought to be essential for DNA synthesis and cell proliferation (Arcangeli *et al.*, 1995). This hypothesis may be supported by an observed up-regulation of the hERG1b subunit in neuroblastoma cells during S phase (Crociani *et al.*, 2003). Moreover, incorporation of the hERG1b subunit may modulate

signalling pathways downstream of hERG channels. A full-length *N*-terminus of hERG1 may be necessary for association with β 1-integrins, since hERG1b subunits fail to co-immunoprecipitate with β 1-integrins (Cherubini *et al.*, 2005) and integrin signalling can fulfil roles in cell proliferation (Zhu *et al.*, 1995). hERG1b-containing channels are also differentially regulated by intracellular signalling molecules, including cyclic GMP, thyrotropin-releasing hormone (TRH) and cell acidosis (Kirchberger *et al.*, 2006, Mewe *et al.*, 2010, Du *et al.*, 2011). Therefore, it is possible that hERG1b expression regulates hERG1-mediated signalling and may facilitate hERG1-mediated transformation.

7.5 What is the potential contribution of hERG1 to tumour progression?

hERG1 channels are up-regulated in many primary tumours including leukaemia (Smith *et al.*, 2002, Pillozzi *et al.*, 2002), glioma (Masi *et al.*, 2005), neuroblastoma (Guasti *et al.*, 2005) and endometrial (Cherubini *et al.*, 2000), colon (Lastraioli *et al.*, 2004) and gastric (Shao *et al.*, 2005) cancers. This broad expression in different cancer cell-types and lack of hERG1-tumour type correlation may suggest that hERG1 overexpression is not the main reason for tumour initiation. Instead, it may be possible that tumour cells up-regulate hERG1 expression (or modulate channel activity) to fulfil specific functional roles and contribute to certain stages of neoplastic progression. Supporting this notion, expression of hERG1 in fibroblast cells only induced a partial cell transformation (Pier, 2007). In this section, I will discuss possible contributions of hERG1, based on the findings of the present study and current literature, to the hallmarks of cancer (Fig. 7.1A).

7.5.1 hERG1 and tumour cell proliferation

The role of hERG1 in tumour cell proliferation is controversial. There is some evidence supporting a growth-enhancing effect of hERG1 expression in tumour cells. The voltage-

dependence of activation and inactivation of hERG1 currents varies throughout the cell cycle (Arcangeli *et al.*, 1995, Meyer *et al.*, 1998). hERG1 expression in tumour cell-lines was found to enhance proliferation induced by low TNF α concentrations (Wang *et al.*, 2002a). Moreover, block of hERG1 currents in leukaemic FLG29.1, gastric cancer and neuroblastoma SH-SY5Y cells caused a block of cell cycle at G1 phase (Pillozzi *et al.*, 2002, Shao *et al.*, 2005, Zhao *et al.*, 2008). On the other hand, stable hERG1 expression in NIH-3T3 cells did not affect proliferation (Pier, 2007). Moreover, although hERG1 was up-regulated in primary leukaemic cells and haematopoietic cell-lines, hERG1 expression was not detected in proliferating non cancerous lymphocytes, indicating that hERG1 expression was not related to proliferation *per se* (Smith *et al.*, 2002). The antiproliferative effects of hERG1 blockers were only observed at concentrations that were many-fold higher than those required to fully block hERG1 currents (e.g. Pillozzi *et al.*, 2002).

In the present study, transient co-expression of hERG1/hERG1b in NIH -3T3 cells enhanced cell proliferation, compared to cells transiently transfected with either isoform alone (Chapter 5). This may suggest that hERG1 can exert a pro-proliferative role only in cells co-expressing the hERG1b isoform. Indeed, the anti-proliferative effect of hERG1 blockers were mostly observed on leukaemia and neuroblastoma cells, which express both hERG1 and hERG1b.

7.5.2 hERG1 and evasion of anti-growth signals

Cancer cells circumvent programs that limit cell growth and proliferation in normal cell populations. An example of this acquired trait is the ability to abolish contact inhibition of growth. hERG1 expression in NIH-3T3 cells conferred the ability to overgrow from a confluent cell monolayer, a property that was not observed in cells transfected with an

empty vector (Pier, 2007). The overgrowth capacity of hERG1-expressing cells seems to be independent of integrin-signalling (Chapter 3). Future investigations are required to explore the mechanistic basis of this transformed behaviour including elucidating mechanisms underlying E-cadherin mediated cell-cell adhesion in hERG1-expressing cells.

7.5.3 hERG1 and resistance to cell death

Cancer cells are subjected to several physiological stresses during tumour progression, such as DNA damage and hypoxia, that can trigger apoptosis and block cancer development. Whether hERG1 channels exhibit pro- or anti-apoptotic effects in cancer cells is not clear. hERG1 conductance facilitates apoptosis induced by high concentrations of TNF α or H₂O₂ in hERG1-expressing tumour cell-lines, as compared to tumour cell-lines that do not express hERG1 (Wang *et al.*, 2002a). Moreover, hERG1 expression did not affect the survival of CHO cells at mild or severe levels of hypoxia (the present study, Chapter 6). In contrast, it has been suggested that hERG1 might contribute to protection against drug-induced apoptosis in childhood Acute B Lymphoblastic Leukaemia (B-ALL) via formation of a hERG1- β 1-integrin-CXCR4 complex. hERG1 channel blockade increased the chemosensitivity of these cells to corticosteroids and induced apoptotic cell death (Pillozzi *et al.*, 2010). This paradox may be related to the cellular context and the stage of cancer progression and thus hERG1 channels may play pro-apoptotic or anti-apoptotic effects in different stages of cancer progression.

7.5.4 hERG1 and tumour angiogenesis

hERG1 channel activity may contribute to malignancy through increasing vascular endothelial growth factor (VEGF) secretion and stimulation of neo-angiogenesis. Inhibition

of hERG1 channel activity reduces both VEGF mRNA expression and secretion in gliomas and AML (Masi *et al.*, 2005, Pillozzi *et al.*, 2007).

7.5.5 hERG1 and invasion/metastasis

hERG1 expression in epithelial cells enhances cell motility (Pier, 2007, Lastraioli *et al.*, 2004). Moreover, hERG1-expressing NIH-3T3 cells exhibited an ECM-dependent transformative activity characterized by altered cell morphology, cytoskeletal reorganization and a modulation of the migratory phenotype (the present study, Chapter 3). These findings support previous reports suggesting hERG1 involvement in invasion and metastasis via formation of integrin-containing signalling complexes triggered by cell adhesion. These macromolecular complexes regulate downstream signalling to enhance cancer cell migration, invasion and metastasis. In AML cells, a signalling complex comprising hERG1, β 1-integrin and VEGF-R1 resulted in more efficient migration through the peripheral circulation to extra-medullary sites in immunodeficient mice (Pillozzi *et al.*, 2007). Moreover, the ability of hERG1 expressing NIH-3T3 cells to overgrow a confluent cell monolayer in saturation density assays (Pier, 2007) may be mediated via down-regulation of E-cadherin, a key cell-cell adhesion molecule, which is a well-known suppressor of invasion and metastasis (Hanahan *et al.*, 2011).

7.5.6 hERG1 and EAG channel expression during cancer development

EAG is a well-established oncogene. Expression of EAG in CHO cells primarily enhanced proliferation and substratum/serum-independence of growth, properties that are required for tumor progression in early cancer stages (Fig. 7.2B). On the other hand, current evidence (see above) suggests that the oncogenic effects of hERG1 are more restricted to late stages of cancer progression (Fig. 7.2B). In these phases, hERG1 expression seems to enhance cell

motility, contribute to invasiveness and metastasis and protect against cytotoxic agents. These effects seem to be mediated via formation of signalling complexes that comprise integrins and other growth factor or chemokine receptors (Pillozzi *et al.*, 2007, Pillozzi *et al.*, 2010).

7.5.7 hERG1 and control of membrane potential of tumour cells.

In neuroblastoma cells, the voltage dependence of activation of hERG1 varies during the cell cycle and correlates with variations to resting membrane potential. This suggests that hERG1 is a key determinant of resting membrane potential of these cells. Interestingly, normal parental neural cells did not express hERG1 currents and only expressed inward rectifier-like K^+ currents. The shift from native K_{ir} currents to hERG1 currents after neoplastic transformation may contribute to the depolarized membrane potential of cancer cells, which is thought to be important for the proliferation of cycling cells (Binggeli *et al.*, 1980, Arcangeli *et al.*, 1995). The hERG1 window current resulting from the overlap between steady-state activation and inactivation curves produces a significant current at a V_m around -40 mV, a value close to resting membrane potential of tumours cells. Moreover, hERG1 currents have a limited hyperpolarizing effect (when compared to inward rectifier-like K^+ currents), since hERG1 channels are deactivated at membrane potentials negative to -60 mV (Bianchi *et al.*, 1998, Arcangeli *et al.*, 1995).

Bibliography

- Abbott, G. W., Sesti, F., Splawski, I., Buck, M. E., Lehmann, M. H., Timothy, K. W., Keating, M. T., Goldstein, S. A., 1999. MiRP1 forms IKr potassium channels with HERG and is associated with cardiac arrhythmia. *Cell*, **97**, 175-187.
- Abdul, M. & Hoosein, N., 2002. Expression and activity of potassium ion channels in human prostate cancer. *Cancer Lett*, **186**, 99-105.
- Achison, M. & Hupp, T. R., 2003. Hypoxia attenuates the p53 response to cellular damage. *Oncogene*, **22**, 3431-3440.
- Afrasiabi, E., Hietamaki, M., Viitanen, T., Sukumaran, P., Bergelin, N., Tornquist, K., 2010. Expression and significance of HERG (KCNH2) potassium channels in the regulation of MDA-MB-435S melanoma cell proliferation and migration. *Cell Signal*, **22**, 57-64.
- Agochiya, M., Brunton, V. G., Owens, D. W., Parkinson, E. K., Paraskeva, C., Keith, W. N., Frame, M. C., 1999. Increased dosage and amplification of the focal adhesion kinase gene in human cancer cells. *Oncogene*, **18**, 5646-5653.
- Akbarali, H. I., Thatte, H., He, X. D., Giles, W. R., Goyal, R. K., 1999. Role of HERG-like K(+) currents in opossum esophageal circular smooth muscle. *Am J Physiol*, **277**, C1284-1290.
- Akhavan, A., Atanasiu, R., Noguchi, T., Han, W., Holder, N., Shrier, A., 2005. Identification of the cyclic-nucleotide-binding domain as a conserved determinant of ion-channel cell-surface localization. *J Cell Sci*, **118**, 2803-2812.
- Alfonso-De Matte, M. Y., Moses-Soto, H., Kruk, P. A., 2002. Calcium-mediated telomerase activity in ovarian epithelial cells. *Arch Biochem Biophys*, **399**, 239-244.
- An, W. G., Kanekal, M., Simon, M. C., Maltepe, E., Blagosklonny, M. V., Neckers, L. M., 1998. Stabilization of wild-type p53 by hypoxia-inducible factor 1alpha. *Nature*, **392**, 405-408.
- Anantharam, A., Lewis, A., Panaghie, G., Gordon, E., McCrossan, Z. A., Lerner, D. J., Abbott, G. W., 2003. RNA interference reveals that endogenous *Xenopus* MinK-related peptides govern mammalian K⁺ channel function in oocyte expression studies. *J Biol Chem*, **278**, 11739-11745.
- Anderson, C. L., Delisle, B. P., Anson, B. D., Kilby, J. A., Will, M. L., Tester, D. J., Gong, Q., Zhou, Z., Ackerman, M. J., January, C. T., 2006. Most LQT2 mutations reduce Kv11.1 (hERG) current by a class 2 (trafficking-deficient) mechanism. *Circulation*, **113**, 365-373.
- Anderson, L. & Seilhamer, J., 1997. A comparison of selected mRNA and protein abundances in human liver. *Electrophoresis*, **18**, 533-537.
- Arcangeli, A. & Becchetti, A., 2006. Complex functional interaction between integrin receptors and ion channels. *Trends Cell Biol*, **16**, 631-639.
- Arcangeli, A., Becchetti, A., Mannini, A., Mugnai, G., De Filippi, P., Tarone, G., Del Bene, M. R., Barletta, E., Wanke, E., Olivotto, M., 1993. Integrin-mediated neurite outgrowth in neuroblastoma cells depends on the activation of potassium channels. *J Cell Biol*, **122**, 1131-1143.

- Arcangeli, A., Bianchi, L., Becchetti, A., Faravelli, L., Coronello, M., Mini, E., Olivotto, M., Wanke, E., 1995. A novel inward-rectifying K⁺ current with a cell-cycle dependence governs the resting potential of mammalian neuroblastoma cells. *Journal of Physiology-London*, **489**, 455-471.
- Arcangeli, A., Crociani, O., Lastraioli, E., Masi, A., Pillozzi, S., Becchetti, A., 2009. Targeting ion channels in cancer: a novel frontier in antineoplastic therapy. *Curr Med Chem*, **16**, 66-93.
- Arcangeli, A., Faravelli, L., Bianchi, L., Rosati, B., Gritti, A., Vescovi, A., Wanke, E., Olivotto, M., 1996. Soluble or bound laminin elicit in human neuroblastoma cells short- or long-term potentiation of a K⁺ inwardly rectifying current: relevance to neuritogenesis. *Cell Adhes Commun*, **4**, 369-385.
- Arcangeli, A., Rosati, B., Cherubini, A., Crociani, O., Fontana, L., Passani, B., Wanke, E., Olivotto, M., 1998. Long-term exposure to retinoic acid induces the expression of IRK1 channels in HERG channel-endowed neuroblastoma cells. *Biochem Biophys Res Commun*, **244**, 706-711.
- Arcangeli, A., Rosati, B., Cherubini, A., Crociani, O., Fontana, L., Ziller, C., Wanke, E., Olivotto, M., 1997. HERG- and IRK-like inward rectifier currents are sequentially expressed during neuronal development of neural crest cells and their derivatives. *Eur J Neurosci*, **9**, 2596-2604.
- Arcangeli, A., Rosati, B., Crociani, O., Cherubini, A., Fontana, L., Passani, B., Wanke, E., Olivotto, M., 1999. Modulation of HERG current and herg gene expression during retinoic acid treatment of human neuroblastoma cells: Potentiating effects of BDNF. *Journal of Neurobiology*, **40**, 214-225.
- Artandi, S. E. & DePinho, R. A., 2010. Telomeres and telomerase in cancer. *Carcinogenesis*, **31**, 9-18.
- Artym, V. V. & Petty, H. R., 2002. Molecular proximity of Kv1.3 voltage-gated potassium channels and beta(1)-integrins on the plasma membrane of melanoma cells: effects of cell adherence and channel blockers. *J Gen Physiol*, **120**, 29-37.
- Atkuri, K. R., Herzenberg, L. A., Niemi, A. K., Cowan, T., 2007. Importance of culturing primary lymphocytes at physiological oxygen levels. *Proc Natl Acad Sci U S A*, **104**, 4547-4552.
- Babij, P., Askew, G. R., Nieuwenhuijsen, B., Su, C. M., Bridal, T. R., Jow, B., Argentieri, T. M., Kulik, J., DeGennaro, L. J., Spinelli, W., Colatsky, T. J., 1998. Inhibition of cardiac delayed rectifier K⁺ current by overexpression of the long-QT syndrome HERG G628S mutation in transgenic mice. *Circ Res*, **83**, 668-678.
- Bauer, C. K., 1998. The erg inwardly rectifying K⁺ current and its modulation by thyrotrophin-releasing hormone in giant clonal rat anterior pituitary cells. *Journal of Physiology-London*, **510**, 63-70.
- Bauer, C. K., Wulfsen, I., Schafer, R., Glassmeier, G., Wimmers, S., Flitsch, J., Ludecke, D. K., Schwarz, J. R., 2003. HERG K(+) currents in human prolactin-secreting adenoma cells. *Pflugers Arch*, **445**, 589-600.
- Beacham, D. A., Amatangelo, M. D., Cukierman, E., 2007. Preparation of extracellular matrices produced by cultured and primary fibroblasts. *Curr Protoc Cell Biol*, **Chapter 10**, Unit 10 19.
- Berkefeld, H., Fakler, B., Schulte, U., 2010. Ca²⁺-activated K⁺ channels: from protein complexes to function. *Physiol Rev*, **90**, 1437-1459.

- Bhattacharyya, M. L., Sarker, S., Mull, K. P., Debnam, Q., 1997. Clofilium-induced block of delayed rectifier type K⁺ current in atrial tumor cells (AT-1 cells). *J Mol Cell Cardiol*, **29**, 301-307.
- Bianchi, L., Wible, B., Arcangeli, A., Taglialatela, M., Morra, F., Castaldo, P., Crociani, O., Rosati, B., Faravelli, L., Olivotto, M., Wanke, E., 1998. hERG encodes a K⁺ current highly conserved in tumors of different histogenesis: A selective advantage for cancer cells? *Cancer Research*, **58**, 815-822.
- Bill, H. M., Knudsen, B., Moores, S. L., Muthuswamy, S. K., Rao, V. R., Brugge, J. S., Miranti, C. K., 2004. Epidermal growth factor receptor-dependent regulation of integrin-mediated signaling and cell cycle entry in epithelial cells. *Mol Cell Biol*, **24**, 8586-8599.
- Binggeli, R. & Cameron, I. L., 1980. Cellular potentials of normal and cancerous fibroblasts and hepatocytes. *Cancer Res*, **40**, 1830-1835.
- Binggeli, R. & Weinstein, R. C., 1986. Membrane potentials and sodium channels: hypotheses for growth regulation and cancer formation based on changes in sodium channels and gap junctions. *J Theor Biol*, **123**, 377-401.
- Blackiston, D. J., McLaughlin, K. A., Levin, M., 2009. Bioelectric controls of cell proliferation: ion channels, membrane voltage and the cell cycle. *Cell Cycle*, **8**, 3519-3528.
- Bonnet, S., Archer, S. L., Allalunis-Turner, J., Haromy, A., Beaulieu, C., Thompson, R., Lee, C. T., Lopaschuk, G. D., Puttagunta, L., Harry, G., Hashimoto, K., Porter, C. J., Andrade, M. A., Thebaud, B., Michelakis, E. D., 2007. A mitochondria-K⁺ channel axis is suppressed in cancer and its normalization promotes apoptosis and inhibits cancer growth. *Cancer Cell*, **11**, 37-51.
- Borowiec, A. S., Hague, F., Harir, N., Guenin, S., Guerineau, F., Gouilleux, F., Roudbaraki, M., Lassoued, K., Ouadid-Ahidouch, H., 2007. IGF-1 activates hEAG K(+) channels through an Akt-dependent signaling pathway in breast cancer cells: role in cell proliferation. *J Cell Physiol*, **212**, 690-701.
- Brackenbury, W. J., Davis, T. H., Chen, C., Slat, E. A., Detrow, M. J., Dickendesher, T. L., Ranscht, B., Isom, L. L., 2008. Voltage-gated Na⁺ channel beta1 subunit-mediated neurite outgrowth requires Fyn kinase and contributes to postnatal CNS development in vivo. *J Neurosci*, **28**, 3246-3256.
- Braga, V. M., Machesky, L. M., Hall, A., Hotchin, N. A., 1997. The small GTPases Rho and Rac are required for the establishment of cadherin-dependent cell-cell contacts. *J Cell Biol*, **137**, 1421-1431.
- Brakebusch, C. & Fassler, R., 2003. The integrin-actin connection, an eternal love affair. *Embo J*, **22**, 2324-2333.
- Brelidze, T. I., Carlson, A. E., Zagotta, W. N., 2009. Absence of direct cyclic nucleotide modulation of mEAG1 and hERG1 channels revealed with fluorescence and electrophysiological methods. *J Biol Chem*, **284**, 27989-27997.
- Bromage, E. S. & Kaattari, S. L., 2007. Simultaneous quantitative analysis of multiple protein species within a single sample using standard scanning densitometry. *J Immunol Methods*, **323**, 109-113.

- Brugada, R., Hong, K., Dumaine, R., Cordeiro, J., Gaita, F., Borggrefe, M., Menendez, T. M., Brugada, J., Pollevick, G. D., Wolpert, C., Burashnikov, E., Matsuo, K., Wu, Y. S., Guerschicoff, A., Bianchi, F., Giustetto, C., Schimpf, R., Brugada, P., Antzelevitch, C., 2004. Sudden death associated with short-QT syndrome linked to mutations in HERG. *Circulation*, **109**, 30-35.
- Bruggemann, A., Stuhmer, W., Pardo, L. A., 1997. Mitosis-promoting factor-mediated suppression of a cloned delayed rectifier potassium channel expressed in *Xenopus* oocytes. *Proc Natl Acad Sci U S A*, **94**, 537-542.
- Bruick, R. K., 2000. Expression of the gene encoding the proapoptotic Nip3 protein is induced by hypoxia. *Proc Natl Acad Sci U S A*, **97**, 9082-9087.
- Brundage, R. A., Fogarty, K. E., Tuft, R. A., Fay, F. S., 1991. Calcium gradients underlying polarization and chemotaxis of eosinophils. *Science*, **254**, 703-706.
- Calabresi, P., Pisani, A., Mercuri, N. B., Bernardi, G., 1995. On the mechanisms underlying hypoxia-induced membrane depolarization in striatal neurons. *Brain*, **118 (Pt 4)**, 1027-1038.
- Camacho, J., Sanchez, A., Stuhmer, W., Pardo, L. A., 2000. Cytoskeletal interactions determine the electrophysiological properties of human EAG potassium channels. *Pflugers Archiv-European Journal of Physiology*, **441**, 167-174.
- Cavarra, M. S., del Monaco, S. M., Assef, Y. A., Ibarra, C., Kotsias, B. A., 2007. HERG1 currents in native K562 leukemic cells. *J Membr Biol*, **219**, 49-61.
- Cayabyab, F. S. & Schlichter, L. C., 2002. Regulation of an ERG K⁺ current by Src tyrosine kinase. *Journal of Biological Chemistry*, **277**, 13673-13681.
- Chadwick, C. C., Ezrin, A. M., O'Connor, B., Volberg, W. A., Smith, D. I., Wedge, K. J., Hill, R. J., Briggs, G. M., Pagani, E. D., Silver, P. J., et al., 1993. Identification of a specific radioligand for the cardiac rapidly activating delayed rectifier K⁺ channel. *Circ Res*, **72**, 707-714.
- Chantome, A., Girault, A., Potier, M., Collin, C., Vaudin, P., Pages, J. C., Vandier, C., Joulin, V., 2009. KCa2.3 channel-dependent hyperpolarization increases melanoma cell motility. *Exp Cell Res*, **315**, 3620-3630.
- Chen, J., Seebohm, G., Sanguinetti, M. C., 2002. Position of aromatic residues in the S6 domain, not inactivation, dictates cisapride sensitivity of HERG and eag potassium channels. *Proc Natl Acad Sci U S A*, **99**, 12461-12466.
- Chen, S. Z., Jiang, M., Zhen, Y. S., 2005a. [Correlation of HERG K⁺ channel protein expression to chemosensitivity of tumor cells to doxorubicin and its modulation by erythromycin]. *Ai Zheng*, **24**, 924-929.
- Chen, S. Z., Jiang, M., Zhen, Y. S., 2005b. hERG K⁺ channel expression-related chemosensitivity in cancer cells and its modulation by erythromycin. *Cancer Chemothererapy and Pharmacology*, **56**, 212-220.
- Cheng, Y. & Prusoff, W. H., 1973. Relationship between the inhibition constant (K₁) and the concentration of inhibitor which causes 50 per cent inhibition (I₅₀) of an enzymatic reaction. *Biochem Pharmacol*, **22**, 3099-3108.

- Cherubini, A., Hofmann, G., Pillozzi, S., Guasti, L., Crociani, O., Cilia, E., Di Stefano, P., Degani, S., Balzi, M., Olivotto, M., Wanke, E., Becchetti, A., Defilippi, P., Wymore, R., Arcangeli, A., 2005. Human ether-a-go-go-related gene 1 channels are physically linked to beta(1) integrins and modulate adhesion-dependent signaling. *Molecular Biology of the Cell*, **16**, 2972-2983.
- Cherubini, A., Pillozzi, S., Hofmann, G., Crociani, O., Guasti, L., Lastraioli, E., Polvani, S., Masi, A., Becchetti, A., Wanke, E., Olivotto, M., Arcangeli, A., 2002. HERG K⁺ channels and beta1 integrins interact through the assembly of a macromolecular complex. *Ann N Y Acad Sci*, **973**, 559-561.
- Cherubini, A., Taddei, G. L., Crociani, O., Paglierani, M., Buccoliero, A. M., Fontana, L., Noci, I., Borri, P., Borrani, E., Giachi, M., Becchetti, A., Rosati, B., Wanke, E., Olivotto, M., Arcangeli, A., 2000. hERG potassium channels are more frequently expressed in human endometrial cancer as compared to non-cancerous endometrium. *British Journal of Cancer*, **83**, 1722-1729.
- Chiesa, N., Rosati, B., Arcangeli, A., Olivotto, M., Wanke, E., 1997. A novel role for hERG K⁺ channels: spike-frequency adaptation. *Journal of Physiology-London*, **501 (Pt 2)**, 313-318.
- Chin, L. S., Park, C. C., Zitnay, K. M., Sinha, M., DiPatri, A. J., Jr., Perillan, P., Simard, J. M., 1997. 4-Aminopyridine causes apoptosis and blocks an outward rectifier K⁺ channel in malignant astrocytoma cell lines. *J Neurosci Res*, **48**, 122-127.
- Choe, S., 2002. Potassium channel structures. *Nat Rev Neurosci*, **3**, 115-121.
- Clarke, C. E., Hill, A. P., Zhao, J., Kondo, M., Subbiah, R. N., Campbell, T. J., Vandenberg, J. I., 2006. Effect of S5P alpha-helix charge mutants on inactivation of hERG K⁺ channels. *J Physiol*, **573**, 291-304.
- Claycomb, W. C., Lanson, N. A., Jr., Stallworth, B. S., Egeland, D. B., Delcarpio, J. B., Bahinski, A., Izzo, N. J., Jr., 1998. HL-1 cells: a cardiac muscle cell line that contracts and retains phenotypic characteristics of the adult cardiomyocyte. *Proc Natl Acad Sci U S A*, **95**, 2979-2984.
- Coghlin, C. & Murray, G. I., 2010. Current and emerging concepts in tumour metastasis. *J Pathol*, **222**, 1-15.
- Coll, J. L., Ben-Ze'ev, A., Ezzell, R. M., Rodriguez Fernandez, J. L., Baribault, H., Oshima, R. G., Adamson, E. D., 1995. Targeted disruption of vinculin genes in F9 and embryonic stem cells changes cell morphology, adhesion, and locomotion. *Proc Natl Acad Sci U S A*, **92**, 9161-9165.
- Coppolino, M. G. & Dedhar, S., 2000. Bi-directional signal transduction by integrin receptors. *Int J Biochem Cell Biol*, **32**, 171-188.
- Cordes, J. S., Sun, Z., Lloyd, D. B., Bradley, J. A., Opsahl, A. C., Tengowski, M. W., Chen, X., Zhou, J., 2005. Pentamidine reduces hERG expression to prolong the QT interval. *British Journal of Pharmacology*, **145**, 15-23.
- Crociani, O., Cherubini, A., Piccini, E., Polvani, S., Costa, L., Fontana, L., Hofmann, G., Rosati, B., Wanke, E., Olivotto, M., Arcangeli, A., 2000. erg gene(s) expression during development of the nervous and muscular system of quail embryos. *Mechanisms of Development*, **95**, 239-243.

- Crociani, O., Guasti, L., Balzi, M., Becchetti, A., Wanke, E., Olivotto, M., Wymore, R. S., Arcangeli, A., 2003. Cell cycle-dependent expression of hERG1 and hERG1B isoforms in tumor cells. *Journal of Biological Chemistry*, **278**, 2947-2955.
- Cui, J., Melman, Y., Palma, E., Fishman, G. I., McDonald, T. V., 2000. Cyclic AMP regulates the HERG K(+) channel by dual pathways. *Curr Biol*, **10**, 671-674.
- Curran, M. E., Splawski, I., Timothy, K. W., Vincent, G. M., Green, E. D., Keating, M. T., 1995. A molecular basis for cardiac arrhythmia: HERG mutations cause long QT syndrome. *Cell*, **80**, 795-803.
- Dalton, S. L., Scharf, E., Briesewitz, R., Marcantonio, E. E., Assoian, R. K., 1995. Cell adhesion to extracellular matrix regulates the life cycle of integrins. *Mol Biol Cell*, **6**, 1781-1791.
- Dartsch, P. C., Ritter, M., Haussinger, D., Lang, F., 1994. Cytoskeletal reorganization in NIH 3T3 fibroblasts expressing the ras oncogene. *European Journal of Cell Biology*, **63**, 316-325.
- deHart, G. W., Jin, T., McCloskey, D. E., Pegg, A. E., Sheppard, D., 2008. The alpha9beta1 integrin enhances cell migration by polyamine-mediated modulation of an inward-rectifier potassium channel. *Proc Natl Acad Sci U S A*, **105**, 7188-7193.
- Desgrosellier, J. S. & Cheresch, D. A., 2010. Integrins in cancer: biological implications and therapeutic opportunities. *Nat Rev Cancer*, **10**, 9-22.
- Ding, X. W., Luo, H. S., Luo, B., Xu, D. Q., Gao, S., 2008. Overexpression of hERG1 in resected esophageal squamous cell carcinomas: a marker for poor prognosis. *J Surg Oncol*, **97**, 57-62.
- Ding, X. W., Yang, W. B., Gao, S., Wang, W., Li, Z., Hu, W. M., Li, J. J., Luo, H. S., 2009. Prognostic significance of hERG1 expression in gastric cancer. *Dig Dis Sci*, **55**, 1004-1010.
- Dolderer, J. H., Schuldes, H., Bockhorn, H., Altmannsberger, M., Lambers, C., von Zabern, D., Jonas, D., Schwegler, H., Linke, R., Schroder, U. H., 2009. HERG1 gene expression as a specific tumor marker in colorectal tissues. *Eur J Surg Oncol*, **36**, 72-77.
- Dolmetsch, R. E., Pajvani, U., Fife, K., Spotts, J. M., Greenberg, M. E., 2001. Signaling to the nucleus by an L-type calcium channel-calmodulin complex through the MAP kinase pathway. *Science*, **294**, 333-339.
- Dong, C., Zhu, S., Yoon, W., Wang, T., Alvarez, R. J., Goldschmidt-Clermont, P. J., 2001. Upregulation of PAI-1 is mediated through TGF beta /SMAD pathway in transplant arteriopathy. *J Heart Lung Transplant*, **20**, 219.
- Downie, B. R., Sanchez, A., Knotgen, H., Contreras-Jurado, C., Gymnopoulos, M., Weber, C., Stuhmer, W., Pardo, L. A., 2008. Eag1 expression interferes with hypoxia homeostasis and induces angiogenesis in tumors. *J Biol Chem*, **283**, 36234-36240.
- Doyle, A., Marganski, W., Lee, J., 2004. Calcium transients induce spatially coordinated increases in traction force during the movement of fish keratocytes. *J Cell Sci*, **117**, 2203-2214.

- Doyle, D. A., Morais Cabral, J., Pfuetzner, R. A., Kuo, A., Gulbis, J. M., Cohen, S. L., Chait, B. T., MacKinnon, R., 1998. The structure of the potassium channel: molecular basis of K⁺ conduction and selectivity. *Science*, **280**, 69-77.
- Draheim, H. J., Repp, H., Dreyer, F., 1995. Src-transformation of mouse fibroblasts induces a Ca²⁺-activated K⁺ current without changing the T-type Ca²⁺ current. *Biochim Biophys Acta*, **1269**, 57-63.
- Du, C. Y., El Harchi, A., McPate, M. J., Orchard, C. H., Hancox, J. C., 2011. Enhanced inhibitory effect of acidosis on hERG potassium channels that incorporate the hERG1b isoform. *Biochem Biophys Res Commun*, **405**, 222-227.
- Dubinsky, J. M., Kristal, B. S., Elizondo-Fournier, M., 1995. An obligate role for oxygen in the early stages of glutamate-induced, delayed neuronal death. *J Neurosci*, **15**, 7071-7078.
- Dubois, J. M. & Rouzair-Dubois, B., 2004. The influence of cell volume changes on tumour cell proliferation. *European Biophysical Journal*, **33**, 227-232. .
- Duesberg, P. & Li, R., 2003. Multistep carcinogenesis: a chain reaction of aneuploidizations. *Cell Cycle*, **2**, 202-210.
- Duff, H. J., Feng, Z. P., Sheldon, R. S., 1995. High- and low-affinity sites for [3H]dofetilide binding to guinea pig myocytes. *Circ Res*, **77**, 718-725.
- Dupuis, D. S., Klaerke, D. A., Olesen, S. P., 2005. Effect of beta-adrenoceptor blockers on human ether-a-go-go-related gene (HERG) potassium channels. *Basic Clin Pharmacol Toxicol*, **96**, 123-130.
- Enyedi, P. & Czirjak, G., 2010. Molecular background of leak K⁺ currents: two-pore domain potassium channels. *Physiol Rev*, **90**, 559-605.
- Faehling, M., Koch, E. D., Raithel, J., Trischler, G., Waltenberger, J., 2001. Vascular endothelial growth factor-A activates Ca²⁺-activated K⁺ channels in human endothelial cells in culture. *Int J Biochem Cell Biol*, **33**, 337-346.
- Faravelli, L., Arcangeli, A., Olivotto, M., Wanke, E., 1996. A HERG-like K⁺ channel in rat F-11 DRG cell line: pharmacological identification and biophysical characterization. *J Physiol*, **496** (Pt 1), 13-23.
- Farber, E., 1984. The multistep nature of cancer development. *Cancer Res*, **44**, 4217-4223.
- Farias, L. M. B., Ocana, D. B., Diaz, L., Larrea, F., Avila-Chavez, E., Cadena, A., Hinojosa, L. M., Lara, G., Villanueva, L. A., Vargas, C., Hernandez-Gallegos, E., Camacho-Arroyo, I., Duenas-Gonzalez, A., Perez-Cardenas, E., Pardo, L. A., Morales, A., Taja-Chayeb, L., Escamilla, J., Sanchez-Pena, C., Camacho, J., 2004. Ether a go-go potassium channels as human cervical cancer markers. *Cancer Research*, **64**, 6996-7001.
- Farrelly, A. M., Ro, S., Callaghan, B. P., Khoyi, M. A., Fleming, N., Horowitz, B., Sanders, K. M., Keef, K. D., 2003. Expression and function of KCNH2 (HERG) in the human jejunum. *Am J Physiol Gastrointest Liver Physiol*, **284**, G883-895.

- Felding-Habermann, B., 2003. Integrin adhesion receptors in tumor metastasis. *Clin Exp Metastasis*, **20**, 203-213.
- Felipe, A., Vicente, R., Villalonga, N., Roura-Ferrer, M., Martinez-Marmol, R., Sole, L., Ferreres, J. C., Condom, E., 2006. Potassium channels: new targets in cancer therapy. *Cancer Detect Prev*, **30**, 375-385.
- Ferrer, T., Rupp, J., Piper, D. R., Tristani-Firouzi, M., 2006. The S4-S5 linker directly couples voltage sensor movement to the activation gate in the human ether-a'-go-go-related gene (hERG) K⁺ channel. *J Biol Chem*, **281**, 12858-12864.
- Ficker, E., Dennis, A. T., Obejero-Paz, C. A., Castaldo, P., Taglialatela, M., Brown, A. M., 2000. Retention in the endoplasmic reticulum as a mechanism of dominant-negative current suppression in human long QT syndrome. *Journal of Molecular and Cellular Cardiology*, **32**, 2327-2337.
- Ficker, E., Jarolimek, W., Kiehn, J., Baumann, A., Brown, A. M., 1998. Molecular determinants of dofetilide block of HERG K⁺ channels. *Circ Res*, **82**, 386-395.
- Ficker, E., Kuryshev, Y. A., Dennis, A. T., Obejero-Paz, C., Lu, W., Hawryluk, P., Wible, B. A., Brown, A. M., 2004. Mechanisms of arsenic-induced prolongation of cardiac repolarization. *Molecular Pharmacology*, **66**, 33-44.
- Ficker, E., Obejero-Paz, C. A., Zhao, S., Brown, A. M., 2002. The binding site for channel blockers that rescue misprocessed human long QT syndrome type 2 ether-a-gogo-related gene (HERG) mutations. *J Biol Chem*, **277**, 4989-4998.
- Finlayson, K., Pennington, A. J., Kelly, J. S., 2001a. [3H]dofetilide binding in SHSY5Y and HEK293 cells expressing a HERG-like K⁺ channel? *Eur J Pharmacol*, **412**, 203-212.
- Finlayson, K., Turnbull, L., January, C. T., Sharkey, J., Kelly, J. S., 2001b. [3H]dofetilide binding to HERG transfected membranes: a potential high throughput preclinical screen. *Eur J Pharmacol*, **430**, 147-148.
- Fleige, S. & Pfaffl, M. W., 2006. RNA integrity and the effect on the real-time qRT-PCR performance. *Mol Aspects Med*, **27**, 126-139.
- Folkman, J., 2002. Role of angiogenesis in tumor growth and metastasis. *Semin Oncol*, **29**, 15-18.
- Fontana, L., D'Amico, M., Crociani, O., Biagiotti, T., Solazzo, M., Rosati, B., Arcangeli, A., Wanke, E., Olivotto, M., 2001. Long-Term Modulation of hERG Channel Gating in Hypoxia. *Biochemical and Biophysical Research Communications*, **286**, 857-862.
- Franco, S. J. & Huttenlocher, A., 2005. Regulating cell migration: calpains make the cut. *J Cell Sci*, **118**, 3829-3838.
- Fraser, S. P., Diss, J. K., Chioni, A. M., Mycielska, M. E., Pan, H., Yamaci, R. F., Pani, F., Siwy, Z., Krasowska, M., Grzywna, Z., Brackenbury, W. J., Theodorou, D., Koyuturk, M., Kaya, H., Battaloglu, E., De Bella, M. T., Slade, M. J., Tolhurst, R., Palmieri, C., Jiang, J., Latchman, D. S., Coombes, R. C., Djamgoz, M. B., 2005. Voltage-gated sodium channel expression and potentiation of human breast cancer metastasis. *Clin Cancer Res*, **11**, 5381-5389.

- Fraser, S. P., Diss, J. K., Lloyd, L. J., Pani, F., Chioni, A. M., George, A. J., Djamgoz, M. B., 2004. T-lymphocyte invasiveness: control by voltage-gated Na⁺ channel activity. *FEBS Lett*, **569**, 191-194.
- Fraser, S. P., Salvador, V., Manning, E. A., Mizal, J., Altun, S., Raza, M., Berridge, R. J., Djamgoz, M. B., 2003. Contribution of functional voltage-gated Na⁺ channel expression to cell behaviors involved in the metastatic cascade in rat prostate cancer: I. Lateral motility. *J Cell Physiol*, **195**, 479-487.
- Freedman, B. D., Price, M. A., Deutsch, C. J., 1992. Evidence for voltage modulation of IL-2 production in mitogen-stimulated human peripheral blood lymphocytes. *J Immunol*, **149**, 3784-3794.
- Friedl, P., Hegerfeldt, Y., Tusch, M., 2004. Collective cell migration in morphogenesis and cancer. *International Journal of developmental biology*, **48**, 441-449.
- Friedl, P., Noble, P. B., Zanker, K. S., 1993. Lymphocyte locomotion in three-dimensional collagen gels. Comparison of three quantitative methods for analysing cell trajectories. *J Immunol Methods*, **165**, 157-165.
- Fulgenzi, G., Graciotti, L., Faronato, M., Soldovieri, M. V., Miceli, F., Amoroso, S., Annunziato, L., Procopio, A., Tagliatela, M., 2006. Human neoplastic mesothelial cells express voltage-gated sodium channels involved in cell motility. *Int J Biochem Cell Biol*, **38**, 1146-1159.
- Gamper, N., Fillon, S., Huber, S. M., Feng, Y., Kobayashi, T., Cohen, P., Lang, F., 2002. IGF-1 up-regulates K⁺ channels via PI3-kinase, PDK1 and SGK1. *Pflugers Arch*, **443**, 625-634.
- Gatenby, R. A., Kessler, H. B., Rosenblum, J. S., Coia, L. R., Moldofsky, P. J., Hartz, W. H., Broder, G. J., 1988. Oxygen distribution in squamous cell carcinoma metastases and its relationship to outcome of radiation therapy. *Int J Radiat Oncol Biol Phys*, **14**, 831-838.
- Gavrilova-Ruch, O., Schonherr, K., Gessner, G., Schonherr, R., Klapperstuck, T., Wohlrab, W., Heinemann, S. H., 2002. Effects of imipramine on ion channels and proliferation of IGR1 melanoma cells. *Journal of Membrane Biology*, **188**, 137-149.
- Gerlach, A. C., Stoehr, S. J., Castle, N. A., 2010. Pharmacological removal of human ether-a-go-go-related gene potassium channel inactivation by 3-nitro-N-(4-phenoxyphenyl) benzamide (ICA-105574). *Mol Pharmacol*, **77**, 58-68.
- Ghiani, C. A., Yuan, X., Eisen, A. M., Knutson, P. L., DePinho, R. A., McBain, C. J., Gallo, V., 1999. Voltage-activated K⁺ channels and membrane depolarization regulate accumulation of the cyclin-dependent kinase inhibitors p27(Kip1) and p21(CIP1) in glial progenitor cells. *J Neurosci*, **19**, 5380-5392.
- Gilles-Gonzalez, M. A. & Gonzalez, G., 2004. Signal transduction by heme-containing PAS-domain proteins. *J Appl Physiol*, **96**, 774-783.
- Gloushankova, N., Ossovskaya, V., Vasiliev, J., Chumakov, P., Kopnin, B., 1997. Changes in p53 expression can modify cell shape of ras-transformed fibroblasts and epitheliocytes. *Oncogene*, **15**, 2985-2989.

- Gloushankova, N. A., Krendel, M. F., Sirotkin, V. A., Bonder, E. M., Feder, H. H., Vasiliev, J. M., Gelfand, I. M., 1995. Dynamics of active lamellae in cultured epithelial cells: effects of expression of exogenous N-ras oncogene. *Proc Natl Acad Sci U S A*, **92**, 5322-5325.
- Gomez-Varela, D., Zwick-Wallasch, E., Knotgen, H., Sanchez, A., Hettmann, T., Ossipov, D., Weseloh, R., Contreras-Jurado, C., Rothe, M., Stuhmer, W., Pardo, L. A., 2007. Monoclonal antibody blockade of the human Eag1 potassium channel function exerts antitumor activity. *Cancer Res*, **67**, 7343-7349.
- Gong, Q., Anderson, C. L., January, C. T., Zhou, Z., 2002. Role of glycosylation in cell surface expression and stability of HERG potassium channels. *American Journal of Physiology-Heart And Circulation Physiology*, **283**, H77-84.
- Gonzalez, C., Vaquero, L. M., Lopez-Lopez, J. R., Perez-Garcia, M. T., 2009. Oxygen-sensitive potassium channels in chemoreceptor cell physiology: making a virtue of necessity. *Ann N Y Acad Sci*, **1177**, 82-88.
- Graeber, T. G., Osmanian, C., Jacks, T., Housman, D. E., Koch, C. J., Lowe, S. W., Giaccia, A. J., 1996. Hypoxia-mediated selection of cells with diminished apoptotic potential in solid tumours. *Nature*, **379**, 88-91.
- Grande-Garcia, A., Echarri, A., de Rooij, J., Alderson, N. B., Waterman-Storer, C. M., Valdivielso, J. M., del Pozo, M. A., 2007. Caveolin-1 regulates cell polarization and directional migration through Src kinase and Rho GTPases. *J Cell Biol*, **177**, 683-694.
- Greenbaum, D., Colangelo, C., Williams, K., Gerstein, M., 2003. Comparing protein abundance and mRNA expression levels on a genomic scale. *Genome Biol*, **4**, 117.
- Griffith, L. C., 2004. Regulation of calcium/calmodulin-dependent protein kinase II activation by intramolecular and intermolecular interactions. *J Neurosci*, **24**, 8394-8398.
- Gu, Y. Z., Hogenesch, J. B., Bradfield, C. A., 2000. The PAS superfamily: sensors of environmental and developmental signals. *Annu Rev Pharmacol Toxicol*, **40**, 519-561.
- Guadagno, T. M., Ohtsubo, M., Roberts, J. M., Assoian, R. K., 1993. A link between cyclin A expression and adhesion-dependent cell cycle progression. *Science*, **262**, 1572-1575.
- Guasti, L., Cilia, E., Crociani, O., Hofmann, G., Polvani, S., Becchetti, A., Wanke, E., Tempia, F., Arcangeli, A., 2005. Expression pattern of the ether-a-go-go-related (ERG) family proteins in the adult mouse central nervous system: evidence for coassembly of different subunits. *J Comp Neurol*, **491**, 157-174.
- Guasti, L., Crociani, O., Redaelli, E., Pillozzi, S., Polvani, S., Masselli, M., Mello, T., Galli, A., Amedei, A., Wymore, R. S., Wanke, E., Arcangeli, A., 2008. Identification of a posttranslational mechanism for the regulation of hERG1 K⁺ channel expression and hERG1 current density in tumor cells. *Mol Cell Biol*, **28**, 5043-5060.
- Gulbis, J. M. & Doyle, D. A., 2004. Potassium channel structures: do they conform? *Curr Opin Struct Biol*, **14**, 440-446.

- Gullo, F., Ales, E., Rosati, B., Lecchi, M., Masi, A., Guasti, L., Cano-Abad, M. F., Arcangeli, A., Lopez, M. G., Wanke, E., 2003. ERG K⁺ channel blockade enhances firing and epinephrine secretion in rat chromaffin cells: the missing link to LQT2-related sudden death? *Faseb J*, **17**, 330-332.
- Guo, T. B., Lu, J., Li, T., Lu, Z., Xu, G., Xu, M., Lu, L., Dai, W., 2005. Insulin-activated, K⁺-channel-sensitive Akt pathway is primary mediator of ML-1 cell proliferation. *American Journal of Physiology - Cell Physiology*, **289**, C257-263.
- Guo, W., Pylayeva, Y., Pepe, A., Yoshioka, T., Muller, W. J., Inghirami, G., Giancotti, F. G., 2006. Beta 4 integrin amplifies ErbB2 signaling to promote mammary tumorigenesis. *Cell*, **126**, 489-502.
- Gygi, S. P., Rochon, Y., Franza, B. R., Aebersold, R., 1999. Correlation between protein and mRNA abundance in yeast. *Mol Cell Biol*, **19**, 1720-1730.
- Hall, C. L., Yang, B., Yang, X., Zhang, S., Turley, M., Samuel, S., Lange, L. A., Wang, C., Curpen, G. D., Savani, R. C., Greenberg, A. H., Turley, E. A., 1995. Overexpression of the hyaluronan receptor RHAMM is transforming and is also required for H-ras transformation. *Cell*, **82**, 19-26.
- Han, H., Wang, J., Zhang, Y., Long, H., Wang, H., Xu, D., Wang, Z., 2004. HERG K channel conductance promotes H₂O₂-induced apoptosis in HEK293 cells: cellular mechanisms. *Cell Physiol Biochem*, **14**, 121-134.
- Han, X., Wang, F., Yao, W., Xing, H., Weng, D., Song, X., Chen, G., Xi, L., Zhu, T., Zhou, J., Xu, G., Wang, S., Meng, L., Iadecola, C., Wang, G., Ma, D., 2007a. Heat shock proteins and p53 play a critical role in K⁺ channel-mediated tumor cell proliferation and apoptosis. *Apoptosis*, **12**, 1837-1846.
- Han, Y., Shi, Y., Han, Z., Sun, L., Fan, D., 2007b. Detection of potassium currents and regulation of multidrug resistance by potassium channels in human gastric cancer cells. *Cell Biol Int*, **31**, 741-747.
- Hanada, T., Lin, L., Chandy, K. G., Oh, S. S., Chishti, A. H., 1997. Human homologue of the Drosophila discs large tumor suppressor binds to p56lck tyrosine kinase and Shaker type Kv1.3 potassium channel in T lymphocytes. *J Biol Chem*, **272**, 26899-26904.
- Hanahan, D. & Weinberg, R. A., 2000. The hallmarks of cancer. *Cell*, **100**, 57-70.
- Hanahan, D. & Weinberg, R. A., 2011. Hallmarks of cancer: the next generation. *Cell*, **144**, 646-674.
- Hancox, J. C., Levi, A. J., Witchel, H. J., 1998. Time course and voltage dependence of expressed HERG current compared with native "rapid" delayed rectifier K current during the cardiac ventricular action potential. *Pflugers Arch*, **436**, 843-853.
- Hansen, A. J., 1985. Effect of anoxia on ion distribution in the brain. *Physiol Rev*, **65**, 101-148.
- Hardy, M. E., Lawrence, C. L., Standen, N. B., Rodrigo, G. C., 2006. Can optical recordings of membrane potential be used to screen for drug-induced action potential prolongation in single cardiac myocytes? *J Pharmacol Toxicol Methods*, **54**, 173-182.
- Haren, N., Khorsi, H., Faouzi, M., Ahidouch, A., Sevestre, H., Ouadid-Ahidouch, H., 2010. Intermediate conductance Ca²⁺ activated K⁺ channels are expressed and functional in breast

- adenocarcinomas: correlation with tumour grade and metastasis status. *Histol Histopathol*, **25**, 1247-1255.
- Harmon, C. S., Lutz, D., Ducote, J., 1993. Potassium channel openers stimulate DNA synthesis in mouse epidermal keratinocyte and whole hair follicle cultures. *Skin Pharmacol*, **6**, 170-178.
- Hartness, M. E., Lewis, A., Searle, G. J., O'Kelly, I., Peers, C., Kemp, P. J., 2001. Combined antisense and pharmacological approaches implicate hTASK as an airway O(2) sensing K(+) channel. *J Biol Chem*, **276**, 26499-26508.
- Hegle, A. P., Marble, D. D., Wilson, G. F., 2006. A voltage-driven switch for ion-independent signaling by ether-a-go-go K⁺ channels. *Proceedings of the National Academy of Sciences of the United States of America*, **103**, 2886-2891.
- Hemmerlein, B., Weseloh, R. M., Mello de Queiroz, F., Knotgen, H., Sanchez, A., Rubio, M. E., Martin, S., Schliephacke, T., Jenke, M., Heinz Joachim, R., Stuhmer, W., Pardo, L. A., 2006. Overexpression of Eag1 potassium channels in clinical tumours. *Mol Cancer*, **5**, 41.
- Henriet, P., Zhong, Z. D., Brooks, P. C., Weinberg, K. I., DeClerck, Y. A., 2000. Contact with fibrillar collagen inhibits melanoma cell proliferation by up-regulating p27KIP1. *Proc Natl Acad Sci U S A*, **97**, 10026-10031.
- Hofmann, G., Bernabei, P. A., Crociani, O., Cherubini, A., Guasti, L., Pillozzi, S., Lastraioli, E., Polvani, S., Bartolozzi, B., Solazzo, V., Gragnani, L., Defilippi, P., Rosati, B., Wanke, E., Olivotto, R., Arcangeli, A., 2001. hERG K⁺ channels activation during beta(1) integrin-mediated adhesion to fibronectin induces an up-regulation of alpha(v)beta(3) integrin in the preosteoclastic leukemia cell line FLG 29.1. *Journal of Biological Chemistry*, **276**, 4923-4931.
- Hood, J. D. & Cheresch, D. A., 2002. Role of integrins in cell invasion and migration. *Nat Rev Cancer*, **2**, 91-100.
- Hu, J., Yuan, X., Ko, M. K., Yin, D., Sacapano, M. R., Wang, X., Konda, B. M., Espinoza, A., Prosolovich, K., Ong, J. M., Irvin, D., Black, K. L., 2007. Calcium-activated potassium channels mediated blood-brain tumor barrier opening in a rat metastatic brain tumor model. *Mol Cancer*, **6**, 22.
- Huang, Y. & Rane, S. G., 1994. Potassium channel induction by the Ras/Raf signal transduction cascade. *J Biol Chem*, **269**, 31183-31189.
- Huffaker, S. J., Chen, J., Nicodemus, K. K., Sambataro, F., Yang, F., Mattay, V., Lipska, B. K., Hyde, T. M., Song, J., Rujescu, D., Giegling, I., Mayilyan, K., Proust, M. J., Soghoyan, A., Caforio, G., Callicott, J. H., Bertolino, A., Meyer-Lindenberg, A., Chang, J., Ji, Y., Egan, M. F., Goldberg, T. E., Kleinman, J. E., Lu, B., Weinberger, D. R., 2009. A primate-specific, brain isoform of KCNH2 affects cortical physiology, cognition, neuronal repolarization and risk of schizophrenia. *Nat Med*, **15**, 509-518.
- Huggett, J., Dheda, K., Bustin, S., Zumla, A., 2005. Real-time RT-PCR normalisation; strategies and considerations. *Genes Immun*, **6**, 279-284.

- Humphries, J. D., Wang, P., Streuli, C., Geiger, B., Humphries, M. J., Ballestrem, C., 2007. Vinculin controls focal adhesion formation by direct interactions with talin and actin. *J Cell Biol*, **179**, 1043-1057.
- Huttenlocher, A., Lakonishok, M., Kinder, M., Wu, S., Truong, T., Knudsen, K. A., Horwitz, A. F., 1998. Integrin and cadherin synergy regulates contact inhibition of migration and motile activity. *J Cell Biol*, **141**, 515-526.
- Hynes, R. O., 2002. Integrins: bidirectional, allosteric signaling machines. *Cell*, **110**, 673-687.
- Iwasaki, H., Murata, Y., Kim, Y., Hossain, M. I., Worby, C. A., Dixon, J. E., McCormack, T., Sasaki, T., Okamura, Y., 2008. A voltage-sensing phosphatase, Ci-VSP, which shares sequence identity with PTEN, dephosphorylates phosphatidylinositol 4,5-bisphosphate. *Proc Natl Acad Sci U S A*, **105**, 7970-7975.
- Izawa, I., Amano, M., Chihara, K., Yamamoto, T., Kaibuchi, K., 1998. Possible involvement of the inactivation of the Rho-Rho-kinase pathway in oncogenic Ras-induced transformation. *Oncogene*, **17**, 2863-2871.
- Jang, S. K., Krausslich, H. G., Nicklin, M. J., Duke, G. M., Palmenberg, A. C., Wimmer, E., 1988. A segment of the 5' nontranslated region of encephalomyocarditis virus RNA directs internal entry of ribosomes during in vitro translation. *J Virol*, **62**, 2636-2643.
- Jiang, Y., Lee, A., Chen, J., Cadene, M., Chait, B. T., MacKinnon, R., 2002a. Crystal structure and mechanism of a calcium-gated potassium channel. *Nature*, **417**, 515-522.
- Jiang, Y., Lee, A., Chen, J., Cadene, M., Chait, B. T., MacKinnon, R., 2002b. The open pore conformation of potassium channels. *Nature*, **417**, 523-526.
- Jiang, Y., Lee, A., Chen, J., Ruta, V., Cadene, M., Chait, B. T., MacKinnon, R., 2003a. X-ray structure of a voltage-dependent K⁺ channel. *Nature*, **423**, 33-41.
- Jiang, Y., Ruta, V., Chen, J., Lee, A., MacKinnon, R., 2003b. The principle of gating charge movement in a voltage-dependent K⁺ channel. *Nature*, **423**, 42-48.
- Jo, S. H., Hong, H. K., Chong, S. H., Choe, H., 2008. Protriptyline block of the human ether-a-go-go-related gene (HERG) K⁺ channel. *Life Sci*, **82**, 331-340.
- Jockusch, B. M. & Rudiger, M., 1996. Crosstalk between cell adhesion molecules: vinculin as a paradigm for regulation by conformation. *Trends Cell Biol*, **6**, 311-315.
- Johansen, T., Bjorkoy, G., Overvatn, A., Diaz-Meco, M. T., Traavik, T., Moscat, J., 1994. NIH 3T3 cells stably transfected with the gene encoding phosphatidylcholine-hydrolyzing phospholipase C from *Bacillus cereus* acquire a transformed phenotype. *Mol Cell Biol*, **14**, 646-654.
- Johnson, J. N., Hofman, N., Haglund, C. M., Cascino, G. D., Wilde, A. A., Ackerman, M. J., 2009. Identification of a possible pathogenic link between congenital long QT syndrome and epilepsy. *Neurology*, **72**, 224-231.
- Jones, E. M., Roti Roti, E. C., Wang, J., Delfosse, S. A., Robertson, G. A., 2004. Cardiac IKr channels minimally comprise hERG 1a and 1b subunits. *J Biol Chem*, **279**, 44690-44694.

- Jones, P. L., Schmidhauser, C., Bissell, M. J., 1993. Regulation of gene expression and cell function by extracellular matrix. *Crit Rev Eukaryot Gene Expr*, **3**, 137-154.
- Jouanneau, J., Longuet, M., Bertrand, S., 1989. Transformed NIH 3T3 cells expressing human melanoma N-ras oncogene metastasize to lymph node in nude mice. *Clin Exp Metastasis*, **7**, 391-403.
- Kabir, S. M., Bhattacharyya, M. L., Robinson, T. R., 2000. Indapamide blocks the rapid component of the delayed rectifier current in atrial tumor cells (AT-1 cells). *Int J Cardiol*, **73**, 27-32.
- Kaczmarek, L. K., 2006. Non-conducting functions of voltage-gated ion channels. *Nat Rev Neurosci*, **7**, 761-771.
- Kaelin, W. G., Jr. & Ratcliffe, P. J., 2008. Oxygen sensing by metazoans: the central role of the HIF hydroxylase pathway. *Mol Cell*, **30**, 393-402.
- Kagan, A., Melman, Y. F., Krumerman, A., McDonald, T. V., 2002. 14-3-3 amplifies and prolongs adrenergic stimulation of HERG K⁺ channel activity. *Embo J*, **21**, 1889-1898.
- Kagan, A., Yu, Z., Fishman, G. I., McDonald, T. V., 2000. The dominant negative LQT2 mutation A561V reduces wild-type HERG expression. *Journal of Biological Chemistry*, **275**, 11241-11248.
- Kaidi, A., Williams, A. C., Paraskeva, C., 2007. Interaction between beta-catenin and HIF-1 promotes cellular adaptation to hypoxia. *Nat Cell Biol*, **9**, 210-217.
- Kamiya, K., Niwa, R., Morishima, M., Honjo, H., Sanguinetti, M. C., 2008. Molecular determinants of hERG channel block by terfenadine and cisapride. *J Pharmacol Sci*, **108**, 301-307.
- Kao, W. Y., Davis, C. E., Kim, Y. I., Beach, J. M., 2001. Fluorescence emission spectral shift measurements of membrane potential in single cells. *Biophys J*, **81**, 1163-1170.
- Kass, R. S., 2005. The channelopathies: novel insights into molecular and genetic mechanisms of human disease. *J Clin Invest*, **115**, 1986-1989.
- Katz, B. Z., Romer, L., Miyamoto, S., Volberg, T., Matsumoto, K., Cukierman, E., Geiger, B., Yamada, K. M., 2003. Targeting membrane-localized focal adhesion kinase to focal adhesions: roles of tyrosine phosphorylation and SRC family kinases. *Journal of Biological Chemistry*, **278**, 29115-29120.
- Kemp, P. J., Telezhkin, V., Wilkinson, W. J., Mears, R., Hanmer, S. B., Gadeberg, H. C., Muller, C. T., Riccardi, D., Brazier, S. P., 2009. Enzyme-linked oxygen sensing by potassium channels. *Ann N Y Acad Sci*, **1177**, 112-118.
- Kessler, W., Budde, T., Gekle, M., Fabian, A., Schwab, A., 2008. Activation of cell migration with fibroblast growth factor-2 requires calcium-sensitive potassium channels. *Pflugers Arch*, **456**, 813-823.
- Kharitonova, M. A., Kopnin, P. B., Vasiliev, J. M., 2007. Transformation by RAS oncogene decreases the width of substrate-spread fibroblasts but not their length. *Cell Biol Int*, **31**, 220-223.

- Khosravi-Far, R., Chrzanowska-Wodnicka, M., Solski, P. A., Eva, A., Burridge, K., Der, C. J., 1994. Dbl and Vav mediate transformation via mitogen-activated protein kinase pathways that are distinct from those activated by oncogenic Ras. *Molecular and Cellular Biology*, **14**, 6848-6857.
- Kim, C. J., Cho, Y. G., Jeong, S. W., Kim, Y. S., Kim, S. Y., Nam, S. W., Lee, S. H., Yoo, N. J., Lee, J. Y., Park, W. S., 2004. Altered expression of KCNK9 in colorectal cancers. *APMIS*, **112**, 588-594.
- Kim, J. A., Kang, Y. S., Jung, M. W., Kang, G. H., Lee, S. H., Lee, Y. S., 2000. Ca²⁺ influx mediates apoptosis induced by 4-aminopyridine, a K⁺ channel blocker, in HepG2 human hepatoblastoma cells. *Pharmacology*, **60**, 74-81.
- Kindzelskii, A. L. & Petty, H. R., 2005. Ion channel clustering enhances weak electric field detection by neutrophils: apparent roles of SKF96365-sensitive cation channels and myeloperoxidase trafficking in cellular responses. *Eur Biophys J*, **35**, 1-26.
- Kindzelskii, A. L., Sitrin, R. G., Petty, H. R., 2004. Cutting edge: optical microspectrophotometry supports the existence of gel phase lipid rafts at the lamellipodium of neutrophils: apparent role in calcium signaling. *J Immunol*, **172**, 4681-4685.
- Kirchberger, N. M., Wulfsen, I., Schwarz, J. R., Bauer, C. K., 2006. Effects of TRH on heteromeric rat erg1a/1b K⁺ channels are dominated by the rerg1b subunit. *J Physiol*, **571**, 27-42.
- Knisley, S. B., Justice, R. K., Kong, W., Johnson, P. L., 2000. Ratiometry of transmembrane voltage-sensitive fluorescent dye emission in hearts. *Am J Physiol Heart Circ Physiol*, **279**, H1421-1433.
- Koh, W. J., Rasey, J. S., Evans, M. L., Grierson, J. R., Lewellen, T. K., Graham, M. M., Krohn, K. A., Griffin, T. W., 1992. Imaging of hypoxia in human tumors with [F-18]fluoromisonidazole. *Int J Radiat Oncol Biol Phys*, **22**, 199-212.
- Kohler, R., Degenhardt, C., Kuhn, M., Runkel, N., Paul, M., Hoyer, J., 2000. Expression and function of endothelial Ca(2+)-activated K(+) channels in human mesenteric artery: A single-cell reverse transcriptase-polymerase chain reaction and electrophysiological study in situ. *Circ Res*, **87**, 496-503.
- Kolbe, K., Schonherr, R., Gessner, G., Sahoo, N., Hoshi, T., Heinemann, S. H., 2010. Cysteine 723 in the C-linker segment confers oxidative inhibition of hERG1 potassium channels. *J Physiol*, **588**, 2999-3009.
- Korn, S. J. & Trapani, J. G., 2005. Potassium channels. *IEEE Trans Nanobioscience*, **4**, 21-33.
- Koumenis, C., Alarcon, R., Hammond, E., Sutphin, P., Hoffman, W., Murphy, M., Derr, J., Taya, Y., Lowe, S. W., Kastan, M., Giaccia, A., 2001. Regulation of p53 by hypoxia: dissociation of transcriptional repression and apoptosis from p53-dependent transactivation. *Mol Cell Biol*, **21**, 1297-1310.
- Kunzelmann, K., 2005. Ion channels and cancer. *Journal of Membrane Biology*, **205**, 159-173.
- Kuo, W., Lin, J., Tang, T. K., 2000. Human glucose-6-phosphate dehydrogenase (G6PD) gene transforms NIH 3T3 cells and induces tumors in nude mice. *Int J Cancer*, **85**, 857-864.

- Kupershmidt, S., Snyders, D. J., Raes, A., Roden, D. M., 1998. A K⁺ channel splice variant common in human heart lacks a C-terminal domain required for expression of rapidly activating delayed rectifier current. *Journal of Biological Chemistry*, **273**, 27231-27235.
- Kuroda, S., Fukata, M., Fujii, K., Nakamura, T., Izawa, I., Kaibuchi, K., 1997. Regulation of cell-cell adhesion of MDCK cells by Cdc42 and Rac1 small GTPases. *Biochem Biophys Res Commun*, **240**, 430-435.
- Kurokawa, H., Lee, D. S., Watanabe, M., Sagami, I., Mikami, B., Raman, C. S., Shimizu, T., 2004. A redox-controlled molecular switch revealed by the crystal structure of a bacterial heme PAS sensor. *Journal of Biological Chemistry*, **279**, 20186-20193.
- Kuryshhev, Y. A., Ficker, E., Wang, L., Hawryluk, P., Dennis, A. T., Wible, B. A., Brown, A. M., Kang, J. S., Chen, X. L., Sawamura, K., Reynolds, W., Rampe, D., 2005. Pentamidine-induced long QT syndrome and block of hERG trafficking. *Journal of Pharmacology and Experimental Therapeutics*, **312**, 316-323.
- Lagrutta, A. A., Trepakova, E. S., Salata, J. J., 2008. The hERG channel and risk of drug-acquired cardiac arrhythmia: an overview. *Curr Top Med Chem*, **8**, 1102-1112.
- Lang, F., Friedrich, F., Kahn, E., Woll, E., Hammerer, M., Waldegger, S., Maly, K., Grunicke, H., 1991. Bradykinin-induced oscillations of cell membrane potential in cells expressing the Ha-ras oncogene. *J Biol Chem*, **266**, 4938-4942.
- Lang, F., Ritter, M., Gamper, N., Huber, S., Fillon, S., Tanneur, V., Lepple-Wienhues, A., Szabo, I., Gulbins, E., 2000. Cell volume in the regulation of cell proliferation and apoptotic cell death. *Cellular Physiology and Biochemistry*, **10**, 417-428.
- Lang, F., Waldegger, S., Woell, E., Ritter, M., Maly, K., Grunicke, H., 1992. Effects of inhibitors and ion substitutions on oscillations of cell membrane potential in cells expressing the RAS oncogene. *Pflugers Arch*, **421**, 416-424.
- Larsen, A. P., 2010. Role of ERG1 isoforms in modulation of ERG1 channel trafficking and function. *Pflugers Arch*, **460**, 803-812.
- Larsen, A. P. & Olesen, S. P., 2010. Differential expression of hERG1 channel isoforms reproduces properties of native I(Kr) and modulates cardiac action potential characteristics. *PLoS One*, **5**, e9021.
- Larsen, A. P., Olesen, S. P., Grunnet, M., Jespersen, T., 2008. Characterization of hERG1a and hERG1b potassium channels—a possible role for hERG1b in the I (Kr) current. *Pflugers Arch*, **456**, 1137-1148.
- Lastraioli, E., Guasti, L., Crociani, O., Polvani, S., Hofmann, G., Witchel, H., Bencini, L., Calistri, M., Messerini, L., Scatizzi, M., Moretti, R., Wanke, E., Olivotto, M., Mugnai, G., Arcangeli, A., 2004. hERG1 gene and hERG1 protein are overexpressed in colorectal cancers and regulate cell invasion of tumor cells. *Cancer Research*, **64**, 606-611.
- Lauritzen, I., Zanzouri, M., Honore, E., Duprat, F., Ehrengruber, M. U., Lazdunski, M., Patel, A. J., 2003. K⁺-dependent cerebellar granule neuron apoptosis. Role of task leak K⁺ channels. *J Biol Chem*, **278**, 32068-32076.

- Lees-Miller, J. P., Kondo, C., Wang, L., Duff, H. J., 1997. Electrophysiological characterization of an alternatively processed ERG K⁺ channel in mouse and human hearts. *Circ Res*, **81**, 719-726.
- LeMasurier, M., Heginbotham, L., Miller, C., 2001. KcsA: it's a potassium channel. *J Gen Physiol*, **118**, 303-314.
- Lepple-Wienhues, A., Berweck, S., Bohmig, M., Leo, C. P., Meyling, B., Garbe, C., Wiederholt, M., 1996. K⁺ channels and the intracellular calcium signal in human melanoma cell proliferation. *J Membr Biol*, **151**, 149-157.
- Levite, M., Cahalon, L., Peretz, A., Hershkovich, R., Sobko, A., Ariel, A., Desai, R., Attali, B., Lider, O., 2000. Extracellular K⁽⁺⁾ and opening of voltage-gated potassium channels activate T cell integrin function: physical and functional association between Kv1.3 channels and beta1 integrins. *J Exp Med*, **191**, 1167-1176.
- Li, H., Du, Y. M., Guo, L., Jie, S., Zhang, S., Du, W., Chen, X., Liu, W., Fan, L., Zhu, J., Zou, A., Huang, S., 2009. The role of hERG1 K⁺ channels and a functional link between hERG1 K⁺ channels and SDF-1 in acute leukemic cell migration. *Exp Cell Res*, **315**, 2256-2264.
- Li, H., Liu, L., Guo, L., Zhang, J., Du, W., Li, X., Liu, W., Chen, X., Huang, S., 2008. HERG K⁺ channel expression in CD34⁺/CD38⁻/CD123^(high) cells and primary leukemia cells and analysis of its regulation in leukemia cells. *Int J Hematol*, **87**, 387-392.
- Li, H., Liu, L., Guo, T., Zhang, J., Li, X., Du, W., Liu, W., Chen, X., Huang, S., 2007a. Expression and functional role of HERG1, K⁺ channels in leukemic cells and leukemic stem cells. *J Huazhong Univ Sci Technolog Med Sci*, **27**, 257-260.
- Li, T. S., Cheng, K., Malliaras, K., Matsushita, N., Sun, B., Marban, L., Zhang, Y., Marban, E., 2010. Expansion of human cardiac stem cells in physiological oxygen improves cell production efficiency and potency for myocardial repair. *Cardiovasc Res*, **89**, 157-165.
- Li, Y., Cui, C. C., Zhao, Y. H., Xue, X. L., Zhang, A. F., Lian, J. F., Huang, C., 2007b. [Functional expression of congenital long QT syndrome related HERG mutation A561V in vitro]. *Zhonghua Xin Xue Guan Bing Za Zhi*, **35**, 143-146.
- Lifschitz-Mercer, B., Czernobilsky, B., Feldberg, E., Geiger, B., 1997. Expression of the adherens junction protein vinculin in human basal and squamous cell tumors: relationship to invasiveness and metastatic potential. *Hum Pathol*, **28**, 1230-1236.
- Lin, H., Xiao, J., Luo, X., Wang, H., Gao, H., Yang, B., Wang, Z., 2007. Overexpression HERG K⁽⁺⁾ channel gene mediates cell-growth signals on activation of oncoproteins SP1 and NF-kappaB and inactivation of tumor suppressor Nkx3.1. *J Cell Physiol*, **212**, 137-147.
- Livak, K. J. & Schmittgen, T. D., 2001. Analysis of relative gene expression data using real-time quantitative PCR and the 2^{(-Delta Delta C(T))} Method. *Methods*, **25**, 402-408.
- London, B., Trudeau, M. C., Newton, K. P., Beyer, A. K., Copeland, N. G., Gilbert, D. J., Jenkins, N. A., Satler, C. A., Robertson, G. A., 1997. Two isoforms of the mouse ether-a-go-go-related gene coassemble to form channels with properties similar to the rapidly activating component of the cardiac delayed rectifier K⁺ current. *Circ Res*, **81**, 870-878.

- Long, S. B., Campbell, E. B., Mackinnon, R., 2005. Crystal structure of a mammalian voltage-dependent Shaker family K⁺ channel. *Science*, **309**, 897-903.
- Lowry, O. H., Rosebrough, N. J., Farr, A. L., Randall, R. J., 1951. Protein measurement with the Folin phenol reagent. *J Biol Chem*, **193**, 265-275.
- Lu, Y., Mahaut-Smith, M. P., Varghese, A., Huang, C. L., Kemp, P. R., Vandenberg, J. I., 2001. Effects of premature stimulation on HERG K(+) channels. *J Physiol*, **537**, 843-851.
- Luo, X., Xiao, J., Lin, H., Lu, Y., Yang, B., Wang, Z., 2008. Genomic structure, transcriptional control, and tissue distribution of HERG1 and KCNQ1 genes. *Am J Physiol Heart Circ Physiol*, **294**, H1371-1380.
- Machesky, L. M., 2008. Lamellipodia and filopodia in metastasis and invasion. *FEBS Lett*, **582**, 2102-2111.
- MacKinnon, R., Cohen, S. L., Kuo, A., Lee, A., Chait, B. T., 1998. Structural conservation in prokaryotic and eukaryotic potassium channels. *Science*, **280**, 106-109.
- Maeno, E., Shimizu, T., Okada, Y., 2006. Normotonic cell shrinkage induces apoptosis under extracellular low Cl conditions in human lymphoid and epithelial cells. *Acta Physiol (Oxf)*, **187**, 217-222.
- Malhi, H., Irani, A. N., Rajvanshi, P., Suadicani, S. O., Spray, D. C., McDonald, T. V., Gupta, S., 2000. KATP channels regulate mitogenically induced proliferation in primary rat hepatocytes and human liver cell lines. Implications for liver growth control and potential therapeutic targeting. *J Biol Chem*, **275**, 26050-26057.
- Malhotra, J. D., Kazen-Gillespie, K., Hortsch, M., Isom, L. L., 2000. Sodium channel beta subunits mediate homophilic cell adhesion and recruit ankyrin to points of cell-cell contact. *J Biol Chem*, **275**, 11383-11388.
- Margulis, M., Sorota, S., Chu, I., Soares, A., Priestley, T., Nomeir, A. A., 2010. Protein binding-dependent decreases in hERG channel blocker potency assessed by whole-cell voltage clamp in serum. *J Cardiovasc Pharmacol*, **55**, 368-376.
- Masi, A., Becchetti, A., Restano-Cassulini, R., Polvani, S., Hofmann, G., Buccoliero, A. M., Paglierani, M., Pollo, B., Taddei, G. L., Gallina, P., Di Lorenzo, N., Franceschetti, S., Wanke, E., Arcangeli, A., 2005. hERG1 channels are overexpressed in glioblastoma multiforme and modulate VEGF secretion in glioblastoma cell lines. *British Journal of Cancer*, **93**, 781-792.
- Mattingly, R. R., Sorisky, A., Brann, M. R., Macara, I. G., 1994. Muscarinic receptors transform NIH 3T3 cells through a Ras-dependent signalling pathway inhibited by the Ras-GTPase-activating protein SH3 domain. *Mol Cell Biol*, **14**, 7943-7952.
- McCaig, C. D., Rajnicek, A. M., Song, B., Zhao, M., 2005. Controlling cell behavior electrically: current views and future potential. *Physiol Rev*, **85**, 943-978.

- McDonald, T. V., Yu, Z., Ming, Z., Palma, E., Meyers, M. B., Wang, K. W., Goldstein, S. A., Fishman, G. I., 1997. A minK-HERG complex regulates the cardiac potassium current I(Kr). *Nature*, **388**, 289-292.
- McFerrin, M. B. & Sontheimer, H., 2006. A role for ion channels in glioma cell invasion. *Neuron Glia Biol*, **2**, 39-49.
- McKeehan, W. L. & Ham, R. G., 1976. Stimulation of clonal growth of normal fibroblasts with substrata coated with basic polymers. *J Cell Biol*, **71**, 727-734.
- McPate, M. J., Duncan, R. S., Milnes, J. T., Witchel, H. J., Hancox, J. C., 2005. The N588K-HERG K⁺ channel mutation in the 'short QT syndrome': mechanism of gain-in-function determined at 37 degrees C. *Biochem Biophys Res Commun*, **334**, 441-449.
- Means, A. R., 1994. Calcium, Calmodulin and Cell-Cycle Regulation. *FEBS Letters*, **347**, 1-4.
- Mello de Queiroz, F., Suarez-Kurtz, G., Stuhmer, W., Pardo, L. A., 2006. Ether a go-go potassium channel expression in soft tissue sarcoma patients. *Mol Cancer*, **5**, 42.
- Meuth, S. G., Herrmann, A. M., Ip, C. W., Kanyshkova, T., Bittner, S., Weishaupt, A., Budde, T., Wiendl, H., 2008. The two-pore domain potassium channel TASK3 functionally impacts glioma cell death. *J Neurooncol*, **87**, 263-270.
- Mewe, M., Mauerhofer, M., Wulfsen, I., Szlachta, K., Zhou, X. B., Schwarz, J. R., Bauer, C. K., 2010. Modulation of cardiac ERG1 K(+) channels by cGMP signaling. *J Mol Cell Cardiol*, **49**, 48-57.
- Mewe, M., Wulfsen, I., Schuster, A. M., Middendorff, R., Glassmeier, G., Schwarz, J. R., Bauer, C. K., 2008. Erg K⁺ channels modulate contractile activity in the bovine epididymal duct. *Am J Physiol Regul Integr Comp Physiol*, **294**, R895-904.
- Meyer, R. & Heinemann, S. H., 1998. Characterization of an eag-like potassium channel in human neuroblastoma cells. *Journal of Physiology-London*, **508**, 49-56.
- Meyer, R., Schonherr, R., Gavrilova-Ruch, O., Wohlrab, W., Heinemann, S. H., 1999. Identification of ether a go-go and calcium-activated potassium channels in human melanoma cells. *Journal of Membrane Biology*, **171**, 107-115.
- Mierke, C. T., Kollmannsberger, P., Zitterbart, D. P., Diez, G., Koch, T. M., Marg, S., Ziegler, W. H., Goldmann, W. H., Fabry, B., 2010. Vinculin facilitates cell invasion into three-dimensional collagen matrices. *J Biol Chem*, **285**, 13121-13130.
- Milosevic, J., Schwarz, S. C., Krohn, K., Poppe, M., Storch, A., Schwarz, J., 2005. Low atmospheric oxygen avoids maturation, senescence and cell death of murine mesencephalic neural precursors. *J Neurochem*, **92**, 718-729.
- Miranda, P., Giraldez, T., de la Pena, P., Manso, D. G., Alonso-Ron, C., Gomez-Varela, D., Dominguez, P., Barros, F., 2005. Specificity of TRH receptor coupling to G-proteins for regulation of ERG K⁺ channels in GH(3) rat anterior pituitary cells. *Journal of Physiology-London*, **566**, 717-736.
- Mitcheson, J. S., Chen, J., Lin, M., Culbertson, C., Sanguinetti, M. C., 2000a. A structural basis for drug-induced long QT syndrome. *Proc Natl Acad Sci U S A*, **97**, 12329-12333.

- Mitcheson, J. S., Chen, J., Sanguinetti, M. C., 2000b. Trapping of a methanesulfonanilide by closure of the HERG potassium channel activation gate. *J Gen Physiol*, **115**, 229-240.
- Mitra, S. K., Hanson, D. A., Schlaepfer, D. D., 2005. Focal adhesion kinase: in command and control of cell motility. *Nat Rev Mol Cell Biol*, **6**, 56-68.
- Mizejewski, G. J., 1999. Role of integrins in cancer: survey of expression patterns. *Proc Soc Exp Biol Med*, **222**, 124-138.
- Mogilner, A. & Oster, G., 2003. Polymer motors: pushing out the front and pulling up the back. *Curr Biol*, **13**, R721-733.
- Morais Cabral, J. H., Lee, A., Cohen, S. L., Chait, B. T., Li, M., Mackinnon, R., 1998. Crystal structure and functional analysis of the HERG potassium channel N terminus: a eukaryotic PAS domain. *Cell*, **95**, 649-655.
- Morino, N., Mimura, T., Hamasaki, K., Tobe, K., Ueki, K., Kikuchi, K., Takehara, K., Kadowaki, T., Yazaki, Y., Nojima, Y., 1995. Matrix/integrin interaction activates the mitogen-activated protein kinase, p44erk-1 and p42erk-2. *J Biol Chem*, **270**, 269-273.
- Mosmann, T., 1983. Rapid colorimetric assay for cellular growth and survival: application to proliferation and cytotoxicity assays. *J Immunol Methods*, **65**, 55-63.
- Mu, D., Chen, L., Zhang, X., See, L. H., Koch, C. M., Yen, C., Tong, J. J., Spiegel, L., Nguyen, K. C., Servoss, A., Peng, Y., Pei, L., Marks, J. R., Lowe, S., Hoey, T., Jan, L. Y., McCombie, W. R., Wigler, M. H., Powers, S., 2003. Genomic amplification and oncogenic properties of the KCNK9 potassium channel gene. *Cancer Cell*, **3**, 297-302.
- Mummery, C. L., Boonstra, J., van der Saag, P. T., de Laat, S. W., 1982. Modulations of Na⁺ transport during the cell cycle of neuroblastoma cells. *J Cell Physiol*, **112**, 27-34.
- Murphy, B. J., Laderoute, K. R., Short, S. M., Sutherland, R. M., 1991. The identification of heme oxygenase as a major hypoxic stress protein in Chinese hamster ovary cells. *Br J Cancer*, **64**, 69-73.
- Muskett, F. W., Thouta, S., Thomson, S. J., Bowen, A., Stansfeld, P. J., Mitcheson, J. S., 2010. Mechanistic insight into hERG K⁺ channel deactivation gating from the solution structure of the EAG domain. *J Biol Chem*.
- Mycielska, M. E. & Djamgoz, M. B., 2004. Cellular mechanisms of direct-current electric field effects: galvanotaxis and metastatic disease. *J Cell Sci*, **117**, 1631-1639.
- Nanduri, J., Bergson, P., Wang, N., Ficker, E., Prabhakar, N. R., 2009. Hypoxia inhibits maturation and trafficking of hERG K(+) channel protein: Role of Hsp90 and ROS. *Biochem Biophys Res Commun*, **388**, 212-216.
- Newby, D., Marks, L., Lyall, F., 2005. Dissolved oxygen concentration in culture medium: assumptions and pitfalls. *Placenta*, **26**, 353-357.

- Nichols, C. G. & Lopatin, A. N., 1997. Inward rectifier potassium channels. *Annu Rev Physiol*, **59**, 171-191.
- Nigg, E. A., Sefton, B. M., Singer, S. J., Vogt, P. K., 1986. Cytoskeletal organization, vinculin-phosphorylation, and fibronectin expression in transformed fibroblasts with different cell morphologies. *Virology*, **151**, 50-65.
- Nilius, B., Schwarz, G., Droogmans, G., 1993. Control of intracellular calcium by membrane potential in human melanoma cells. *Am J Physiol*, **265**, C1501-1510.
- Nilius, B. & Wohlrab, W., 1992. Potassium Channels and Regulation of Proliferation of Human-Melanoma Cells. *Journal of Physiology-London*, **445**, 537-548.
- Nobes, C. D. & Hall, A., 1999. Rho GTPases control polarity, protrusion, and adhesion during cell movement. *J Cell Biol*, **144**, 1235-1244.
- Nutile-McMenemy, N., Elfenbein, A., Deleo, J. A., 2007. Minocycline decreases in vitro microglial motility, beta1-integrin, and Kv1.3 channel expression. *J Neurochem*, **103**, 2035-2046.
- O'Grady, S. M. & Lee, S. Y., 2005. Molecular diversity and function of voltage-gated (Kv) potassium channels in epithelial cells. *Int J Biochem Cell Biol*, **37**, 1578-1594.
- Ohya, S., Horowitz, B., Greenwood, I. A., 2002. Functional and molecular identification of ERG channels in murine portal vein myocytes. *Am J Physiol Cell Physiol*, **283**, C866-877.
- Omichi, C., Momose, Y., Kitahara, S., 2009. Congenital long QT syndrome presenting with a history of epilepsy: misdiagnosis or relationship between channelopathies of the heart and brain? *Epilepsia*, **51**, 289-292.
- Orlando, C., Pinzani, P., Pazzagli, M., 1998. Developments in quantitative PCR. *Clin Chem Lab Med*, **36**, 255-269.
- Orrenius, S., Zhivotovsky, B., Nicotera, P., 2003. Regulation of cell death: the calcium-apoptosis link. *Nat Rev Mol Cell Biol*, **4**, 552-565.
- Ouadid-Ahidouch, H., Le Bourhis, X., Roudbaraki, M., Toillon, R. A., Delcourt, P., Prevarskaya, N., 2001. Changes in the K⁺ current-density of MCF-7 cells during progression through the cell cycle: possible involvement of a h-ether.a-gogo K⁺ channel. *Receptors Channels*, **7**, 345-356.
- Ouadid-Ahidouch, H., Roudbaraki, M., Delcourt, P., Ahidouch, A., Joury, N., Prevarskaya, N., 2004. Functional and molecular identification of intermediate-conductance Ca(2+)-activated K(+) channels in breast cancer cells: association with cell cycle progression. *Am J Physiol Cell Physiol*, **287**, C125-134.
- Overholt, J. L., Ficker, E., Yang, T., Shams, H., Bright, G. R., Prabhakar, N. R., 2000. HERG-Like potassium current regulates the resting membrane potential in glomus cells of the rabbit carotid body. *J Neurophysiol*, **83**, 1150-1157.
- Pancrazio, J. J., Ma, W., Grant, G. M., Shaffer, K. M., Kao, W. Y., Liu, Q. Y., Manos, P., Barker, J. L., Stenger, D. A., 1999. A role for inwardly rectifying K⁺ channels in differentiation of NG108-15 neuroblastoma x glioma cells. *Journal of Neurobiology*, **38**, 466-474.

- Pandiella, A., Magni, M., Lovisolo, D., Meldolesi, J., 1989. The effect of epidermal growth factor on membrane potential. Rapid hyperpolarization followed by persistent fluctuations. *J Biol Chem*, **264**, 12914-12921.
- Pankov, R., Endo, Y., Even-Ram, S., Araki, M., Clark, K., Cukierman, E., Matsumoto, K., Yamada, K. M., 2005. A Rac switch regulates random versus directionally persistent cell migration. *J Cell Biol*, **170**, 793-802.
- Papa, M., Boscia, F., Canitano, A., Castaldo, P., Sellitti, S., Annunziato, L., Tagliatela, M., 2003. Expression pattern of the ether-a-gogo-related (ERG) K⁺ channel-encoding genes ERG1, ERG2, and ERG3 in the adult rat central nervous system. *J Comp Neurol*, **466**, 119-135.
- Pardo, L. A., 2004. Voltage-gated potassium channels in cell proliferation. *Physiology (Bethesda)*, **19**, 285-292.
- Pardo, L. A., Bruggemann, A., Camacho, J., Stuhmer, W., 1998. Cell cycle-related changes in the conducting properties of r-eag K⁺ channels. *J Cell Biol*, **143**, 767-775.
- Pardo, L. A., del Camino, D., Sanchez, A., Alves, F., Bruggemann, A., Beckh, S., Stuhmer, W., 1999. Oncogenic potential of EAG K⁺ channels. *Embo Journal*, **18**, 5540-5547.
- Pardo, L. A. & Stuhmer, W., 2008. Eag1: an emerging oncological target. *Cancer Res*, **68**, 1611-1613.
- Parihar, A. S., Coghlan, M. J., Gopalakrishnan, M., Shieh, C. C., 2003. Effects of intermediate-conductance Ca²⁺-activated K⁺ channel modulators on human prostate cancer cell proliferation. *Eur J Pharmacol*, **471**, 157-164.
- Park, C. C., Zhang, H., Pallavicini, M., Gray, J. W., Baehner, F., Park, C. J., Bissell, M. J., 2006. Beta1 integrin inhibitory antibody induces apoptosis of breast cancer cells, inhibits growth, and distinguishes malignant from normal phenotype in three dimensional cultures and in vivo. *Cancer Res*, **66**, 1526-1535.
- Partin, A. W., Isaacs, J. T., Treiger, B., Coffey, D. S., 1988. Early cell motility changes associated with an increase in metastatic ability in rat prostatic cancer cells transfected with the v-Harvey-ras oncogene. *Cancer Res*, **48**, 6050-6053.
- Patel, A. J. & Lazdunski, M., 2004. The 2P-domain K⁺ channels: role in apoptosis and tumorigenesis. *Pflugers Arch*, **448**, 261-273.
- Patel, R., Holt, M., Philipova, R., Moss, S., Schulman, H., Hidaka, H., Whitaker, M., 1999. Calcium/calmodulin-dependent phosphorylation and activation of human Cdc25-C at the G2/M phase transition in HeLa cells. *J Biol Chem*, **274**, 7958-7968.
- Patt, S., Preussat, K., Beetz, C., Kraft, R., Schrey, M., Kalff, R., Schonherr, K., Heinemann, S. H., 2004. Expression of ether a go-go potassium channels in human gliomas. *Neuroscience Letters*, **368**, 249-253.
- Pedersen, S. F., Hoffmann, E. K., Mills, J. W., 2001. The cytoskeleton and cell volume regulation. *Comp Biochem Physiol A Mol Integr Physiol*, **130**, 385-399.

- Pei, L., Wiser, O., Slavin, A., Mu, D., Powers, S., Jan, L. Y., Hoey, T., 2003. Oncogenic potential of TASK3 (Kcnk9) depends on K⁺ channel function. *Proceedings of the National Academy of Sciences of the United States of America*, **100**, 7803-7807.
- Peng, B., Fleming, J. B., Breslin, T., Grau, A. M., Fojioka, S., Abbruzzese, J. L., Evans, D. B., Ayers, D., Wathen, K., Wu, T., Robertson, K. D., Chiao, P. J., 2002. Suppression of tumorigenesis and induction of p15(ink4b) by Smad4/DPC4 in human pancreatic cancer cells. *Clin Cancer Res*, **8**, 3628-3638.
- Perrin, M. J., Subbiah, R. N., Vandenberg, J. I., Hill, A. P., 2008. Human ether-a-go-go related gene (hERG) K⁺ channels: function and dysfunction. *Prog Biophys Mol Biol*, **98**, 137-148.
- Perry, M., Sanguinetti, M., Mitcheson, J., 2010. Revealing the structural basis of action of hERG potassium channel activators and blockers. *J Physiol*, **588**, 3157-3167.
- Pessia, M., Servettini, I., Panichi, R., Guasti, L., Grassi, S., Arcangeli, A., Wanke, E., Pettorossi, V. E., 2008. ERG voltage-gated K⁺ channels regulate excitability and discharge dynamics of the medial vestibular nucleus neurones. *J Physiol*, **586**, 4877-4890.
- Phartiyal, P., Jones, E. M., Robertson, G. A., 2007. Heteromeric assembly of human ether-a-go-go-related gene (hERG) 1a/1b channels occurs cotranslationally via N-terminal interactions. *J Biol Chem*, **282**, 9874-9882.
- Phartiyal, P., Sale, H., Jones, E. M., Robertson, G. A., 2008. Endoplasmic reticulum retention and rescue by heteromeric assembly regulate human ERG 1a/1b surface channel composition. *J Biol Chem*, **283**, 3702-3707.
- Pier, D. 2007. *The oncogenic potential of human ether-a-go-go-related gene (hERG) potassium channels. Ph,D thesis*. Ph. D. University of leicester.
- Pillozzi, S., Brizzi, M. F., Balzi, M., Crociani, O., Cherubini, A., Guasti, L., Bartolozzi, B., Becchetti, A., Wanke, E., Bernabei, P. A., Olivotto, M., Pegoraro, L., Arcangeli, A., 2002. HERG potassium channels are constitutively expressed in primary human acute myeloid leukemias and regulate cell proliferation of normal and leukemic hemopoietic progenitors. *Leukemia*, **16**, 1791-1798.
- Pillozzi, S., Brizzi, M. F., Bernabei, P. A., Bartolozzi, B., Caporale, R., Basile, V., Boddi, V., Pegoraro, L., Becchetti, A., Arcangeli, A., 2007. VEGFR-1 (FLT-1), beta1 integrin, and hERG K⁺ channel for a macromolecular signaling complex in acute myeloid leukemia: role in cell migration and clinical outcome. *Blood*, **110**, 1238-1250.
- Pillozzi, S., Masselli, M., De Lorenzo, E., Accordi, B., Cilia, E., Crociani, O., Amedei, A., Veltroni, M., D'Amico, M., Basso, G., Becchetti, A., Campana, D., Arcangeli, A., 2010. Chemotherapy resistance in acute lymphoblastic leukemia requires hERG1 channels and is overcome by hERG1 blockers. *Blood*.
- Piper, D. R., Hinz, W. A., Tallurri, C. K., Sanguinetti, M. C., Tristani-Firouzi, M., 2005. Regional specificity of human ether-a-go-go-related gene channel activation and inactivation gating. *J Biol Chem*, **280**, 7206-7217.

- Piper, D. R., Varghese, A., Sanguinetti, M. C., Tristani-Firouzi, M., 2003. Gating currents associated with intramembrane charge displacement in HERG potassium channels. *Proc Natl Acad Sci U S A*, **100**, 10534-10539.
- Pond, A. L., Scheve, B. K., Benedict, A. T., Petrecca, K., Van Wagoner, D. R., Shrier, A., Nerbonne, J. M., 2000. Expression of distinct ERG proteins in rat, mouse, and human heart. Relation to functional I(Kr) channels. *J Biol Chem*, **275**, 5997-6006.
- Potier, M., Joulin, V., Roger, S., Besson, P., Jourdan, M. L., Leguennec, J. Y., Bougnoux, P., Vandier, C., 2006. Identification of SK3 channel as a new mediator of breast cancer cell migration. *Mol Cancer Ther*, **5**, 2946-2953.
- Prevarskaya, N., Skryma, R., Shuba, Y., 2010. Ion channels and the hallmarks of cancer. *Trends Mol Med*, **16**, 107-121.
- Price, M., Lee, S. C., Deutsch, C., 1989. Charybdotoxin inhibits proliferation and interleukin 2 production in human peripheral blood lymphocytes. *Proc Natl Acad Sci U S A*, **86**, 10171-10175.
- Pritchard, C. A., Hayes, L., Wojnowski, L., Zimmer, A., Marais, R. M., Norman, J. C., 2004. B-raf acts via the ROCKII/LIMK/cofilin pathway to maintain actin stress fibers in fibroblasts. *Molecular and Cellular Biology*, **24**, 5937-5952.
- Pylayeva, Y., Gillen, K. M., Gerald, W., Beggs, H. E., Reichardt, L. F., Giancotti, F. G., 2009. Ras- and PI3K-dependent breast tumorigenesis in mice and humans requires focal adhesion kinase signaling. *J Clin Invest*, **119**, 252-266.
- Qiu, R. G., Chen, J., Kirn, D., McCormick, F., Symons, M., 1995a. An essential role for Rac in Ras transformation. *Nature*, **374**, 457-459.
- Qiu, R. G., Chen, J., McCormick, F., Symons, M., 1995b. A role for Rho in Ras transformation. *Proc Natl Acad Sci U S A*, **92**, 11781-11785.
- Rajah, T. T., Abidi, S. M., Rambo, D. J., Dmytryk, J. J., Pento, J. T., 1998. The motile behavior of human breast cancer cells characterized by time-lapse videomicroscopy. *In Vitro Cell Dev Biol Anim*, **34**, 626-628.
- Rajamani, S., Anderson, C. L., Anson, B. D., January, C. T., 2002. Pharmacological rescue of human K(+) channel long-QT2 mutations: human ether-a-go-go-related gene rescue without block. *Circulation*, **105**, 2830-2835.
- Rao, J. N., Platoshyn, O., Li, L., Guo, X., Golovina, V. A., Yuan, J. X., Wang, J. Y., 2002. Activation of K(+) channels and increased migration of differentiated intestinal epithelial cells after wounding. *Am J Physiol Cell Physiol*, **282**, C885-898.
- Raschi, E., Vasina, V., Poluzzi, E., De Ponti, F., 2008. The hERG K+ channel: target and antitarget strategies in drug development. *Pharmacol Res*, **57**, 181-195.
- Raz, A. & Geiger, B., 1982. Altered organization of cell-substrate contacts and membrane-associated cytoskeleton in tumor cell variants exhibiting different metastatic capabilities. *Cancer Res*, **42**, 5183-5190.

- Redmann, K., Muller, V., Tanneberger, S., Kalkoff, W., 1972. The membrane potential of primary ovarian tumor cells in vitro and its dependence on the cell cycle. *Acta Biol Med Ger*, **28**, 853-856.
- Rees, S., Coote, J., Stables, J., Goodson, S., Harris, S., Lee, M. G., 1996. Bicistronic vector for the creation of stable mammalian cell lines that predisposes all antibiotic-resistant cells to express recombinant protein. *Biotechniques*, **20**, 102-104, 106, 108-110.
- Reinhardt, J., Golenhofen, N., Pongs, O., Oberleithner, H., Schwab, A., 1998. Migrating transformed MDCK cells are able to structurally polarize a voltage-activated K⁺ channel. *Proc Natl Acad Sci U S A*, **95**, 5378-5382.
- Renaudo, A., Watry, V., Chassot, A. A., Ponzio, G., Ehrenfeld, J., Soriani, O., 2004. Inhibition of tumor cell proliferation by sigma ligands is associated with K⁺ Channel inhibition and p27kip1 accumulation. *J Pharmacol Exp Ther*, **311**, 1105-1114.
- Repp, H., Draheim, H., Ruland, J., Seidel, G., Beise, J., Presek, P., Dreyer, F., 1993. Profound differences in potassium current properties of normal and Rous sarcoma virus-transformed chicken embryo fibroblasts. *Proc Natl Acad Sci U S A*, **90**, 3403-3407.
- Rezzonico, R., Cayatte, C., Bourget-Ponzio, I., Romey, G., Belhacene, N., Loubat, A., Rocchi, S., Van Obberghen, E., Girault, J. A., Rossi, B., Schmid-Antomarchi, H., 2003. Focal adhesion kinase pp125FAK interacts with the large conductance calcium-activated hSlo potassium channel in human osteoblasts: potential role in mechanotransduction. *J Bone Miner Res*, **18**, 1863-1871.
- Riccardi, C. & Nicoletti, I., 2006. Analysis of apoptosis by propidium iodide staining and flow cytometry. *Nat Protoc*, **1**, 1458-1461.
- Richmond, A., 2002. Nf-kappa B, chemokine gene transcription and tumour growth. *Nature Reviews Immunology*, **2**, 664-674.
- Ridley, A. J. & Hall, A., 1992a. The small GTP-binding protein rho regulates the assembly of focal adhesions and actin stress fibers in response to growth factors. *Cell*, **70**, 389-399.
- Ridley, A. J., Paterson, H. F., Johnston, C. L., Diekmann, D., Hall, A., 1992b. The small GTP-binding protein rac regulates growth factor-induced membrane ruffling. *Cell*, **70**, 401-410.
- Ridley, A. J., Schwartz, M. A., Burridge, K., Firtel, R. A., Ginsberg, M. H., Borisy, G., Parsons, J. T., Horwitz, A. R., 2003. Cell migration: integrating signals from front to back. *Science*, **302**, 1704-1709.
- Rodriguez Fernandez, J. L., Geiger, B., Salomon, D., Ben-Ze'ev, A., 1993. Suppression of vinculin expression by antisense transfection confers changes in cell morphology, motility, and anchorage-dependent growth of 3T3 cells. *Journal of Cell Biology*, **122**, 1285-1294.
- Rodriguez Fernandez, J. L., Geiger, B., Salomon, D., Sabanay, I., Zoller, M., Ben-Ze'ev, A., 1992. Suppression of tumorigenicity in transformed cells after transfection with vinculin cDNA. *Journal of Cell Biology*, **119**, 427-438.
- Rodriguez-Viciano, P., Warne, P. H., Khwaja, A., Marte, B. M., Pappin, D., Das, P., Waterfield, M. D., Ridley, A., Downward, J., 1997. Role of phosphoinositide 3-OH kinase in cell transformation and control of the actin cytoskeleton by Ras. *Cell*, **89**, 457-467.

- Rosati, B., Marchetti, P., Crociani, O., Lecchi, M., Lupi, R., Arcangeli, A., Olivotto, M., Wanke, E., 2000. Glucose- and arginine-induced insulin secretion by human pancreatic beta-cells: the role of HERG K(+) channels in firing and release. *Faseb J*, **14**, 2601-2610.
- Roti, E. C., Myers, C. D., Ayers, R. A., Boatman, D. E., Delfosse, S. A., Chan, E. K., Ackerman, M. J., January, C. T., Robertson, G. A., 2002. Interaction with GM130 during HERG ion channel trafficking. Disruption by type 2 congenital long QT syndrome mutations. Human Ether-a-go-go-Related Gene. *J Biol Chem*, **277**, 47779-47785.
- Rotsch, C., Jacobson, K., Condeelis, J., Radmacher, M., 2001. EGF-stimulated lamellipod extension in adenocarcinoma cells. *Ultramicroscopy*, **86**, 97-106.
- Rouzaire-Dubois, B. & Dubois, J. M., 1998. K⁺ channel block-induced mammalian neuroblastoma cell swelling: a possible mechanism to influence proliferation. *Journal of Physiology-London*, **510**, 93-102.
- Rouzaire-Dubois, B., Malo, M., Milandri, J. B., Dubois, J. M., 2004. Cell size-proliferation relationship in rat glioma cells. *Glia*, **45**, 249-257.
- Rouzaire-Dubois, B., Milandri, J. B., Bostel, S., Dubois, J. M., 2000. Control of cell proliferation by cell volume alterations in rat C6 glioma cells. *Pflugers Archiv-European Journal of Physiology*, **440**, 881-888.
- Roy, J., Vantol, B., Cowley, E. A., Blay, J., Linsdell, P., 2008. Pharmacological separation of hEAG and hERG K⁺ channel function in the human mammary carcinoma cell line MCF-7. *Oncol Rep*, **19**, 1511-1516.
- Roy, M., Dumaine, R., Brown, A. M., 1996. HERG, a primary human ventricular target of the non-sedating antihistamine terfenadine. *Circulation*, **94**, 817-823.
- Ruan, K., Song, G., Ouyang, G., 2009. Role of hypoxia in the hallmarks of human cancer. *J Cell Biochem*, **107**, 1053-1062.
- Ruffolo, R. R., Jr., 1982. Review important concepts of receptor theory. *J Auton Pharmacol*, **2**, 277-295.
- Runnels, L. W., Yue, L., Clapham, D. E., 2001. TRP-PLIK, a bifunctional protein with kinase and ion channel activities. *Science*, **291**, 1043-1047.
- Sacco, T., Bruno, A., Wanke, E., Tempia, F., 2003. Functional roles of an ERG current isolated in cerebellar Purkinje neurons. *J Neurophysiol*, **90**, 1817-1828.
- Sale, H., Wang, J., O'Hara, T. J., Tester, D. J., Phartiyal, P., He, J. Q., Rudy, Y., Ackerman, M. J., Robertson, G. A., 2008. Physiological properties of hERG 1a/1b heteromeric currents and a hERG 1b-specific mutation associated with Long-QT syndrome. *Circ Res*, **103**, e81-95.
- Sanguinetti, M. C., 2010. HERG1 channelopathies. *Pflugers Arch*, **460**, 265-276.
- Sanguinetti, M. C., Curran, M. E., Spector, P. S., Keating, M. T., 1996. Spectrum of hERG K⁺-channel dysfunction in an inherited cardiac arrhythmia. *Proceedings of the National Academy of Sciences of the United States of America*, **93**, 2208-2212.

- Sanguinetti, M. C., Jiang, C., Curran, M. E., Keating, M. T., 1995. A mechanistic link between an inherited and an acquired cardiac arrhythmia: HERG encodes the IKr potassium channel. *Cell*, **81**, 299-307.
- Sanguinetti, M. C. & Mitcheson, J. S., 2005. Predicting drug-hERG channel interactions that cause acquired long QT syndrome. *Trends Pharmacol Sci*, **26**, 119-124.
- Sanguinetti, M. C. & Tristani-Firouzi, M., 2006. hERG potassium channels and cardiac arrhythmia. *Nature*, **440**, 463-469.
- Saunders, R. M., Holt, M. R., Jennings, L., Sutton, D. H., Barsukov, I. L., Bobkov, A., Liddington, R. C., Adamson, E. A., Dunn, G. A., Critchley, D. R., 2006. Role of vinculin in regulating focal adhesion turnover. *Eur J Cell Biol*, **85**, 487-500.
- Schlaepfer, D. D., Hanks, S. K., Hunter, T., van der Geer, P., 1994. Integrin-mediated signal transduction linked to Ras pathway by GRB2 binding to focal adhesion kinase. *Nature*, **372**, 786-791.
- Schmid, T., Zhou, J., Brune, B., 2004. HIF-1 and p53: communication of transcription factors under hypoxia. *Journal of Cellular and Molecular Medicine*, **8**, 423-431.
- Schneider, S. W., Pagel, P., Rotsch, C., Danker, T., Oberleithner, H., Radmacher, M., Schwab, A., 2000. Volume dynamics in migrating epithelial cells measured with atomic force microscopy. *Pflugers Arch*, **439**, 297-303.
- Schoenwaelder, S. M. & Burridge, K., 1999. Bidirectional signaling between the cytoskeleton and integrins. *Curr Opin Cell Biol*, **11**, 274-286.
- Schonherr, R., 2005. Clinical relevance of ion channels for diagnosis and therapy of cancer. *J Membr Biol*, **205**, 175-184.
- Schonherr, R. & Heinemann, S. H., 1996. Molecular determinants for activation and inactivation of hERG, a human inward rectifier potassium channel. *Journal of Physiology-London*, **493**, 635-642.
- Schrempf, H., Schmidt, O., Kummerlen, R., Hinnah, S., Muller, D., Betzler, M., Steinkamp, T., Wagner, R., 1995. A prokaryotic potassium ion channel with two predicted transmembrane segments from *Streptomyces lividans*. *Embo J*, **14**, 5170-5178.
- Schwab, A., Finsterwalder, F., Kersting, U., Danker, T., Oberleithner, H., 1997. Intracellular Ca²⁺ distribution in migrating transformed epithelial cells. *Pflugers Arch*, **434**, 70-76.
- Schwab, A., Reinhardt, J., Schneider, S. W., Gassner, B., Schuricht, B., 1999a. K(+) channel-dependent migration of fibroblasts and human melanoma cells. *Cell Physiol Biochem*, **9**, 126-132.
- Schwab, A., Schuricht, B., Seeger, P., Reinhardt, J., Dartsch, P. C., 1999b. Migration of transformed renal epithelial cells is regulated by K⁺ channel modulation of actin cytoskeleton and cell volume. *Pflugers Arch*, **438**, 330-337.

- Schwab, A., Wojnowski, L., Gabriel, K., Oberleithner, H., 1994. Oscillating activity of a Ca(2+)-sensitive K⁺ channel. A prerequisite for migration of transformed Madin-Darby canine kidney focus cells. *J Clin Invest*, **93**, 1631-1636.
- Schwab, A., Wulf, A., Schulz, C., Kessler, W., Nechyporuk-Zloy, V., Romer, M., Reinhardt, J., Weinhold, D., Dieterich, P., Stock, C., Hebert, S. C., 2006. Subcellular distribution of calcium-sensitive potassium channels (IK1) in migrating cells. *J Cell Physiol*, **206**, 86-94.
- Sciacaluga, M., Fioretti, B., Catacuzzeno, L., Pagani, F., Bertollini, C., Rosito, M., Catalano, M., D'Alessandro, G., Santoro, A., Cantore, G., Ragozzino, D., Castigli, E., Franciolini, F., Limatola, C., 2010. CXCL12-induced glioblastoma cell migration requires intermediate conductance Ca²⁺-activated K⁺ channel activity. *Am J Physiol Cell Physiol*, **299**, C175-184.
- Semenza, G. L., 2007. Life with oxygen. *Science*, **318**, 62-64.
- Shao, X. D., Wu, K. C., Guo, X. Z., Xie, M. J., Zhang, J., Fan, D. M., 2008. Expression and significance of HERG protein in gastric cancer. *Cancer Biol Ther*, **7**, 45-50.
- Shao, X. D., Wu, K. C., Hao, Z. M., Hong, L., Zhang, J., Fan, D. M., 2005. The potent inhibitory effects of cisapride, a specific blocker for human ether-a-go-go-related gene (HERG) channel, on gastric cancer cells. *Cancer Biol Ther*, **4**, 295-301.
- Shattil, S. J., Kim, C., Ginsberg, M. H., 2010. The final steps of integrin activation: the end game. *Nat Rev Mol Cell Biol*, **11**, 288-300.
- Shen, M. R., Yang, T. P., Tang, M. J., 2002. A novel function of BCL-2 overexpression in regulatory volume decrease. Enhancing swelling-activated Ca(2+) entry and Cl(-) channel activity. *Journal of Biological Chemistry*, **277**, 15592-15599.
- Shi, W., Wymore, R. S., Wang, H. S., Pan, Z., Cohen, I. S., McKinnon, D., Dixon, J. E., 1997. Identification of two nervous system-specific members of the erg potassium channel gene family. *J Neurosci*, **17**, 9423-9432.
- Smith, G. A. M., Tsui, H. W., Newell, E. W., Jiang, X. P., Zhu, X. P., Tsui, F. W. L., Schlichter, L. C., 2002a. Functional up-regulation of hERG K⁺ channels in neoplastic hematopoietic cells. *Journal of Biological Chemistry*, **277**, 18528-18534.
- Smith, P. L., Baukrowitz, T., Yellen, G., 1996. The inward rectification mechanism of the HERG cardiac potassium channel. *Nature*, **379**, 833-836.
- Smith, P. L. & Yellen, G., 2002b. Fast and slow voltage sensor movements in HERG potassium channels. *J Gen Physiol*, **119**, 275-293.
- Smith, T. C. & Levinson, C., 1975. Direct measurement of the membrane potential of Ehrlich ascites tumor cells: lack of effect of valinomycin and ouabain. *J Membr Biol*, **23**, 349-365.
- Snyders, D. J. & Chaudhary, A., 1996. High affinity open channel block by dofetilide of HERG expressed in a human cell line. *Mol Pharmacol*, **49**, 949-955.

- Sowter, H. M., Ratcliffe, P. J., Watson, P., Greenberg, A. H., Harris, A. L., 2001. HIF-1-dependent regulation of hypoxic induction of the cell death factors BNIP3 and NIX in human tumors. *Cancer Res*, **61**, 6669-6673.
- Spangenberg, C., Lausch, E. U., Trost, T. M., Prawitt, D., May, A., Keppler, R., Fees, S. A., Reutzel, D., Bell, C., Schmitt, S., Schiffer, I. B., Weber, A., Brenner, W., Hermes, M., Sahin, U., Tureci, O., Koelbl, H., Hengstler, J. G., Zabel, B. U., 2006. ERBB2-mediated transcriptional up-regulation of the alpha5beta1 integrin fibronectin receptor promotes tumor cell survival under adverse conditions. *Cancer Res*, **66**, 3715-3725.
- Spector, P. S., Curran, M. E., Zou, A. R., Sanguinetti, M. C., 1996. Fast inactivation causes rectification of the I-Kr channel. *Journal of General Physiology*, **107**, 611-619.
- Spitzner, M., Ousingsawat, J., Scheidt, K., Kunzelmann, K., Schreiber, R., 2007. Voltage-gated K⁺ channels support proliferation of colonic carcinoma cells. *Faseb J*, **21**, 35-44.
- Srinivasan, S., Wang, F., Glavas, S., Ott, A., Hofmann, F., Aktories, K., Kalman, D., Bourne, H. R., 2003. Rac and Cdc42 play distinct roles in regulating PI(3,4,5)P3 and polarity during neutrophil chemotaxis. *J Cell Biol*, **160**, 375-385.
- Stringer, B. K., Cooper, A. G., Shepard, S. B., 2001. Overexpression of the G-protein inwardly rectifying potassium channel 1 (GIRK1) in primary breast carcinomas correlates with axillary lymph node metastasis. *Cancer Res*, **61**, 582-588.
- Sturm, P., Wimmers, S., Schwarz, J. R., Bauer, C. K., 2005. Extracellular potassium effects are conserved within the rat erg K⁺ channel family. *Journal of Physiology-London*, **564**, 329-345.
- Suessbrich, H., Waldegger, S., Lang, F., Busch, A. E., 1996. Blockade of HERG channels expressed in *Xenopus* oocytes by the histamine receptor antagonists terfenadine and astemizole. *FEBS Lett*, **385**, 77-80.
- Sun, X. X., Hodge, J. J., Zhou, Y., Nguyen, M., Griffith, L. C., 2004. The eag potassium channel binds and locally activates calcium/calmodulin-dependent protein kinase II. *J Biol Chem*, **279**, 10206-10214.
- Suzuki, T. & Takimoto, K., 2004. Selective expression of hERG and Kv2 channels influences proliferation of uterine cancer cells. *International Journal of Oncology*, **25**, 153-159.
- Szabo, I., Gulbins, E., Apfel, H., Zhang, X., Barth, P., Busch, A. E., Schlottmann, K., Pongs, O., Lang, F., 1996. Tyrosine phosphorylation-dependent suppression of a voltage-gated K⁺ channel in T lymphocytes upon Fas stimulation. *J Biol Chem*, **271**, 20465-20469.
- Tagliatela, M., Castaldo, P., Iossa, S., Pannaccione, A., Fresi, A., Ficker, E., Annunziato, L., 1997. Regulation of the human ether-a-gogo related gene (HERG) K⁺ channels by reactive oxygen species. *Proceedings of the National Academy of Sciences of the United States of America*, **94**, 11698-11703.
- Tajima, N., Schonherr, K., Niedling, S., Kaatz, M., Kanno, H., Schonherr, R., Heinemann, S. H., 2006. Ca²⁺-activated K⁺ channels in human melanoma cells are up-regulated by hypoxia involving hypoxia-inducible factor-1alpha and the von Hippel-Lindau protein. *J Physiol*, **571**, 349-359.

- Takaishi, K., Sasaki, T., Kotani, H., Nishioka, H., Takai, Y., 1997. Regulation of cell-cell adhesion by rac and rho small G proteins in MDCK cells. *J Cell Biol*, **139**, 1047-1059.
- Teicher, B. A., Lazo, J. S., Sartorelli, A. C., 1981. Classification of antineoplastic agents by their selective toxicities toward oxygenated and hypoxic tumor cells. *Cancer Res*, **41**, 73-81.
- Teulon, J., Ronco, P. M., Geniteau-Legendre, M., Baudouin, B., Estrade, S., Cassingena, R., Vandewalle, A., 1992. Transformation of renal tubule epithelial cells by simian virus-40 is associated with emergence of Ca(2+)-insensitive K⁺ channels and altered mitogenic sensitivity to K⁺ channel blockers. *J Cell Physiol*, **151**, 113-125.
- Thomas, D., Bloehs, R., Koschny, R., Ficker, E., Sykora, J., Kiehn, J., Schlomer, K., Gierten, J., Kathofer, S., Zitron, E., Scholz, E. P., Kiesecker, C., Katus, H. A., Karle, C. A., 2008. Doxazosin induces apoptosis of cells expressing hERG K⁺ channels. *Eur J Pharmacol*, **579**, 98-103.
- Thomas, D., Wendt-Nordahl, G., Rockl, K., Ficker, E., Brown, A. M., Kiehn, J., 2001. High-affinity blockade of human ether-a-go-go-related gene human cardiac potassium channels by the novel antiarrhythmic drug BRL-32872. *J Pharmacol Exp Ther*, **297**, 753-761.
- Thomas, D., Wimmer, A. B., Wu, K., Hammerling, B. C., Ficker, E. K., Kuryshev, Y. A., Kiehn, J., Katus, H. A., Schoels, W., Karle, C. A., 2004. Inhibition of human ether-a-go-go-related gene potassium channels by alpha 1-adrenoceptor antagonists prazosin, doxazosin, and terazosin. *Naunyn Schmiedebergs Arch Pharmacol*, **369**, 462-472.
- Toral, C., Mendoza-Garrido, M. E., Azorin, E., Hernandez-Gallegos, E., Gomora, J. C., Delgadillo, D. M., Solano-Agama, C., Camacho, J., 2007. Effect of extracellular matrix on adhesion, viability, actin cytoskeleton and K⁺ currents of cells expressing human ether a go-go channels. *Life Sci*, **81**, 255-265.
- Tristani-Firouzi, M., Chen, J., Sanguinetti, M. C., 2002. Interactions between S4-S5 linker and S6 transmembrane domain modulate gating of HERG K⁺ channels. *J Biol Chem*, **277**, 18994-19000.
- Trudeau, M. C., Warmke, J. W., Ganetzky, B., Robertson, G. A., 1995. HERG, a human inward rectifier in the voltage-gated potassium channel family. *Science*, **269**, 92-95.
- Tu, Z., Gui, L., Wang, J., Li, X., Sun, P., Wei, L., 2006. Tumorigenesis of K-ras mutation in human endometrial carcinoma via upregulation of estrogen receptor. *Gynecol Oncol*, **101**, 274-279.
- Umemoto, T., Inomoto, T., Ueda, K., Hamaguchi, M., Kioka, N., 2009. v-Src-mediated transformation suppresses the expression of focal adhesion protein vincenin. *Cancer Lett*, **279**, 22-29.
- Ungar, F., Geiger, B., Ben-Ze'ev, A., 1986. Cell contact- and shape-dependent regulation of vinculin synthesis in cultured fibroblasts. *Nature*, **319**, 787-791.
- Vaupel, P., Kallinowski, F., Okunieff, P., 1989. Blood flow, oxygen and nutrient supply, and metabolic microenvironment of human tumors: a review. *Cancer Res*, **49**, 6449-6465.
- Vial, E., Sahai, E., Marshall, C. J., 2003. ERK-MAPK signaling coordinately regulates activity of Rac1 and RhoA for tumor cell motility. *Cancer Cell*, **4**, 67-79.

- Viloria, C. G., Barros, F., Giraldez, T., Gomez-Varela, D., de la Pena, P., 2000. Differential effects of amino-terminal distal and proximal domains in the regulation of human erg K(+) channel gating. *Biophys J*, **79**, 231-246.
- Volberg, T., Geiger, B., Kam, Z., Pankov, R., Simcha, I., Sabanay, H., Coll, J. L., Adamson, E., Ben-Ze'ev, A., 1995. Focal adhesion formation by F9 embryonal carcinoma cells after vinculin gene disruption. *J Cell Sci*, **108 (Pt 6)**, 2253-2260.
- Vreede, J., van der Horst, M. A., Hellingwerf, K. J., Crielaard, W., van Aalten, D. M. F., 2003. PAS domains - Common structure and common flexibility. *Journal of Biological Chemistry*, **278**, 18434-18439.
- Walker, J. L. & Assoian, R. K., 2005. Integrin-dependent signal transduction regulating cyclin D1 expression and G1 phase cell cycle progression. *Cancer Metastasis Rev*, **24**, 383-393.
- Wang, H. Z., Zhang, Y. Q., Cao, L. W., Han, H., Wang, J. X., Yang, B. F., Nattel, S., Wang, Z. G., 2002a. hERG K⁺ channel, a regulator of tumor cell apoptosis and proliferation. *Cancer Research*, **62**, 4843-4848.
- Wang, J., Myers, C. D., Robertson, G. A., 2000. Dynamic control of deactivation gating by a soluble amino-terminal domain in HERG K(+) channels. *J Gen Physiol*, **115**, 749-758.
- Wang, J., Trudeau, M. C., Zappia, A. M., Robertson, G. A., 1998. Regulation of deactivation by an amino terminal domain in human ether-a-go-go-related gene potassium channels. *Journal of General Physiology*, **112**, 637-647.
- Wang, L. & Duff, H. J., 1996a. Identification and characteristics of delayed rectifier K⁺ current in fetal mouse ventricular myocytes. *Am J Physiol*, **270**, H2088-2093.
- Wang, L., Feng, Z. P., Kondo, C. S., Sheldon, R. S., Duff, H. J., 1996b. Developmental changes in the delayed rectifier K⁺ channels in mouse heart. *Circ Res*, **79**, 79-85.
- Wang, L., Xu, B., White, R. E., Lu, L., 1997a. Growth factor-mediated K⁺ channel activity associated with human myeloblastic ML-1 cell proliferation. *Am J Physiol*, **273**, C1657-1665.
- Wang, S., Liu, S., Morales, M. J., Strauss, H. C., Rasmusson, R. L., 1997b. A quantitative analysis of the activation and inactivation kinetics of hERG expressed in *Xenopus* oocytes. *Journal of Physiology-London*, **502**, 45-60.
- Wang, W., Goswami, S., Sahai, E., Wyckoff, J. B., Segall, J. E., Condeelis, J. S., 2005. Tumor cells caught in the act of invading: their strategy for enhanced cell motility. *Trends Cell Biol*, **15**, 138-145.
- Wang, W., Wyckoff, J. B., Frohlich, V. C., Oleynikov, Y., Huttelmaier, S., Zavadil, J., Cermak, L., Bottinger, E. P., Singer, R. H., White, J. G., Segall, J. E., Condeelis, J. S., 2002b. Single cell behavior in metastatic primary mammary tumors correlated with gene expression patterns revealed by molecular profiling. *Cancer Res*, **62**, 6278-6288.
- Wang, Y. L., 1985. Exchange of actin subunits at the leading edge of living fibroblasts: possible role of treadmilling. *J Cell Biol*, **101**, 597-602.

- Wang, Z., 2004. Roles of K⁺ channels in regulating tumour cell proliferation and apoptosis. *Pflugers Arch*, **448**, 274-286.
- Warmke, J. W. & Ganetzky, B., 1994. A family of potassium channel genes related to eag in *Drosophila* and mammals. *Proceedings of the National Academy of Sciences of the United States of America*, **91**, 3438-3442.
- Weaver, A. K., Bomben, V. C., Sontheimer, H., 2006. Expression and function of calcium-activated potassium channels in human glioma cells. *Glia*, **54**, 223-233.
- Weber, C., Mello de Queiroz, F., Downie, B. R., Suckow, A., Stuhmer, W., Pardo, L. A., 2006. Silencing the activity and proliferative properties of the human Eag1 potassium channel by RNAi. *Journal of Biological Chemistry*, **281**, 13030-13037.
- Weerapura, M., Nattel, S., Chartier, D., Caballero, R., Hebert, T. E., 2002. A comparison of currents carried by HERG, with and without coexpression of MiRP1, and the native rapid delayed rectifier current. Is MiRP1 the missing link? *J Physiol*, **540**, 15-27.
- Weinberg, R. A., 2008. Mechanisms of malignant progression. *Carcinogenesis*, **29**, 1092-1095.
- Weiner, T. M., Liu, E. T., Craven, R. J., Cance, W. G., 1993. Expression of focal adhesion kinase gene and invasive cancer. *Lancet*, **342**, 1024-1025.
- Whitfield, R. A. & Jacobson, B. S., 1999. The beta1-integrin cytosolic domain optimizes phospholipase A2-mediated arachidonic acid release required for NIH-3T3 cell spreading. *Biochem Biophys Res Commun*, **258**, 306-312.
- Wiecha, J., Munz, B., Wu, Y., Noll, T., Tillmanns, H., Waldecker, B., 1998. Blockade of Ca²⁺-activated K⁺ channels inhibits proliferation of human endothelial cells induced by basic fibroblast growth factor. *J Vasc Res*, **35**, 363-371.
- Wilson, G. F. & Chiu, S. Y., 1993. Mitogenic factors regulate ion channels in Schwann cells cultured from newborn rat sciatic nerve. *J Physiol*, **470**, 501-520.
- Wimmers, S., Bauer, C. K., Schwarz, J. R., 2002. Biophysical properties of heteromultimeric erg K⁺ channels. *Pflugers Arch*, **445**, 423-430.
- Wimmers, S., Wulfsen, I., Bauer, C. K., Schwarz, J. R., 2001. Erg1, erg2 and erg3 K channel subunits are able to form heteromultimers. *Pflugers Arch*, **441**, 450-455.
- Witchel, H. J., 2007. The hERG potassium channel as a therapeutic target. *Expert Opin Ther Targets*, **11**, 321-336.
- Wonderlin, W. F. & Strobl, J. S., 1996. Potassium channels, proliferation and G1 progression. *Journal of Membrane Biology*, **154**, 91-107.
- Wood, S. M., Wiesener, M. S., Yeates, K. M., Okada, N., Pugh, C. W., Maxwell, P. H., Ratcliffe, P. J., 1998. Selection and analysis of a mutant cell line defective in the hypoxia-inducible factor-1 alpha-subunit (HIF-1alpha). Characterization of hif-1alpha-dependent and -independent hypoxia-inducible gene expression. *J Biol Chem*, **273**, 8360-8368.

- Wozniak, M. A., Modzelewska, K., Kwong, L., Keely, P. J., 2004. Focal adhesion regulation of cell behavior. *Biochimica Et Biophysica Acta*, **1692**, 103-119.
- Wu, D., 2005. Signaling mechanisms for regulation of chemotaxis. *Cell Res*, **15**, 52-56.
- Xu, D., Wang, L., Dai, W., Lu, L., 1999. A requirement for K⁺-channel activity in growth factor-mediated extracellular signal-regulated kinase activation in human myeloblastic leukemia ML-1 cells. *Blood*, **94**, 139-145.
- Xu, L. H., Yang, X., Bradham, C. A., Brenner, D. A., Baldwin, A. S., Jr., Craven, R. J., Cance, W. G., 2000. The focal adhesion kinase suppresses transformation-associated, anchorage-independent apoptosis in human breast cancer cells. Involvement of death receptor-related signaling pathways. *Journal of Biological Chemistry*, **275**, 30597-30604.
- Xu, W., Baribault, H., Adamson, E. D., 1998. Vinculin knockout results in heart and brain defects during embryonic development. *Development*, **125**, 327-337.
- Yang, T., Snyders, D. J., Roden, D. M., 1997. Rapid inactivation determines the rectification and [K⁺]_o dependence of the rapid component of the delayed rectifier K⁺ current in cardiac cells. *Circ Res*, **80**, 782-789.
- Yao, X. & Kwan, H. Y., 1999. Activity of voltage-gated K⁺ channels is associated with cell proliferation and Ca²⁺ influx in carcinoma cells of colon cancer. *Life Sci*, **65**, 55-62.
- Yifrach, O. & MacKinnon, R., 2002. Energetics of pore opening in a voltage-gated K(+) channel. *Cell*, **111**, 231-239.
- Yoon, S. O., Shin, S., Lipscomb, E. A., 2006. A novel mechanism for integrin-mediated ras activation in breast carcinoma cells: the alpha6beta4 integrin regulates ErbB2 translation and transactivates epidermal growth factor receptor/ErbB2 signaling. *Cancer Res*, **66**, 2732-2739.
- Yu, H., Wu, J., Potapova, I., Wymore, R. T., Holmes, B., Zuckerman, J., Pan, Z., Wang, H., Shi, W., Robinson, R. B., El-Maghrabi, M. R., Benjamin, W., Dixon, J., McKinnon, D., Cohen, I. S., Wymore, R., 2001a. MinK-related peptide 1: A beta subunit for the HCN ion channel subunit family enhances expression and speeds activation. *Circ Res*, **88**, E84-87.
- Yu, S. P., Canzoniero, L. M. T., Choi, D. W., 2001b. Ion homeostasis and apoptosis. *Current Opinion in Cell Biology*, **13**, 405-411.
- Zeng, H., Lozinskaya, I. M., Lin, Z., Willette, R. N., Brooks, D. P., Xu, X., 2006. Mallotoxin is a novel human ether-a-go-go-related gene (hERG) potassium channel activator. *J Pharmacol Exp Ther*, **319**, 957-962.
- Zhang, L., Bewick, M., Lafrenie, R. M., 2002. Role of Raf-1 and FAK in cell density-dependent regulation of integrin-dependent activation of MAP kinase. *Carcinogenesis*, **23**, 1251-1258.
- Zhang, L. & Hill, R. P., 2004. Hypoxia enhances metastatic efficiency by up-regulating Mdm2 in KHT cells and increasing resistance to apoptosis. *Cancer Res*, **64**, 4180-4189.

- Zhang, M., Liu, J., Jiang, M., Wu, D. M., Sonawane, K., Guy, H. R., Tseng, G. N., 2005. Interactions between charged residues in the transmembrane segments of the voltage-sensing domain in the hERG channel. *J Membr Biol*, **207**, 169-181.
- Zhao, J., Wei, X. L., Jia, Y. S., Zheng, J. Q., 2008. Silencing of hERG gene by shRNA inhibits SH-SY5Y cell growth in vitro and in vivo. *Eur J Pharmacol*, **579**, 50-57.
- Zhong, C., Kinch, M. S., Burridge, K., 1997. Rho-stimulated contractility contributes to the fibroblastic phenotype of Ras-transformed epithelial cells. *Mol Biol Cell*, **8**, 2329-2344.
- Zhou, Z., Gong, Q., Epstein, M. L., January, C. T., 1998a. HERG channel dysfunction in human long QT syndrome. Intracellular transport and functional defects. *J Biol Chem*, **273**, 21061-21066.
- Zhou, Z., Gong, Q., Ye, B., Fan, Z., Makielski, J. C., Robertson, G. A., January, C. T., 1998b. Properties of HERG channels stably expressed in HEK 293 cells studied at physiological temperature. *Biophysical Journal*, **74**, 230-241.
- Zhu, X. & Assoian, R. K., 1995. Integrin-dependent activation of MAP kinase: a link to shape-dependent cell proliferation. *Mol Biol Cell*, **6**, 273-282.
- Zutter, M. M., Santoro, S. A., Staatz, W. D., Tsung, Y. L., 1995. Re-expression of the alpha 2 beta 1 integrin abrogates the malignant phenotype of breast carcinoma cells. *Proc Natl Acad Sci U S A*, **92**, 7411-7415.